ISSN 1881-7815 Online ISSN 1881-7823

BST BioScience Trends

Volume 12, Number 6
December, 2018

IRCA BSSA

IACMHR

www.biosciencetrends.com

BST
BioScience Trends

ISSN: 1881-7815
Online ISSN: 1881-7823
CODEN: BTIRCZ
Issues/Year: 6
Language: English
Publisher: IACMHR Co., Ltd.

BioScience Trends is one of a series of peer-reviewed journals of the International Research and Cooperation Association for Bio & Socio-Sciences Advancement (IRCA-BSSA) Group and is published bimonthly by the International Advancement Center for Medicine & Health Research Co., Ltd. (IACMHR Co., Ltd.) and supported by the IRCA-BSSA and Shandong University China-Japan Cooperation Center for Drug Discovery & Screening (SDU-DDSC).

BioScience Trends devotes to publishing the latest and most exciting advances in scientific research. Articles cover fields of life science such as biochemistry, molecular biology, clinical research, public health, medical care system, and social science in order to encourage cooperation and exchange among scientists and clinical researchers.

BioScience Trends publishes Original Articles, Brief Reports, Reviews, Policy Forum articles, Case Reports, News, and Letters on all aspects of the field of life science. All contributions should seek to promote international collaboration.

Editorial Board

Editorial Office

Pearl City Koishikawa 603,
2-4-5 Kasuga, Bunkyo-ku, Tokyo 112-0003, Japan
Tel: +81-3-5840-8764 Fax: +81-3-5840-8765
E-mail: office@biosciencetrends.com

BioScience Trends

Editorial and Head Office

Pearl City Koishikawa 603, 2-4-5 Kasuga, Bunkyo-ku,
Tokyo 112-0003, Japan

Tel: +81-3-5840-8764, Fax: +81-3-5840-8765
E-mail: office@biosciencetrends.com
URL: www.biosciencetrends.com

Editorial Board Members

CONTENTS

Volume 12, Number 6, 2018

Review

Original Article

Brief Report

Guide for Authors

Copyright

Review

DOI: 10.5582/bst.2018.01172

The beneficial and deleterious role of dietary polyphenols on chronic degenerative diseases by regulating gene expression

Guojing Qu[1], Jinhua Chen[2], Xiuli Guo[2,*]

[1] *Shandong University Taishan College (Biological Research Training Program for Top-notch Students), Ji'nan, Shandong, China;*
[2] *Department of Pharmacology, School of Pharmaceutical Sciences, Shandong University, Ji'nan, Shandong, China.*

Summary **Dietary polyphenols, a natural component in many kinds of foods such as fruits and vegetables, play essential roles in a wide range of plant functions. Importantly, the discovery of the functions of polyphenols including anti-oxidant, anti-carcinogenic and anti-inflammatory has been appealing to researchers' attentions. Dietary polyphenols have shown protective effects on chronic degenerative diseases (CDD) such as cardiovascular diseases, cancers, and neurodegenerative diseases by regulating gene expression. Dietary polyphenols also affect the composition and activity of gut microbiota, in reverse, gut microbiota influences the bioavailability and physiological activity of dietary polyphenols. However, not all kinds of dietary polyphenols are beneficial for human health. The potential deleterious effects of several dietary polyphenols have been reported by inducing DNA damage and gene mutants. This review summarizes the potential therapeutic effects of dietary polyphenols on chronic degeneration diseases, the polyphenols-gut microbiota interactions, and the potential dangers of individual dietary polyphenols on human health.**

Keywords: Dietary polyphenols, chronic degenerative diseases, expression regulation, therapeutic effects, deleterious effects

1. Introduction

Dietary polyphenols are common secondary metabolites in various plant foods, which derive from L-phenylalanine and play an important role in the normal growth and functions of the plants (*1*). They are available for the pigmentation of flower, fruit and vegetables to adapt to use bees or moths as pollinators and seed dispersers. They protect plants against ultraviolet light, act as the plant defense against pathogenic microorganisms, for example, phenolic monoterpenes (such as carvacrol, thymol, *etc*.) have antifungal activity against plant pathogenic fungi (*2,3*). Recently, human epidemiological studies have shown that there is a positive correlation between the intake of polyphenols and the incidence of many chronic degenerative diseases, such as cardiovascular diseases, cancers, neurodegenerative diseases and diabetes (*4,5*). One typical case is "French Paradox phenomenon" which is referred to as a relatively low incidence of coronary heart disease (CHD) in the French population, despite consuming a diet rich in saturated fat (*6*). The possible explanation for the lower CHD in the French is the large consumption of wines, which are rich in some polyphenols. Another typical case is "Mediterranean diet" which was characterized by high consumption of olive oil, unrefined cereals, vegetables, fruits; moderate consumption of fish, cheese and wine, which was rich in dietary polyphenols. The health benefits and protective effects of "Mediterranean diet" against age-related cognitive decline and cognitive impairment of Alzheimer's disease (AD) and vascular dementia (VaD) were well documented (*7,8*). Therefore, there has been growing scientific interest in various chemical properties and biological effects of dietary polyphenols on chronic degenerative diseases.

More than 8,000 different polyphenols have been identified in edible plants. Their diverse chemical structures contribute to their multiple functions including anti-oxidative, anti-inflammatory, anti-carcinogenic,

Released online in J-STAGE as advance publication December 28, 2018.

**Address correspondence to:*
Dr. Xiuli Guo, Department of Pharmacology, School of Pharmaceutical Sciences, Shandong University, No. 44, WenHuaXi Road, Ji'nan 250012, P.R. China.
E-mail: guoxl@sdu.edu.cn

cardioprotective actions and anti-platelet properties, *etc*. (*9,10*). However, the structure-activity relationship of dietary polyphenols is still unclear. Importantly, dietary polyphenols are found to bring potential danger to human health (*11*). Some dietary polyphenols have mutagenic and/or pro-oxidant effects, as well as interference with endogenous essential biochemical pathways (*12-14*). Therefore, this review will summarize the recent understanding of the structure and structure-activity relationship, the therapeutic effects and molecular mechanism of dietary polyphenols on human diseases, and the polyphenols-gut microbiota interactions as well as the potential dangers of individual dietary polyphenols.

2. The molecular structure and structure-activity relationship of dietary polyphenols

Chemically, dietary polyphenols consist of one or more hydroxyl groups directly attached to a benzene ring. They can be classified according to their structure as flavonoids, phenolic acid derivatives, and the less common stilbenes or lignans in Table 1, and most percentages exist in the form of flavonoids (*4,15*). Flavonoids have a common C6-C3-C6 structure consisting of two aromatic rings linked by a three carbon chain, and are usually organized as an oxygenated heterocycle in Figure 1. Among non-flavoniods polyphenols (Figure 2), stilbenes have a common C6-C2-C6 structure consisting of two aromatic rings linked through a two carbon bridge with a double bond in Figure 2B (*16*). One of Stilbenes, resveratrol, has gotten more attention because of its multiple biological functions. Lignans consist of mostly two phenylpropanoid moieties connected *via* their side chain C8 carbons (*17*). They can be converted to enterodiol and enterolactone by intestinal bacteria in Figure 2C.

On the basis of the structural discrepancies, the structure-activity relationships of polyphenols have been established *in vitro* and *in vivo* (Table 2). Several catechins have shown their ability to induce apoptosis in human cancer cells (*18*). It has been found that catechins with a pyrogallol-type structure in a B-ring induced apoptosis and a 3-O-gallate group in a cis-relationship to the B ring enhanced the activity, whereas catechins without a pyrogallol-type structure in a molecule lacked this activity. (-)-epigallocatechin-3-gallate (EGCG) and its metabolite products, such as pyrogallol, gallic acid or quinones also have been reported to have important roles in inducing apoptosis (*19*). By investigating the molecular structure-affinity relationship of natural polyphenols for γ-globulin, Xiao *et al*. demonstrated that galloylated catechins and catechol-type catechins exhibited higher binding affinities for γ-globulin than non-galloylated and pyrogallol-type catechins (*20*). They also found that the glycosylation of resveratrol

Table 1. The categories of the representative polyphenolic compounds

Categories	Representative compounds
1. Flavonoids	
Flavanols	(-)-Epigallocatechin-3-gallate (EGCG); Epigallocatechin (EGC); (+)-Catechin.
Flavonols	Myricetin; Quercetin.
Flavones	Apigenin; Luteolin; Chrysin.
Isoflavones	Genistein; Daidzein; Glycitein.
Flavanones	Hesperetin; Naringenin.
Anthocyanins	Anthocyanidins; Procyanidine.
2. Phenolic acids derivatives	Caffeic acid
3. Stilbenes	Resveratrol; Piceatannol.
4. Lignans	Secoisolariciresinol; Matairesinol.
5. Phenolic monoterpenes	Carvacrol, Thymol

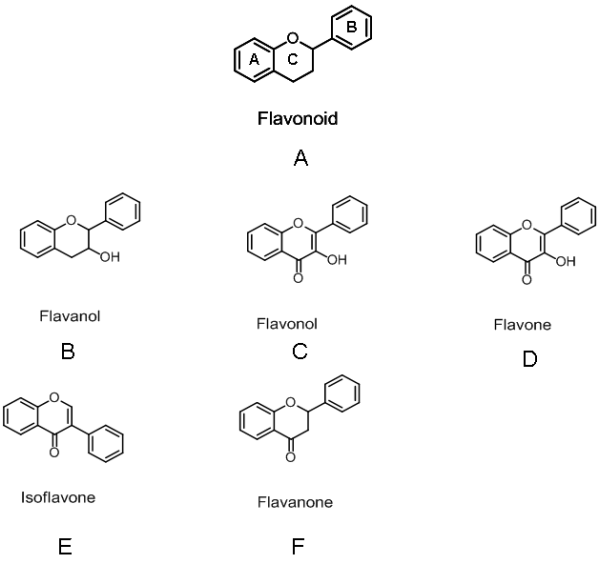

Figure 1. The chemical structure of different classes of Flavonoids. (A) The basic skeleton of flavonoid; (B) Flavanol; **(C)** Flavonol; **(D)** Flavone; **(E)** Isoflavone; **(F)** Flavanone.

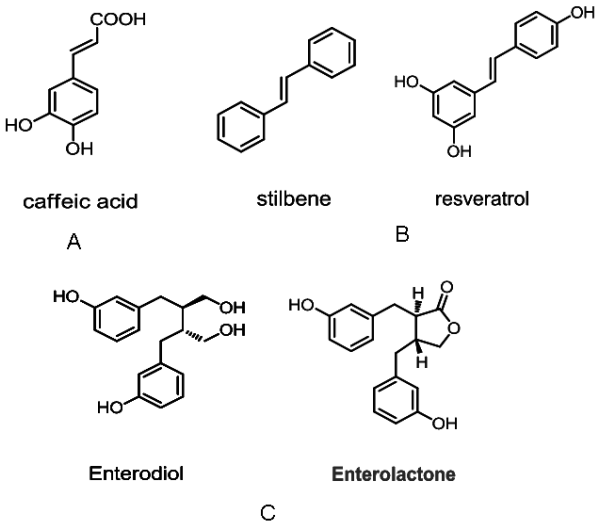

Figure 2. The chemical structure of non-flavoniods polyphenols. (A) Caffeic acid (phenolic acids); **(B)** The basic skeleton of stilbene and resveratrol (stilbenes); **(C)** Enterodiol and enterolactone (lignans).

Table 2. Structure-activity relationship of dietary polyphenols

Polyphenol compounds	Group in structure	Activity
Flavonoids	Methoxy groups	Decrease antioxidation
	Multiple hydroxyl groups	Inhibition on lipid peroxidation and ROS, chelating redox-active metals
	A double bond and carbonyl in the heterocycle	Increase free radical scavenging activity
	R3'-OH and R4'-OH substitutions	Inhibit MMP-9 activity
Catechins	pyrogallol-type structure in B ring	Apoptosis induction
	Without pyrogallol-type structure in B ring	Lack of apoptosis induction
	3-O-gallate group in cis- relationship to the B ring in catechins	Increase apoptosis induction
	Galloylated catechins and Catechol-type catechins	Higher affinity to γ-globulin than non-galloylated or pyrogallol-type
Isoflavones	4'-OH and 7'-OH site of daidzein	Increase hydroxyl radical scavenging activity
Anthocyanins	3-OH group	Better antiradical and reductant activities than trolox and catechol
Stibenes	Glycosylation of resveratrol	Decreased affinity to γ-globulin
Lignans	Without ortho-dihydroxy group	Weak radical scavenging activity
Phenolic monoterpenes	Phenolic hydroxyl and monoterpene in carvacrol or thymol	Antifungal activity
	Ester derivatives of carvacrol or thymol	Increased antifungal activity

decreased its affinity for γ-globulin. Moreover, cardioprotective effects of flavonoids are mainly due to the multiple hydroxyl groups in their molecules. Multiple hydroxyl groups conferred upon the molecule inhibition of lipid peroxidation, chelating redox-active metals and attenuating other processes involving reactive oxygen species. Methoxy groups in flavonoids introduce unfavorable steric effects and increase the lipophilicity and membrane partitioning, which result in decreased antioxidation. A double bond and carbonyl function in the heterocycle or polymerization of the nuclear structure increases free radical scavenging activity by affording a more stable flavonoid radical through conjugation and electron delocalization (*21*). Daidzein, a soy isoflavone, possessed potent hydroxyl radical scavenging activity through forming stable daidzein radicals with highly reactive hydroxyl radicals by a hydrogen abstraction reaction with both OH functional groups, the 4'-OH and 7'-OH site of daidzein. The high enthalpic stabilization involved in daidzein radical formation at the 4'-OH site can be partly attributed to better solvation through hydrogen-bonding interactions with water and higher electron density delocalization of the radical over the adjacent aromatic ring (*22*). Both anthocyanidins and anthocyanins showed better antiradical and reductant activities than trolox and catechol. A structure-activity relationship study showed that, the 3-OH group improved hydrogen atom donation because of the stabilization by anthocyanidins semiquinone-like resonance, while radicals of the 4, 5 or 7-OH groups could only be stabilized by resonance through pyrylium oxygen in the presence of the 3-OH group. The 3-OH group also enhanced electron donation (**23**). Furthermore, Saragusti *et al*. have demonstrated that flavonoid R3'-OH and R4'-OH substitutions were relevant to the inhibitory property against the activity of matrix metalloproteinase 9 (MMP-9), which plays an important role in the turnover of basement membrane type IV collagen during the formation of atherosclerotic plaques (*24*). However, Cai *et al*. reported that although lignans had hydroxyl groups, their radical scavenging activity was very weak. Lack of the *ortho*-dihydroxy structure was the main reason (*25*). In addition, the antifungal activity of phenolic monoterpenes (carvacrol, thymol) was related to the basic structures of phenolic hydroxyl and monoterpene, while the position of phenolic hydroxyl has no significant effect. Moreover, the ester derivatives of carvacrol or thymol showed stronger antifungal activity against pathogenic fungi than their parent structure (2).

3. The beneficial effects of polyphenols on several chronic degenerative diseases

Numerous action mechanisms of polyphenols including anti-oxidation, free radical scavenging, mitochondrial protection and anti-cancerization, regulation on transcription factors and membrane receptors have been investigated. Some research demonstrated that dietary polyphenols have important potential for effective treatment of chronic degenerative diseases (CDD) like cardiovascular diseases (CVD), cancers and neurodegenerative diseases (*4*).

3.1. *Dietary polyphenols and cardiovascular diseases*

Dietary polyphenols are beneficial in many cardiovascular diseases, including myocardial ischemia/reperfusion, platelet aggregation, inflammation and atherosclerosis (*26*). Among numerous plausible

mechanisms, which may be involved in cardiovascular protection, improvement of endothelial function and inhibition of angiogenesis in blood vessels has been shown. Yang *et al*. reported that resveratrol, an antioxidant existing in red wine, was effective in preventing myocardial ischemia/reperfusion injury which may be due to its antioxidant activity and upregulation of vascular endothelial growth factor B (*27*). EGCG, a bioactive ingredient of green tea, plays a protective role in the cardiovascular system by inhibiting the expression of angiotensin II type 1 receptor (AT-1R) and extracellular regulated protein kinases 1/2 (ERK1/2) and p38 mitogen-activated protein kinase (MAPK) signals, resulting in a decrease of proliferation of human vascular smooth muscle cells (HVSMCs) induced by homocysteine (Hcy) (*28*). Furthermore, dietary polyphenols have positive effects on vascular function and platelet function in humans to attenuate thrombosis. The consumption of polyphenol rich foods might impart anti-thrombotic and cardiovascular protective effects *via* their inhibition of platelet hyperactivation or aggregation. Polyphenols also alleviated fibrinogen binding to platelet surface (GPIIb-IIIa) receptors to reduce platelet recruitment for aggregation and inhibit platelet degranulation by targeting various additional platelet activation pathways (*e.g*. by blocking platelet-ADP, collagen receptors) (*29*). Khan *et al*. demonstrated that flavonoids were responsible for several health-promoting properties, such as outstanding preclinical antiplatelet effects, and provided an ideal approach as templates for new, clinically effective and safe antiplatelet agents (*30*). Omega-3 polyunsaturated fatty acids (PUFA) rich Mediterranean diet has protective effects for CVD by reducing the risk for sudden death induced by cardiac arrhythmias and could treat hyperlipidemia and hypertension. Foods with omega-3 PUFA, purple grape juice (PGJ), and wine all reduce platelet aggregation and P-selectin expression (*31*). PGJ suppressed platelet-mediated thrombosis by decreasing platelet aggregation and superoxide production, increasing platelet-derived NO release which represented a potential mechanism for the beneficial effects of PGJ in CVD. An abundance of new evidence points to inflammation as a major participant in the pathogenesis and development of cardiovascular diseases. Polyphenols have been reported to directly inhibit inflammatory responses of the innate immune system, such as nuclear factor-kappa B (NF-κB), and activate anti-inflammatory gene transcription factors, such as peroxisome proliferators-activated receptors-γ (PPAR-γ), adenosine monophosphate activated protein kinase (AMPK), *etc*. to exert a protective effect against hypertension, atherosclerosis, dyslipidemias (*32*). The impact of polyphenols on the same molecular targets as pharmacological interventions on inflammation makes it possible to develop a unique, non-pharmacological approach for CVD treatment.

3.2. *Dietary polyphenols and cancers*

Though great progress has been made in cancer therapy in the past several decades, the incidence and mortality of cancer has been increasing endlessly. By epidemiologic investigation, polyphenols-rich diets have been shown to be associated with a lower risk of cancers. Therefore, numerous studies have been conducted to explore the beneficial effects of polyphenols on various cancers. Green tea polyphenols defend healthy cells from malignant transformation and induce apoptosis locally in oral cancer cells (*33*). Polyphenols extracted from both green tea and ginger showed antiproliferative and apoptosis-mediated cytotoxic effects on human non-small lung cancer cells (*34*). Polyphenols and sterols extracted from virgin argan oil have also shown antiproliferative and pro-apoptotic effects on human prostate cancer cell lines (*35*). Lignans, recognized as the greatest class of phytoestrogens in the Western diet, have a negative correlation with breast cancer risk in postmenopausal women (*36*). Apigenin (4',5,7-trihydroxyflavone), a major plant flavone, has shown anticancer properties reducing the risk of certain cancers alone and/or increasing the efficacy of several chemotherapeutic drugs. It could affect several molecular and cellular targets related to a variety of human cancers, in particular, inducing differential effects in causing minimal toxicity to normal cells (*37*). However, the underlying mechanisms are still unclear. Kang *et al*. indicated that polyphenols exerted anti-tumor actions as small molecular inhibitors of signaling cascades and src family kinase (*38*). EGCG induced apoptosis in human acute promyelocytic leukemia NB4 cells and increased the level of Bcl-2-associated X protein (Bax) protein expression *via* upregulating Src homology 1 domain-containing protein tyrosine phosphatase (SHP-1)-p38αMAPK- Bax cascade (*10*). EGCG in combination with Am80 (a synthetic retinoid) synergistically induced apoptosis in human lung cancer cell line PC-9 and up-regulated expressions of growth arrest and DNA damage-inducible gene 153 (*GADD153*), death receptor 5, p21waf1 genes by increasing acetylation levels in nonhistone proteins such as p53, α-tubulin *via* down-regulation of histone deacetylase 4, 5, 6 (*39*). In addition, inflammation is increasingly found to be involved in the development of different types of cancer and the anti-inflammatory property of some polyphenols might provide a therapeutic window for the treatment of cancer. For example, curcumin and rutin reduced tumor-associated inflammation in HPV16-transgenic FVB/n mice through inhibition of the expression of cyclo-oxygenase-2 (COX-2) (*40*). Curcumin has also been reported to restore the level of tumor suppressor p53 through increasing nuclear factor-erythroid 2 related factor 2 (Nrf2) activation and upregulation of tumor growth factor β (TGF-β) and inducible nitric oxide

synthase (iNOS) in lymphoma bearing mice (*41*). These indicate that polyphenols have the potential for the development of new strategies for cancer prevention.

3.3. *Dietary polyphenols and neurodegenerative diseases*

The typical diagnosis of AD includes neuropathological lesions, such as amyloid plaques and cerebral amyloid angiopathy, and substantial neuronal loss (*42*). Resveratrol, which has been found in more than 70 plant species, promotes the non-amyloidogenic cleavage of the amyloid precursor protein, enhances clearance of amyloid beta-peptides, and reduces neuronal damage (*43*). EGCG, the major component of green tea, exerted a neurorescue effect against functional and neurochemical deficits in a mouse model of Parkinson disease (PD) by regulating the iron-export protein ferroportin in substantia nigra and reducing oxidative stress (*44*). The flavanone hesperetin, has also been shown to have a protective effect on an early model of PD induced by 6-hydroxydopamine *via* mitigation of nigral DNA fragmentation as an index of apoptosis and prevention of loss of substantia nigra pars compacta (SNC) dopaminergic neurons (*45*). Except for the amyloid neurotoxicity, mitochondrial dysfunction and oxidative damage may also play important roles in the slowly progressive neuronal death (*46,47*). Numerous studies have indicated that dietary polyphenolic compounds exhibited neuroprotective effects through scavenging free radicals and increasing anti-oxidant capacity *in vitro* and *in vivo* AD models. Furthermore, they could facilitate the endogenous antioxidant system by stimulating transcription (*48,49*). Feng *et al*. reported that grape seed extract (GSE) reduced the concentration of brain 8-isoprostaglandin F2α and proapoptotic protein c-jun in the brain cortex improving neurofunctional abnormalities caused by hypoxia-ischemia. GSE also reduced brain injury by suppressing lipid peroxidation after reoxygenation in rat pups (*50*). Long-term consumption of fermented rooibos herbal tea significantly reduced brain edema and neuronal apoptosis by reducing lipid peroxidation levels and increasing total antioxidant capacity in Wistar rats following cerebral ischemia induced by bilateral occlusion of the common carotid arteries (*51*). Oral consumption of flavonoids may promote neural protection by facilitating the expression of gene products responsible for detoxifying the ischemic microenvironment through both anti-oxidative and anti-inflammatory actions. In particular, the transcriptional factor, nuclear factor erythroid 2-related factor 2 (NFE2L2), has emerged as a critical regulator of flavonoid-mediated protection through induction of various cytoprotective genes (*52*). Some reports have shown that the neuroprotective effects of polyphenols may be associated with activation or inhibition of some cellular signaling pathways involving Sirtuin 1 (SIRT1), AMPK, *etc*. Resveratrol is the first polyphenolic compound, which has been shown to activate SIRT1 (*53*). SIRT1 plays an essential role in the ability of moderate doses of resveratrol to stimulate AMPK and improve mitochondrial function both *in vitro* and *in vivo* (*54*). Wang *et al*. reported that resveratrol reversed rotenone-induced neurotoxicity through activation of the SIRT/Akt1 signaling pathway and reduction of reactive oxygen species (ROS) production in PC12 cells (*55*). A recent report showed that strawberry supplementation improved aging-associated impairments in mitochondrial function and biogenesis through increasing the expression of AMPK cascade genes and decreasing intracellular ROS levels and lipid and DNA damage in old rats (*56*). Studies with lower organisms have also revealed that the increase of AMPK activity could extend lifespan (*57*).

4. The potential cellular and molecular mechanism of polyphenols on chronic degenerative diseases

Molecular mechanisms underlying the potential therapeutic role of polyphenols on CDD have been investigated (Table 3). Here, we will briefly summarize the regulation effects of dietary polyphenols on DNA damage, transcription factors and mRNA expression.

4.1. *Dietary polyphenols inhibit DNA damage*

DNA is easily assaulted by the byproducts of cellular metabolism, background radiation and environmental mutagens. Particularly, DNA double-strand breaks may result in cell death or cancer if improperly repaired. It could be induced by reactive oxygen species, ionizing radiation and some anti-cancer drugs. Polyphenols and flavonoids in artichoke leaf tincture have been shown to inhibit oxidative DNA damage to limit the effects of the atherogenic diet through reducing monocyte chemoattractant protein-1 (MCP-1) expression (*58*). Seo and Lee demonstrated that antioxidant supplementation including polyphenols, ascorbate and curcumin to lymphocytes inhibited benz[a]anthracene-induced oxidative DNA damage *in vitro* (*59*). Resveratrol has also shown the ability to antagonize DNA damage induced by aflatoxin B1 in human lymphocytes (*60*). Dietary polyphenols such as quercetin, myricetin and catechin could protect HepG2 cells against DNA strand breaks and oxidized pyrimidines induced by N-nitrosodimethylamine, N-nitrosopyrrolidine and benzo(a)pyrene, which are three carcinogenic compounds in the environment (*61*). Furthermore, the hypermethylation of promoter sequences is the main mechanism of epigenetic inactivation of various genes that are necessary for the accurate regulation of apoptosis, cell cycle or DNA repair. Studies reported that polyphenols (EGCG, dietary black tea and coffee polyphenols, annurca apple polyphenols) have

Table 3. Molecular mechanism of dietary polyphenols for treatment of CDD

Disease	Action	Signal pathway
Cardiovascular disease	Antiproliferation of HVSMCs	↓AT-1R, ↓p-ERK1/2, ↓p-P38/MAPK
	Antiplatelet aggregation	↓Fibrinogen binding to GPIIb-IIIa receptor; ↓P-selectin expression
	Free radical scavenging	
	Anti-inflammation	↓NF-kB, ↑PPAR-γ and AMPK
	Anti-arthrosclerosis	↓MCP-1
	Endothelial NO production	↓Cav-1 mRNA level
	Endothelial protection by inhibiting PAI-1	↑EC p38, ↑ERK1/2, ↑JNK
Neurodegenerative disease	Clearance of amyloid beta-peptides; Reduction of oxidative stress and lipid peroxidation; Mitigation of DNA fragmentation; Prevention of loss of dopaminergic neurons;	
	Antihypoxia-ischemia	↓brain 8-isoPGF2α, ↓c-jun
	Neuroprotection	↑NFE2L2; Regulation on iron-export protein ferroportin
	Relieve neurotoxicity and improve mitochondrial function	↑SIRT/Akt1, ↑AMPK
	Demethylation activity to improve brain performance	↓Dnmt3a
Cancer	Anti-tumor actions	↓Src family kinase
	Apoptosis induction	↑Bax, upregualtion of SHP-1-p38MAPK-Bax; ↑GADD153; ↑death receptor 5; ↑p21waf1 genes; ↑p53, ↑Nrf2, ↑TGF-β, ↑iNOS ↑SIRT1/Akt
	Antiproliferation	↓Telomerase mRNA level
	Reduced tumor-associated inflammation	↓COX2; ↓NF-kB/p65 activation; ↑PPAR-γ

HVSMCs: human vascular smooth muscle cells; AT-1R: angiotensin II type 1 receptor; ERK1/2: extracellular regulated protein kinases 1/2; MAPK: mitogen-activated protein kinase; NF-κB: Nuclear transcription factor; PPAR-γ: peroxisome proliferators-activated receptors-γ; AMPK: AMP-activated protein kinase; MCP-1: monocyte chemoattractant protein-1; Cav-1: caveolin-1; EC p38: endothelial cell p38; PAI-1: plasminogen activator inhibitor type-1; JNK: c-Jun N-terminal kinase; 8-isoPGF2α: 8-iso-prostaglandin F2α; NFE2L2: nuclear factor erythroid 2-related factor 2; SIRT: Sirtuin 1; Dnmt3a: DNA methyltransferase 3a; SHP-1: Src homology 1 domain-containing protein tyrosine phosphatase; GADD153: growth arrest and DNA damage-inducible gene 153; iNOS: inducible nitric oxide synthase; COX2: cyclooxygenase 2.

demethylation activity by inhibiting mammalian DNA methyltransferase 3a (Dnmt3a) to show potential anti-cancer effects, or improvement of brain performance (*62,63*).

4.2. *Dietary polyphenols regulate transcription factors*

Nuclear transcription factor NF-κB regulates the expression of many genes, which encode proteins involved in immune response, inflammatory reaction, apoptosis and neurodegenerative diseases (*64,65*). Special polyphenols could modulate the expression of genes, which are regulated by NF-κB at multiple levels. For example, Epicatechin and dimeric procyanidins B2 restrained NF-κB activation in Jurkat T cells and Hodgkin's lymphoma cells by interacting with NF-κB proteins and preventing the binding of NF-κB to the DNAκB sites (*66,67*). It is noteworthy that NF-κB can be constitutively activated in most types of human cancer including breast, colon, skin, lung, esophagus, pancreas, prostate and gliomas and plays a critical role in the regulation of cell survival, proliferation and apoptosis (*68,69*). A polyphenolic fraction of green tea (GTP) inhibited cell proliferation and induced apoptosis of human osteosarcoma SAOS-2 cells by decreasing nuclear DNA binding of NF-κB/p65 and lowering the NF-κB/p65 and p50 levels in the cytoplasm and nucleus (*70*). Moreover, red wine metabolites may delay the activation of different transcription factors, NF-κB and activator protein-1 induced by TNF-α to prevent cell adhesion (*71*). PPAR-γ is another nuclear receptor and transcription factor, which is involved in cell control, proliferation and differentiation, exerting anti-inflammatory, anti-cancer and insulin-sensitizing actions. Polyphenols have been reported to regulate the expression of both PPAR-γ and NF-κB. Curcuma longa polyphenols have been shown to improve obesity-related metabolic disorders by upregulating the gene expression of PPAR-γ and decreasing the production of pro-inflammatory molecules such as NF-κB, MCP-1, interleukin 6 (IL-6), *etc*. in 3T3-L1 adipose cells exposed to hydrogen peroxide (H_2O_2)-mediated oxidative stress (*72*). Choi *et al*. has also shown that galangin exerts anti-inflammatory effects by inhibiting NF-κB activity and increasing expression and transcriptional activity of PPAR-γ in polyinosinic-polycytidylic acid (poly(I:C)) (a viral mimic dsRNA analog)-stimulated microglia (*73*).

4.3. *Dietary polyphenols regulate mRNA expression*

Telomerase, a specialized reverse transcriptase, has an important role in cell fate, for example, sustaining cell proliferation resulting in tumorigenesis and mutagenesis. The activity of telomerase correlates with the degree of malignancy and senescence (*74*). Tea

polyphenols of EGCG and epigallocatechin (EGC) showed repression activities on carcinogenesis by inhibiting mRNA expression of human telomerase reverse transcriptase (hTERT) in human lung carcinoma H1299 cells, human oral cancer OECM-1 cells and tongue squamous-cell carcinoma cells (SAS) (*75*). In the cardiovascular system, caveolin-1 (Cav-1), a negative regulator of endothelial nitric oxide synthase, influences various aspects of cardiovascular function. Green tea polyphenols could down-regulate mRNA levels of Cav-1 in bovine aortic endothelial cells time- and dose-dependently *via* activating ERK1/2 and inhibiting p38MAPK signaling (*76*). Furthermore, there is a positive association between plasminogen activator inhibitor type-1 (PAI-1) and the development and progression of CVD. Catechin and quercetin showed cardiovascular protection through down-regulating the PAI-1 mRNA level in endothelial cells *via* activating ERK1/2 and c-Jun N-terminal kinase (JNK) (*77*). A resveratrol-rich grape has also been reported to reduce low-density lipoprotein (LDL)-cholesterol, oxidized LDL and apolipoprotein B (ApoB) and improve the inflammatory and fibrinolytic status in patients undergoing primary prevention of CVD through decreasing thrombogenic PAI-1 by modulating six key inflammation-related transcription factors involved in inflammation and cell migration (*78*).

5. The polyphenols-gut microbiota interactions

There exists a complex microbial ecosystem comprising considerable metabolic versatility in the human intestinal tract (*79*). Reports have shown that dietary polyphenols could affect the composition and function of gut microbiota involved in the maintenance of gastrointestinal health. The equilibrium of the gut microbiota in return keeps the bioavailability and physiological activity of dietary polyphenols. The growth of certain pathogenic bacteria such as *Clostridium perfringens*, *Clostridium difficile* and *Bacteroides spp*. were significantly repressed by tea phenolics and their derivatives, while the growth of commensal anaerobes like *Clostridium spp*., *Bifidobacterium spp*. and probiotics such as *Lactobacillus sp*. were not affected. This suggested that different strains of intestinal bacteria had different sensitivity to tea phenolics and their metabolites (*80*). Moreover, consistent evidence from Shanthi *et al*. indicates that polyphenols have potential to alter gut microecology and confer positive gut health benefits by regulating the total number of beneficial microflora in the gut (*81*). There is a growing body of evidence that gut microbiota contributes to colon tumorigenesis. Polyphenols can inhibit the development of colon tumorigenesis through affecting the composition and activity of the gut microbiota and anti-inflammation. On the other hand, gut microbiota are involved in the metabolism of polyphenols and convert dietary polyphenols into active and bioavailable metabolites. As gut microbiota vary among individuals, variations in gut microbiota can affect polyphenol activity by producing metabolites with different physiological significance (*82*). For example, the soy isoflavone daidzein is microbially biotransformed to equol, which has a more potent estrogenic action than the precursor itself. Being overweight or obese induced the gut microbial environment alteration and contributed to being incapable of metabolizing the soy isoflavone daidzine to O-desmethylangolensin (ODMA) in peri- and post-menopausal women (*83*). What's more, human intestinal bacteria could rapidly degrade cyranidin 3-glucoside (C3G, one of the major dietary anthocyanins) to phenolic acids *in vitro*. However, higher concentrations of phenolic acids were observed in the presence of intestinal bacteria, while these products appeared at considerably lower levels in the absence of bacteria (*84*).

6. The potential danger of dietary polyphenols on human health

Many types of polyphenols are considered to be traditional herbal medicines and safety drug candidates. However, it is noteworthy that some actions of individual dietary polyphenols may have a potential danger to human health. Tannins, catechins, flavones and isoflavones have been considered as topo poisons, which could cause high numbers of broken and recombined chromosomes and chromosome aberrations in treated cells (*85,86*). Green tea polyphenols (GTPs) showed toxicity at high doses presumably due to pro-oxidative properties in experimental rodents, such as hepatotoxicity, GTP-deteriorated dextran sodium sulfate (DSS)-induced intestinal inflammation and carcinogenesis, 1% GTPs induced nephrotoxicity in colitis mode mice, *etc*. (*87*). Quercetin transformed into an *ortho*-quinone after scavenging free radicals to decrease the level of many anti-oxidative cellular substances such as glutathione (GSH), and total anti-oxidative capacity (*88*). Biso *et al*. reported that quercetin, quercetin-3-O-α-l-rhamnoside (quercitrin), myricetin and gallic acid derivatives showed mutagenic potential for peripheral blood cells by micronucleus test (Ames test), while they didn't show genotoxic activity in the mouse cells (*90*). Another study observed the mutagenicity of ten flavonoids, results showed that some flavonoids such as galangin, kaemferol and quercetin could be biotransformed into more genotoxic metabolites and showed signs of mutagenicity in Ames test (*90*). The structural requirements for mutagenicity is a flavonoid ring structure with a free hydroxyl group at the 3-position, a double bond at the 2,3-position and a keto-group at the 4-position allowing the proton of the 3-hydroxyl group to tautomerize to

a 3-keto moiety. When free hydroxyl groups are not present in the B-ring, a metabolic activating system is required for the formation of a mutagenic compound (*91*). In addition, flavonoids in propolis induced both mutagenic and antimutagenic effects depending on its concentration (*92*). The result is consistent with the study that green propolis caused an increase in the damage to DNA in the peripheral blood cells of mice using micronucleus and single-cell gel electrophoresis assays (*93*). Comparable to green propolis, the extracts of baccharis dracunculifolia showed genotoxic and mutagenic effects by increasing the DNA damage in blood and liver tissues and the frequency of micronuclei in bone marrow in mice (*94*). *Cecropia pachystachya*, which contains chlorogenic acid, isoorientin, orientin, and isovitexin, were shown to be genotoxic to brain tissue because of the ability to cross the blood-brain barrier and act on the central nervous system and had mutagenic effects at higher doses (*95*).

7. Prospects of dietary polyphenols in treatment of CDD

Recent investigations of the pharmacological actions of dietary polyphenols have showed that they have neuroprotection, free radical scavenging, anti-oxidation, reduction of LDL-cholesterol and ApoB, anti-inflammation, carcinogenesis repression, inhibition on DNA damage, *etc*. which promised strong potential for treatment of AD, PD, CVD, and cancers. However, more research will be needed to further investigate the structure-activity relationship of polyphenols molecules and the mechanism of biological effects including beneficial or deleterious effects before treating dietary polyphenols as therapeutic agents.

Acknowledgements

This work was supported by Research Training Project of Taishan College, Shandong University.

References

1. Boudet AM. Evolution and current status of research in phenolic compounds. Phytochemistry. 2007; 68:2722-2735.
2. Wang K, Jiang S, Pu T, Fan L, Su F, Ye M. Antifungal activity of phenolic monoterpenes and structure-related compounds against plant pathogenic fungi. Nat Prod Res. 2018; 15:1-8.
3. Petti S, Scully C. Polyphenols, oral health and disease: a review. J Dent. 2009; 37:413-423.
4. Adefegha SA. Functional foods and nutraceuticals as dietary intervention in chronic diseases; novel perspectives for health promotion and disease prevention. J Diet Suppl. 2017; 27:1-33.
5. Tomás-Barberán FA, Andrés-Lacueva C. Polyphenols and health: current state and progress. J Agr Food Chem. 2012; 60:8773-8775.
6. Visioli F, Davalos A. Polyphenols and cardiovascular disease: a critical summary of the evidence. Mini-Rev Med Chem. 2011; 11:1186-1190.
7. Féart C, Samieri C, Barberger-Gateau P. Mediterranean diet and cognitive function in older adults. Curr Opin Clin Nutr Metab Care. 2010; 13:14-18.
8. Leifert WR, Abeywardena MY. Cardioprotective actions of grape polyphenols. Nutr Res. 2008; 28:729-737.
9. Rodrigo R, Miranda A, Vergara L. Modulation of endogenous antioxidant system by wine polyphenols in human disease. Clin Chim Acta. 2011; 412:410-424.
10. Gan L, Zhong L, Shan Z, Xiao C, Xu T, Song H, Li L, Yang R, Liu B. Epigallocatechin-3-gallate induces apoptosis in acute promyelocytic leukemia cells *via* a SHP-1-p38α MAPK-Bax cascade. Oncol Lett. 2017; 14:6314-6320.
11. Coniglio MS, Busto VD, González PS, Medina MI, Milrad S, Agostini E. Application of *Brassica napus* hairy root cultures for phenol removal from aqueous solutions. Chemosphere. 2008; 72:1035-1042.
12. Belcavello L, Vencioneck Dutra JC, de Freitas JV, Aranha IP, do Carmo Pimentel, Batitucci M. Mutagenicity of ipriflavone *in vivo* and *in vitro*. Food Chem Toxicol. 2012; 50:996-1000.
13. Macáková K, Mladěnka P, Filipský T, Říha M, Jahodář L, Trejtnar F, Bovicelli P, Proietti Silvestri I, Hrdina R, Saso L. Iron reduction potentiates hydroxyl radical formation only in flavonols. Food Chem. 2012; 135:2584-2592.
14. Fraga CG, Galleano M, Verstraeten SV, Oteiza PI. Basic biochemical mechanisms behind the health benefits of polyphenols. Mol Aspects Med. 2010; 31:435-445.
15. Davin LB, Lewis NG. An historical perspective on lignan biosynthesis: monolignol, allylphenol and hydroxycinnamic acid coupling and downstream metabolism. Phytochem Rev. 2003; 2: 257-288.
16. Rodríguez-Cabo T, Rodríguez I, Ramil M, Cela R. Comprehensive evaluation of the photo-transformation routes of trans-resveratrol. J Chromatogr A. 2015; 1410:129-139.
17. Gaya P, Medina M, Sánchez-Jiménez A, Landete JM. Phytoestrogen metabolism by adult human gut microbiota. Molecules. 2016; 21:pii: E1034.
18. Bhattacharjee R, Devi A, Mishra S. Molecular docking and molecular dynamics studies reveal structural basis of inhibition and selectivity of inhibitors EGCG and OSU-03012 toward glucose regulated protein-78 (GRP78) overexpressed in glioblastoma. J Mol Model. 2015; 21:272.
19. Berindan-Neagoe I, Braicu C, Tudoran O, Balacescu O, Irimie A. Early apoptosis signals induced by a low dose of epigallocatechin 3-gallate interfere with apoptotic and cell death pathways. J Nanosci Nanotechno. 2012; 12:2113-2119.
20. Xiao J, Kai G, Yang F, Liu C, Xu X, Yamamoto K. Molecular structure-affinity relationship of natural polyphenols for bovine γ-globulin. Mol Nutr Food Res. 2011; 55(Suppl 1):S86-92.
21. Heim KE, Tagliaferro AR, Bobilya DJ. Flavonoid antioxidants: chemistry, metabolism and structure-activity relationships. J Nutr Biochem. 2002; 13:572-584.
22. Chakraborty S, Biswas PK. Elucidation of the mechanistic pathways of the hydroxyl radical scavenging reaction by daidzein using hybrid QM/MM dynamics. J Phys Chem A. 2012; 116:8775-8785.
23. Ali HM, Almagribi W, Al-Rashidi MN. Antiradical and

reductant activities of anthocyanidins and anthocyanins, structure-activity relationship and synthesis. Food Chem. 2016; 194:1275-1282.
24. Saragusti AC, Ortega MG, Cabrera JL, Estrin DA, Marti MA, Chiabrando GA. Inhibitory effect of quercetin on matrix metalloproteinase 9 activity Molecular mechanism and structure-activity relationship of the flavonoid-enzyme interaction. Eur J Pharmacol. 2010; 644:138-145.
25. Cai YZ, Sun M, Xing J, Luo Q, Corke H. Structure-radical scavenging activity relationships of phenolic compounds from traditional Chinese medicinal plants. Life Sci. 2006; 78:2872-2888.
26. Vasanthi HR, Shrishrimal N, Das DK. Phytochemicals from plants to combat cardiovascular disease. Curr Med Chem. 2012; 19:2242-2251.
27. Yang L, Zhang Y, Zhu M, Zhang Q, Wang X, Wang Y, Zhang J, Li J, Yang L, Liu J, Liu F, Yang Y, Kang L, Shen Y, Qi Z. Resveratrol attenuates myocardial ischemia/reperfusion injury through up-regulation of vascular endothelial growth factor B. Free Radic Biol Med. 2016; 101:1-9.
28. Zhan XL, Yang XH, Gu YH, Guo LL, Jin HM. Epigallocatechin gallate protects against homocysteine-induced vascular smooth muscle cell proliferation. Mol Cell Biochem. 2018; 439:131-140.
29. Santhakumar AB, Bulmer AC, Singh I. A review of the mechanisms and effectiveness of dietary polyphenols in reducing oxidative stress and thrombotic risk. J Hum Nutr Diet. 2014; 27:1-21.
30. Khan H, Jawad M, Kamal MA, Baldi A, Xiao J, Nabavi SM, Daglia M. Evidence and prospective of plant derived flavonoids as antiplatelet agents: Strong candidates to be drugs of future. Food Chem Toxicol. 2018; 119:355-367.
31. McEwen BJ. The influence of diet and nutrients on platelet function. Semin Thromb Hemost. 2014; 40:214-226.
32. Sears B, Ricordi C. Role of fatty acids and polyphenols in inflammatory gene transcription and their impact on obesity, metabolic syndrome and diabetes. Eur Rev Med Pharmacol Sci. 2012; 16:1137-1154.
33. Singhal K, Raj N, Gupta K, Singh S. Probable benefits of green tea with genetic implications. J Oral Maxillofac Pathol. 2017; 21:107-114.
34. Hessien M, El-Gendy S, Donia T, Sikkena MA. Growth inhibition of human non-small lung cancer cells h460 by green tea and ginger polyphenols. Anticancer Agents Med Chem. 2012; 12:383-390.
35. Bennani H, Drissi A, Giton F, Kheuang L, Fiet J, Adlouni A. Antiproliferative effect of polyphenols and sterols of virgin argan oil on human prostate cancer cell lines. Cancer Detect Prev. 2007; 31:64-69.
36. Buck K, Zaineddin AK, Vrieling A, Linseisen J, Chang-Claude J.. Meta-analyses of lignans and enterolignans in relation to breast cancer risk. Am J Clin Nutr. 2010; 92:141-153.
37. Shankar E, Goel A, Gupta K, Gupta S. Plant flavone apigenin: an emerging anticancer agent. Curr Pharmacol Rep. 2017; 3:423-446.
38. Kang NJ, Shin SH, Lee HJ, Lee KW. Polyphenols as small molecular inhibitors of signaling cascades in carcinogenesis. Pharmacol Ther. 2011; 130:310-324.
39. Oya Y, Mondal A, Rawangkan A, Umsumarng S, Iida K, Watanabe T, Kanno M, Suzuki K, Li Z, Kagechika H, Shudo K, Fujiki H, Suganuma M. Down-regulation of histone deacetylase 4, -5 and -6 as a mechanism of synergistic enhancement of apoptosis in human lung cancer cells treated with the combination of a synthetic retinoid, Am80 and green tea catechin. J Nutr Biochem. 2017; 42:7-16.
40. Das L, Vinayak M. Long term effect of curcumin in restoration of tumour suppressor p53 and phase-II antioxidant enzymes *via* activation of Nrf2 signalling and modulation of inflammation in prevention of cancer. PLoS One. 2015; 10:e0124000.
41. Moutinho MSS, Aragão S, Carmo D, Casaca F, Silva S, Ribeiro J, Sousa H, Pires I, Queiroga F, Colaço B, Medeiros R, Oliveira PA, Lopes C, Bastos MMSM, DA Costa RMG. Curcumin and Rutin down-regulate cyclooxygenase-2 and reduce tumor-associated inflammation in HPV16-Transgenic Mice. Anticancer Res. 2018; 38:1461-1466.
42. Serrano-Pozo A, Frosch MP, Masliah E, Hyman BT. Neuropathological alterations in Alzheimer disease. Cold Spring Harb Perspect Med. 2011; 1:a006189.
43. Li F, Gong Q, Dong H, Shi J. Resveratrol, a neuroprotective supplement for Alzheimer's disease. Curr Pharm Design. 2012; 18:27-33.
44. Xu Q, Langley M, Kanthasamy AG, Reddy MB. Epigallocatechin gallate has a neurorescue effect in a mouse model of Parkinson disease. J Nutr. 2017; 147:1926-1931.
45. Kiasalari Z, Khalili M, Baluchnejadmojarad T, Roghani M. Protective effect of oral hesperetin against unilateral striatal 6-hydroxydopamine damage in the rat. Neurochem Res. 2016; 41:1065-1072.
46. Schapira AH. Mitochondrial dysfunction in neurodegenerative diseases. Neurochem Res. 2008; 33:2502-2509.
47. Trushina E, McMurray CT. Oxidative stress and mitochondrial dysfunction in neurodegenerative diseases. Neuroscience. 2007; 145:1233-1248.
48. Singh M, Arseneault M, Sanderson T, Murthy V, Ramassamy C. Challenges for research on polyphenols from foods in Alzheimer's disease: bioavailability, metabolism, and cellular and molecular mechanisms. J Agr Food Chem. 2008; 56:4855-4873.
49. Choi DY, Lee YJ, Hong JT, Lee HJ. Antioxidant properties of natural polyphenols and their therapeutic potentials for Alzheimer's disease. Brain Res Bull. 2012; 87:144-153.
50. Feng Y, Liu YM, Leblanc MH, Bhatt AJ, Rhodes PG. Grape seed extract given three hours after injury suppresses lipid peroxidation and reduces hypoxic-ischemic brain injury in neonatal rats. Pediatr Res. 2007; 61:295-300.
51. Akinrinmade O, Omoruyi S, Dietrich D, Ekpo O. Long-term consumption of fermented rooibos herbal tea offers neuroprotection against ischemic brain injury in rats. Acta Neurobiol Exp (Wars). 2017; 77:94-105.
52. Leonardo CC, Doré S. Dietary flavonoids are neuroprotective through Nrf2-coordinated induction of endogenous cytoprotective proteins. Nutr Neurosci. 2011; 14:226-236.
53. Baur JA, Pearson KJ, Price NL, *et al*. Resveratrol improves health and survival of mice on a high-calorie diet. Nature. 2006; 444:337-342.
54. Price NL, Gomes PG, Ling AJ, *et al*. SIRT1 is required for AMPK activation and the beneficial effects of resveratrol on mitochondrial function. Cell Metab. 2012; 15:675-690.
55. Wang H, Dong X, Liu Z, *et al*. Resveratrol suppresses

rotenone-induced neurotoxicity through activation of SIRT1/Akt1 signaling pathway. Anat Rec (Hoboken). 2018; 301:1115-1125.
56. Giampieri F, Alvarez-Suarez JM, Cordero MD, Gasparrini M, Forbes-Hernandez TY, Afrin S, Santos-Buelga C, González-Paramás AM, Astolfi P, Rubini C, Zizzi A, Tulipani S, Quiles JL, Mezzetti B, Battino M. Strawberry consumption improves aging-associated impairments, mitochondrial biogenesis and functionality through the AMP-activated protein kinase signaling cascade. Food Chem. 2017; 234:464-471.
57. Salminen A, Kaarniranta K. AMP-activated protein kinase (AMPK) controls the aging process *via* an integrated signaling network. Ageing Res Rev. 2012; 11:230-241.
58. Bogavac-Stanojevic N, Kotur Stevuljevic J, Cerne D, Zupan J, Marc J, Vujic Z, Crevar-Sakac M, Sopic M, Munjas J, Radenkovic M, Jelic-lvanovic Z. The role of artichoke leaf tincture (*Cynara scolymus*) in the suppression of DNA damage and atherosclerosis in rats fed an atherogenic diet. Pharm Biol. 2018; 56:138-144.
59. Seo YN, Lee MY. Inhibitory effect of antioxidants on the benz[a]anthracene- induced oxidative DNA damage in lymphocytes. J Environ Biol. 2011; 32:7-10.
60. Türkez H, Sisman T. The genoprotective activity of resveratrol on aflatoxin B1-induced DNA damage in human lymphocytes *in vitro*. Toxicol Ind Health. 2012; 28:474-480.
61. Delgado ME, Haza AI, Arranz N, Garcia A, Morales P. Dietary polyphenols protect against N-nitrosamines and benzo(a)pyrene-induced DNA damage (strand breaks and oxidized purines/pyrimidines) in HepG2 human hepatoma cells. Eur J Nutr. 2008; 47:479-490.
62. Rajavelu A, Tulyasheva Z, Jaiswal R, Jeltsch A, Kuhnert N. The inhibition of the mammalian DNA methyltransferase 3a (Dnmt 3a) by dietary black tea and coffee polyphenols. BMC Biochem. 2011; 12:16.
63. Fini L, Selgrad M, Fogliano V, Graziani G, Romano M, Hotchkiss E, Daoud YA, De Vol EB, Boland CR, Ricciardiello L. Annurca apple polyphenols have potent demethylation activity and can reactivate silenced tumor suppressor genes in colorectal cancer cells. J Nutr. 2007; 137:2622-2628.
64. Radhakrishnan SK, Kamalakaran S. Pro-apoptotic role of NF-kappaB: implications for cancer therapy. Biochim Biophys Acta. 2006; 1766:53-62.
65. Perkins ND. Integrating cell-signalling pathways with NF-kappaB and IKK function. Nat Rev Mol Cell Biol. 2007; 8:49-62.
66. Mackenzie GG, Oteiza PI. Modulation of transcription factor NF-kappaB in Hodgkin's lymphoma cell lines: effect of (-)-epicatechin. Free Radic Res. 2006; 40:1086-1094.
67. Mackenzie GG, Adamo AM, Decker NP, Oteiza PI. Dimeric procyanidin B2 inhibits constitutively active NF-kappaB in Hodgkin's lymphoma cells independently of the presence of IkappaB mutations. Biochem Pharmacol. 2008; 75:1461-1471.
68. Li F, Zhang J, Arfuso F, Chinnathambi A, Zayed ME, Alharbi SA, Kumar AP, Ahn KS, Sethi G. NF-κB in cancer therapy. Arch Toxicol. 2015; 89:711-731.
69. Shostak K, Chariot A. EGFR and NF-κB: partners in cancer. Trends Mol Med. 2015; 21:385-393.
70. Hafeez BB, Ahmed S, Wang N, Gupta S, Zhang A, Haqqi TM. Green tea polyphenols-induced apoptosis in human osteosarcoma SAOS-2 cells involves a caspase-dependent mechanism with downregulation of nuclear factor-κB. Toxicol Appl Pharmacol. 2006; 216:11-19.
71. Canali R, Comitato R, Ambra R, Virgili F. Red wine metabolites modulate NF-kappaB, activator protein-1 and cAMP response element-binding proteins in human endothelial cells. Brit J Nutr. 2010; 103:807-814.
72. Septembre-Malaterre A, Le Sage F, Hatia S, Catan A, Janci L, Gonthier MP. Curcuma longa polyphenols improve insulin-mediated lipid accumulation and attenuate proinflammatory response of 3T3-L1 adipose cells during oxidative stress through regulation of key adipokines and antioxidant enzymes. Biofactors. 2016; 42:418-430.
73. Choi MJ, Park JS, Park JE, Kim HS, Kim HS. Galangin suppresses pro-inflammatory gene expression in polyinosinic-polycytidylic acid-stimulated microglial Cells. Biomol Ther (Seoul). 2017; 25:641-647.
74. Xu Y, He K, Goldkorn A. Telomerase targeted therapy in cancer and cancer stem cells. Clin Adv Hematol Oncol. 2011; 9:442-455.
75. Lin SC, Li WC, Shin JW, Hong KF, Pan YR, Lin JJ. The tea polyphenols EGCG and EGC repress mRNA expression of human telomerase reverse transcriptase (hTERT) in carcinoma cells. Cancer Lett. 2006; 23:80-88.
76. Li Y, Ying C, Zuo X, Yi H, Yi W, Meng Y, Ikeda K, Ye X, Yamori Y, Sun X. Green tea polyphenols down-regulate caveolin-1 expression *via* ERK1/2 and p38MAPK in endothelial cells. J Nutr Biochem. 2009; 20:1021-1027.
77. Pasten C, Olave NC, Zhou L, Tabengwa EM, Wolkowicz PE, Grenett HE. Polyphenols downregulate PAI-1 gene expression in cultured human coronary artery endothelial cells: Molecular contributor to cardiovascular protection. Thromb Res. 2007; 121:59-65.
78. Wang S, Moustaid-Moussa N, Chen L, Mo H, Shastri A, Su R, Bapat P, Kwun I, Shen CL. Novel insights of dietary polyphenols and obesity. J Nutr Biochem. 2014; 25:1-18.
79. Qin J, Li R, Raes J, *et al*. A human gut microbial gene catalogue established by metagenomic sequencing. Nature. 2010; 464:59-65.
80. Lee HC, Jenner AM, Low CS, Lee YK. Effect of tea phenolics and their aromatic fecal bacterial metabolites on intestinal microbiota. Res Microbiol. 2006; 157:876-884.
81. Parkar SG, Stevenson DE, Skinner MA. The potential influence of fruit polyphenols on colonic microflora and human gut health. Int J Food Microbiol. 2008; 124:295-298.
82. Tomás-Barberán FA, Selma MV, Espín JC. Interactions of gut microbiota with dietary polyphenols and consequences to human health. Curr Opin Clin Nutr Metab Care. 2016; 19:471-476.
83. Miller LM, Lampe JW, Newton KM, Gundersen G, Fuller S, Reed SD, Frankenfeld CL. Being overweight or obese is associated with harboring a gut microbial community not capable of metabolizing the soy isoflavone daidzein to O-desmethylangolensin in peri- and post-menopausal women. Maturitas. 2017; 99:37-42.
84. Hanske L, Engst W, Loh G, Sczesny S, Blaut M, Braune A. Contribution of gut bacteria to the metabolism of cyanidin 3-glucoside in human microbiota-associated rats. Br J Nutr. 2013; 10:1433-1441.
85. Cantero G, Campanella C, Mateos S, Cortés F. Topoisomerase II inhibition and high yield of endoreduplication induced by the flavonoids luteolin and quercetin. Mutagenesis. 2006; 21:321-325.

86. Zhoum N, Yanm Y, Lim W, Wangm Y, Zhengm L, Hanm S, Yanm Y, Lim Y. Genistein inhibition of topoisomerase IIalpha expression participated by Sp1 and Sp3 in HeLa cells. Int J Mol Sci. 2009; 10:3255-3268.
87. Murakami A. Dose-dependent functionality and toxicity of green tea polyphenols in experimental rodents. Arch Biochem Biophys. 2014; 557:3-10.
88. Rpbaszkiewicz A, Balcerczyk A, Bartosz G. Antioxidative and prooxidative effects of quercetin on A549 cells. Cell Biol Int. 2007; 31:1245-1250.
89. Biso FI, Rodrigues CM, Rinaldo D, Reis MB, Bernardi CC, de Mattos JC, Caldeira-de-Araújo A, Vilegas W, Cólus IM, Varanda EA. Assessment of DNA damage induced by extracts fractions and isolated compounds of *Davilla nitida* and *Davilla elliptica* (Dilleniaceae). Mutat Res. 2010; 702:92-99.
90. Resende FA, Vilegas W, Dos Santos LC, Varanda EA. Mutagenicity of flavonoids assayed by bacterial reverse mutation (Ames) test. Molecules. 2012; 17:5255-5268.
91. MacGregor JT, Jurd L. Mutagenicity of plant flavonoids: structural requirements for mutagenic activity in *Salmonella typhimurium*. Mutat Res. 1978; 54:297-309.
92. Tavares DC, Mazzaron Barcelos GR, Silva LF, Chacon Tonin CC, Bastos JK. Propolis-induced genotoxicity and antigenotoxicity in Chinese hamster ovary cells. Toxicol in Vitro. 2006; 20:1154-1158.
93. Pereira AD, de Andrade SF, de Oliveira-Swerts MS, Maistro EL. First *in vivo* evaluation of the mutagenic effect of Brazilian green propolis by comet assay and micronucleus test. Food Chem Toxicol. 2008; 46:2580-2584.
94. Rodrigues CR, Dias JH, Semedo JG, da Silva J, Ferraz AB, Picada JN. Mutagenic and genotoxic effects of *Baccharis dracunculifolia* (D.C.). J Ethnopharmacol. 2009; 124:321-324.
95. Mendonça ED, da Silva J, Dos Santos MS, Carvalho P, Papke DK, Ortmann CF, Picada JN, Reginatto FH, de Barros Falcão Ferraz A. Genotoxic, mutagenic and antigenotoxic effects of *Cecropia pachystachya* Trécul aqueous extract using *in vivo* and *in vitro* assays. J Ethnopharmacol. 2016; 193:214-220.

(Received July 23, 2018; Revised November 8, 2018; Accepted December 9, 2018)

Review

DOI: 10.5582/bst.2018.01246

Update review of skin adverse events during treatment of lung cancer and colorectal carcinoma with epidermal growth receptor factor inhibitors

Yanmei Peng[1], Qiang Li[1], Jingyi Zhang[1], Wen Shen[1], Xu Zhang[1], Chenyao Sun[1], Huijuan Cui[2,*]

[1] *Beijing University of Chinese Medicine, China-Japan Friendship Hospital, Beijing, China;*
[2] *Department of Integrative Oncology, China-Japan Friendship Hospital, Beijing, China.*

Summary **The past decades have witnessed a rapid increase in the use of molecularly targeted therapies. One class of agents includes the epidermal growth factor receptor inhibitors (EGFRIs), which afford patients longer progression-free survival (PFS) times, especially among non-small cell lung cancer (NSCLC) and metastatic colorectal carcinoma (mCRC). Certain adverse effects, particularly skin toxicity, are mainly manifested as rash, xerosis, pruritus, nails changes, hair changes and mucositis. Previous studies reported the adverse events occurred based on the cutaneous inflammation reaction. Treatment recommended glucocorticoids and antibiotics. It is suggested that skin toxicity is an important issue because it usually affects patients' quality of life (QoL) and still causes dose reduction or discontinuation of targeted therapies. For these reasons, more and more oncologists and dermatologists recognize the importance of recognition and management of skin toxicities with the expansion in availability of EGFRIs. In this review, we conducted a systematic review of recent data to examine the types and frequencies of dermatologic toxicities associated with anti-epidermal growth factor receptor (EGFR) therapies in NSCLC and mCRC. In addition, we would like to explore the management and treatment options currently used by clinicians based on the possible mechanism.**

Keywords: EGFRIs, skin toxicities, non-small cell lung cancer, colorectal carcinoma, review

1. Introduction

Epidermal growth factor receptor (EGFR) is often over-expressed or overactivated in human cancer, which makes EGFR a key therapeutic target. Frequently administered inhibiting EGFR have different mechanisms of action that are specific for the intracellular tyrosine kinase inhibitors (TKIs) erlotinib gefitinib, icotinib, osimertinib, dacomitinib and the monoclonal antibodies (mAbs) cetuximab and panitumumab binding the extracellular domain of the EGFR. TKIs have been recommended as the first-line treatment for non-small cell lung cancer (NSCLC) with EGFR mutation. In the IPASS study, the first-line therapy with gefitinib significantly prolonged progression-free survival compared with paclitaxel plus carboplatin in pulmonary adenocarcinoma patients (*1*). The mAbs have been recommended for patients with wild-type RAS metastatic colorectal carcinoma (mCRC) by the National Comprehensive Cancer Network (NCCN) at the first line (*2*).

The adverse events of these targeted drugs are usually minimal in terms of frequency and severity. However, epidermal growth factor receptor inhibitors (EGFRIs) are commonly associated with dermatological toxicities that may less be seen with conventional chemotherapy or radiotherapy. They are usually manifested as acneiform rash, xerosis, pruritus, paronychia, hair changes and mucostitis. The overall incidence was skin rash 47-100% (grade 3/4 1-10%), xerosis 10-49% (grade 3/4 0-7%),

Released online in J-STAGE as advance publication December 17, 2018.

**Address correspondence to:*
Dr. Huijuan Cui, Department of Integrative Oncology, China-Japan Friendship Hospital, No. 2 Yinghua Dongjie, Hepingli Beijing 100029, Beijing, China.
E-mail: chjzryhyy@sina.com

pruritus 8-57% (grade 3/4 0-2%), paronychia 3-25% (grade 3/4 0-2%), hair abnormalities 0-13% (grade 3/4 0-12%), mucositis 0-44% (grade 3/4 0-1%), while skin reactions occur more frequently in mAbs than in TKIs (*3*). EGFRIs-related skin toxicities usually lead to infection, pain, discomfort and greatly affect quality of life, causing depression, sleep interruptions and feel self-abasement. Most importantly, skin toxicities influence anti-cancer therapies adherence of patients. Gefitinib induced skin toxicity led to drug interruption of 6.9% patients (*4*). Herein, skin adverse events perhaps present the greatest concern with EGFRIs use. Prevention and treatment are recommended by experts and constitutions, mostly using topical or systematic glucocorticoids and antibiotics. But these recommendations rarely are supported by large clinical trials (*5*).

The use of EGFRIs in cancer therapy is very likely to expand, and oncologists should be familiar with the incidence, manifestion, possible mechanism and appropriate management of their associated a constellation of adverse effects. Here, we summarize the characteristics of commonly encountered skin toxicities associated with EGFR-inhibiting mAbs and TKIs among lung cancer and colorectal carcinoma patients, and provide recommendations for prophylaxis and treatment. When reviewed clinical study articles, priority was granted to the randomized clinical trials (RCT).

2. The common dermatological adverse events (dAEs) occurred in TKIs and mAbs

The main safety profiles of current clinical used EGFRIs are comparable between TKIs and mAbs, while the difference in incidence of each drug is observed. Evidence in EURTAC and CTONG0806 may further demonstrate the rash is more likely to occur in Eastern patients (all grades 80%, grade 3/4 13%) compared to western patients (all grades 42%, grade 3/4 0) (*6,7*).

2.1. *TKIs*

There are inherent differences in active and skin toxicities of the first-generation reversible TKIs, gefitinib, erlotinib and icotinib, the second-generation irreversible TKI, afatinib, and the third-generation TKI, osimertinib, who has activity in patients with T790M-negative acquired resistance (*8*). Dacomitinib is a novel second-generation, irreversible TKI, which showed potent EGFR signaling inhibition in experimental models, including first-generation TKI-resistant NSCLC cell lines (*9*).

In Table S1 (*http://www.biosciencetrends.com/action/getSupplementalData.php?ID=32*) (*1,11,44,48,101-116*), the review of gefitinib showed rash and pruritus were prominent, while Wo HM *et al*. reported dry skin, grade 3/4 rash, pruritus was significantly prominent in gefitinib groups than in other agent-based regimens (*10*). As for erlotinib, the skin toxicity occurred in more patients. The TITAN study not included in the table demonstrated erlotinib associated skin toxicity was in 52% patients, and grade 3/4 5% (*11*). In this review, icotinib involved significant CONVINCE and BRAIN study and the most dAEs were in mild grade. However, a cohort study of first-line icotinib treatment in 152 advanced NSCLC patients with mutated EGFR reported the main safety profiles that 43.4% and 5.9% patients appeared rash and paronychia (*12*). Rash (36.0%) was one of the most common afatinib-related dAEs, while only 0.3% rates of discontinuation due to rash provided the expanded access program (*13*). In LUX-Lung series trials, afatinib-related dAEs had higher rates in patients (*14*). Investigator assessed the osimertinib associated adverse events in the AURA Study Phase II Extension Component, showing rash was also predominant (*8*). Future safety analyses from AURA extension and AURA2 included clustered terms of rash (41%), dry skin (31%), and nail toxicity (25%) (*15*). The result of AURA3 presented that osimertinib did not share more incidence of skin toxicity than first-generation and second-generation TKI. In the phase 2 trial of dacomitinib, the most common all-grade treatment-related adverse events of dacomitinib were dermatitis acneiform in 78% patients, dry skin in 44% patients, and stomatitis in 40% patients (*16*). The phase 3 NCIC CTG BR.26 study in this review had similar results.

In Table S2 (*http://www.biosciencetrends.com/action/getSupplementalData.php?ID=32*) (*25,117-134*), the third-generation TKI seemed to induce less skin toxicity than other TKIs, while the second-generation TKI showed predominant incidence of dAEs and dose modification among TKIs (*17*). Grade 3/4 adverse events rate of afatinib was comparable to that of erlotinib but higher than that of gefitinib (*18*). As for first-generation TKI, skin toxicity most commonly occurred in erlotinib, followed by gefitinib, icotinib in terms of incidence and severity (*19*).

2.2. *EGFR-mAbs*

Panitumumab and cetuximab have been approved by the US Food and Drug Administration for the treatment of certain patients with mCRC to treat patients with wild-type RAS mCRC. Necitumumab is a second-generation recombinant human EGFR mAb to blocks ligand-induced receptor phosphorylation and downstream signaling.

The adverse events most frequently associated with EGFR TKIs are skin conditions, notably rash, pruritus, and as with the EGFR mAbs, it appeared to be associated with an increased risk of some forms of mucosal inflammation, notably stomatitis, when used in combination with chemotherapy except for rash (*20*). In Table S3 (*http://www.biosciencetrends.com/action/getSupplementalData.php?ID=32*) (*25,125-134*), the review also illustrated the skin toxicity profile: cetuximab

and panitumumab have comparable skin disorders, and necitumumab seem to induce less skin disorders. Rash is likely to occur, while pruritus and mucositis are less likely to be observed (*21*). Few patients had grade 3 skin-related toxicities (*22*). In phase I/II study of necitumumab, rash (70.5%), dry skin (18.2-67%), pruritus (11.4-60%), paronychia (36.4%) and grade ≥ 3 events, rash (20.5%) were observed (*23,24*). In SQUIRE study, rash (1.1%) led to necitumumab interruption (*25*).

Evidences showed that the overall incidence of skin toxicities for EGFR-MoAbs was 77.1% and high-grade (≥grade 3) occurred in 24.6%. Longer treatment with EGFR-MoAbs (≥ 5 months) was more likely to cause skin toxicity and rash than in the shorter duration (< 5 months) (*26*).

Compared with cetuximab, panitumumab was associated with less incidence of rash, pruritus, mucositis, while overall skin toxicity has a higher rate. However, a meta-analysis of different toxicity of cetuximab and panitumumab in mCRC treatment showed cetuximab was associated with fewer grade 3/4 skin toxicities, slightly more frequent grade 3/4 acne-like rash, and paronychia, but fewer cases of skin fissures and pruritus than panitumumab (*27*).

2.3. *Other EGFRIs under study*

Poziotinib, a second-generation EGFR-TKI in patients with lung adenocarcinoma with EGFR mutation was reported the most frequent grade 3 adverse events were rash (59%), mucosal inflammation (26%), and stomatitis (18%) in a phase II study (*28*). AC0010, a mutation-selective third-generation TKI, reported the incidence of skin rash was 48% in the treatment-emergent adverse events and grade 3 or higher was 4% in the first-in-human phase I trial (*29*). In BLOOM study of AZD3759 in EGFR-mutant NSCLC, grade 3 skin disorders occurred in 17% patients at a dose of 200 mg twice a day, and in 40% patients at a dose of 300 mg twice a day (*30*). The EGFR-MoAbs against the EGFRT790M resistance mutation under study, HM61713 and EGF816, also reported the skin toxicities (*31*).

3. The appearance of dAEs occurred in TKIs and mAbs

3.1. *Grading algorithm of skin toxicity*

The Common Terminology Criteria for Adverse Events version 4.03 (CTCAE v4.03) is a widely used classification system (*32*). The Multinational Association of Supportive Care in Cancer (MASCC) Skin Toxicity Study Group conducted a new grading system, which is specially proposed for EGFRIs-induced dAEs and maintains consistency with the grading principles CTCAE system. Moreover, MASCC grading algorithm includes relevant patient-reported health-related quality of life factors and is commonly used as well (*33*).

There have been concerted efforts to develop more precise and clinically relevant tools to quantify and monitor EGFRI-related skin toxicities, including the MASCC EGFRI Skin Toxicity Tool (MESTT) (*34*) and the EGFRI related Skin Toxicity Index (EGFRISTI) (*35*). However, the MESTT requires individual pustules to be counted, which is impractical in a busy clinic, and the EGFRISTI is again based on the surface area affected, whose score ranged from 6.0 to 64.5 (*36*). In addition, Wollenberg A *et al*. presented a new scoring tool for acneiform skin eruptions by calculating from body involvement, facial involvement and clinical grading of the skin items erythema, papulation, pustulation and scaling/crusts (*37*).

3.2. *The distribution and typical time course of skin appearance*

Rash is the earliest and most common cutaneous reaction. Braden RL *et al*. conducted a retrospective chart review on 157 patients with EGFRIs-induced skin reactions. Papulopustular eruption was observed at the average duration of 9.4 weeks, and eruption mostly involved in face with 97 % of patients affected, followed by the chest (75%) and back (61%). The abdomen (8%), upper extremity (8%), and lower extremity (4%) were less frequently observed. Bacterial skin infection accounted for 21% patients, in which the upper extremity (64%), lower extremity (52%), and abdomen (33%) were the most common infectious locations. The mean time to onset of the acneiform rash was 1.5 weeks after initiation of EGFRIs, while the mean time to onset of bacterial superinfection was 28.6 weeks (*38*). Xerosis generally occurs late, after the patient has been on anti-EGFR treatment for at least 30-60 days. This condition usually follows or accompanies by acneiform eruption and itch. Dry skin is also a cause of increased susceptibility to injuries and fissures, whose secondary causes include bacterial and viral infections. Deep painful fissures are most often seen in the area of fingertips, heels, periungual skin and dorsal surface of the interphalangeal joints (*39*). Pruritus often coexists with xerosis (50%) and papulopustular rash (62%), and also commonly accompanies rash at onset (*40*). Similarly, paronychia frequently accompanies papulopustular rash. It develops later on, usually 4-8 weeks after starting treatment (*41*). The lesions develop 2-5 months after the onset of treatment.

3.3. *Common appearances involved in anti-EGFR treatment*

Rash, xerosis, pruritus, nail changes, hair changes, mucositis are common skin toxicities involved in TKIs and mAbs, and in some extreme cases, severe cutaneous

Grade 1 **Grade 2** **Grade 3**

Grade 1: Papular and/or pustular lesions covering < 10% BSA, not associated with itching or pain.
Grade 2: Papular and/or pustular lesions covering 10-30% BSA; may cause pruritus, pain, and adverse psychosocial effects.
Grade 3: Papular and/or pustular lesions covering > 30% BSA; may cause pruritus, pain, and adverse psychosocial effects, secondary infection requiring oral antibiotic therapy, limiting self-care.

Figure 1. The different degrees of severity of the rash according to CTCAE v4.03. In grade 1, the rash only occurred on head and face dispersedly. In grade 2, papular lesions occurred on the patient's face and all his back with pain and pruritus. In grade 3, the head of the patient suffered secondary infection, and the face was swelling and red, which effected his daily life obviously. *Note*: No patients with grade 4/5 rash were observed. BSA = body surface area. The pictures were taken from 2014 to 2018.

adverse reactions (SCARs) may occur, while they specifically have some differences.

3.3.1. *Rash*

The eruption generally evolves through four distinct phases. The skin rash lesions can be manifested as 24% rash, 16% dermatitis acneiform, 7% rash maculopapular, 11% acne (*42*). At the first 1-2 weeks from initial treatment, rash occurred with dysesthesia, erythema and edema, then erythematous papules and pustules. Until 3-6 weeks purulent crusts appear, progressing to telangiectasias with pain and pruritus. Symptoms typically resolved within 4 weeks after EGFR TKI is ceased; but there could be partial or even complete resolution despite continued EGFR TKI therapy. The duration and severity of symptoms depend on the dose and kinds of EGFRIs, if properly managed, the symptoms may also self-relieve to some extent, even disappear. Complete disappearance of lesions but hyperpigmentation left is observed about one month after discontinuity of treatment. Sibaud V reported 4 patients presented an unusual presentation of acneiform rash, characterized by late development after several months of EGFRIs treatment, localization to the limbs with sparing of the face, and association with severe pruritus and Staphylococcus aureus superinfection in all cases (*43*). Seriously, skin exfoliation and toxic epidermal necrolysis are diagnosed (*44,45*). The different degrees of severity of the papulopustular rash are illustrated in Figure 1.

3.3.2. *Xerosis*

EGFRIs impair the epidermal barrier based on keratinocyte differentiation, causing shortage of water and abnormal oil production in the epidermis. Skin secondary infection may contribute to xerosis. The risk of skin dryness during treatment increases with age, pre-eczema, and prior cytotoxic use. Evidence showed patients who received gefitinib experienced xerosis cutis, acneiform have mean Transepidermal Water Loss values higher than normal (*46*). The different degrees of severity of the xerosis are illustrated in Figure 2.

3.3.3. *Pruritus*

Pruritus is an uncomfortable sensation leading to intensive scratching. Your skin looks dry and scaly. During treatment, generalized or localized itching is observed in arms, legs or body, ranging in strength from mild to severe pruritus. The severe condition shows the skin on the fingertips and heels crack. Dry mouth, eyes and nose also can be observed in the late. The different degrees of severity of the pruritus are illustrated in Figure 3.

3.3.4. *Nail changes*

Paronychia is the typical appearance of nail changes

Grade 1 **Grade 2** **Grade 3**

Grade 1: Covering < 10% BSA and no associated erythema or pruritus.
Grade 2: Covering 10-30% BSA and associated with erythema or pruritus; limiting instrumental ADL.
Grade 3: Covering > 30% BSA and associated with pruritis; limiting self-care ADL.

Figure 2. The different degrees of severity of the xerosis according to CTCAE v4.03. In grade 1, the calf of patient was exposed to xerosis without erythema or pruritus. When progressed to grade 2, all the limbs suffered from xerosis with rhagades and pruritus. In grade 3, the patient suffered from a wide range of xerosis and pruritus with obvious scratch. *Note*: ADL = activities of daily living; BSA = body surface area. The tags with words and time in the pictures represented as code names from their name acronyms and the time of collection.

Grade 1 **Grade 2** **Grade 3**

Grade 1: Moderately intensive, limited to a particular part of the body, requires topical treatment.
Grade 2: Increased local or periodically generalized, present lesions resulting from scratching, impairment of basic patient activity, requires systemic treatment.
Grade 3: Increased local or permanently generalized, significant limitation of selfcare activity or impairment of sleep, requires oral corticosteroids or immunosuppressive therapy.

Figure 3. The different degrees of severity of the pruritus according to CTCAE v4.03. In grade 1, pruritus only occurred in regional area of the leg with erythema. In grade 2, pruritus induced obvious scratch with hemorrhagic spot and hyperpigmentation. In grade 3, the scratch because of skin itch caused secondary infection and need systematic therapy. *Note*: The tags with words and time in the pictures represented as code names from their name acronyms and the time of collection.

usually with secondary inflammation, characterized by edema, redness, nail fold and severe pain in the area around the nail plate, even progression to onycholysis or onychodystrophy. The big toe is commonly the first area to be affected, and eventually one or more fingers and toes were involved (*47*). The different degrees of severity of the paronychia are illustrated in Figure 4.

Grade 1 **Grade 2** **Grade 3**

Grade 1: Nail fold edema or erythema; disruption of the cuticle.
Grade 2: Localized intervention indicated; oral intervention indicated (*e.g.*, antibiotic, antifungal, antiviral); nail fold edema or erythema with pain; associated with discharge or nail plate separation; limiting instrumental ADL.
Grade 3: Surgical intervention or intravenous antibiotics indicated; limiting self-care ADL.

Figure 4. The different degrees of severity of the paronychia according to CTCAE v4.03. In grade 1, the first picture showed mild edema and erythema of fingernails without limiting daily life. In grade 2, the edema erythema and bleeding occurred with intervention of antibiotic. In grade 3, the inflammation occurred around the fingernails and need surgery treatment. *Note*: The pictures were taken from 2014 to 2018.

3.3.5. *Hair changes*

Hair changes are characterized as the alterations in the hair structure, accompanied by curly hair, and thin, as well as a change in color. The typical manifestation is alopecia, reported in 1.9-4.9% of patients (*48*). Non-scarring hair loss is reversible, slow, and usually does not lead to complete baldness. Alopecia is not the only described changes to hair during EGFRIs use. A five-year review of spectrum of ocular toxicities from EGFRIs showed eyelash changes (trichomegaly and trichiasis) were also the commonly observed appearances

Figure 5. The appearance of eyelash changes. In these two pictures, the patients suffered from trichomegaly and trichiasis. The eyelash grew irregular and disturbed their sight. *Note*: The pictures were taken from 2014 to 2018. The tags with words and time in the pictures represented as code names from their name acronyms and the time of collection.

(*49*). Excessive hypertrichosis also included of the face (*50*). The appearance of eyelash change is presented in Figure 5.

3.3.6. *Mucositis*

EGFRIs result in a range of alterations in visible mucosal tissues, mainly in oral cavity. Patients may suffer from mild red and swollen to severe ulceration and pain, which lead to discomfort and influence eating and drinking (*34*).

3.3.7. *SCARs*

There have been a substantial number of reports concerning life-threatening SCARs, including Stevens-Johnson syndrome (SJS), toxic epidermal necrolysis (TEN), drug rash with eosinophilia and systemic symptoms, drug-induced hypersensitivity syndrome, and acute generalized exanthematous pustulosis. Literature review showed a total of 12 patients suffered from SCAR episodes: two SJS caused by afatinib, one SJS, one SJS/TEN and two TEN (one death) caused by cetuximab, one SJS caused by erlotinib, two TEN (one death) and two acute generalized exanthematous pustulosis caused by gefitinib, one SJS caused by panitumumab (*51*).

4. The possible mechanism of dAEs

The skin toxicity due to EGFRI is not yet fully understood. Evidences demonstrated the skin reactions may be illustrated from point of pathogensis, signal molecule, polymorphism, and pharmacokinetics.

4.1. *Pathogenesis and molecular biomarkers*

Biomarkers of skin toxicity induced by anti-EGFR treatment mainly include three major signalling outputs, namely RAS/RAF/MEK/ERK with the function of cell proliferation, cell cycle and cell migration and on the expression of inflammatory mediators, JAK/STAT pathway reaction to proliferative response, protection from apoptosis and PI3K/Akt pathway governing survival responses (*52*). Lacouture ME firstly systematically reviewed the underlying pathobiological mechanism of EGFRIs-associated skin reactions based on previous experimental and clinical data (*53*). Then Paul *et al*. explored the changes of signal molecules among cancer patients (*54*). The chemokine expression in keratinocytes further illustrated skin inflammation mechanism when treated with EGFRIs (*55*).

In general, the molecular mechanism is the following aspects: a. EGFRIs inhibit the PI3K-Akt and MAPK pathways, contributing to the inhibition of keratinocyte growth and survival; b. EGFRIs has an inhibitory effect on differentiation of keratinocyte by interfering in the expression of signal molecular, such as keratin 1 (KRT1), KRT10, ASK1, STAT3 BCL2 and BCL-XL; c. EGFRIs change the function of attachment and migration by the up-regulation or down-regulation of related proteins. d. EGFRIs induced the release of chemokines and cytokines, CCL2, CCL5, CXCL10, CCL18, XCL1, CXCL9 (CXC chemokine ligand 9), CCL3, NFκB, IL6, IL7, and IFN regulatory factor 5, which developed inflammation. e. EGFRIs damage the protection function of skin from ultraviolet radiation. Consequently, the effects of proinflammatory chemokines in the epidermis lead to inflammation.

The abnormal signal processes accordingly lead to pathological changes. The EGFR is known to be expressed in skin keratinocytes, the sebaceous glands, hair follicle epithelium, and periungual tissue (*56*). EGFR inhibition leads to dysfunction of keratinocyte migration, maturation, and proliferation, resulting in inflammatory cell recruitment and cutaneous injury (*53*). Release of pro-inflammatory cytokines contributes to ubsequent tissue damage and apoptosis (*55*). EGFRIs associated skin lesions are formed owing to secondary bacterial infections and other complications as well (*57*). The possible pathogenesis of pruritus may involve cutaneous nerve endings, unmyelinated C-fibers, and neurotransmitters or regulation of various receptors, included serotonin, neurokinin (NK)-1 receptor, opioid receptors, and gammaaminobutyric acid (GABA). Mast cell degranulation and maturation may be the important activation way (*58*).

4.2. *Gene polymorphisms*

Pharmacogenomic analyses of EGFR polymorphisms and several genomic mutations have been undertaken to determine their predictive value in the development of skin toxicity after anti-EGFR treatment (Table S4, *http://www.biosciencetrends.com/action/getSupplementalData.php?ID=32*) (*135-141*)). From the literatures review, molecular markers of EGFR polymorphisms can

predict skin toxicity, and also has association with the efficacy of the anti-cancer. Unfortunately, these studies are sporadic and have not been validated by larger and further research to reveal the occurrence mechanism and clinical biomarkers.

4.3. *Pharmacokinetics*

Concentration of HGF might be significantly inversely correlated with severity of rash. Increased HGF/MET signaling might compensate the inhibitory effect of EGFRIs in skin as well as tumor cells, leading to less severe skin rash and decreased efficacy of the anti-tumor therapy (*59*). Kimura K *et al*. used the average binding occupancies (Phi ss) of EGFR-TKIs, gefitinib and erlotinib to evaluate frequency of rash (*60*). Vasavda C *et al*. found gefitinib, erlotinib, osimertinib had responsible proteins by reverse phase protein arrays among 301 proteins associated with EGFR signaling. These three EGFRIs equally suppressed phosphorylation of 12 proteins, while they respectively regulated phosphorylation of 13 other proteins, such as 4E-BP1 and eIF4E. Gefitinib most potently inhibited the 13 proteins, whereas osimertinib blocked fewer, and erlotinib even fewer. Osimertinib also independently resulted in phosphorylation of histone H2AX, suggesting that osimertinib may promote double-strand DNA breaks. These differences may explain why patients treated with different inhibitors experience differing dermatologic effects (*61*). Erlotinib concentration was also associated with occurrence and severity of skin rash (*62*). Accordingly, the proteins identified as differentially regulated by these inhibitors may be candidates for evaluating the mechanisms underlying their dermatologic toxicities.

Raman spectroscopy is novel method to distinguish the patients with or without skin toxicity by correlating the skin patients Raman signature and the drugs concentration into patient's blood. Raman spectroscopy can be a pharmacodynamic biomarker for EGFRIs-related adverse reactions (*63*).

5. Management

EGFRIs treatment associated dAEs has caused a substantial economic burden and lower quality of life (*64*). Hence, it is essential to establish appropriate strategies, including prophylactic treatment, reactive treatment, dose reductions and drug discontinuance, to deal with skin toxicity, especially the management does not compromise anti-cancer efficacy. At present, recommendations are almost based on expert opinion and consensus, which large randomized clinical trials are insufficient. The existing guidelines include CTCAEv4.0 suggestions for interventions (*65*), MASCC Skin Toxicity Study Group Clinical Practice Guidelines (*66*), NCCN dermatologic toxicities management guidelines (*5*), disciplinary therapeutic algorithm from various areas (*67-70*). The management treatment options for dAEs mainly consist of topical moisturizers or corticosteroid creams for mild reactions or systemic treatments of antibiotics and corticosteroids. Supportive care, such as prevention from sun exposure, comfortable clothes and shoes, non-irritating bath products are recommended. (Table S5, *http://www.biosciencetrends.com/action/getSupplementalData.php?ID=32*) (*142-159*))

5.1. *Patient education*

Patient and doctor education are fundamental to treatment. The explanation of the care strategies and symptoms management are especially important. The oncologists and dermatologists should provide patients with specific instructions on when to ask for medical attention to manage the skin reactions and give appropriate advice on basic dermatologic care, such as maintaining cleanliness, moisturisation, and prevention from stimuli. In general, patients should recognize and early evaluate the signs and symptoms of EGFRIs-associated dAEs. They should be instructed to realize the risk of skin infection, avoid scratching and sun, protect arms and legs from extreme heat or cold, and wear loose cotton clothing and shoes (*71*).

5.2. *Rash*

Lacouture *et al*. recommended topical and systemic treatment for EGFRIs-induced rash according to the severity of rash (*66*). Dose modification is unnecessary for grade one. Apply low to mid potency topical steroids such as hydrocortisone, betamethasone dipropionate and antibiotics such as clindamycin, gentamicin externally daily until rash resolution. As for grade two, oral antibiotics, for example doxycycline or minocycline 100 mg twice a day, are applied until rash eases except for recommendations of grade one. Dose reduction is essential for grade three, as well as the recommendations of grade two. The grade four rash would lead to treatment discontinuity and be managed refer to grade three.

Pophylactic treatment of EGFRIs-related rashes, oral antibiotics and steroid creams, is more effective than reactive treatment, which does not compromise survival (*72*). Doxycycline and tetracycline appear to be a favorable option in rash with safety profile either prophylactic treatment or reactive treatment (*70*). Case reports of topical recombinant human EGF or topical vitamin K cream resulting in a reduction of rash grade within a few weeks are very promising. Vitamin K3 (menadione), a synthetic pro-drug of vitamin K, has been suggested to be able to re-phosphorylate EGFR-even during treatment with EGFR-inhibitors (*73*) (Table S5, *http://www.biosciencetrends.com/action/getSupplementalData.php?ID=32*) (*142-159*)).

5.3. *Pruritus*

Pruritus intervention can be challenging. The prevention of scratching is the first management strategy for patient, which may induce secondary infections. The mechanism of EGFRIs-associated pruritus has not yet been explained. In general, the classical mediators, such as histamine and neurotransmitters, are chosen as the target to provide symptom relief (*74*). Emollients or moisturizing creams are recommended if pruritus is caused by skin xerosis. Topical and systematic glucocorticosteroids are recommended for moderate and severe pruritus. Besides, gabapentin and pregabalin, doxepin also reported as candidates (*65*). Recently, aprepitant, a neurokinin-1 receptor antagonist was demonstrated to reduce pruritus caused by erlotinib, which may imply substance P is one of key itch-induced neurotransmitters (*75*).

5.4. *Xerosis*

Staying hydrated is the key to preventing xerosis. Xerosis rarely lead to dose changes of EGFRIs. Patients should be encouraged to adopt emollients without irritants. If hyperkeratotic skin appeared, exfoliants and urea cream can be used. Other management includes steroid creams, salicylic acid, zinc oxide (*76*).

5.5. *Nail changes*

Paronychia is the most commonly appearance of nail changes. Lacouture *et al*. recommend prevention of paronychia by comfortable footwear, avoiding irritants and treatment of topical corticosteroids or calcineurin inhibitors, systemic tetracyclines if diagnosed infection (*76*). A series of cases of nail changes from cetuximab, panitumumab, erlotinib showed the topical povidone-iodine/dimethyl sufoxide solution described is very effective in alleviating the signs and symptoms. There was a total of 25 nails affected in the case series, and 21/25 (84%) resolved overall. The culture results suggested the microorganisms included Staphylcoccus aureus, Pseudomonas, T. mentagrophytes, Streptococcal pyogenes, Trichophyton mentagrophytes (*77*).

5.6. *Hair changes*

The EGFRIs-associated hair changes mainly manifest as trichomegaly and alopecia. Abnormal trichomegaly may be treated with temporary or permanent hair removal (*66*). Alopecia generally resolves after target drugs discontinuation.

5.7. *Mucositis*

Oral mucositis is the prominent factor that affects the daily life of patient. The principles of treating stomatitis are oral care, pain management, maintaining oral function, oral complications control, and the quality of life improvement (*78*). The prevention approaches include soft tooth brushing, frequent mouse and teeth clean and avoiding alcohol and tobacco products (*79*). The treatment recommendations of EGFRIs-associated mucositis in expert consensus and ESMO guideline are as follows (*76,80*).

5.8. *Traditional Chinese medicines (TCM) and Japanese kampo for skin toxicity*

There is only one study, none for TCM, on the effects of Japanese kampo on EGFRIs-related rash in English. Still, a few reports are designed to observe proved prescriptions on EGFRIs-associated dAEs in China (Table S6, *http://www.biosciencetrends.com/action/getSupplementalData.php?ID=32*) (*82-87*)). We conducted a meta-analysis to evaluate the effect of TCM on EGFRIs-induced rash, suggesting that TCM could significantly relieve EGFRIs induced rash and symptoms and improve patients' quality of life (*81*).

5.8.1. *Japanese kampo*

Ichiki M (*82*) studied Japanese kampo on afatinib-induced rash, diarrhea, and oral mucositis with prophylactic use of minocycline and TJ-14 in Japan. The result showed TJ-14 mainly reduced the risk of diarrhea rather than skin toxicity compared with minocycline. Therefore, the effect of Japanese kampo for EGFRIs-associated dAEs seems to be absence of evidence.

5.8.2. *TCM herbs*

TCM herbs are used on the foundation of TCM theory. The EGFRIs-associated dAEs belongs to the category of “drug toxicity”. The pathogenesis is that wind, dampness and heat invade lung on the foundation of deficiency. The basic principle of treatment is dispelling wind and dampness to promote eruption and itch, clearing heat-toxin and cooling blood, nourishing yin and blood and moistening dryness. In TCM, couplet medicines are the commonly used prescribing method, which was also applied for the skin toxicity. Herba Schizonepetae (Jing jie) and Radix Saposhnikoviae (Fang feng) are combined to dispel wind to promote eruption. Flos Lonicerae (Jin yin hua) and Fructus Forsythiae (Lian qiao) are combined to clear heat-toxin. Cortex Moutan Radicis (Mu dan pi) and Radix Paeoniae Rubra (Chi shao) are combined to clear heat and cool blood. Herba Taraxaci (Pu gong ying) is also used to remove toxin for detumescence in the condition of secondary infection. Cortex Dictamni (Bai xian pi), and Radix Sophorae Flavescentis (Ku shen) are adopted to promote diuresis and itch if pruritus is the cardinal symptom.

5.8.3. *TCM formula*

TCM formula mainly included external or oral decoction, and another study involving the combination of auricular acupuncture. The basic formulas included Xiaofeng powder (from Waike Zhengzong), Jingfang Baidu powder (from Shesheng Zhong miao Fang), Siwu decoction (from Xianshou Lishang Xuduan Mifang), Wuwei Xiaodu drink (from Yizong Jinjian). The auricular acupuncture chosen was to regulate qi and blood, balance yin and yang, improve immunity and defense against tumor.

Xu JX *et al*. studied oral and external Jingfang Baidu San Jiawei combined with auricular acupuncture on EGFRIs-related dAEs, which confirmed that TCM could lower the incidence and grade of skin toxicity, improve quality of life (QoL) as well (*83*). Zhao ZW *et al*. recommended oral Siwu Xiaofeng San to treat gefitinib-related rash. All the patients treated with TCM had therapeutic effect and the rash discontinuation rate in treatment group was lower than the control group (*84*). Similarly, the efficacy of Xiaozhen San was also verified by Zhang PY *et al*. (*85*). In Sun T *et al*. researched the efficacy of oral Yangfei Xiaozhen Tang, suggesting that TCM had an advantage in effective rate, recovery rate of TCM syndromes and QoL improvement (*86*). Peng YM *et al*. conducted a trial to confirm the effect of external Zhiyang Pingfu Lotion. The result showed that the effective rates of TCM in the treatment of rash, cutaneous pruritus, xerosis cutis and nail changes were higher than that of the standard treatment group (*87*).

However, the efficacy of TCM and Japanese kampo for skin toxicity based on present studies may not draw a definitive conclusion because of the poor methodological quality and further large clinical trials are needed to confirm results (*88*).

6. Skin toxicity, clinical outcomes, QoL

Series of studies have confirmed that the occurrence and the severity of dAEs are related to better anti-cancer efficacy and survival benefits (*89*), however, the dAEs are also involved in with lower QoL and higher financial burden (*90*), especially for serious skin reactions. The identical standard of tools used to measure QoL of patients with EGFRIs treatment is actually unclear.

6.1. *The association of dAEs and response rates*

As we known, numerous studies have varied the association between skin toxicity caused by EGFRIs and clinical outcomes. Recently, retrospective analyses further showed that skin toxicity might be a positive indicative of EGFRIs for lung cancer and mCRC. Grade 2 or higher skin rash of afatinib might be a useful marker for long-term efficacy (*91*). Erlotinib-associated rash may be a valuable biomarker for the prediction of clinical response and overall survival (OS) in advanced NSCLC patients (*92*). Patients treated with cetuximab also showed that early skin toxicity suggested significantly longer OS and higher skin toxicity grades indicated longer PFS (*93*).

6.2. *QoL evaluation algorithm*

The Dermatologic toxicity of EGFRIs may affect the physical, emotional, and social well-being, which suggests the potential to severely influence patients' QoL (*94*). No uniform evaluation standard for QoL is provided and researchers recommend some useful tools, such as dermatology-specific quality-of-life questionnaire (Skindex-16) (*95*) and the EGFRI-specific Functional Assessment of Cancer Therapy Questionnaire-EGFRI (FACT-EGFRI-18) (*96*).

Skindex-16 is a general instrument to be used in skin disorders, including acne and psoriasis. Although it is not specific for EGFRIs-associated skin toxicity, its item content focused on multidimensional evaluation of skin disorders and related ease of management, making it a feasible measure. In a subsequent study using Skindex-16 to evaluate the QoL of EGFRIs-associated skin toxicity found that the rash grade in CTCAE system was significantly connected with Skindex-16 scores (*97*). Using Skindex-16 to evaluate patients' QoL with EGFRIs therapy including symptoms, emotion, and function, Rosen *et al*. found higher scores across all 3 domains in patients who experienced rash or pruritus than those not experience these skin reactions (*98*).

The FACT-EGFRI-18, an 18-item patient questionnaire, assesses the influence of EGFRIs-related skin, nail, and hair toxicities on physical, emotional, social, and functional impact, which proved useful to clinicians and researchers in prevention protocol and clinical study. In Dutch practice, the FACT-EGFRI-18 was identified as an appropriate measurement for dAEs-related QoL (*99*).

In addition, a valid instrument, Eruption Scoring System (ESS), was introduced for cetuximab-related dAEs, which covered evaluation of the consequences of skin toxicity on the QoL, similar to FACT-EGFRI-18 and the severity of dermatological toxicity induced by cetuximab, compared with the standard CTCAE system (*100*).

7. Conclusion

It is no doubt that EGFRIs prolong the survival time of lung cancer and mCRC patients. The dAEs is potentially should be taken into consideration by oncologists and dermatologists when taking the implementation of such target strategies. Just as Tischer B *et al*. promoted, these four missing information should be addressed in further study: patient's voice, the communication between physician and patient regarding dAEs, acceptance

of skin toxicities compared with other AEs, and the balance of the risk of skin toxicities and the efficacy of the therapy (*3*).

Recognizing EGFRIs induced dAEs and understanding possible mechanism, then correct evaluating skin toxicity and choosing proper treatment for practitioners and patients are critical. We systematically reviewed the recent literatures of dAEs associated with the most frequently used EGFRIs in lung cancer and mCRC, including the frequency of occurrence, clinical appearance, methods of grading, underlining mechanisms, algorithm of management and the association of skin toxicity, clinical outcomes, quality of life. Our goal is to provide an adequate decision regarding treatment dose or discontinuation, impacting therapeutic efficacy and patient survival when dAEs occur, contributing better use of target drugs.

Acknowledgements

This project was supported by Capital's funds for health improvement and research (2018-2-4065). We sincerely thank patients from outpatient from 2014 to 2018 for providing their pictures.

References

1. Mok TS, Wu YL, Thongprasert s, *et al*. Gefitinib or Carboplatin-Paclitaxel in Pulmonary Adenocarcinoma. N Engl J Med. 2009; 361:947-957.
2. National Comprehensive Cancer Network. Clinical Practice Guidelines in Oncology: Head and Neck Cancers. *https://www.nccn.org/professionals/physician_gls/default.aspx* (accessed September 14, 2018).
3. Tischer B, Huber R, Kraemer M, Lacouture ME. Dermatologic events from EGFR inhibitors: The issue of the missing patient voice. Support Care Cancer, 2017; 25:651-660.
4. Patil VM, Noronha V, Joshi A, *et al*. Phase III study of gefitinib or pemetrexed with carboplatin in EGFR-mutated advanced lung adenocarcinoma. ESMO Open. 2017; 2:e000168.
5. Burtness B, Anadkat M, Basti S, Hughes M, Lacouture ME, McClure JS, Myskowski PL, Paul J, Perlis CS, Saltz L, Spencer S. NCCN Task Force Report: Management of Dermatologic and Other Toxicities Associated With EGFR Inhibition in Patients With Cancer. J Natl Compr Canc Netw. 2009; 71:S5-S21.
6. Rosell R, Carcereny E, Gervais R, *et al*. Erlotinib versus standard chemotherapy as first-line treatment for European patients with advanced EGFR mutation-positive non-small-cell lung cancer (EURTAC): A multicentre, open-label, randomised phase 3 trial. Lancet Oncol. 2012; 13:239-246.
7. Zhou Q, Cheng Y, Yang JJ, *et al*. Pemetrexed versus gefitinib as a second-line treatment in advanced nonsquamous nonsmall-cell lung cancer patients harboring wild-type EGFR (CTONG0806): A multicenter randomized trial. Ann Oncol. 2014; 25:2385-2391.
8. Yang JC, Ahn MJ, Kim DW, *et al*. Osimertinib in Pretreated T790M-Positive Advanced Non-Small-Cell Lung Cancer: AURA Study Phase II Extension Component. J Clin Oncol. 2017; 35:1288-1296.
9. Zugazagoitia J, Díaz A, Jimenez E, Nuñez JA, Iglesias L, Ponce-Aix S, Paz-Ares L. Second-line Treatment of Non-Small Cell Lung Cancer: Focus on the Clinical Development of Dacomitinib. Front Med (Lausanne). 2017; 4:36.
10. Wo HM, He J, Zhao Y, Yu H, Chen F, Yi HG. The Efficacy and Toxicity of Gefitinib in Treating Non-small Cell Lung Cancer: A Meta-analysis of 19 Randomized Clinical Trials. J Cancer. 2018; 9:1455-1465.
11. Ciuleanu T, Stelmakh L, Cicenas S, Miliauskas S, Grigorescu AC, Hillenbach C, Johannsdottir HK, Klughammer B, Gonzalez EE. Efficacy and safety of erlotinib versus chemotherapy in second-line treatment of patients with advanced, non-small-cell lung cancer with poor prognosis (TITAN): A randomised multicentre, open-label, phase 3 study. Lancet Oncol. 2012; 13:300-308.
12. Huang AM, Shen Q, Yu XL, Wang HM, Shi CL, Han BH, Gu AQ. Efficacy, safety and prognostic factors analysis of first-line icotinib treatment in advanced non-small cell lung cancer patients with mutated EGFR. Transl Cancer Res. 2018; 7:600-608.
13. Kim ES, Halmos B, Kohut IF, Patel T, Rostorfer RD, Spira AI, Cseh A, McKay J, Wallenstein G, Mileham KF. Efficacy and safety results of the afatinib expanded access program. Oncol Ther. 2017; 5:103-110.
14. Yang JC, Wu YL, Schuler M, *et al*. Afatinib versus cisplatin-based chemotherapy for EGFR mutation-positive lung adenocarcinoma (LUX-Lung 3 and LUX-Lung 6): Analysis of overall survival data from two randomised, phase 3 trials. Lancet Oncol. 2015; 16:141-151.
15. Khozin S, Weinstock C, Blumenthal GM, Cheng J, He K, Zhuang L, Zhao H, Charlab R, Fan I, Keegan P, Pazdur R. Osimertinib for the Treatment of Metastatic EGFR T790M Mutation-Positive Non-Small Cell Lung Cancer. Clin Cancer Res. 2017; 23:2131-2135.
16. Jänne PA, Ou SH, Kim DW, Oxnard GR, Martins R, Kris MG, Dunphy F, Nishio M, O'Connell J, Paweletz C, Taylor I, Zhang H, Goldberg Z, Mok T. Dacomitinib as first-line treatment in patients with clinically or molecularly selected advanced non-small-cell lung cancer: A multicentre, open-label, phase 2 trial. Lancet Oncol. 2014; 15:1433-1441.
17. Ding PN, Lord SJ, Gebski V, Links M, Bray V, Gralla RJ, Yang JC, Lee CK. Risk of Treatment-Related Toxicities from EGFR Tyrosine Kinase Inhibitors: A Meta-analysis of Clinical Trials of Gefitinib, Erlotinib, and Afatinib in Advanced EGFR-Mutated Non-Small Cell Lung Cancer. J Thorac Oncol. 2017; 12:633-643.
18. Yang Z, Hackshaw A, Feng Q, Fu X, Zhang Y, Mao C, Tang J. Comparison of gefitinib, erlotinib and afatinib in non-small cell lung cancer: A meta-analysis. Int J Cancer. 2017; 140:2805-2819.
19. Chu CY, Choi J, Eaby-Sandy B, Langer CJ, Lacouture ME. Osimertinib: A Novel Dermatologic Adverse Event Profile in Patients with Lung Cancer. Oncologist. 2018; 23:891-899.
20. Hofheinz RD, Segaert S, Safont MJ, Demonty G, Prenen H. Management of adverse events during treatment of gastrointestinal cancers with epidermal growth factor inhibitors. Crit Rev Oncol Hematol. 2017; 114:102-113.
21. Venook AP, Niedzwiecki D, Lenz HJ, *et al*. Effect of First-Line Chemotherapy Combined With Cetuximab or

Bevacizumab on Overall Survival in Patients With KRAS Wild-Type Advanced or Metastatic Colorectal Cancer: A Randomized Clinical Trial. JAMA. 2017; 317:2392-2401.
22. Lacouture ME, Anadkat M, Jatoi A, Garawin T, Bohac C, Mitchell E. Dermatologic Toxicity Occurring During Anti-EGFR Monoclonal Inhibitor Therapy in Patients With Metastatic Colorectal Cancer: A Systematic Review. Clin Colorectal Cancer. 2018; 17:85-96.
23. Tamura Y, Nokihara H, Honda K, Tanabe Y, Asahina H, Yamada Y, Enatsu S, Kurek R, Yamamoto N, Tamura T. Phase I study of the second-generation, recombinant, human EGFR antibody necitumumab in Japanese patients with advanced solid tumors. Cancer Chemother Pharmacol. 2016; 78:995-1002.
24. Elez E, Hendlisz A, Delaunoit T, Sastre J, Cervantes A, Varea R, Chao G, Wallin J, Tabernero J. Phase II study of necitumumab plus modified FOLFOX6 as first-line treatment in patients with locally advanced or metastatic colorectal cancer. Br J Cancer. 2016; 114:372-380.
25. Paz-Ares L, Socinski MA, Shahidi J, Hozak RR, Soldatenkova V, Kurek R, Varella-Garcia M, Thatcher N, Hirsch FR. Correlation of EGFR-expression with safety and efficacy outcomes in SQUIRE: A randomized, multicenter, open-label, phase III study of gemcitabine-cisplatin plus necitumumab versus gemcitabine-cisplatin alone in the first-line treatment of patients with stage IV squamous non-small-cell lung cancer. Ann Oncol. 2016; 27:1573-1579.
26. Li J, Yan H. Skin toxicity with anti-EGFR monoclonal antibody in cancer patients: A meta-analysis of 65 randomized controlled trials. Cancer Chemother Pharmacol. 2018; 82:571-583.
27. Petrelli F, Ardito R, Ghidini A, Zaniboni A, Ghidini M, Barni S, Tomasello G, Different Toxicity of Cetuximab and Panitumumab in Metastatic Colorectal Cancer Treatment: A Systematic Review and Meta-Analysis. Oncology. 2018; 94:191-199.
28. Han JY, Lee KH, Kim SW, Min YJ, Cho E, Lee Y, Lee SH, Kim HY, Lee GK, Nam BH, Han H, Jung J, Lee JS. A Phase II Study of Poziotinib in Patients with Epidermal Growth Factor Receptor (EGFR)-Mutant Lung Adenocarcinoma Who Have Acquired Resistance to EGFR Tyrosine Kinase Inhibitors. Cancer Res Treat. 2017; 49:10-19.
29. Ma Y, Zheng X, Zhao H, Fang W, Zhang Y, Ge J, Wang L, Wang W, Jiang J, Chuai S, Zhang Z, Xu W, Xu X, Hu P, Zhang L. First-in-Human Phase I Study of AC0010, a Mutant-Selective EGFR Inhibitor in Non-Small Cell Lung Cancer: Safety, Efficacy, and Potential Mechanism of Resistance. J Thorac Oncol. 2018; 13:968-977.
30. Ahn MJ, Kim DW, Cho BC, *et al*. Activity and safety of AZD3759 in EGFR-mutant non-small-cell lung cancer with CNS metastases (BLOOM): A phase 1, open-label, dose-escalation and dose-expansion study. Lancet Respir Med. 2017; 5:891-902.
31. Tran PN, Klempner SJ. Profile of rociletinib and its potential in the treatment of non-small-cell lung cancer. Lung Cancer (Auckl). 2016; 7:91-97.
32. Chen AP, Setser A, Anadkat MJ, Cotliar J, Olsen EA, Garden BC, Lacouture ME. Grading dermatologic adverse events of cancer treatments: The Common Terminology Criteria for Adverse Events Version 4.0. J Am Acad Dermatol. 2012; 67:1025-1039.
33. Lacouture ME, Maitland ML, Segaert S, *et al*. A proposed EGFR inhibitor dermatologic adverse event-specific grading scale from the MASCC skin toxicity study group. Support Care Cancer. 2010; 18:509-522.
34. MASCC. EGFR Inhibitor Skin Toxicity Tool (MESTT). *http://www.mascc.org/MESTT* (accessed September 14, 2018).
35. Lisi P, Bellini V, Bianchi L. The epidermal growth factor receptor inhibitor-related Skin Toxicity Index (EGFRISTI): A new tool for grading and managing skin adverse reactions to epidermal growth factor receptor inhibitors. Oncology. 2014; 87:311-319.
36. Chan A, Tan EH. How well does the MESTT correlate with CTCAE scale for the grading of dermatological toxicities associated with oral tyrosine kinase inhibitors? Support Care Cancer. 2011; 19:1667-1674.
37. Wollenberg A, Moosmann N, Klein E, Katzer K. A tool for scoring of acneiform skin eruptions induced by EGF receptor inhibition. Exp Dermatol. 2008; 17:790-792.
38. Braden RL, Anadkat MJ. EGFR inhibitor-induced skin reactions: Differentiating acneiform rash from superimposed bacterial infections. Support Care Cancer. 2016; 24:3943-3950.
39. Clabbers JMK, Boers-Doets CB, Gelderblom H, Stijnen T, Lacouture, ME, van der Hoeven KJM, Kaptein AA. Xerosis and pruritus as major EGFRI-associated adverse events. Support Care Cancer. 2016; 24:513-521.
40. Wu J, Lacouture ME. Pruritus Associated with Targeted Anticancer Therapies and Their Management. Dermatol Clin. 2018; 36:315-324.
41. Fischer A, Rosen AC, Ensslin CJ, Wu S, Lacouture ME. Pruritus to anticancer agents targeting the EGFR, BRAF, and CTLA-4. Dermatol Ther. 2013; 26:135-148.
42. Natale RB, Bodkin D, Govindan R, Sleckman BG, Rizvi NA, Capó A, Germonpré P, Eberhardt WE, Stockman PK, Kennedy SJ, Ranson M. Vandetanib Versus Gefitinib in Patients With Advanced Non-Small-Cell Lung Cancer: Results From a Two-Part, Double-Blind, Randomized Phase II Study. J Clin Oncol. 2009; 27:2523-2529.
43. Sibaud V, Tournier E, Roché H, Del Giudice P, Delord JP, Hubiche T. Late epidermal growth factor receptor inhibitor-related papulopustular rash: A distinct clinical entity. Clin Exp Dermatol. 2016; 41:34-37.
44. Zhang L, Ma S, Song X, *et al*. Gefitinib versus placebo as maintenance therapy in patients with locally advanced or metastatic non-small-cell lung cancer (INFORM; C-TONG 0804): A multicentre, double-blind randomised phase 3 trial. Lancet Oncol. 2012; 13:466-475.
45. Wang J, Cheng X, Lu Y, Zhou B. A case report of toxic epidermal necrolysis associated with AZD-9291. Drug Des Devel Ther. 2018; 12:2163-2167.
46. Chandra F, Chandra F, Sandiono D, Sugiri U, Suwarsa O, Gunawan H. Cutaneous Side Effects and Transepidermal Water Loss To Gefitinib: A Study of 11 Patients. Dermatol Ther (Heidelb). 2017; 7:133-141.
47. Goto H, Yoshikawa S, Mori K, Otsuka M, Omodaka T, Yoshimi K, Yoshida Y, Yamamoto O, Kiyohara Y. Effective treatments for paronychia caused by oncology pharmacotherapy. J Dermatol. 2016; 43:670-673.
48. Scagliotti GV, Shuster D, Orlov S, von Pawel J, Shepherd FA, Ross JS, Wang Q, Schwartz B, Akerley W. Tivantinib in Combination with Erlotinib versus Erlotinib Alone for EGFR-Mutant NSCLC: An Exploratory Analysis of the Phase 3 MARQUEE Study. J Thorac Oncol. 2018; 13:849-854.
49. Borkar DS, Lacouture ME, Basti S. Spectrum of ocular toxicities from epidermal growth factor receptor inhibitors

and their intermediate-term follow-up: A five-year review. Support Care Cancer. 2013; 21:1167-1174.
50. Zheng H, Zhang H, Zhang T, Wang Q, Hu F, Li B. Trichomegaly and scalp hair changes following treatment with erlotinib in pulmonary adenocarcinoma patients: A case report and literature review. Exp Ther Med. 2016; 12:1287-1292.
51. Chen CB, Wu MY, Ng CY, Lu CW, Wu J, Kao PH, Yang CK, Peng MT, Huang CY, Chang WC, Hui RC, Yang CH, Yang SF, Chung WH, Su SC. Severe cutaneous adverse reactions induced by targeted anticancer therapies and immunotherapies. Cancer Manag Res. 2018; 10:1259-1273.
52. Pastore S, Lulli D, Girolomoni G. Epidermal growth factor receptor signalling in keratinocyte biology: Implications for skin toxicity of tyrosine kinase inhibitors. Arch Toxicol. 2014; 88:1189-1203.
53. Lacouture ME. Mechanisms of cutaneous toxicities to EGFR inhibitors. Nat Rev Cancer. 2006; 6:803-812
54. Paul T, Schumann C, Rüdiger S, Boeck S, Heinemann V, Kächele V, Steffens M, Scholl C, Hichert V, Seufferlein T, Stingl JC. Cytokine regulation by epidermal growth factor receptor inhibitors and epidermal growth factor receptor inhibitor associated skin toxicity in cancer patients. Eur J Cancer. 2014; 50:1855-1863.
55. Mascia F, Mariani V, Girolomoni G, Pastore S. Blockade of the EGF receptor induces a deranged chemokine expression in keratinocytes leading to enhanced skin inflammation. Am J Pathol. 2003; 163:303-312.
56. Nanney LB, Stoscheck CM, King LE Jr, Underwood RA, Holbrook KA. Immunolocalization of epidermal growth factor receptors in normal developing human skin. J Invest Dermatol. 1990; 94:742-748.
57. Abdullah SE, Haigentz M Jr, Piperd B. Dermatologic toxicities from monoclonal-antibodies and tyrosine kinase inhibitors against EGFR: Pathophysiology and management. Chemother Res Pract. 2012; 2012:351210.
58. Munoz M, Covenas R. Involvement of substance P and the NK-1 receptor in human pathology. Amino Acids. 2014; 46:1727-1750.
59. Hichert V, Scholl C, Steffens M, Paul T, Schumann C, Rüdiger S, Boeck S, Heinemann V, Kächele V, Seufferlein T, Stingl J. Predictive blood plasma biomarkers for EGFR inhibitor-induced skin rash. Oncotarget, 2017; 8:35193-35204.
60. Kimura K, Takayanagi R, Fukushima T, Yamada Y. Theoretical method for evaluation of therapeutic effects and adverse effects of epidermal growth factor receptor tyrosine kinase inhibitors in clinical treatment. Med Oncol, 2017; 34:178.
61. Vasavda C, Kwatra MM, Kwatra, SG. Phospho-proteomic profiling reveals distinct signaling pathways by first and third generation EGFR inhibitors in human keratinocytes: Implications for adverse dermatologic reactions. J Invest Dermatol. 2018; 138:S183-S183 abstract 1079.
62. Fiala O, Hosek P, Pesek M, Finek J, Racek J, Stehlik P, Sorejs O, Minarik M, Benesova L, Celer A, Nemcova I, Kucera R, Topolcan O. Serum Concentration of Erlotinib and its Correlation with Outcome and Toxicity in Patients with Advanced-stage NSCLC. Anticancer Res. 2017; 37:6469-6476.
63. Azan A, Caspers PJ, Bakker Schut TC, *et al*. A Novel Spectroscopically Determined Pharmacodynamic Biomarker for Skin Toxicity in Cancer Patients Treated with Targeted Agents. Cancer Res. 2017; 77:557-565.
64. Ray S, Bonthapally V, Holen KD, Gauthier G, Wu EQ, Cloutier M, Guérin A. Economic burden of dermatologic adverse drug reactions in the treatment of colorectal, non-small cell lung, and head and neck cancers with epidermal growth factor receptor inhibitors. J Med Econ. 2013; 16:221-230.
65. Lacouture M. Dermatologic principles and practice in oncology: Conditions of the skin, hair, and nails in cancer patients. New York: Wiley-Blackwell. 2014.
66. Lacouture ME, Anadkat MJ, Bensadoun RJ, Bryce J, Chan A, Epstein JB, Eaby-Sandy B, Murphy BA; MASCC Skin Toxicity Study Group. Clinical practice guidelines for the prevention and treatment of EGFR inhibitor-associated dermatologic toxicities. Support Care Cancer. 2011; 19:1079-1095.
67. Potthoff K, Hofheinz R, Hassel JC, Volkenandt M, Lordick F, Hartmann JT, Karthaus M, Riess H, Lipp HP, Hauschild A, Trarbach T, Wollenberg A. Interdisciplinary management of EGFR-inhibitor-induced skin reactions: A German expert opinion. Ann Oncol. 2011; 22:524-535.
68. Reguiai Z, Bachet JB, Bachmeyer C, *et al*. Management of cutaneous adverse events induced by anti-EGFR (epidermal growth factor receptor): A French interdisciplinary therapeutic algorithm. Support Care Cancer. 2012; 20:1395-1404.
69. Melosky B, Burkes R, Rayson D, Alcindor T, Shear N, Lacouture M. Management of skin rash during EGFR-targeted monoclonal antibody treatment for gastrointestinal malignancies: Canadian recommendations. Curr Oncol. 2009; 16:16-26.
70. Arriola E, Reguart N, Artal A, Cobo M, García-Campelo R, Esteban E, Rodríguez MC, García-Muret MP. Management of the adverse events of afatinib: A consensus of the recommendations of the Spanish expert panel. Future Oncol. 2015; 11:267-77.
71. American Society of Clinical Oncology. Skin reactions to targeted therapy and immotherapy. *http://www.cancer.net/navigating-cancer-care/side-effects/skin-reactions-targeted-therapy-and-immunotherapy* (accessed September 14, 2018).
72. Dascalu B, Kennecke HF, Lim HJ, Renouf DJ, Ruan JY, Chang JT, Cheung WY. Prophylactic versus reactive treatment of acneiform skin rashes from epidermal growth factor receptor inhibitors in metastatic colorectal cancer. Support Care Cancer. 2016; 24:799-805.
73. Perez-Soler R, Zou Y, Li T, Ling YH. The phosphatase inhibitor menadione (vitamin K3) protects cells from EGFR inhibition by erlotinib and cetuximab. Clin Cancer Res. 2011; 17:6766-6777.
74. Porzio G, Aielli F, Verna L, Porto C, Tudini M, Cannita K, Ficorella C. Efficacy of pregabalin in the management of cetuximab-related itch. J Pain Symptom Manage. 2006; 32:397-398
75. Santini D, Vincenzi B, Guida FM, Imperatori M, Schiavon G, Venditti O, Frezza AM, Berti P, Tonini G. Aprepitant for management of severe pruritus related to biological cancer treatments: A pilot study. The Lancet Oncology. 2012; 13:1020-1024.
76. Califano R, Tariq N, Compton S, Fitzgerald DA, Harwood CA, Lal R, Lester J, McPhelim J, Mulatero C, Subramanian S, Thomas A, Thatcher N, Nicolson M. Expert Consensus on the Management of Adverse Events from EGFR Tyrosine Kinase Inhibitors in the UK. Drugs. 2015; 75:1335-1348.
77. Capriotti K, Capriotti J, Pelletier J, Stewart K.

Chemotherapy-associated paronychia treated with 2% povidone-iodine: A series of cases. Cancer Manag Res. 2017; 9:225-228.
78. Elad S, Raber-Durlacher JE, Brennan MT, *et al*. Basic oral care for hematology-oncology patients and hematopoietic stem cell transplantation recipients: A position paper from the joint task force of the Multinational Association of Supportive Care in cancer/International Society of Oral Oncology (MASCC/ISOO) and the European Society for Blood and Marrow Transplantation (EBMT). Support Care Cancer. 2015; 23:223-236.
79. Lalla RV, Bowen J, Barasch A, Elting L, Epstein J, Keefe DM, McGuire DB, Migliorati C, Nicolatou-Galitis O, Peterson DE, Raber-Durlacher JE, Sonis ST, Elad S; Mucositis Guidelines Leadership Group of the Multinational Association of Supportive Care in Cancer and International Society of Oral Oncology (MASCC/ISOO). MASCC/ISOO clinical practice guidelines for the management of mucositis secondary to cancer therapy. Cancer. 2014; 120:1453-1461.
80. Peterson DE, Boers-Doets CB, Bensadoun RJ, Herrstedt J; ESMO Guidelines Committee. Management of oral and gastrointestinal mucosal injury: ESMO Clinical Practice Guidelines for diagnosis, treatment, and follow-up. Ann Oncol. 2015; 26:139-151.
81. Deng B, Jia LQ, Cui HJ. Effects of traditional Chinese medicine on epidermal growth factor receptor inhibitors induced rash: A meta-analysis. Journal of China-Japan Friendship Hospital. 2016; 30:30-35. (in Chinese)
82. Ichiki M, Wataya H, Yamada K, Tsuruta N, Takeoka H, Okayama Y, Sasaki J, Hoshino T. Preventive effect of kampo medicine (hangeshashin-to, TJ-14) plus minocycline against afatinib-induced diarrhea and skin rash in patients with non-small cell lung cancer. Onco Targets Ther. 2017; 10:5107-5113.
83. Xu JX, Zhang MJ, Wang AR, Li LM, Gu ML, Li SK. Clinical Application of Jingfang Baidu San Jiawei Combined with Auricular Acupuncture in Prophylaxis and Treatment of Epidermal Growth Factor Receptor Inhibitor Related Skin Toxicity. Chinese Archives of Traditional Chinese Medicine. 2018; 36:417-429. (in Chinese)
84. Zhao ZW, Chen XJ. Efficacy of Siwu Xiaofeng San on treating rash from EGF receptor inhibitor. Chinese Journal of Chinese Medicine. 2015; 7:22-23. (in Chinese)
85. Zhang PY, Pei JW. The Clinical Research of The Powder for Removing Rashes United Gefitinib on Adenocarcinoma of Lung. Journal of Chinese Medicine. 2010; 25:21-23. (in Chinese)
86. Sun T, Yang J, Hu KW. Clinical observation on treatment of EGFR-TKIs-related adverse skin reactions with Yangfei Xiaozhen Tang. Journal of Beijing University of Traditional Chinese Medicine. 2013; 20:17-19. (in Chinese)
87. Peng YM, Cui HJ, Liu Z, Jing FF, Chu YP, Bai YP, Liu DW, Song YZ, Duan H, Qiu YQ. Treatment of EGFRIs-related Skin Adverse Reactions by Zhiyang Pingfu Lotion. Chinese Journal of Integrated Traditional and Western Medicine. 2017; 37:149-154. (in Chinese)
88. Wang Z, Qi F, Cui Y, Zhao L, Sun X, Tang W, Cai P. An update on Chinese herbal medicines as adjuvant treatment of anticancer therapeutics. Biosci Trends. 2018; 12:220-239.
89. Dienstmann R, Braña I, Rodon J, Tabernero J. Toxicity as a biomarker of efficacy of molecular targeted therapies: Focus on EGFR and VEGF inhibiting anticancer drugs. Oncologist. 2011; 16:1729-1740.
90. Chen L, Brown J, Marmaduke DQ, Mayo C, Grau G, Lau YK, Obasaju CK. Rash management and treatment persistence of cancer patients treated with epidermal growth factor receptor inhibitors in the Truven MarketScan® research database. Support Care Cancer. 2018; 26:2369-2377.
91. Nasu S, Suzuki H, Shiroyama T, Tanaka A, Iwata K, Ryota N, Ueda Y, Takata SO, Masuhiro K, Morita S, Morishita N, Okamoto N, Hirashima T. Skin Rash Can Be a Useful Marker for Afatinib Efficacy. Anticancer Res, 2018; 38:1783-1788.
92. Kainis I, Syrigos N, Kopitopoulou A, Gkiozos I, Filiou E, Nikolaou V, Papadavid E. Erlotinib-Associated Rash in Advanced Non-Small Cell Lung Cancer: Relation to Clinicopathological Characteristics, Treatment Response, and Survival. Oncol Res. 2018; 26:59-69.
93. Kogawa T, Doi A, Shimokawa M, *et al*. Early skin toxicity predicts better outcomes, and early tumor shrinkage predicts better response after cetuximab treatment in advanced colorectal cancer. Target Oncol. 2015; 10:125-133.
94. Cella DF. Quality of life: Concepts and definition. J Pain Symptom Manage. 1994; 9:186-192.
95. Chren MM, Lasek JR, Sahay AP, Sands LP. Measurement properties of Skindex-16: A brief quality-of-life measure for patients with skin diseases. J Cutan Med Surg. 2001; 5:105-110.
96. Wagner LI, Berg SR, Gandhi M, Hlubocky FJ, Webster K, Aneja M, Cella D, Lacouture ME. The development of a Functional Assessment of Cancer Therapy (FACT) questionnaire to assess dermatologic symptoms associated with epidermal growth factor receptor inhibitors (FACT-EGFRI-18). Support Care Cancer. 2013; 21:1033-1041.
97. Joshi SS, Ortiz S, Witherspoon JN, *et al*. Effects of epidermal growth factor receptor inhibitor-induced dermatologic toxicities on quality of life. Cancer. 2010; 116:3916-3923.
98. Rosen AC, Case EC, Dusza SW, Balagula Y, Gordon J, West DP, Lacouture ME. Impact of dermatologic adverse events on quality of life in 283 cancer patients: A questionnaire study in a dermatology referral clinic. Am J Clin Dermatol. 2013; 14:327-333.
99. Boers-Doets CB, Gelderblom H, Lacouture ME, Epstein JB, Nortier JW, Kaptein AA. Experiences with the FACT-EGFRI-18 instrument in EGFRI-associated mucocutaneous adverse events. Support Care Cancer. 2013; 2:1919-1926.
100. De Tursi M, Zilli M, Carella C, Auriemma M, Lisco MN, Di Nicola M, Di Martino G, Natoli C, Amerio P. Skin toxicity evaluation in patients treated with cetuximab for metastatic colorectal cancer: A new tool for more accurate comprehension of quality of life impacts. Onco Targets Ther. 2017; 10:3007-3015.
101. Mok TS, Wu Y-L, Ahn M-J, *et al*. Osimertinib or Platinum-Pemetrexed in EGFR T790M-Positive Lung Cancer. N Engl J Med. 2017; 376:629-640.
102. Shi YK, Wang L, Han BH, *et al*. First-line icotinib versus cisplatin/pemetrexed plus pemetrexed maintenance therapy for patients with advanced EGFR mutation-positive lung adenocarcinoma (CONVINCE): A phase 3, open-label, randomized study. Ann Oncol. 2017; 28:2443-2450.
103. Yang JJ, Zhou C, Huang Y, *et al*. Icotinib versus whole-brain irradiation in patients with EGFR-mutant non-small-

cell lung cancer and multiple brain metastases (BRAIN): A multicentre, phase 3, open-label, parallel, randomised controlled trial. Lancet Respir Med. 2017; 5:707-716.
104. Schuler M, Yang JC, Park K, *et al*. Afatinib beyond progression in patients with non-small-cell lung cancer following chemotherapy, erlotinib/gefitinib and afatinib: Phase III randomized LUX-Lung 5 trial. Ann Oncol, 2016; 27:417-423.
105. Zhou C, Wu YL, Chen G, *et al*. Final overall survival results from a randomised, phase III study of erlotinib versus chemotherapy as first-line treatment of EGFR mutation-positive advanced non-small-cell lung cancer (OPTIMAL, CTONG-0802). Ann Oncol. 2015; 26:1877-1883.
106. Wu YL, Zhou C, Liam CK, *et al*. First-line erlotinib versus gemcitabine/cisplatin in patients with advanced EGFR mutation-positive non-small-cell lung cancer: Analyses from the phase III, randomized, open-label, ENSURE study. Ann Oncol. 2015; 26:1883-1889.
107. Wu YL, Zhou C, Hu CP, Feng J, Lu S, Huang Y, Li W, Hou M, Shi JH, Lee KY, Xu CR, Massey D, Kim M, Shi Y, Geater SL. Afatinib versus cisplatin plus gemcitabine for first-line treatment of Asian patients with advanced non-small-cell lung cancer harbouring EGFR mutations (LUX-Lung 6): An open-label, randomised phase 3 trial. Lancet Oncol. 2014; 15:213-222.
108. Seto T, Kato T, Nishio M, *et al*. Erlotinib alone or with bevacizumab as first-line therapy in patients with advanced non-squamous non-small-cell lung cancer harbouring EGFR mutations (JO25567): An open-label, randomised, multicentre, phase 2 study. Lancet Oncol. 2014; 15:1236-1244.
109. Ellis PM, Shepherd FA, Millward M, *et al*. Dacomitinib compared with placebo in pretreated patients with advanced or metastatic non-small-cell lung cancer (NCIC CTG BR.26): A double-blind, randomised, phase 3 trial. Lancet Oncol. 2014; 15:1379-1388.
110. Sequist LV, Yang JC, Yamamoto N, *et al*. Phase III study of afatinib or cisplatin plus pemetrexed in patients with metastatic lung adenocarcinoma with EGFR mutations. J Clin Oncol. 2013; 31:3327-3334.
111. Sun JM, Lee KH, Kim SW, *et al*. Gefitinib versus pemetrexed as second-line treatment in patients with nonsmall cell lung cancer previously treated with platinum-based chemotherapy (KCSG-LU08-01): An open-label, phase 3 trial. Cancer. 2012; 118:6234-6242.
112. Cappuzzo F, Ciuleanu T, Stelmakh L, Cicenas S, Szczésna A, Juhász E, Esteban E, Molinier O, Brugger W, Melezínek I, Klingelschmitt G, Klughammer B, Giaccone G; SATURN investigators. Erlotinib as maintenance treatment in advanced non-small-cell lung cancer: A multicentre, randomised, placebo-controlled phase 3 study. Lancet Oncol. 2010; 11:521-529.
113. Mitsudomi T, Morita S, Yatabe Y, *et al*. Gefitinib versus cisplatin plus docetaxel in patients with non-small-cell lung cancer harbouring mutations of the epidermal growth factor receptor (WJTOG3405): An open label, randomised phase 3 trial. Lancet Oncol. 2010; 11:121-128.
114. Lee DH, Park K, Kim JH, Lee JS, Shin SW, Kang JH, Ahn MJ, Ahn JS, Suh C, Kim SW. Randomized Phase III trial of gefitinib versus docetaxel in non-small cell lung cancer patients who have previously received platinum-based chemotherapy. Clin Cancer Res. 2010; 16:1307-1314.
115. Kim ES, Hirsh V, Mok T, *et al*. Gefitinib versus docetaxel in previously treated non-small-cell lung cancer (INTEREST): A randomised phase III trial. Lancet. 2008; 372:1809-1818.
116. Crinò L, Cappuzzo F, Zatloukal P, Reck M, Pesek M, Thompson JC, Ford HE, Hirsch FR, Varella-Garcia M, Ghiorghiu S, Duffield EL, Armour AA, Speake G, Cullen M. Gefitinib versus vinorelbine in chemotherapy-naive elderly patients with advanced non-small-cell lung cancer (INVITE): A randomized, phase II study. J Clin Oncol. 2008; 26:4253-4260.
117. Soria JC, Ohe Y, Vansteenkiste J, *et al*. Osimertinib in Untreated EGFR-Mutated Advanced Non-Small-Cell Lung Cancer. N Engl J Med. 2018; 378:113-125.
118. Wu YL, Cheng Y, Zhou X,*et al*. Dacomitinib versus gefitinib as first-line treatment for patients with EGFR-mutation-positive non-small-cell lung cancer (ARCHER 1050): A randomised, open-label, phase 3 trial. Lancet Oncol. 2017; 18:1454-1466.
119. Yang JJ, Zhou Q, Yan HH, Zhang XC, Chen HJ, Tu HY, Wang Z, Xu CR, Su J, Wang BC, Jiang BY, Bai XY, Zhong WZ, Yang XN, Wu YL. A phase III randomised controlled trial of erlotinib *vs* gefitinib in advanced non-small cell lung cancer with EGFR mutations. Br J Cancer. 2017; 116:568-574.
120. Paz-Ares L, Tan EH, O'Byrne K, *et al*. Afatinib versus gefitinib in patients with EGFR mutation-positive advanced non-small-cell lung cancer: Overall survival data from the phase IIb LUX-Lung 7 trial. Ann Oncol. 2017; 28:270-277.
121. Soria JC, Felip E, Cobo M, *et al*. Afatinib versus erlotinib as second-line treatment of patients with advanced squamous cell carcinoma of the lung (LUX-Lung 8): An open-label randomised controlled phase 3 trial. Lancet Oncol. 2015; 16:897-907.
122. Ramalingam SS, Jänne PA, Mok T, *et al*. Dacomitinib versus erlotinib in patients with advanced-stage, previously treated non-small-cell lung cancer (ARCHER 1009): A randomised, double-blind, phase 3 trial. Lancet Oncol. 2014; 15:1369-1378.
123. Shi Y, Zhang L, Liu X, *et al*. Icotinib versus gefitinib in previously treated advanced non-small-cell lung cancer (ICOGEN): A randomised, double-blind phase 3 non-inferiority trial. Lancet Oncol. 2013; 14:953-961.
124. Ramalingam SS, Blackhall F, Krzakowski M, *et al*. Randomized phase II study of dacomitinib (PF-00299804), an irreversible pan-human epidermal growth factor receptor inhibitor, versus erlotinib in patients with advanced non-small-cell lung cancer. J Clin Oncol. 2012; 30:3337-3344.
125. Herbst RS, Redman MW, Kim ES, *et al*. Cetuximab plus carboplatin and paclitaxel with or without bevacizumab versus carboplatin and paclitaxel with or without bevacizumab in advanced NSCLC (SWOG S0819): A randomised, phase 3 study. Lancet Oncol. 2018; 19:101-114.
126. Cremolini C, Antoniotti C, Lonardi S, *et al*. Activity and Safety of Cetuximab Plus Modified FOLFOXIRI Followed by Maintenance With Cetuximab or Bevacizumab for RAS and BRAF Wild-type Metastatic Colorectal Cancer: A Rmized Phase 2 Clinical Triaandol. JAMA Oncol. 2018; 4:529-536.
127. Schwartzberg LS, Rivera F, Karthaus M, Fasola G, Canon JL, Hecht JR, Yu H, Oliner KS, Go WY. PEAK: A randomized, multicenter phase II study of panitumumab plus modified fluorouracil, leucovorin, and oxaliplatin

(mFOLFOX6) or bevacizumab plus mFOLFOX6 in patients with previously untreated, unresectable, wild-type KRAS exon 2 metastatic colorectal cancer. J Clin Oncol. 2014; 32:2240-2247.
128. Shitara K, Yonesaka K, Denda T, *et al*. Randomized study of FOLFIRI plus either panitumumab or bevacizumab for wild-type KRAS colorectal cancer-WJOG 6210G. Cancer Sci. 2016; 107:1843-1850.
129. Hecht JR, Cohn A, Dakhil S, Saleh M, Piperdi B, Cline-Burkhardt M, Tian Y, Go WY. SPIRITT: A Randomized, Multicenter, Phase II Study of Panitumumab with FOLFIRI and Bevacizumab with FOLFIRI as Second-Line Treatment in Patients with Unresectable Wild Type KRAS Metastatic Colorectal Cancer. Clin Colorectal Cancer. 2015; 14:72-80.
130. Paz-Ares L, Mezger J, Ciuleanu TE, *et al*. Necitumumab plus pemetrexed and cisplatin as first-line therapy in patients with stage IV non-squamous non-small-cell lung cancer (INSPIRE): An open-label, randomised, controlled phase 3 study. Lancet Oncol. 2015; 16:328-337.
131. Heinemann V, von Weikersthal LF, Decker T, *et al*. FOLFIRI plus cetuximab versus FOLFIRI plus bevacizumab as first-line treatment for patients with metastatic colorectal cancer (FIRE-3): A randomised, open-label, phase 3 trial. Lancet Oncol. 2014; 15:1065-1075.
132. Douillard JY, Siena S, Cassidy J, *et al*. Final results from PRIME: Randomized phase III study of panitumumab with FOLFOX4 for first-line treatment of metastatic colorectal cancer. Ann Oncol. 2014; 25:1346-1355.
133. Price TJ, Peeters M, Kim TW, Li J, Cascinu S, Ruff P, Suresh AS, Thomas A, Tjulandin S, Zhang K, Murugappan S, Sidhu R. Panitumumab versus cetuximab in patients with chemotherapy-refractory wild-type KRAS exon 2 metastatic colorectal cancer (ASPECCT): A randomised, multicentre, open-label, non-inferiority phase 3 study. Lancet Oncol. 2014; 15:569-579.
134. Seymour MT, Brown SR, Middleton G, *et al*. Panitumumab and irinotecan versus irinotecan alone for patients with KRAS wild-type, fluorouracil-resistant advanced colorectal cancer (PICCOLO): A prospectively stratified randomised trial. Lancet Oncol. 2013; 14:749-759.
135. Brøndum L, Alsner J, Sørensen BS, Maare C, Johansen J, Primdahl H, Evensen JF, Kristensen CA, Andersen LJ, Overgaard J, Eriksen JG. Associations between skin rash, treatment outcome, and single nucleotide polymorphisms in head and neck cancer patients receiving the EGFR-inhibitor zalutumumab: Results from the DAHANCA 19 trial. Acta Oncol. 2018; 57:1159-1164.
136. Ma Y, Xin S, Huang M, Yang Y, Zhu C, Zhao H, Zhang Y, Chen L, Zhao Y, Li J, Zhuang W, Zhu X, Zhang L, Wang X. Determinants of Gefitinib toxicity in advanced non-small cell lung cancer (NSCLC): A pharmacogenomic study of metabolic enzymes and transporters. Pharmacogenomics J. 2017; 17:325-330.
137. Fernández-Mateos J, Seijas-Tamayo R, Mesía R, Taberna M, Pastor Borgoñón M, Pérez-Ruiz E, Adansa Klain JC, Vázquez Fernández S, Del Barco Morillo E, Lozano A, González Sarmiento R, Cruz-Hernández JJ, Spanish Head and Neck Cancer Cooperative Group (TTCC). Epidermal growth factor receptor (EGFR) pathway polymorphisms as predictive markers of cetuximab toxicity in locally advanced head and neck squamous cell carcinoma (HNSCC) in a Spanish population. Oral Oncol. 2016; 63:38-43.
138. Caba O, Irigoyen A, Jimenez-Luna C, Benavides M, Ortuño FM, Gallego J, Rojas I, Guillen-Ponce C, Torres C, Aranda E, Prados J. Identification of gene expression profiling associated with erlotinib-related skin toxicity in pancreatic adenocarcinoma patients. Toxicol Appl Pharmacol. 2016; 311:113-116.
139. Jarząbek T, Rucińska M, Rogowski W, Lewandowska M, Tujakowski J, Habib M, Kowalczyk A, Byszek A, Dziadziuszko R, Nawrocki S. CA-SSR1 Polymorphism in Intron 1 of the EGFR Gene in Patients with Malignant Tumors Who Develop Acneiform Rash Associated with the Use of Cetuximab. Mol Diagn Ther. 2015; 19:79-89.
140. Hasheminasab SM, Tzvetkov MV, Schumann C, Rüdiger S, Boeck S, Heinemann V, Kächele V, Steffens M, Scholl C, Hichert V, Seufferlein T, Brockmöller J, Stingl JC. High-throughput screening identified inherited genetic variations in the EGFR pathway contributing to skin toxicity of EGFR inhibitors. Pharmacogenomics. 2015; 16:1605-1619.
141. Jaka A, Gutiérrez-Rivera A, Ormaechea N, Blanco J, La Casta A, Sarasqueta C, Izeta A, Tuneu A. Association between EGFR gene polymorphisms, skin rash and response to anti-EGFR therapy in metastatic colorectal cancer patients. Exp Dermatol. 2014; 23:751-753.
142. Hofheinz RD, Lorenzen S, Trojan J, *et al*. EVITA-a double-blind, vehicle-controlled, randomized phase II trial of vitamin K1 cream as prophylaxis for cetuximab-induced skin toxicity. Ann Oncol. 2018; 29:1010-1015.
143. Eriksen JG, Kaalund I, Clemmensen O, Overgaard J, Pfeiffer P. Placebo-controlled phase II study of vitamin K3 cream for the treatment of cetuximab-induced rash. Support Care Cancer. 2017; 25:2179-2185.
144. Kripp M, Prasnikar N, Vehling-Kaiser U, Quidde J, Al-Batran SE, Stein A, Neben K, Hannig CV, Tessen HW, Trarbach T, Hinke A, Hofheinz RD. AIO LQ-0110: A randomized phase II trial comparing oral doxycycline versus local administration of erythromycin as preemptive treatment strategies of panitumumab-mediated skin toxicity in patients with metastatic colorectal cancer. Oncotarget. 2017; 8:105061-105071.
145. Watanabe S, Nakamura M, Takahashi H, Hara M, Ijichi K, Kawakita D, Morita A. Dermopathy associated with cetuximab and panitumumab: Investigation of the usefulness of moisturizers in its management. Clin Cosmet Investig Dermatol. 2017; 10:353-361.
146. Deplanque G, Gervais R, Vergnenegre A, Falchero L, Souquet PJ, Chavaillon JM, Taviot B, Fraboulet G, Saal H, Robert C, Chosidow O;CYTAR investigators. Doxycycline for prevention of erlotinib-induce rash in non-small-cell lung cancer patients after failure of first-line chemotherapy: A randomized, open-label trial. J Am Acad Dermatol. 2016; 74:1077-1085.
147. Melosky B, Anderson H, Burkes RL, Chu Q, Hao D, Ho V, Ho C, Lam W, Lee CW, Leighl NB, Murray N, Sun S, Winston R, Laskin JJ. Pan Canadian rash trial: A randomized phase III trial evaluating the impact of a prophylactic skin treatment regimen on epidermal growth factor receptor-tyrosine kinase inhibitor-induced skin toxicities in patients with metastatic lung cancer. J Clin Oncol. 2016; 34:810-815.
148. Vaccaro M, Guarneri F, Borgia F, Pollicino A, Altavilla G, Cannavò SP. Efficacy, tolerability and impact on quality of life of clindamycin phosphate and benzoyl peroxide for the treatment of cetuximab-associated acneiform eruption

in patients with metastatic colorectal cancer. J Dermatolog Treat. 2016; 27:148-152.
149. Arrieta O, Vega-González MT, López-Macías D, Martínez-Hernández JN, Bacon-Fonseca L, Macedo-Pérez EO, Ramírez-Tirado LA, Flores-Estrada D, de la Garza-Salazar J. Randomized, open-label trial evaluating the preventive effect of tetracycline on afatinib induced-skin toxicities in non-small cell lung cancer patients. Lung Cancer. 2015; 88:282-288.
150. Yamada M, Iihara H, Fujii H, Ishihara M, Matsuhashi N, Takahashi T, Yoshida K, Itoh Y. Prophylactic effect of oral minocycline in combination with topical steroid and skin care against panitumumab-induced acneiform rash in metastatic colorectal cancer patients. Anticancer Res. 2015; 35:6175-6181.
151. Li AM, Miao JH, Liu H, Ma YZ, Sun ZC. Drug-induced skin toxicity and clinical nursing of VitK cream on colorectal cancer patients. Pak J Pharm Sci. 2015; 28:1499-1503.
152. Kobayashi Y, Komatsu Y, Yuki S, *et al*. Randomized controlled trial on the skin toxicity of panitumumab in Japanese patients with metastatic colorectal cancer: HGCSG1001 study; J-STEPP. Future Oncol. 2015; 11:617-627.
153. Tastekin D, Tambas M, Kilic K, Erturk K, Arslan D. The efficacy of Pistacia Terebinthus soap in the treatment of cetuximab-induced skin toxicity. Invest New Drugs. 2014; 32:1295-300.
154. Pinta F, Ponzetti A, Spadi R. Pilot clinical trial on the efficacy of prophylactic use of vitamin K1-based cream (Vigorskin) to prevent cetuximab-induced skin rash in patients with metastatic colorectal cancer. Clin Colorectal Cancer. 2014; 13:62-67.
155. Jatoi A, Dakhil SR, Sloan JA, Kugler JW, Rowland KM Jr, Schaefer PL, Novotny PJ, Wender DB, Gross HM, Loprinzi CL; North Central Cancer Treatment Group. Prophylactic tetracycline does not diminish the severity of epidermal growth factor receptor (EGFR) inhibitor-induced rash: Results from the North Central Cancer Treatment Group (Supplementary N03CB). Support Care Cancer. 2011; 19:1601-1607.
156. Lacouture ME, Mitchell EP, Piperdi B, Pillai MV, Shearer H, Iannotti N, Xu F, Yassine M. Skin toxicity evaluation protocol with panitumumab (STEPP), a phase II, open-label, randomized trial evaluating the impact of a pre-emptive skin treatment regimen on skin toxicities and quality of life in patients with metastatic colorectal cancer. J Clin Oncol. 2010; 28:1351-1357.
157. Jatoi A, Thrower A, Sloan JA, Flynn PJ, Wentworth-Hartung NL, Dakhil SR, Mattar BI, Nikcevich DA, Novotny P, Sekulic A, Loprinzi CL. Does sunscreen prevent epidermal growth factor receptor (EGFR) inhibitor-induced rash? Results of a placebo-controlled trial from the North Central Cancer Treatment Group (N05C4). Oncologist. 2010; 15:1016-1022.
158. Jatoi A, Rowland K, Sloan JA, Gross HM, Fishkin PA, Kahanic SP, Novotny PJ, Schaefer PL, Johnson DB, Tschetter LK, Loprinzi CL. Tetracycline to prevent epidermal growth factor receptor inhibitor-induced skin rashes: Results of a placebo-controlled trial from the North Central Cancer Treatment Group (N03CB) Cancer. 2008; 113:847-853.
159. Scope A, Agero AL, Dusza SW, Myskowski PL, Lieb JA, Saltz L, Kemeny NE, Halpern AC. Randomized double-blind trial of prophylactic oral minocycline and topical tazarotene for cetuximab-associated acne-like eruption. J Clin Oncol. 2007; 25:5390-5396.

(Received October 12, 2018 Revised November 28, 2018; Accepted December 2, 2018)

Mini-Review

DOI: 10.5582/bst.2018.01264

On medical application of neural networks trained with various types of data

Kenji Karako[1], Yu Chen[1,*], Wei Tang[2]

[1] *Department of Human and Engineered Environmental Studies, Graduate School of Frontier Sciences, The University of Tokyo, Chiba, Japan;*
[2] *Department of International Trial, Center for Clinical Sciences; Hospital International Health Care Center, National Center for Global Health and Medicine, Tokyo, Japan.*

Summary **Neural networks have garnered attention over the past few years. A neural network is a typical model of machine learning that is used to identify visual patterns. Neural networks are used to solve a wide variety of problems, including image recognition problems and time series prediction problems. In addition, neural networks have been applied to medicine over the past few years. This paper classifies the ways in which neural networks have been applied to medicine based on the type of data used to train those networks. Applications of neural networks to medicine can be categorized two types: automated diagnosis and physician aids. Considering the number of patients per physician, neural networks could be used to diagnose diseases related to the vascular system, heart, brain, spinal column, head, neck, and tumors/cancer in three fields: vascular and interventional radiology, interventional cardiology, and neuroradiology. Lastly, this paper also considers areas of medicine where neural networks can be effectively applied in the future.**

Keywords: Neural network, convolutional neural network, recurrent neural network, CT, X-ray, MRI, PET, EHR

1. Introduction

Neural networks have garnered attention over the past few years. Essentially, a neural network is a mathematical model of neurons (*1*). A neural network is capable of approximating arbitrary functions mathematically based on the universal approximation theorem (*1*). Because of this characteristic, a neural network is used as a model to identify visual patterns. Over the past few years, neural networks have been used extensively to solve various problems. Examples are a convolutional neural network, which is used in image recognition (*2,3*), and a recurrent neural network, which is used model sequential data for speech recognition (*4,5*).

Neural networks have also been applied to medicine over the past few years. This paper will make a mini-review on this topic by classifying the application of neural networks to medicine based on the type of data used to train those networks. This paper also considers areas of medicine where neural networks can be applied in the future.

This paper is organized as follows. In Section 2, the applications of neural networks trained with medical images are described. Section 3 describes applications involving neural network trained with data from examination notes and other medical records. Areas of medicine where neural networks can be applied in the future are discussed in Section 4.

2. Applications of neural network trained with medical images

The aim of this section is to specify what neural networks can do with medical images. A diagram depicting classification using a convolutional neural network is shown in Figure. 1. The convolutional

Released online in J-STAGE as advance publication December 17, 2018.

**Address correspondence to:*
Dr. Yu Chen, Department of Human and Engineered Environmental Studies, Graduate School of Frontier Sciences, The University of Tokyo, 5-1-5 Kashiwa-no-ha, Kashiwa Chiba 227-8568, Japan.
E-mail: chen@edu.k.u-tokyo.ac.jp

neural network consists of an input layer, hidden layers, and an output layer. The images to classify constitute the input layer. The hidden layers identify features in those images. Based on those features, the output layer classifies those images. The hidden layers consist of a series of convolutional layers and pooling layers. A convolutional layer consists of neurons that connect to a grid of neurons in the previous layer. Convolution extracts the features of the grid of neurons in the previous layer. Pooling extracts representative features from the convolutional layer. Through repeated convolution and pooling, information can be compressed and the features needed to classify images can be identified. To classify the images, training a convolutional neural network is necessary. Each layer of neural networks has parameters that decide outputs of neural networks. By following training step, the parameters are set to the values that neural networks can classify the images. The procedures of training neural networks are as follows. The first step is the collection of training data that is the correct pairs of input and output. The second step is optimization of the parameters to reduce the error between the correct output and the neural networks' output calculated from the pair input. The third step is the iteration of the second step in order to determine the parameters that reduce the loss for the entire training data. The neural networks can output the same value as the training data using the parameters determined in the third step. Nevertheless, the neural networks could not output correct values that has features not existing in the training data. Therefore, it is preferable to use as much data as possible for training data and use various possible forms of the actual input data.

2.1. *Applications involving pathology images*

Whether cancer cells are metastatic is an important factor in determining treatment. One proposal is to use a convolutional neural network to detect metastasis in pathology images (*6*). This method was used to analyze a set of pathology images from patients with breast cancer (the Camelyon16 dataset (*7*)), and it had a diagnostic accuracy of 92.4%, which is much higher than the accuracy of pathologists (73.2%). With the neural networks, the program can rapidly detect metastasis in large numbers of images. Methods of classifying breast cancer using a neural network trained with pathology images have been proposed (*8-14*).

2.2. *Applications involving magnetic resonance imaging (MRI), positron emission tomography (PET), and computed tomography (CT) images*

The accurate diagnosis of Alzheimer's disease (AD) and its early stage is essential to its timely treatment and possible delay. A method of identifying AD from MRI and PET images using a neural network has been proposed (*15*). This method extracts features from MRI and PET images of the brain and it detects AD based on features from those two types of images. This is accomplished using multimodal stacked deep polynomial networks to identify the features of AD (*16*). Multimodal stacked deep polynomial networks were used to analyze multimodal neuroimaging data from patients with AD (ADNI dataset (*17*)) and that approach identified AD with an accuracy of 97.13%, which was higher than the accuracy of other multimodal learning methods. Methods of classifying brain conditions and cancers using a neural network trained with MRI, PET, and CT images have also been proposed (*18-25*).

2.3. *Applications involving X-rays Images*

Like the method of diagnosing disease based on MRI and PET images described in Section 2.2, a method of diagnosing disease based on X-rays images has been proposed (*26*). This method diagnoses disease based

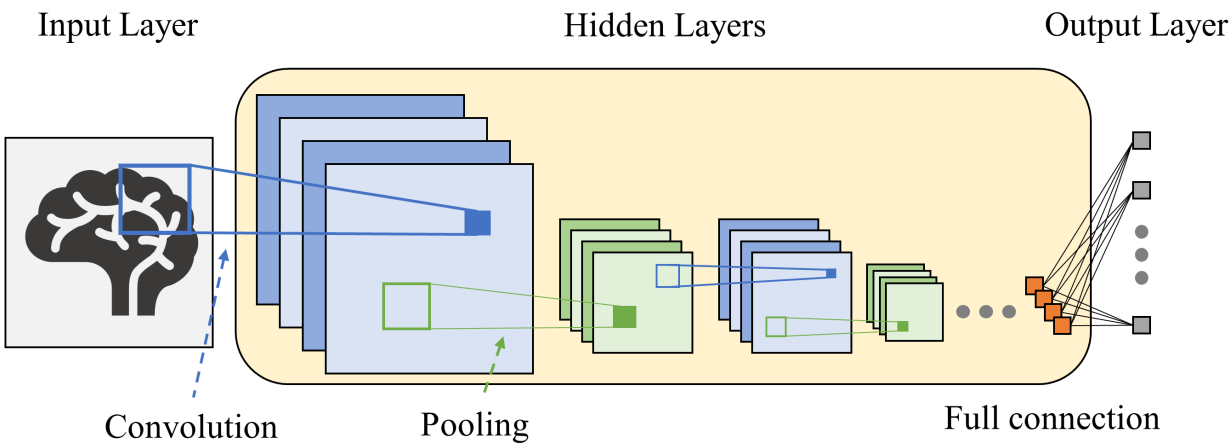

Figure 1. Classification using a convolutional neural network.

on chest X-rays using a convolutional neural network. This approach was better at detecting pneumonia than practicing radiologists. In addition, this method identified 14 types of diseases in a chest X-ray dataset (Chest X-ray 14 (*27*)) at a higher rate than other methods. Methods of classifying chest conditions and dental caries using a neural network trained with X-rays have also been proposed (*28-34*).

2.4. *Applications involving endoscopy images*

A method of detecting gastrointestinal disease in endoscopy videos has been proposed (*35*). This method can classify multiple types of gastrointestinal diseases using a convolutional neural network. This method had an accuracy of 96.9% at distinguishing six classes of images (blurry images, images of the cecum, images of the normal colon, images of polyps, images of a tumor, and images showing the Z-line). This method can be used to provide physicians with endoscopic images of the gastrointestinal tract in real time. Methods of identifying angiodysplasia and other conditions using a neural network trained with endoscopy images have also been proposed (*36-37*).

2.5. *Applications involving images of the skin*

Neural networks have been trained with images from diagnostic equipment, and they have also been trained with images of the skin. A method of classifying skin lesions based on images of the skin has been proposed (*38*). This method uses a dataset of 12,945 images of the skin including 2,032 diseases to train a convolution neural network. This method separated lesions into three classes (benign lesions, malignant lesions, and non-neoplastic lesions) with an accuracy of 72.1 ± 0.9% (mean ± standard deviation), which is higher than the accuracy of two dermatologists (65.56 and 66.0%). In addition, dedicated equipment is not needed to obtain images of the skin, so this method could be used on a mobile device such as a smartphone. Methods of classifying melanoma and other skin lesions using a neural network trained with images of the skin have also been proposed (*39-44*).

2.6. *Summary of Section 2*

Each of the methods described involves a neural network trained using various medical images to replace diagnosis by a physician. This is because diagnosis is often based on imaging and because a convolution neural network facilitates image analysis. The applications described in Sections 2.1 to 2.5 suggest that a convolution neural network can diagnose disease more accurately than a physician. Thus, diagnosis based on imaging is likely to be performed entirely by neural networks in the future. Neural networks improve both the accuracy and speed of diagnosis. In addition, images could be obtained and used to train a neural network with no involvement of a specialist. Medical images could be obtained at a hospital that lacks a specialist and transferred remotely to a specialist for diagnosis. Physicians can only diagnose a limited number of patients, but automated diagnosis using a neural network can diagnose a large number of patients all over the world. These advantages are why neural networks will be increasingly applied to fields with a shortage of specialists.

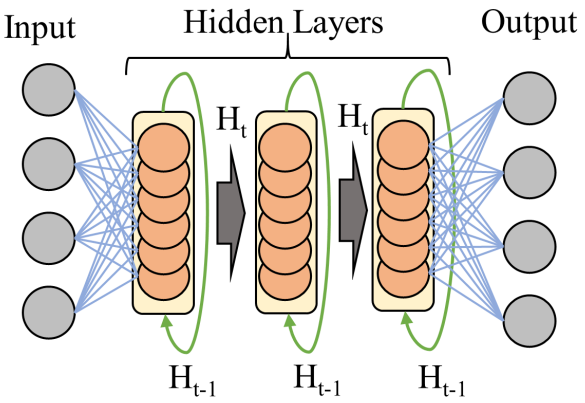

Figure 2. Prediction using a recurrent neural network.

3. Applications of neural networks trained with data from medical records

This section describes what neural network can predict with data from medical records (*45-52*). Prediction using a recurrent neural network is shown in Figure. 2. The main purpose of the use of neural network is to aid a physician. Predicting a medical event allows a physician to know where to focus his or her attention. Based on the prediction of a patient's next visit, the physician can instruct the patient to come to the hospital earlier so that symptoms will not worsen. A normal neural network cannot be applied to time-series problems because it uses only current data. A recurrent neural network can be applied to sequential data. The output of each hidden layer is generated based on its previous output and its current input. Thus, current output includes both the previous output and current input. This allows a recurrent neural network to forecast a time series over a long period of time.

3.1. *Prediction of medical events based on electronic health records (EHRs)*

A method of predicting medical events (symptom information, medication information, timing of visits, *etc*.) based on past electronic medical records has been proposed (*53*). This method uses a recurrent neural

network, which is effective at analyzing sequential data. A recurrent neural network that was trained with 8 years of electronic medical records from 260,000 patients and 2,128 physicians predicts future medical events. This method performed 79.58% recall using 85% of that data as training and 15% as the test.

3.2. *Predicting medications in use based on EHRs*

Estimates are that 50% of the medicines being taken by patients are not listed in electronic medical records (*54*). Therefore, a method of predicting medicines being taken by patients has been proposed (*55*). This method uses a recurrent neural network trained with electronic medical records, and it is highly accurate. In multi-label classification of medicines, micro-averaged area under the curve of this method is 0.926.

3.3. *Summary of Section 3*

Applications involving a neural network trained with data from medical records aid physicians rather than replacing them. The application described in Section 3.1 provides information needed for patient care and the application described in Section 3.2 augments the information given to a physician. This is because a neural network generates a rule based on a large volume of input data. These data are mainly EHRs. Developing a system that uses a neural network to aid a physician is difficult. Data are needed to train the neural network, and those data must contain information that the network can use to generate rules. Moreover, generating a rule may not always be possible. Furthermore, there may not be sufficient data with which to train the neural network. A diagnosis is made based on a physician's knowledge and imaging, so a neural network can generate a diagnostic rule. A neural network is effective at making predictions based on existing information with a certain level of accuracy. When a neural network is used to make a prediction without such information, knowing whether data are insufficient or whether generation of a rule is not possible is difficult. Thus, neural networks can aid physicians. Physicians are human beings, and they can make mistakes and they have limitations. A neural network can be used to alleviate or compensate for those flaws.

4. Application of neural networks to medicine in the future

The applications in Sections 2 and 3 can be categorized into two types: automated diagnosis and physician aids. Currently, 45% of WHO member countries have less than 1 physician per 1,000 population (*56*). Considering the current shortage of physicians, automated diagnostic systems using neural networks are needed more than physician aids.

Automated diagnosis could be used in several areas of medicine in the future. Developing an automated diagnostic system for each disease and examination would prove costly, so automated diagnostic systems are most needed in fields where physicians are in short supply. Given the number of patients per specialist, the top three fields in which those systems can be applied are vascular and interventional radiology, interventional cardiology, and neuroradiology (*57*).

Vascular and interventional radiology is a medical sub-specialty of radiology utilizing minimally-invasive image-guided procedures to diagnose and treat diseases in nearly every organ system. Imaging is guided by X-rays, ultrasonography, or CT. In interventional cardiology, the heart is depicted on X-rays *via* catheterization so that a procedure can be performed. Fluoroscopy is often used to depict the heart. Neuroradiology is a subspecialty of radiology focusing on the diagnosis and characterization of abnormalities of the central and peripheral nervous system, spine, head, and neck using neuroimaging techniques. Imaging modalities include MRI, CT, and ultrasonography.

In the three specialties above, a diagnosis is made and treatment is provided using MRI, CT, X-rays, and ultrasonography. Automated diagnosis using a neural network would be useful in these fields. Diseases encountered in the three specialties above relate to the vascular system, heart, brain, spinal column, head, neck, and tumors/cancer. Hence, neural networks will be applied to a wider range of diseases related to the vascular system, heart, brain, spinal column, head, neck, and tumors/cancer in the future.

5. Conclusion

Medical applications of the neural networks mentioned in Section 2 - 3 are shown in Table 1. Applications of neural networks can mainly be classified into two types. Neural networks like those in Sections 2.1 to 2.5 take the place of a physician to identify or detect disease. Neural networks like those in Sections 3.1 to 3.2 assist a physician in providing care.

A diagnosis based on imaging is likely to be highly accurate because the images have features that a neural network can extract. Diagnosis using a neural network seems to be the main way in which neural networks will be applied to medicine in the future. Considering the number of patients per physician, neural networks could be used to diagnose diseases related to the vascular system, heart, brain, spinal column, head, neck, and tumors/cancer in three fields: vascular and interventional radiology, interventional cardiology, and neuroradiology. This would not only decrease the workload for physicians but it would also increase diagnostic accuracy and lead to the early detection of disease.

Table 1. Uses of neural networks trained with varied data

Input data	Application	Use
Pathology images	Classification of metastasis	CNN (*6*)
	Classification of breast cancer	CNN (*8-9*), Deep NN (*10*)
	Classification of cellular and non-cellular structures	CNN (*11*)
	Detection of mitosis in breast cancer	CNN (*12*)
	Identification of endothelial cells derived from induced pluripotent stem cells	CNN (*13*)
	Classification of HEp-2 cell images	CNN (*14*)
MRI & PET images	Diagnosis of Alzheimer's disease	MM-DPN(PN-based) (*15*)
MRI images	Classification of prostate cancer	CNN (*18*)
	Segmentation of brain tumors	CNN (*19*)
	Segmentation of volumetric medical images	3D CNN (*20*)
	Classification of Alzheimer's disease	CNN (*21*)
PET & CT images	Detection of pulmonary nodules	CNN (*22*)
CT images	Classification of hematomas in the brain	NN (*23*)
	Detection of lung nodules	3D CNN (*24-25*)
X-ray images	Detection of pneumonia	CNN (*26*)
	Classification of chest pathologies	CNN (*28*)
	Classification of dental caries	Deep NN (*29*)
	Reading frontal and lateral chest X-rays	CNN (*30*)
	Classification of X-rays	CNN (*31*)
	Reading chest X-rays	CNN & RNN (*32*), CNN (*33*)
	Identification of the spine and pelvis in frontal X-rays	CNN (*34*)
Images of endoscope	Detection of gastrointestinal disease in videos	CNN (*35*)
	Detection of angiodysplasia	CNN (*36*)
	Detection of abnormalities in wireless capsule endoscopy	CNN (*37*)
Images of the skin	Classification of skin cancer	CNN (*38-39*)
	Diagnosis of melanoma	CNN (*40-43*), RNN & CNN (*44*)
EHRs	Classification of 128 conditions based on clinical data	RNN (*45*)
	Labeling to extract medical events and their attributes from unstructured text	RNN (*46*)
	Generation of multi-label discrete EHRs	RNN (*47*)
	Detection of the onset of heart failure	RNN (*48*)
	Phenotyping youth depression based on text notes in EHRs	Deep NN (*49*)
	Prediction of risk	CNN (*50*)
	Detection of preterm births	Feed-Forward NN, Radial Basis Function NN, Random NN (*51*)
	Prediction of colorectal cancer	RNN (*52*)
	Prediction of medical events	RNN (*53*)
	Prediction of medications in use	RNN (*55*)

Acknowledgement

This work was supported by Grants-in-Aid from the Ministry of Education, Science, Sports, and Culture of Japan.

References

1. Goodfellow I, Bengio Y, Courville A. Deep Learning. Deep Learning. MIT Press. 2016; pp. 164-223.
2. Krizhevsky A, Sutskever I, Hinton GE. ImageNet classification with deep convolutional neural networks. NIPS. 2012; 1:1097-1105.
3. He K, Zhang X, Ren S, Sun J . Spatial pyramid pooling in deep convolutional networks for visual recognition. IEEE Trans Pattern Anal Mach Intell. 2014; 37:1904-1916.
4. Graves A, Mohamed A, Hinton GE. Speech recognition with deep recurrent neural networks. IEEE Int Conf Acoust Speech Signal Process. 2013; 6645-6649.
5. Sutskever I, Martens J, Hinton GE. Generating text with recurrent neural networks. ICML. 2011; 1017-1024.
6. Liu Y, Gadepalli K, Norouzi M, Dahl GE, Kohlberger T, Boyko A, Venugopalan S, Timofeev A, Nelson PQ, Corrado GS, Hipp JD, Peng L, Stumpe MC. Detecting cancer metastases on gigapixel pathology images. 2017; CoRR, abs/1703.02442.
7. CAMELYON16. *https://camelyon16.grand-challenge.org/* (accessed October 6, 2018).
8. Nawaz M, Sewissy AA, Soliman TH. Multi-class breast cancer classification using deep learning convolutional neural network. IJACSA. 2018; 9:316-322.
9. Spanhol FA, Oliveira LE, Petitjean C, Heutte L. Breast cancer histopathological image classification using Convolutional Neural Networks. IJCNN. 2016; 2560-2567.

10. Feng Y, Zhang L, Yi Z. Breast cancer cell nuclei classification in histopathology images using deep neural networks. Int J Comput Assist Radiol Surg. 2017; 13:179-191.
11. Hatipoglu N, Bilgin G. Classification of histopathological images using convolutional neural network. IPTA. 2014; 1-6.
12. Ciresan DC, Giusti A, Gambardella LM, Schmidhuber J. Mitosis detection in breast cancer histology images with deep neural networks. Med Image Comput Comput Assist Interv. 2013; 16:411-418.
13. Kusumoto D, Lachmann MJ, Kunihiro T, Yuasa S, Kishino Y, Kimura M, Katsuki T, Itoh S, Seki T, Fukuda K. Automated deep learning-based system to identify endothelial cells derived from induced pluripotent stem cells. Stem cell reports. 2018; 10:1687-1695.
14. Gao Z, Wang L, Zhou L, Zhang J. HEp-2 cell image classification with deep convolutional neural networks. IEEE J Biomed Health Inform. 2017; 21:416-428.
15. Shi J, Zheng X, Li Y, Zhang Q, Ying S. Multimodal neuroimaging feature learning with multimodal stacked deep polynomial networks for diagnosis of Alzheimer's disease, IEEE J Biomed Health Inform. 2018; 22:173-183.
16. Livni R, Shalev-Shwartz S, Shamir O. An algorithm for training polynomial networks. 2013; CoRR, abs/1304.7045.
17. ADNI. Alzheimer's Disease Neuroimaging Initiative. *http://adni.loni.usc.edu/* (accessed October 6, 2018).
18. Liu Y, An X. A classification model for the prostate cancer based on deep learning. CISP-BMEI. 2017; 1-6.
19. Pereira S, Pinto A, Alves V, Silva CA. Brain tumor segmentation using convolutional neural networks in MRI images. IEEE Trans Med Imaging. 2016; 35:1240-1251.
20. Milletari F, Navab N, Ahmadi S. V-Net: Fully convolutional neural networks for volumetric medical image segmentation. 3DV. 2016; 565-571.
21. Sarraf S, Tofighi G. DeepAD: Alzheimer's disease classification *via* deep convolutional neural networks using MRI and fMRI. 2016; bioRxiv. (doi:10.1101/070441).
22. Teramoto A, Fujita H, Yamamuro O, Tamaki T. Automated detection of pulmonary nodules in PET/CT images: Ensemble false-positive reduction using a convolutional neural network technique. Medical physics. 2016; 43:2821-2827.
23. Sharma B, Venugopalan K. Classification of hematomas in brain CT images using neural network. ICICT. 2014; 41-46.
24. Huang X, Shan J, Vaidya V. Lung nodule detection in CT using 3D convolutional neural networks. ISBI. 2017; 379-383.
25. Hamidian S, Sahiner B, Petrick N, Pezeshk A. 3D convolutional neural network for automatic detection of lung nodules in chest CT. Proc SPIE Int Soc Opt Eng. 2017; 10134.
26. Rajpurkar P, Irvin J, Zhu K, Yang B, Mehta H, Duan T, Ding D, Bagul A, Langlotz CP, Shpanskaya K, Lungren MP, Ng AY. CheXNet: Radiologist-level pneumonia detection on chest X-rays with deep learning. 2017; CoRR, abs/1711.05225.
27. NIH Chest X-rays. Kaggle. *https://www.kaggle.com/nih-chest-xrays/data* (accessed October 6, 2018).
28. Salehinejad H, Valaee S, Dowdell T, Colak E, Barfett J. Generalization of deep neural networks for chest pathology classification in X-rays using generative adversarial networks. ICASSP. 2018; 990-994.
29. Ali RB, Ejbali R, Zaied M. Detection and classification of dental caries in X-ray images using deep neural networks. ICSEA. 2016; 223-227.
30. Rubin J, Sanghavi D, Zhao C, Lee K, Qadir A, Xu-Wilson M. Large scale automated reading of frontal and lateral chest X-rays using dual convolutional neural networks. 2018; CoRR, abs/1804.07839.
31. Ahn E, Kumar A, Kim J, Li C, Feng DD, Fulham MJ. X-ray image classification using domain transferred convolutional neural networks and local sparse spatial pyramid. ISBI. 2016; 855-858.
32. Shin H, Roberts K, Lu L, Demner-Fushman D, Yao J, Summers RM. Learning to read chest X-rays: Recurrent neural cascade model for automated image annotation. CVPR. 2016; 2497-2506.
33. Dong Y, Pan Y, Zhang J, Xu W. Learning to read chest X-ray images from 16000+ examples using CNN. CHASE. 2017; 51-57.
34. Aubert B, Vazquez C, Cresson T, Parent S, Guise JA. Automatic spine and pelvis detection in frontal X-rays using deep neural networks for patch displacement learning. ISBI. 2016; 1426-1429.
35. Pogorelov K, Riegler M, Eskeland SL, Lange TD, Johansen D, Griwodz C, Schmidt PT, Halvorsen P. Efficient disease detection in gastrointestinal videos – Global features versus neural networks. Multimedia Tools and Applications. 2017; 76:22493-22525.
36. Shvets A, Iglovikov VI, Rakhlin A, Kalinin AA. Angiodysplasia detection and localization using deep convolutional neural networks. 2018; CoRR, abs/1804.08024.
37. Sekuboyina AK, Devarakonda ST, Seelamantula CS. A convolutional neural network approach for abnormality detection in Wireless Capsule Endoscopy. ISBI. 2017; 1057-1060.
38. Esteva A, Kuprel B, Novoa RA, Ko J, Swetter SM, Blau HM, Thrun S. Dermatologist-level classification of skin cancer with deep neural networks. Nature. 2017; 542:115-118.
39. Harangi B. Skin lesion detection based on an ensemble of deep convolutional neural network. 2017; CoRR, abs/1705.03360.
40. Jivtode SS, Ukalkar A. Neural network based detection of melanoma skin cancer. IJSR. 2016; 5:860-864.
41. Bastürk A, Yuksei ME, Badem H, Caliskan A. Deep neural network based diagnosis system for melanoma skin cancer. SIU. 2017; 1-4.
42. Sivaranjani N, Kalaimani MM. Diagnosis of melanoma skin cancer using neural network. IJRD. 2016; 2:13-24.
43. Ali AA, Al-Marzouqi H. Melanoma detection using regular convolutional neural networks. ICECTA. 2017; 1-5.
44. Attia M, Hossny M, Nahavandi S, Yazdabadi A. Skin melanoma segmentation using recurrent and convolutional neural networks. ISBI. 2017; 292-296.
45. Lipton ZC, Kale DC, Elkan C, Wetzel RC. Learning to diagnose with LSTM recurrent neural networks. 2015; CoRR, abs/1511.03677.
46. Jagannatha AN, Yu H. Bidirectional RNN for medical event detection in electronic health records. Conference Proceedings. Association for Computational Linguistics. North American Chapter. Meeting. 2016; 473-482.
47. Choi E, Biswal S, Malin BA, Duke J, Stewart WF, Sun J. Generating multi-label discrete electronic health records

using generative adversarial networks. 2017; CoRR, abs/1703.06490.
48. Choi E, Schuetz A, Stewart WF, Sun J. Using recurrent neural network models for early detection of heart failure onset. JAMIA. 2017; 24:361–370.
49. Geraci J, Wilansky P, Luca VD, Roy A, Kennedy JL, Strauss J. Applying deep neural networks to unstructured text notes in electronic medical records for phenotyping youth depression. EBMH. 2017; 20:83-87.
50. Che Z, Cheng Y, Sun Z, Liu Y. Exploiting convolutional neural network for risk prediction with medical feature embedding. 2017; CoRR, abs/1701.07474.
51. Fergus P, Idowu IO, Hussain AJ, Dobbins C. Advanced artificial neural network classification for detecting preterm births using EHG records. Neurocomputing. 2016; 188:42-49.
52. Amirkhan R, Hoogendoorn M, Numans ME, Moons LM. Using recurrent neural networks to predict colorectal cancer among patients. SSCI. 2017; 1-8.
53. Choi E, Bahadori MT, Sun J. Doctor AI: Predicting clinical events *via* recurrent neural networks. JMLR Workshop Conf Proc. 2016; 56:301-318.
54. Caglar S, Henneman PL, Blank FS, Smithline HA, Henneman EA. Emergency department medication lists are not accurate. The Journal of Emergency Medicine. 2011; 40:613-616.
55. Bajor JM, Lasko TA. Predicting medications from diagnostic codes with recurrent neural networks. ICLR. 2017.
56. WHO. Density of physicians (total number per 1000 population, latest available year). *http://www.who.int/gho/health_workforce/physicians_density/en/* (accessed October 23, 2018).
57. Data and Reports - Workforce - Data and Analysis - AAMC. *https://www.aamc.org/data/workforce/reports/458490/1-2-chart.html* (accessed October 23, 2018).

(Received September 17, 2018; Revised November 20, 2018; Accepted November 26, 2018)

Original Article

DOI: 10.5582/bst.2018.01226

Regulation on introducing process of the highly difficult new medical technologies: A survey on the current status of practice guidelines in Japan and overseas

Kazuo Minamikawa[1,2,3], Akiko Okumura[3,4], Norihiro Kokudo[3,5], Koji Kono[1,3,*]

[1] *Departments of Gastrointestinal Tract Surgery, Fukushima Medical University, Fukushima, Japan;*
[2] *Medical Research Center, Fukushima Medical University, Fukushima, Japan;*
[3] *Special Research Group on Evaluation and Improvement of Clinical Guidelines for Introduction Process of Highly Difficult New Medical Technologies, Japan;*
[4] *Department of EBM and Guidelines, Japan Council for Quality Health Care, Tokyo, Japan;*
[5] *Department of Surgery, University of Tokyo, Tokyo, Japan.*

Summary **Since serious problematic cases regarding the technical safety of technically demanding operations were reported in Japan, the Ministry of Health, Labor and Welfare issued new regulations on June 10, 2016 requiring each hospital to check the status of informed consent, skill of surgery team and governance system of the surgical unit, when the highly difficult new medical technologies were introduced to a hospital. In order to firmly establish this new system for highly difficult new medical technologies, it is very important and informative to survey the current situation for guidelines and consensus regarding introduction of medical technology with special skills in Japan and overseas. Based on the survey of questionnaires, document retrieval, and expert interviews, we found that documentation related to the introduction process of highly difficult medical technologies is very rare, and the regulations were mainly issued by academic societies. Moreover, even if such documentation existed, the quality of the regulations is poor and not sufficient enough to perform surgical practice safely. Therefore, for medical practitioners, comprehensive and concrete regulations should be issued by the government or ministry to legally follow in regard to technically demanding operations. A new practice guideline was proposed by our special research group to regulate the introduction process of highly difficult new medical technologies in hospitals in Japan. This guideline, gained understanding from relevant academic societies, provided a comprehensive view on the interpretation of "high difficulty new medical technology" prescribed by the law and show the basic idea at a preliminary examination from the viewpoints of "Surgeon's requirement", "Guidance system", "Medical safety" , and "Informed consent". These efforts will contribute to the improvement of the quality of guidelines regarding "highly difficult new medical technology".**

Keywords: Technically demanding operation, guidelines, technical safety, medical safety

1. Introduction

There have been great advances in surgical techniques resulting in improved quality of life (QOL) and better overall survival in several types of operations, including laparoscopic and thoracoscopic approaches (*1,2*). However, in 2014, serious problematic cases in technical safety for technically demanding operations such as laparoscopic liver resection and laparoscopic pancreatic resection were reported one after another in Japan, in hospitals such as university hospitals, which provide advanced medical care (*3,4*).

On June 10, 2016, the Japanese Ministry of Health, Labor and Welfare revised the ministerial ordinance for

Released online in J-STAGE as advance publication December 28, 2018.

*Address correspondence to:
Dr. Koji Kono, Departments of Gastrointestinal Tract Surgery, Fukushima Medical University, 1 Hikarigaoka, Fukushima, Fukushima 960-1295, Japan.
E-mail: kojikono@fmu.ac.jp

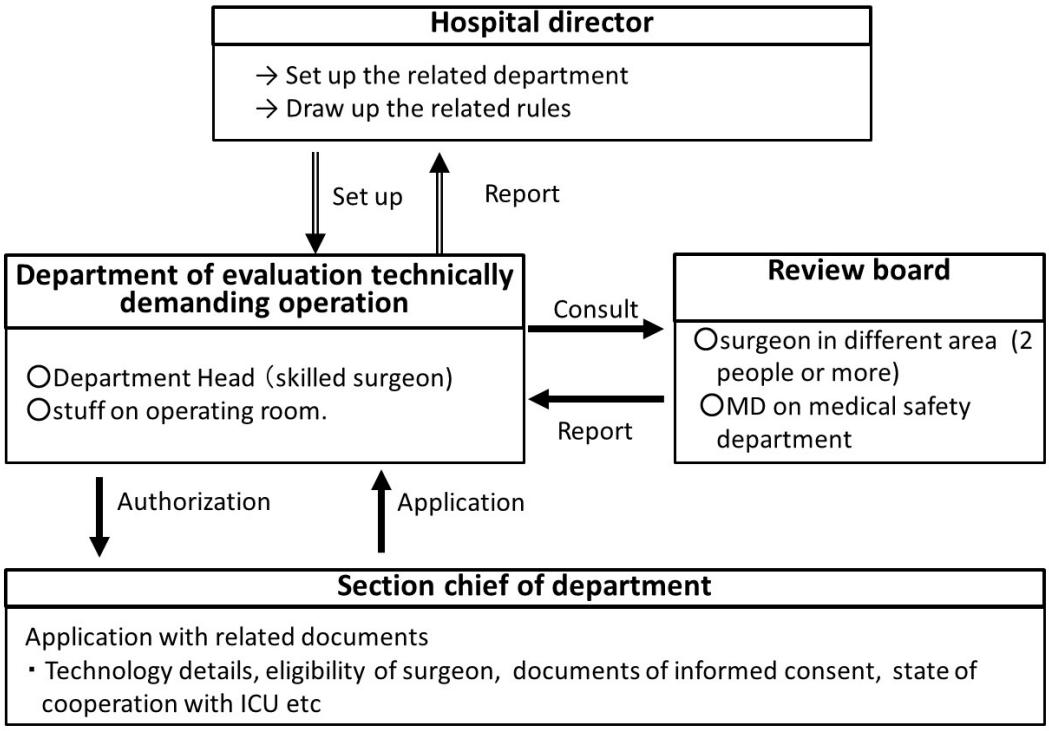

Figure 1. Framework of regulations when newly introducing a technically demanding operation imposed by medical care act. This regulation was enforced on the 10 of June in 2016. Special Functioning Hospitals are obligated, and other hospitals are obligated to make a sincere effort.

the Medical Service Law (*5*), and decided to impose certain procedures or regulations on each hospital in Japan, requiring them to check the status of informed consent, skill of surgery team and governance system of the surgical unit, when medical practitioners are going to introduce highly difficult new medical technologies that severely effects patients (Figure 1) (*6*).

In addition, in order to firmly establish this new system for the introducing process of highly difficult medical technologies, the Ministry of Health, Labor and Welfare organized a Special Research Group on Evaluation and Improvement of Clinical Guidelines Concerning Introducing Process of Highly Difficult New Medical Technologies (hereinafter referred to as "special research group"), where they, together with related academic societies, tried to survey the current situation for guidelines and consensus regarding introducing processes of highly difficult new medical technologies in Japan and overseas (*7*).

In this study, we present the research findings on current status of such clinical guidelines in Japan and overseas, *via* survey of questionnaires, document retrieval, and expert interviews. Furthermore, with reference to the survey results, we proposed a new practice guideline to regulate the introduction process of highly difficult new medical technologies in each hospital in Japan.

2. Materials and Methods

2.1. *Survey of the guidelines in Japan*

A questionnaire survey conducted between August 12 and September 28, 2016 for the documents related to the introduction process of the highly difficult new medical technologies were sent to the 18 academic societies (Table 1) belonging to the Japanese Medical Specialty Board. Based on the inquires, we received a response from all 18 academic societies, and 38 related documents were gathered. After second-round selection, 32 published documents were assigned to this study for further analysis. Especially, among these documents, we investigated the presence/absence of descriptions of "surgeon's requirement", "guidance system for the introduction", "medical safety related to facility standards" and "informed consent".

2.2. *Survey of the guidelines overseas*

From the information published at the National Guideline Clearinghouse (NGC, issued from 2004 to 2016) operated by the Agency for Healthcare Research and Quality (AHRQ, USA) and the National Institute for Health and Care Excellence (NICE, UK), literature surveys were conducted in July 2016 regarding the presence or absence of overseas clinical practice guidelines related to surgery and procedures. The retrieval keywords included "technology appraisal guidance", "medical technologies guidance", "surgeon credentialing", "training guidelines", "privileging qualified surgeons", "minimal requirements for granting privileging surgeons", and "technically demanding surgery".

Table 1. Survey on the documents related to introduction process of the highly difficult new medical technologies in 18 academic societies in Japan

Title of documents	Organization	Contents			
		Surgeon's requirement	Guidance system	Medical safety	Informed consent
▪ Guidelines for endoscopic surgical procedures	Japan Society for Endoscope Surgery	○	○	–	–
▪ Recommendations on introducing endoscopic surgery assisted robotic surgery		○	○	○	–
▪ Consensus for introduction of new medical devices		–	–	–	–
▪ Compliance with the conditions for introducing robot-assisted endoscopic surgery		–	–	–	–
▪ Proper usage guidelines for percutaneous transluminal cerebral thrombus collection device	The Japan Stroe Society, the Japan Neurosurgical Society, the Japanese Society for NeuroEndovascular Therapy	○	–	○	–
▪ Proper usage guidelines for intracranial artery stent (for arteriosclerosis)		○	–	○	–
▪ Intracranial artery stent (Flow Diverter for treatment of cerebral aneurysm) Proper usage guidelines		○	–	○	–
▪ Requirements such as system for appropriate use of cranial nerve area medical devices	The Japan Society for Endoscopic Surgery, The Japan Neurosurgical Society, Japanese Society of Interventional Radiology	○	○	–	–
▪ Transcatheteric aortic valve replacement surgery implementation facility standard	Council for Transcatheteric Aortic Valve Replacement Surgery Related Association	○	○	○	–
▪ Institutional criteria for use of human skeletal muscle derived cell sheets and practicing medical standards	Human Skeletal Muscle Derived Cell Sheet Related Academic Conference	○	–	○	–
▪ Implantable assistant artificial heart certification facility · Physician update standard	Association for Assistive Cardiac Therapy	○	○	○	–
▪ Certification Criteria for Heart Transplant Implementation Facilities	Council for Heart Transplant Association	○	○	○	○
▪ Criteria for thoracic aortic aneurysm stent graft implementation	Japan Stent Graft Implementation Standards Management Committee	○	○	○	–
▪ Call attention to academic society members	Japan Society for Endoscope Surgery, Japanese Society of Hepato–Biliary–Pancreatic Surgery, The Japanese Society of Gastroenterological Surgery, Japan Surgical Society	–	–	–	○
▪ Implementation guidelines for vagal nerve stimulation therapy for epilepsy	Japan Epilepsy Society	○	○	–	–
▪ Guidelines on indication for epilepsy surgery		–	–	–	–
▪ Guidelines on the diagnosis of internal medial temporal lobe epilepsy and surgical adaptation		–	–	–	–
▪ Surgical treatment guidelines for neocortical epilepsy		–	–	–	–
▪ Brain tumor clinical practice guidelines	The Japan Society for Neuro–Oncology	–	–	–	–
▪ Brain tumor clinical practice guideline: central nervous system primary malignant lymphoma		–	–	–	–
▪ Urological laparoscopic surgery guideline 2014 edition	Japanese Society of Endourology	–	–	–	–
▪ Guidelines for conducting da Vinci assisted surgery in the field of urology	The Japanese Urological Association, Japanese Society of Endourology	○	○	○	○
▪ Guidelines on robot–assisted surgery for gynecological malignancies	Japan Society of Obstetrics and Gynecology	○	○	○	○
▪ Guidelines on robot–assisted surgery for gynecological malignancies	Japanese Ophthalmological Society	○	–	–	○
▪ Cataract surgery Combined intraocular drain requirement criteria		○	–	–	–
▪ Guidelines for refractive surgery		○	–	–	○
▪ Lens Expansion Ring Usage Guidelines		○	–	–	○
▪ Endoscopic surgical guidelines for obstetrics and gynecology	Japan Society of Obstetrics and Gynecology	○	○	–	○
▪ Guidelines for Certification System for Awakening Brain Surgery Facilities	The Japan Neurosurgical Society	○	–	○	–
▪ Guidelines for Acute Blood Purification Therapy for Neonates by Extracorporeal Circulation	Japan Pediatric Society	–	–	–	○
▪ Adaptation guidelines for catheter treatment for congenital and childhood onset heart disease		○	–	–	–
▪ Congenital heart disease, Guidelines for catheter treatment for structural heart disease of cardiovascular vessels (structural heart disease)		○	–	○	○

NICE and NGC were main databases of trustworthy clinical practice guidelines. NICE has integrated the systematic methods of clinical practice guidelines development, and NGC has adopted criteria for inclusion of clinical practice guidelines in NGC (→2013 (Revised) Criteria for Inclusion of Clinical Practice Guidelines in NGC).

2.3. *Expert interview for in-depth discussion*

We also interviewed two surgical professors, a gastrointestinal surgeon and a cardiac surgeon at the National University of Singapore, about the process of introducing highly difficult new medical technologies in Singapore, and discussed the current situation in Western and Asia-Pacific countries.

3. Results

3.1. *Survey of the guidelines in Japan*

We examined the contents of 32 published documents released by 18 academic societies belonging to the Japanese Medical Specialty Board out of 38 related documents gathered as a result of the survey in Japan. Among the 32 documents, 22 included at least one of the following items: surgeon's requirement (22 documents, 68.8%); guidance system (11 documents, 34.4%); medical safety matters (13 documents, 40.6%), and informed consent (10 documents, 31.3%). These descriptions were described as the general parts of the guidelines, or were commented on as the question and answer (Q & A) system. These documents belonged to guidelines (9 documents, 28.1%), guidance (4 documents, 12.5%) and other categories. A list of the documents is shown in Table l.

3.2. *Survey of the guidelines overseas*

We surveyed the website of the NGC (issued from 2004 to 2016) operated by the AHRQ (*https://www.guideline.gov*) as the category of "Surgery" and 390 guidelines were selected. Among them, 75 were further selected (published in 2011-2016) after a quality control based on whether the guidelines matched the criteria for NGC publication was performed (*8*). A list of these documents is shown in Table 2. Although two of the 75 documents were listed through a title search for corresponding documents, we found no descriptions regarding clinical practice guidelines when newly introducing highly difficult new medical technologies (*9,10*).

On the NICE website (*https://www.nice.org.uk/guidance*), we searched the category of "Technology appraisal guidance" and "Medical technologies guidance". We found 188 cases and 28 cases, respectively (issued between 2011 and 2016). However, after conducting a title search for these cases, there were no documents describing the introduction of the highly difficult new medical technologies.

Also on the NICE website, we searched for keywords such as "surgeon credentialing", "training guidelines", "privileging qualified surgeons", "minimal requirements for granting privileging surgeons", and "technically demanding surgery", and as a result, eight documents were selected. After an extensive evaluation of the contents, two documents were matched, "Laparoscopic repair of abdominal aortic aneurysm" and "Laparoscopic retroperitoneal lymph node dissection for testicular cancer" (*11,12*) (Table 3). Both documents included guidance for "informed consent that the procedure is technically difficult", "registering the procedure in a database", and "performing the procedure with a multidisciplinary team", although the contents are simple and thin with only one page.

3.3. *Expert interview for in-depth discussion*

As a result of the interview survey with the surgeons from the National University of Singapore, there is no unified rule in Singapore regulated by the government, and there is a unique arrangement in the National University of Singapore Hospital that a preliminary review is carried out when newly introducing technically demanding operations. In addition, as clinical practice for robotic surgery in Singapore, "A consensus document on robotic surgery" (*13*) is routinely used. This document was prepared by a consensus group consisting of academic organizations in the United States, and contained necessary and sufficient conditions for technically demanding operations, in which detailed descriptions regarding surgeon's requirements, guidance system for the introduction, and medical safety related to the facility standards are included (Table 4).

3.4. *The new practice guideline proposed in Japan to regulate the introducing process of highly difficult new medical technologies in the hospital*

With reference to the survey of questionnaire and document retrieval, our special research group proposed a new practice guideline to regulate the introducing process of highly difficult new medical technologies in each hospital in Japan (*14*), which are controlled by the ministerial ordinance for the Medical Service Law (Table 5). This guideline provided a comprehensive view on the interpretation of "high difficulty new medical technology" prescribed by the law so that the medical institution can properly understand or judge. In addition, we show the basic idea at preliminary examination from the viewpoints of "Surgeon's requirement ", "Guidance system", "Medical safety" , and "Informed consent".

Table 2. Survey of national guidelines overseas from NGC operated by the AHRQ published from 2011 to 2016

Published Year	Title of clinical practice guidelines
2016	▪ Practice guidelines for the prevention, detection, and management of respiratory depression associated with neuraxial opioid administration: an updated report by the American Society of Anesthesiologists Task Force on Neuraxial Opioids and the American Society of Regional Anesthesia and Pain Medicine. ▪ Guideline for prevention of retained surgical items. ▪ Guideline for care of the patient receiving moderate sedation/analgesia.
2015	▪ Blood transfusion. ▪ Guideline for prevention of unplanned patient hypothermia. ▪ Prophylaxis against infective endocarditis: antimicrobial prophylaxis against infective endocarditis in adults and children undergoing interventional ▪ procedures. ▪ Treatment of Cushing's syndrome: an Endocrine Society clinical practice guideline. ▪ Everolimus for preventing organ rejection in liver transplantation. ▪ Merkel cell carcinoma. ▪ Lower urinary tract symptoms in men: assessment and management. ▪ Venous thromboembolism in adults admitted to hospital: reducing the risk. ▪ Society for Vascular Surgery practice guidelines for atherosclerotic occlusive disease of the lower extremities: management of asymptomatic ▪ disease and claudication. ▪ Bladder cancer: diagnosis and management. ▪ Platelet transfusion: a clinical practice guideline from the AABB. ▪ Practice guidelines for perioperative blood management: an updated report by the American Society of Anesthesiologists Task Force on ▪ Perioperative Blood Management. ▪ Gastro-oesophageal reflux disease: recognition, diagnosis and management in children and young people. ▪ Peyronie's disease: AUA guideline. ▪ ACR Appropriateness Criteria® radiologic management of hepatic malignancy. ▪ American Geriatrics Society abstracted clinical practice guideline for postoperative delirium in older adults. ▪ ACR Appropriateness Criteria® routine chest radiography.
2014	▪ Guideline for autologous tissue management. ▪ Intrapartum care: care of healthy women and their babies during childbirth. ▪ Acromegaly: an Endocrine Society clinical practice guideline. ▪ Guideline for preoperative patient skin antisepsis. ▪ Optimal systemic therapy for early female breast cancer. ▪ Locoregional therapy of locally advanced breast cancer (LABC). ▪ Dyspepsia and gastro-oesophageal reflux disease. Investigation and management of dyspepsia, symptoms suggestive of gastro-oesophageal reflux ▪ disease, or both. ▪ Drug allergy: diagnosis and management of drug allergy in adults, children and young people. ▪ Management of venous leg ulcers: clinical practice guidelines of the Society for Vascular Surgery and the American Venous Forum. ▪ Systemic therapy for patients with advanced human epidermal growth factor receptor 2-positive breast cancer: American Society of Clinical ▪ Oncology clinical practice guideline. ▪ 2013 AHA/ACC/TOS guideline for the management of overweight and obesity in adults: a report of the American College of Cardiology/American Heart Association Task Force on Practice Guidelines and The Obesity Society. ▪ Pheochromocytoma and paraganglioma: an Endocrine Society clinical practice guideline. ▪ Guidelines for laparoscopic peritoneal dialysis access surgery. ▪ Management of primary cutaneous squamous cell carcinoma. A national clinical guideline. ▪ Timing and type of surgical treatment of Clostridium difficile-associated disease: a practice management guideline from the Eastern Association ▪ for the Surgery of Trauma. ▪ Sentinel lymph node biopsy for patients with early-stage breast cancer: American Society of Clinical Oncology clinical practice guideline update. ▪ Clinical practice guideline on diagnosis and treatment of hyponatraemia. ▪ Pressure ulcers: prevention and management of pressure ulcers. ▪ Medical management of kidney stones: AUA guideline. ▪ Cervical spine injury medical treatment guidelines. ▪ Low back pain medical treatment guidelines. ▪ Total hip replacement and resurfacing arthroplasty for end-stage arthritis of the hip (review of technology appraisal guidance 2 and 44). ▪ Guideline for care of the patient receiving local anesthesia. ▪ Interventions for prevention and treatment of pressure ulcers. In: Prevention and treatment of pressure ulcers: clinical practice guideline. ▪ Adult weight management evidence-based nutrition practice guideline ▪ VA/DoD clinical practice guideline for the management of upper extremity amputation rehabilitation. ▪ ACR Appropriateness Criteria® aggressive nonmelanomatous skin cancer of the head and neck. ▪ ACR Appropriateness Criteria® blunt chest trauma – suspected aortic injury. ▪ Treatment of pressure ulcers. In: Prevention and treatment of pressure ulcers: clinical practice guideline. ▪ Blood transfusion in the management of sickle cell disease. In: Evidence-based management of sickle cell disease. ▪ ACR Appropriateness Criteria® radiologic management of lower gastrointestinal tract bleeding ▪ Special populations. In: Prevention and treatment of pressure ulcers: clinical practice guideline. ▪ ACR Appropriateness Criteria® resectable stomach cancer. ▪ Guideline for surgical attire. ▪ Managing acute complications of sickle cell disease. In: Evidence-based management of sickle cell disease. ▪ ACR Appropriateness Criteria® radiologic management of infected fluid collections. ▪ ACR Appropriateness Criteria® ductal carcinoma in situ. ▪ Guideline for management of wounds in patients with lower-extremity arterial disease. ▪ VA/DoD clinical practice guideline for screening and management of overweight and obesity

AHRQ, Agency for Healthcare Research and Quality; NGC, National Guideline Clearinghouse.

Table 2. Survey of national guidelines overseas from NGC operated by the AHRQ published from 2011 to 2016 (Continued)

Published Year	Title of clinical practice guidelines
2013	▪ Management of obstructive sleep apnea in adults: a clinical practice guideline from the American College of Physicians. ▪ Intraoperative tests (RD-100i OSNA system and Metasin test) for detecting sentinel lymph node metastases in breast cancer. ▪ Summary of evidence-based guideline: periprocedural management of antithrombotic medications in patients with ischemic cerebrovascular disease. Report of the Guideline Development Subcommittee of the American Academy of Neurology. ▪ Clinical practice guideline on the management of invasive meningococcal disease. ▪ Clinical practice guidelines for the management of overweight and obesity in adults, adolescents and children in Australia. ▪ Clinical practice guidelines for the management of rotator cuff syndrome in the workplace.
2012	▪ Depth of anaesthesia monitors – Bispectral Index (BIS), E-Entropy and Narcotrend-Compact M. ▪ SonoVue (sulphur hexafluoride microbubbles) – contrast agent for contrast-enhanced ultrasound imaging of the liver. ▪ Red blood cell transfusion: a clinical practice guideline from the AABB. ▪ Early thrombus removal strategies for acute deep venous thrombosis: clinical practice guidelines for the Society for Vascular Surgery and the ▪ American Venous Forum. ▪ Patient blood management guidelines: module 4 - critical care. ▪ Patient blood management guidelines: module 2 - perioperative.
2011	▪ Updated Society for Vascular Surgery guidelines for management of extracranial carotid disease. ▪ The care of patients with varicose veins and associated chronic venous diseases: clinical practice guidelines of the Society for Vascular Surgery and ▪ the American Venous Forum. ▪ Patient blood management guidelines: module 1 - critical bleeding/massive transfusion. ▪ Guideline for processing flexible endoscopes.

AHRQ, Agency for Healthcare Research and Quality; NGC, National Guideline Clearinghouse.

Table 3. Survey of national guidelines overseas from NICE

Title of documents	Organization	Contents			
		Surgeon's requirement	Guidance system	Medical safety	Informed consent
▪ Laparoscopic retroperitoneal lymph node dissection for testicular cancer	National Institute for Health and Care Excellence	○		○	○
▪ Laparoscopic repair of abdominal aortic aneurysm		○		○	○

NICE, National Institute for Health and Care Excellence.

4. Discussion

In Japan, medical safety incidents in medical institutions that are well-equipped with medical facilities and human resources happen one after another when introducing high difficulty medical technology, and these incidents have become a social problem in 2016. Difficulty of hospital governance especially regarding the high level of expertise in surgery and procedures has been pointed out as the cause of these incidents. Therefore, it is an effective approach for the government to impose certain procedures from the viewpoint of securing medical safety for hospitals providing advanced medical care on the process of introducing "high difficulty new medical technology" and to establish cooperative relationships between government and hospitals and relevant academic societies by law.

The results of the present report indicate that before June 2016, there were no rules or guidelines regarding the introducing process of highly difficult new medical technologies at the governmental or ministerial levels in Japan and/or overseas.

Through our survey of document retrieval from Japan, we found that there are several documents specific to certain diseases or surgical procedures that describe the surgeon's requirements, a governance system for the surgical team, and other medical safety matters such as informed consent, and that the rules are organized by academic bodies or special committees, with the rules published as recommendations or guidance for the members of academic societies (Table 1). Thus, since these documents are recommendations or guidance, medical practitioners are not legally obliged to follow them.

Through the overseas survey, we were only able to find two simple regulations for laparoscopic surgery (*11,12*) and one comprehensive guidance for robotic surgery (A consensus document on robotic surgery) (*13*). The robotic surgery guidance was made by a consensus group consisting of academic organizations, and had detailed descriptions of the surgeon's requirements, guidance system for introducing the procedure, and medical safety related to the facility standards (Table 4). However, these documents are also recommendations and guidance, and there are no rules issued at governmental or ministerial levels that legally have to be followed.

The results of our survey confirm that documentation related to the introduction process of highly difficult new

Table 4. Description about "surgeon's requirement", "guidance system for the introduction", "medical safety related to the facility standards" on "A consensus document on robotic surgery, Appendix I: Guidelines for Institutions Granting Privileges in Therapeutic Robotic Procedures"

Contents	Description
Surgeon's requirement	II. Minimum Requirements for Granting Privileges Part A. Formal Specialty Training Prerequisite training must include satisfactory completion of an accredited surgical residency program, with subsequent certification by the applicable specialty board or an equivalent as required by the institution. D. Practical Experience 1. Applicant's Experience – Documented experience that includes an appropriate volume of cases with satisfactory outcomes, equivalent to the procedure in question in terms of complexity. The chief of service should determine the appropriateness of this experience.
Guidance system for the introduction	II. Minimum Requirements for Granting Privileges Part D. Practical Experience 1. Initial clinical experience on the specific procedure must be undertaken under the review of an expert and may include assisting. An adequate number of cases to allow proficient completion of the procedure should be performed with this expert review IV. Maintenance of Privileges C. Continuing Medical Education Continuing medical education related to the field should be required as part of the periodic renewal of privileges. Attendance at appropriate local, national or international meetings and courses is encouraged.
Medical safety related to the facility standards	I. Principles of Privileging C. Responsibility for Privileging The privileging structure and process remain the responsibility of the institution at which privileges are being sought. It should be the responsibility of the specialty department, through its chief to recommend privileges for individual surgeons to perform procedures. These recommendations should then be approved by the appropriate institutional committee, board, or governing body. III. Institutional Support It is necessary that the staff and technical support team undergo a similar formal technical training with the device before its use in a clinical scenario. Therapeutic robotic surgery requires technical support and must be approached with a team concept. IV. Maintenance of Privileges A. Provisional Privileges Once competence has been determined, a period of provisional privileges may be appropriate. The time frame and/or number of cases during this period should be determined by the chief of service and/or the appropriate institutional committee, board, or governing body. B. Monitoring of Performance Once privileges have been granted, performance should be monitored through existing quality assurance mechanisms at the institution. These mechanisms may be modified as appropriate, and should evaluate outcomes, as well as competency in the complete patient care process. E. Denial of Privileges Institutions denying, withdrawing, or restricting privileges should have an appropriate mechanism for appeal in place. The procedural details of this should be developed by the institution, and must satisfy the institution's bylaws and institutional recommendations

medical technologies is very rare, and the regulations that we found were mainly issued by academic societies. Moreover, even if such documentation existed, the quality of the regulations is poor and not enough to perform surgical practice safely. Therefore, for medical practitioners, comprehensive and concrete regulations should be issued by the government or ministry to follow legally with regard to technically demanding operations. With exceptional cases in the drug development and organ transplantation fields, there are several rules that have been issued by academic societies that are supported by law, such as the Pharmaceuticals and Medical Devices Act, and the Organ Transplant Act".

Before June 2016, there had been no consensus or rules for the introduction process for the technically demanding surgical procedures, and the process basically relies on the surgeon's decision or institutional common sense. However, these situations may cause a risk for patients with serious complications due to poor surgical technique and, in Japan, there have been reported problematic cases regarding technical safety for technically demanding operations such as laparoscopic liver resection and laparoscopic pancreatic resection. Therefore, for the Japanese Ministry of Health, Labor and Welfare to impose a certain procedure or regulations for a newly introducing process of a technically demanding operation is a very meaningful, impactful and innovative approach, from a medical safety point of view. Based on the new rules in Japan, each hospital needs to check the status of informed consent, skill of the surgery team, and governance system of the surgical unit, when medical practitioners are going to introduce highly difficult medical technology or technically demanding operation, each step of which is followed by an audit, evaluating and reporting system.

Furthermore, in introducing regulations to areas with high specialization, a special research group was established composed of experts before the system was enforced. This special research group, with the cooperation of the Japan Medical Society, proposed a new practice guideline which showed a comprehensive idea on preliminary review conducted at the hospital in introducing highly difficult new medical technology. This guideline is made with reference to relevant descriptions

Table 5. Basic approach for the introduction of highly difficult new medical technologies in each hospital of Japan proposed by our special research group

Criteria	Contents
Criteria "highly difficult" for "highly difficult new difficult medical technologies"	It is stipulated by laws and regulations that "high difficult" means that the death or other serious effects of the patient will be assumed by the implementation for the hospital due to the high level of technical difficulty of the medical technology. We showed our views , other serious effects includes "Permanent or prominent Failure or malfunction". We also showed our views, when each hospital judges the suitability of "high difficulty", the list that comprehensively grasp the technical difficulty level of surgical operations and procedures performed in Japan in cooperation with related academic societies in relation to the public insurance system, will be helpful for Medical institutions. In addition Medical technologies that are not widely disseminated should be judged individually and carefully at individual medical institutions for their suitability.
Criteria "new" for "highly difficult new medical technologies"	It is stipulated by laws and regulations that "New" is judged depending on whether it corresponds to "medical technology that has never been implemented at the hospital excluding minor modification, and so forth,)" or not. We showed our views that whether or not it corresponds to the "minor modification,and so forth" is judged on the degree of difference in "target disease", "expected result", "degree of difference in frequency and content of complications". And Emergency operation also corresponds to "minor modification, and so forth".
Surgeon's requirement	Skill of surgeon's should be matched to the standards established by academic societies If there is a standard the "highly difficult new medical technologies" the hospital is try to introduce. If academic society have a specific training course or qualification for the "highly difficult new medical technologies", it is desirable that surgeon's have completed the training or qualified. If there is no standard by academic societies, surgeon need Professional qualifications of basic area academic societies related to the "highly difficult new medical technologies". Regarding new medical technology that is not widely spread in the public, the surgeon should have the experience of similar surgery to "highly difficult new medical technologies".
Guidance system	Meet the criteria on the way of "guidance system" based on the guidelines, *etc*. established by academic societies. In addition, take one of the following measures: 1. Before introduction, as a medical team including surgeons *etc*., visit medical institutions that are experienced in providing the "highly difficult new medical technologies"; 2. When the "highly difficult new medical technologies" is provided, those who are experienced in the technology are invited, and surgeons should be under the guidance.
Medical safety	Meet the criteria on the way of "Facility standards" and "implementation standards" based on the guidelines, *etc*. established by academic societies. Take sufficient cooperation before performing surgery among staff concerned such as operating room, intensive care room, anesthesiologist, nursing department *etc*. About 5 cases after introduction should report the description contents such as surgical record, medical record, *etc*. to the department in charge. ※Regarding the specific number of cases requiring reporting, the department in charge of " highly difficult new medical technologies" should fully set up the contents of the offer from the department and set it in advance based on the opinion of the high-difficulty new medical technology evaluation committee.
Informed consent	A doctor who provides highly difficult medical technology or the attending doctor of the patient should explain to the patient under the presence of medical persons of different paramedical personal. Explanation is done by the document, and the description content should include the following items: 1. Past surgical results in medical institutions related to the "highly difficult medical technology"; 2. Provision of facilities and systems; 3. Professional qualifications of surgeons and previous surgical experience; 4. Efficacy and safety (including comparison with alternative therapies).

special research group, Special Research Group on Evaluation and Improvement of Clinical Guidelines Concerning Introducing Process of Highly Difficult New Medical Technologies.

of domestic and foreign guidelines revealed in this survey for the purpose that the hospital can comply with laws and regulations and conduct the appropriate preliminary examination.

By introducing high-difficulty new medical technology based on these guidelines, Hospitals will comply with laws and regulations by introducing high-difficulty new medical technology based on these guidelines, and as a result, hospitals will be able to appropriately provide medical care with adequate difficulty to patients.

Also the special research group asked academic societies in each specialized field to actively disseminate information necessary for preliminary examination,"surgeon's requirement","guidance system"," medical safety" "informed consent", with

respect to individual high-difficulty new medical technologies. These efforts will contribute to the improvement of the quality of guidelines created by academic societies regarding "Highly Difficult New Medical Technology". Hopefully, Cooperative efforts by medical institutions, academic societies, and administrative agencies can contribute to reduce risk for patients receiving the technically demanding surgical procedures.

In conclusion, through domestic and overseas surveys, we found that there are no rules for how to introduce technically demanding operations at the governmental or ministerial levels. Therefore, new rules presupposing cooperation between administration, academia and medical institutions issued by the Japanese Ministry of Health, Labor and Welfare are a meaningful and novel approach.

Acknowledgements

This survey was supported by Ministry of Health, Labour and Welfare Sciences Research Grants, Special Research. The findings and conclusions of this article are solely the responsibility of the authors, and do not represent the official views of the Ministry of Health, Labour and Welfare.

We thank Prof. Jimmy So, Head & Senior Consultant, Division of General Surgery; Prof. Lee Chuen Neng, Head, Department of Surgery, the National University of Singapore for interviewing. The authors thank Peipei Song Ph.D. for her devoted work in preparing the manuscript.

We thank all members from Special Research Group, ADACHI Hideo, ICHIKAWA Tomohiko,UETAKE Yuzaburo, SETO Yasuyuki, TOGASHI Junichi, HASEGAWA Kiyoshi, FUJII Tomoyuki, MATSUNO Akira, DOKI Yuuichirou, and NAKAMURA Masafumi.

References

1. Angst E, Hiatt J R, Gloor B, Reber H A ,Hines O J. Laparoscopic surgery for cancer: A systematic review and a way forward. J Am Coll Surg. 2010; 211:412-423 .
2. D'Amico TA. Long-term outcomes of thoracoscopic lobectomy. Thorac Surg Clin. 2008; 18:259-262.
3. The Japan Times. Gunma hospital reveals ninth death following laparoscopic surgery. *https://www.japantimes.co.jp/news/2014/11/19/national/gunma-hospital-reveals-ninth-death-following-laparoscopic-surgery/#.W4DqNegzaUk* (accessed August 25, 2018)
4. Kaneko H, Otsuka Y, Kubota Y, Wakabayashi G. Evolution and revolution of laparoscopic liver resection in Japan. Ann Gastroenterol Surg. 2017; 1:33-43.
5. Government of Japan. Medical Care Act. *http://www.japaneselawtranslation.go.jp/law/detail/?id=2199&vm=04&re=01* (accessed August 25, 2018) (in Japanese)
6. Ministy of Health Labor and Welfare. About Medical Care by the newly introducing technically demanding operation Technologies and Unapproved Medical Products. *https://www.mhlw.go.jp/stf/seisakunitsuite/bunya/0000145803.html* (accessed August 25, 2018) (in Japanese)
7. Chairman of The Japanese Association of Medical Sciences. Basic Approach to Medical safety assessed for the newly introducing process of the technically demanding operation. *http://jams.med.or.jp/news/043.html* (accessed August 25, 2018) (in Japanese)
8. Special Research group on evaluation and improvement of clinical practice guideline for newly introducing process of the technically demanding operation. Basic concept of newly introducing process of the technically demanding operation. *http://jams.med.or.jp/news/043_1.pdf* (accessed August 25, 2018) (in Japanese)
9. Criteria for Inclusion in The National Guideline Clearinghouse (NGC) – Get Help, and give us Suggestions and Feedback. *http://help.magicapp.org/knowledgebase/articles/297449-criteria-for-inclusion-in-the-national-guideline-c* (accessed August 25, 2018)
10. NICE. Total hip replacement and resurfacing arthroplasty for end-stage arthritis of the hip. *https://www.nice.org.uk/guidance/ta304/resources/total-hip-replacement-and-resurfacing-arthroplasty-for-endstage-arthritis-of-the-hip-review-of-technology-appraisal-guidance-2-and-44-82602365977285* (accessed August 25, 2018)
11. Lyman, GH, Somerfield MR, Bosserman LD, Perkins CL, Weaver DL, Giuliano AE. Sentinel lymph node biopsy for patients with early-stage breast cancer. American Society of Clinical Oncology Clinical Practice Guideline Update. J Clin Oncol. 2017; 35:561-564.
12. NICE. Laparoscopic repair of abdominal aortic aneurysm. *https://www.nice.org.uk/guidance/ipg229/resources/laparoscopic-repair-of-abdominal-aortic-aneurysm-pdf-1899865283911621* (accessed August 25, 2018).
13. NICE. Laparoscopic retroperitoneal lymph node dissection for testicular cancer. *https://www.nice.org.uk/guidance/ipg158/resources/laparoscopic-retroperitoneal-lymph-node-dissection-for-testicular-cancer-pdf* (accessed August 25, 2018).
14. Herron DM, Marohn M, SAGES-MIRA Robotic Surgery Consensus Group. A consensus document on robotic surgery. Surg Endosc. 2008; 22:313-325.

(Received September 17, 2018; Revised December 13, 2018; Accepted December 20, 2018)

Original Article

DOI: 10.5582/bst.2018.01178

Tissue-specific alternative splicing of pentatricopeptide repeat (PPR) family genes in *Arabidopsis thaliana*

Umme Qulsum[1], Toshifumi Tsukahara[1,2,3,*]

[1] *School of Materials Science, Japan Advanced Institute of Science and Technology (JAIST), Nomi City, Ishikawa, Japan;*
[2] *Area of Bioscience and Biotechnology, School of Materials Science, Japan Advanced Institute of Science and Technology (JAIST), Nomi City, Ishikawa, Japan;*
[3] *Division of Transdisciplinary Science, Japan Advanced Institute of Science and Technology (JAIST), Nomi City, Ishikawa, Japan.*

Summary **Alternative splicing is a post- and co-transcriptional regulatory mechanism of gene expression. Pentatricopeptide repeat (PPR) family proteins were recently found to be involved in RNA editing in plants. The aim of this study was to investigate the tissue-specific expression and alternative splicing of PPR family genes and their effects on protein structure and functionality. Of the 27 *PPR* genes in *Arabidopsis thaliana*, we selected six *PPR* genes of the P subfamily that are likely alternatively spliced, which were confirmed by sequencing. Four of these genes show intron retention, and the two remaining genes have 3' alternative-splicing sites. Alternative-splicing events occurred in the coding regions of three genes and in the 3' UTRs of the three remaining genes. We also identified five previously unannotated alternatively spliced isoforms of these *PPR* genes, which were confirmed by PCR and sequencing. Among these, three contain 3' alternative-splicing sites, one contains a 5' alternative-splicing site, and the remaining gene contains a 3'-5' alternative-splicing site. The new isoforms of two genes affect protein structure, and three other alternative-splicing sites are located in 3' UTRs. These findings suggest that tissue-specific expression of different alternatively spliced transcripts occurs in Arabidopsis, even at different developmental stages.**

Keywords: RNA editing, alternative splicing, PPR, Arabidopsis

1. Introduction

Alternative splicing is a bimolecular process in which multiple mRNAs are generated from the same gene through the selection of different splicing sites. This key process occurs in living organisms during development and is regulated in response to environmental factors (*1-3*). Surprisingly, up to 60% of multiexon-containing genes undergo alternative splicing (*4*). Core circadian clock genes are also controlled by alternative splicing in Arabidopsis under different environmental conditions (*4,5*). The functional consequences and effects of alternative splicing on plant phenotypes are an important focus of study (*4*).

Arabidopsis contains approximately 450 pentatricopeptide repeat (PPR) proteins (*6*). PPR proteins were first identified almost two decades ago (*7*). This important protein family is involved in a wide variety of cellular processes in plants, such as RNA editing (*8-10*), RNA stabilization (*11,12*), post-transcriptional RNA maturation (*13,14*), seed development (*15*), endonuclease activity (*16*), and various phenotypic effects (*17*). The PPR protein family comprises the P and PLS subfamilies. P proteins contain a 35 amino-acid classical tandem repeat known as the P motif. PLS subfamily proteins consist of a P motif, an S (short) 31 amino-acid motif, and an L (long) 35-36 amino-acid motif. The PLS subfamily can be divided into the PLS, DYW, and E subclasses. DYW and E proteins contain an additional, conserved C-terminal motif with deaminase properties that plays a distinct role in RNA editing in plants (*18-*

Released online in J-STAGE as advance publication December 17, 2018.

**Address correspondence to:*
Professor Toshifumi Tsukahara, Area of Bioscience and Biotechnology, School of Materials Science, Japan Advanced Institute of Science and Technology (JAIST), 1-1 Asahidai, Nomi City, Ishikawa 923-1292, Japan.
E-mail: tukahara@jaist.ac.jp

21). The DYW domain has C-to-U converting activity and shares similarity with the domain found in cytidine deaminase (*22*). The P subfamily members are mainly involved in RNA splicing, stabilization, cleavage, and the activation or repression of translation (*23*). PPR proteins primarily form complexes with other family members or sometimes with associated group members to form editosome complexes (*9*). In addition to the PLS subfamily, the P subfamily of PPR proteins is involved in RNA editing in plants (*21,24*).

RNA editing efficiency varies in different tissues and developmental stages, such as non-green tissues in seedlings and mature plants, although most RNA editing sites are found in green tissues (*25*). The PPR motif can be reprogrammed to target any RNA molecule (*26*). Recent advancements in the use of synthetic PPR molecules have created interest in programmable targeting to RNA substrates. Most PPR proteins localize to the mitochondria, chloroplasts, or both organelles, whereas very few localize to the cytoplasm and nucleus (*27*). Tissue-specific alternative splicing affects protein phosphorylation, which ultimately alters protein stability, enzymatic activity, subcellular localization in mammalian tissues (*28*). However, the role of extensive tissue-specific alternative splicing in plants is less well understood.

To date, most studies investigating alternative splicing have been performed using whole plants. However, we were interested in investigating this process in specific tissues and at particular developmental stages. The aim of the current study was to investigate tissue-specific alternative splicing of selected *PPR* genes in Arabidopsis seedling, leaf, stem, stipe, and root tissue. We also investigated the expression patterns of alternatively spliced transcripts in various Arabidopsis tissues on day 4, 8, 12, 16, 21, 27, and 32 of plant development. Finally, we performed bioinformatics analysis to investigate how alternative splicing affects protein diversity in this plant, shedding light on this important process during plant development.

2. Materials and Methods

2.1. *Plant growth conditions and sample collection*

Arabidopsis thaliana ecotype Colombia (Col-0) seeds were sown in paper pots containing a 1:2:1 mixture of horticultural perlite, peat moss, and vermiculite, covered with plastic wrap, and incubated for 3 to 4 days in the dark. The pots were transferred to a U-ING Green Farm hydroponic grow box (Osaka, Japan) in a growth room at 22°C, relative humidity 45%, and a 16 h light/8 h dark cycle. After germination, the plants were watered every morning and evening and fertilized twice weekly. Seedlings (whole plants on days 4, 8, and 12) and 16-, 21-, 27-, and 32-day-old leaf, stipe, stem, and root tissue were collected for analysis.

2.2. *RNA extraction and cDNA synthesis*

RNA was extracted from the samples using a Qiagen Plant Mini kit (Hilden, Germany, catalog no. 74904) according to the manufacturer's instructions. The RNA was treated with DNase (RQ1 RNase free DNase; Promega, Madison, WI, USA) to digest contaminating genomic DNA. After DNase treatment, the samples were purified by phenol-chloroform and ethanol precipitation. The final purified RNA was quantified using a NanoDrop (Thermo Fisher Scientific, Waltham, MA, USA). The cDNA was synthesized using reverse transcriptase (Superscript III, Invitrogen, Carlsbad, CA, USA) with oligo dT primers, which was confirmed using primers for the Arabidopsis housekeeping gene GAPDH: forward primer: GTTGTCATCTCTGCCCCAAG, reverse primer: TGCAACTAGCGTTGGAAACA.

2.3. *Selection of PPR candidate genes from the Arabidopsis genome and mRNA database*

Candidate of alternatively spliced genes were selected from various databases as follows: The accession numbers of 425 *PPR* genes were obtained from *https://www.ncbi.nlm.nih.gov/*. The accession numbers were used as queries against the www.plantgdb.org/AtGDB/ database to obtain a genomic map of each gene. Based on these genomic maps, likely alternatively spliced genes (whole genome model) were selected using At-TAIR10. After identifying 27 genes that are alternatively spliced and expressed in different tissues from the Arabidopsis information resource (TAIR; *https://www.arabidopsis.org/*), the full-length genomic DNA, mRNA, and cDNA of each gene was identified as well. Finally, for each gene, the whole genome sequence, intron-exon sequences, CDS, transcript sequence, and deduced protein sequence were downloaded from *http://atgenie.org and crosschecked*.

2.4. *Primer design*

Primers were designed using Primer3 primer design software (bioinfo.ut.ee/primer3-0.4.0/primer3/), and BLAST analysis was performed using NCBI/Primer BLAST. When the primers failed to produce the desired product, another set of primers was designed and tested. The primers (in TE buffer at a concentration of 50 pmol/μL under salt-free conditions) were purchased from Eurofins Genomics (Tokyo, Japan). Each primer set was diluted to 10 pmol/μL with TE buffer (working concentration).

2.5. *PCR and polyacrylamide gel image analysis*

PCR was performed using 30-35 cycles at a denaturation temperature of 94°C and an elongation temperature

Table 1. Candidates studied genes and accession number of PPR family proteins

Tentative Gene Name	Accession number	AT°C	Cycle	Sequence (5' → 3')	
				Forward	Reverse
PPR1	AT5G24060	55	30	GAACACAGAGGACGGAGGAG	TTGACTTCCCAGTTGGCTTC
PPR2	AT5G27300	58	30	GTTTTGATCCCACCCATCAC	TGAACGTGTTGGGACTGAAG
PPR3	AT2G19280	58	30	TGATCCCGAACAGTCTCAAGT	CTCTCATCTTCCTCCGGCTA
PPR4	AT4G38150	59	35	ATTTCCGTCTTTGGCTTGG	CAGTGCCTTTGGAGGATGAT
PPR5	AT1G30610	58	30	GGATATGGAAAGCCGTGGTA	GCCAGTGTAAGTCACCACGA
PPR6	AT1G05670	58	30	AAGAACTGATGCTGGTGCAA	TGGAGAGATGATGTGGCTCTT

All genes belong to the P-subfamily of PPR family proteins which were confirmed by PCR and sequencing. The table indicates annealing temperature, thermal cycle and primer sequences.

of 72°C (Table 1); the annealing temperature varied depending on the primer. The PCR products were subjected to electrophoresis on a ~6% polyacrylamide gel and stained with SYBR Green Dye (Lonza, Rockland, ME, USA). An equal amount of PCR product was subjected to polyacrylamide gel electrophoresis in a gel containing ethidium bromide. Each gel image was photographed using different exposure times to obtain high-quality images for analysis. The gel images were analyzed using LAS3000 software (Fujifilm, Tokyo, Japan). The experiments were conducted thrice ($n = 3$).

2.6. *Transcript sequencing*

The PCR products were sequenced on an Applied Biosystems 3130xl Genetic Analyzer (Foster City, CA, USA). The desired bands from PAGE were excised, transferred to a disposable pellet pestle/tissue grinder (Kimble®, Capitol Scientific, Inc., Austin, TX, USA, catalog no. 749520-0090), and incubated in a -80°C freezer for 1 h. The frozen gel piece was ground well with a pestle. Approximately 10 µL of 0.1× TE was added to the gel powder, followed by additional grinding. After discarding the pestle, the tube was vortexed for 10 min and centrifuged at full speed at 4°C for 20 min in a tabletop centrifuge. The supernatant was transferred to another tube, and 3 µL of sample was used for sequencing with a BigDye Terminator V3.1 Sequencing Standard kit (Applied Biosystems, Austin, TX, USA, catalog no. 4336935). However, in some samples where the PCR product was unable to sequence, in that case the PCR product was amplified by TA cloning using the pGEMT-Easy vector system (Promega, catalog no. A1360). The sequencing results using the reverse primers were reverse complemented using the online software, *http://www.bioinformatics.org/sms2/reference.html* (*29*). All sequencing results were aligned with the Arabidopsis genome *via* BLAST searches (*30*). The experiments were conducted thrice ($n = 3$).

2.7. *Analyzing the tissue-specific expression patterns of the isoforms of different PPR genes*

The PCR products were subjected to 6% polyacrylamide gel electrophoreses in 1× TBE buffer at 200 volts for 20 min. The gel was stained with SYBR Green Dye (Lonza) for 20 min in 1× TBE buffer in a constant rotating shaker. The gels were imaged using an LAS3000 Imaging System (Fujifilm). Image J software (NIH, MD, USA) was used for densitometry analysis of the bands for comparative expression analysis of the different alternatively spliced transcripts, which were confirmed by sequencing.

2.8. *Determining the effect of alternative splicing on protein diversity*

I-TASSER (Iterative Threading ASSEmbly Refinement) bioinformatics tools (*31-33*) were used to examine the effects of alternatively spliced isoforms on protein levels, as well as ligand-binding sites and the distances between residues. Each full-length amino-acid sequence was submitted to the I-TASSER server. The amino-acid sequence of each isoform was obtained from *http://atgenie.org*. However, the sequences of newly identified isoforms were transcribed using the ExPASy Translate tool. The amino-acid sequences were then submitted to the server with the desired output parameters, and data were obtained 1-2 weeks later. Various parameters were comparatively analyzed between the alternatively spliced isoforms.

3. Results

We identified 27 alternatively spliced genes of PPR family proteins from an Arabidopsis database (*https://www.ncbi.nlm.nih.gov*) that were differentially expressed in different tissues. Of these genes, we have selected six genes due to their functional importance for further analysis by semi-quantitative PCR and sequencing. We have represented the alternatively spliced isoforms of a gene in alphabetic order a, b, c, d.

3.1. *Tissue-specific expression patterns of the isoforms of different PPR geness*

In *PPR1* harboring a 3' alternative-splicing site, a 39 nucleotide (nt) sequence was added to exon 3, creating

PPR1c. This 3' alternative-splicing site was identified in 4, 8 and 12-day-old seedlings, in leaves on days 16, 21, 27, and 32, in stipes on days 16, 21, 27, and 32, in stems on days 16, 21, 27, and 32, and in roots on days 16, 21, 27, and 32 (Figure 1A-C). We detected another new, unannotated splice isoform containing a 3' alternatively spliced site resulting in an additional 15 nt sequence in exon 3, creating *PPR1b*, which was expressed in leaves on day 21 (Figure 1A-C). *PPR1c* expression gradually increased in stipes but gradually decreased in stems and roots; however, this isoform was highly expressed in all of these tissues on day 27 (Figure 1B).

In *PPR2* harboring a 3' alternatively spliced site, a 26 nt sequence was added to exon 2, creating *PPR2b*, a previously unannotated splicing product. The only 3' alternative-splicing site was activated in leaves on day 32 and in stems on days 16, 21, 27, and 32, but not in leaves on day 16 (Figure 2A-C). Both isoforms were expressed in leaf 21 and 27 days but *PPR2b* expression found higher in 21 days whereas *PPR2a* expression higher in 27 days. In leaves, *PPR2b* was expressed at gradually decreasing levels on days 21, 27, and 32 whereas *PPR2a* highly expressed on day 16 (Figure 2B). In stems, *PPR2a* was not expressed, but *PPR2b* was highly expressed. The expression of *PPR2b* in stems gradually increased on days 16, 21, and 27 but decreased on day 32 (Figure 2B).

In *PPR3*, a 73 bp intron sequence was retained within exons 3 and 4, creating *PPR3b*. This isoform was not expressed in seedlings on days 4 and 12, leaves on day 27, stipes on days 16, 21, and 32, stems on days 21 and 32, or roots on days 16, 21, and 32 (Figure 3A). In leaves, *PPR3a* expression gradually increased on days 16, 21, 27, and 32, with the expression level on day 32 almost twice that on day 16. In stipes, the expression of this splice isoform gradually decreased on days 16, 21, 27, and 32 (Figure 3B); this expression pattern is opposite to that detected in leaves.

In *PPR4*, a 325 bp intron sequence was retained between exons 1 and 2, producing *PPR4d* (Figure 4A). This splice isoform was expressed in almost all tissues except 21 days old stem and root (Figure 4A). We detected two new, unannotated splice isoforms, including one with an additional 5' 80 nt sequence in exon 1, creating *PPR4b*, and another with a 201 bp 5'-3' sequence within exons 1 and 2, creating *PPR4c*, as confirmed by Sanger sequencing (Figure 4A-C). *PPR4d* expression was higher in almost all tissues but *PPR4c* highly expressed in stipe 16 days and stem 32 days (Figure 4B).

In *PPR5*, an 84 bp intron sequence was retained between exons 7 and 8, creating *PPR5b* (Figure 5A). This splice isoform was not activated in seedlings on day 4, leaves on days 16 and 27, stipes on days 21 and 32, stems on day 21, or roots on days 21, 27, and 32 (Figure 5A). In *PPR6*, a 106 bp intron sequence was retained between exons 2 and 3, creating *PPR6c*. This isoform was not activated in seedlings on days 4, 8, and 12, leaves on days 16 and 32, stipes on days 16, 21, and 27, stems on days 16, 21, 27, and 32, or roots on days 16, 21, 27, and 32 (Figure 6A).

Finally, we detected another unannotated alternative-splicing event: a 3' alternative-splicing site resulting in a 9 nt deletion in exon 3, which was detected in stems on day 16, as confirmed by Sanger sequencing (Figure 6A-C). *PPR6b*, containing a 3' alternative-splicing site, is expressed in all tissues. On the other hand, a splice isoform, *PPR6c* with intron retention between exons 2 and 3 was expressed only in leaves on days 21 and 27 and in stipes on day 32 (Figure 6B).

3.2. *Determining the effect of alternative splicing on protein structure*

We detected alternative-splicing events in the coding regions of PPR1, PPR2, and PPR5. Next, we investigated whether alternative splicing affects protein structure. The secondary structure of PPR1 differs among the three isoforms (Table 2). Reference isoform PPR1c, a 3' alternative-splicing site leads to the in-frame addition of 39 nt encoding 13 amino acids: (CGFLKCYSDYITR; amino acids 48th-60th). Due to a 13 amino-acid addition to PPR1a, the number of alpha helices, beta sheets, and random coils is altered in the resulting isoform, PPR1c; PPR1c lacks a beta sheet in its upstream region but contains an additional alpha helix at its C-terminus (Figure 7D). Moreover, the distance among the first 100 residues in the upstream regions of these isoforms is nearly identical (Figure 7D). The addition or deletion of 13 amino acids may alter the ligand-binding ability of the isoforms (Figure 7F-G). PPR1b harbors a new 3' alternative-splicing site leading to the addition of a 15 nt sequence with an in-frame addition of five amino acids: DYITR (48th-52th) (Table 2). Interestingly, however, despite the addition of five amino acids in PPR1a, the number of alpha helices, beta sheets, and random coils remains unchanged (Table 2).

In PPR2, the reference isoform is PPR2a, and another new isoform, PPR2b (Table 2). In PPR2, a 26 nt addition resulted in a frameshift. In this case, the number of alpha helices and beta sheets changed, but the number of coils remained the same (Table 2). In PPR5, due to the addition of 28 amino acids (VNFVNPVVLKLIENLIYKADLVHTIQFQ; amino acids 719th–746th), number of alpha helices, beta sheets and random coil changed (Table 2).

4. Discussion

Much is known about alternative splicing in humans and animals, but little is known about this process in plants. In plants, alternative splicing is a highly diversified process, which greatly affects transcript diversity; in Arabidopsis, even a single nucleotide exon has been reported (*34*). In this study, we focused on

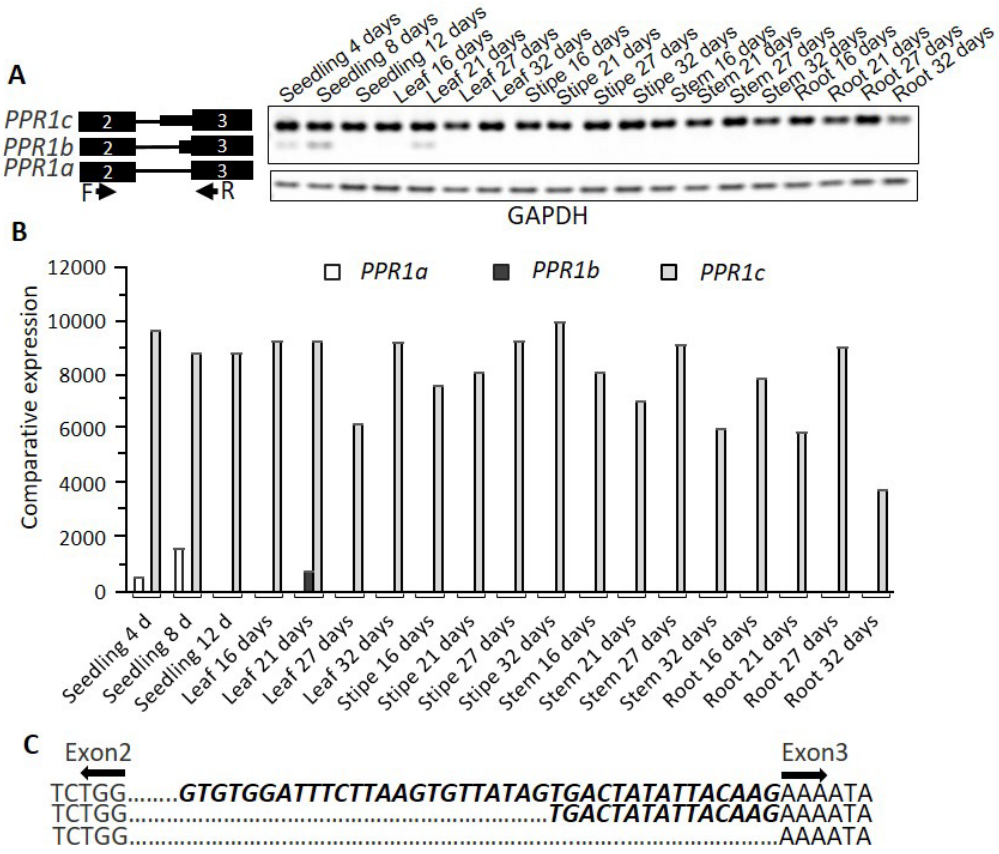

Figure 1. PCR and sequence analysis of PPR1 (accession no. AT5G24060). (A) PCR analysis of seedling, leaf, stipe, stem, and root tissue. Fragment size estimated from the gel in base pairs (bp). **(B)** Comparative expression analysis of three alternatively spliced isoforms in different tissues. **(C)** Genomic sequence of PPR1 from exon 2 to exon 3. Arrow indicates exon 2 and 3 boundary, and dots indicate intron sequences. Sequences in bold and italics indicate a 3′ alternative-splicing site.

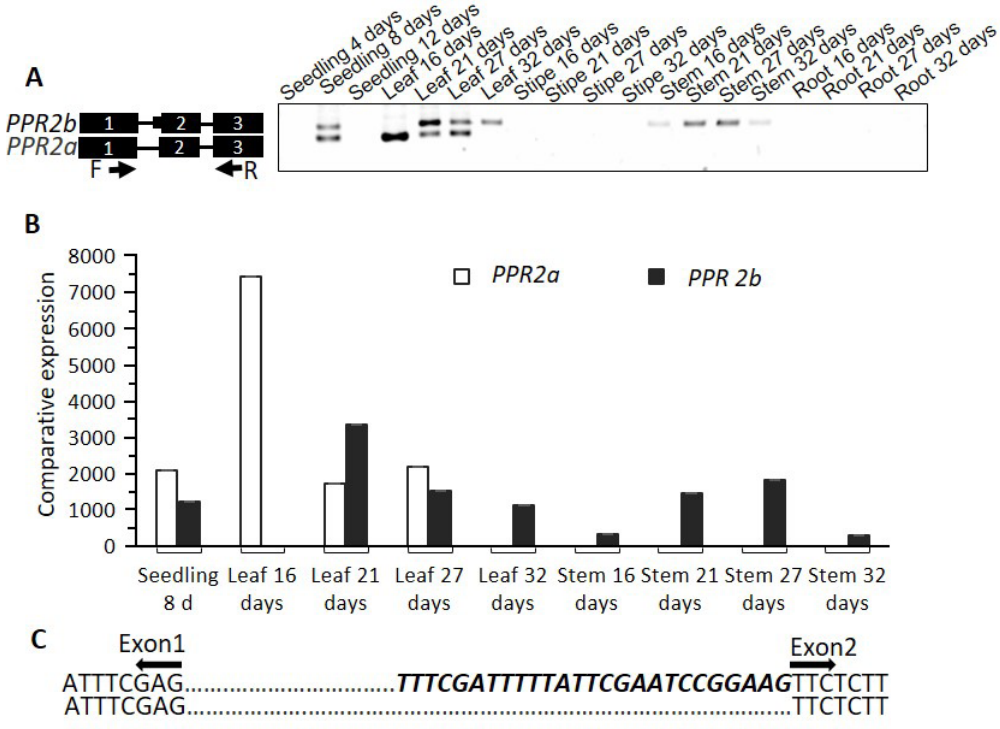

Figure 2. PCR and sequence analysis of PPR2 (accession no. AT5G27300). (A) PCR analysis of seedling, leaf, stipe, stem, and root tissue. Fragment size estimated from the gel in base pairs (bp). **(B)** Comparative expression analysis of two splice isoforms in different tissues. **(C)** Genomic sequence of PPR2 from exon 1 to exon 2. Arrow indicates the exon 1 and 2 boundary, and dots indicate intron sequences. Sequences in bold and italics indicate a 3′ alternative-splicing site.

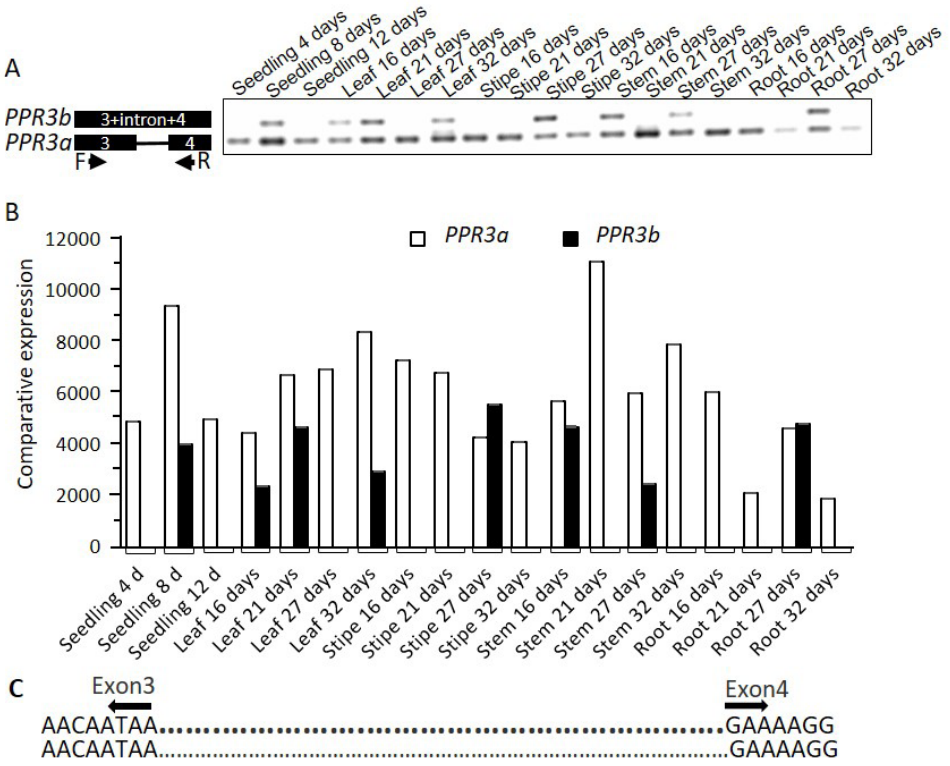

Figure 3. PCR and sequence analysis of PPR3 (accession no. AT2G19280). (A) PCR analysis of seedling, leaf, stipe, stem, and root tissue. Fragment size estimated from the gel in base pairs (bp). **(B)** Comparative expression analysis of the two splice isoforms in different tissues. **(C)** Genomic sequence of PPR3 from exon 3 to exon 4. Arrow indicates the exon 3 and 4 boundary, and dots indicate intron sequences. Bold dot indicate intron retained.

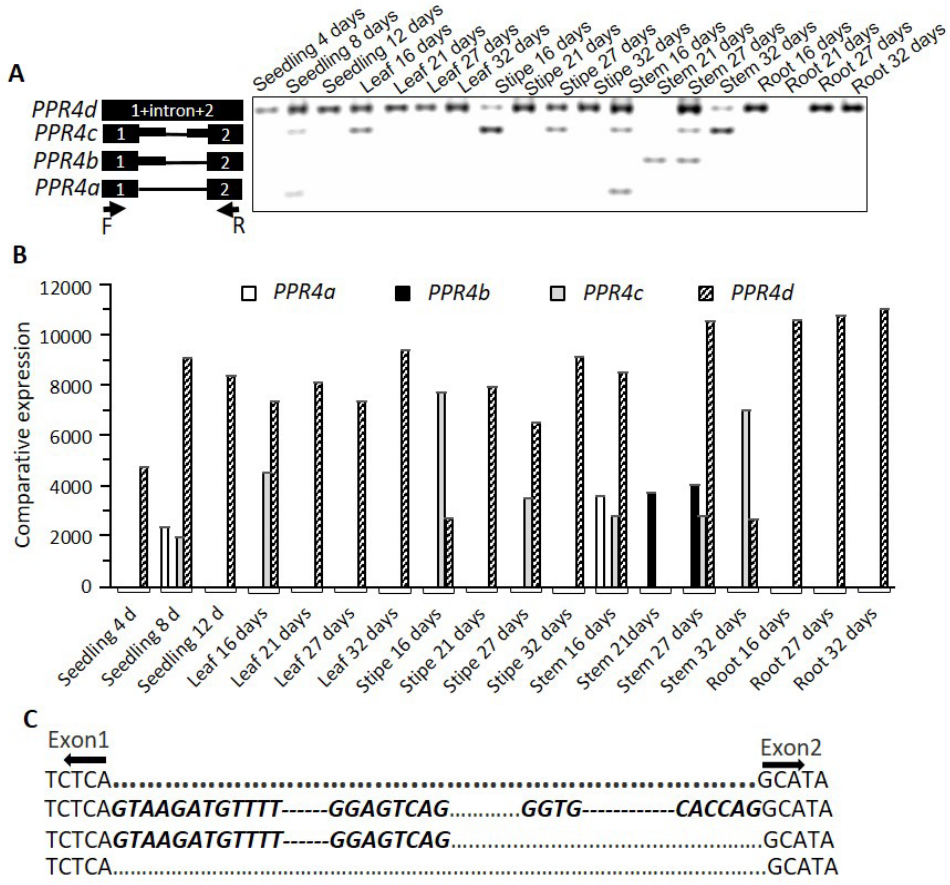

Figure 4. PCR and sequence analysis of PPR4 (accession no. AT4G38150). (A) PCR analysis of seedling, leaf, stipe, stem, and root tissue. Fragment size estimated from the gel in base pairs (bp). **(B)** Comparative expression analysis of the splice isoforms in different tissues. **(C)** Genomic sequence of PPR4 from exon 1 to exon 2. Arrow indicates the exon 1 and 2 boundary, and dots indicate intron sequences. Sequences in bold and italics and dashes indicate a 3′-5′ alternative-splicing site. Bold dot indicate intron retained.

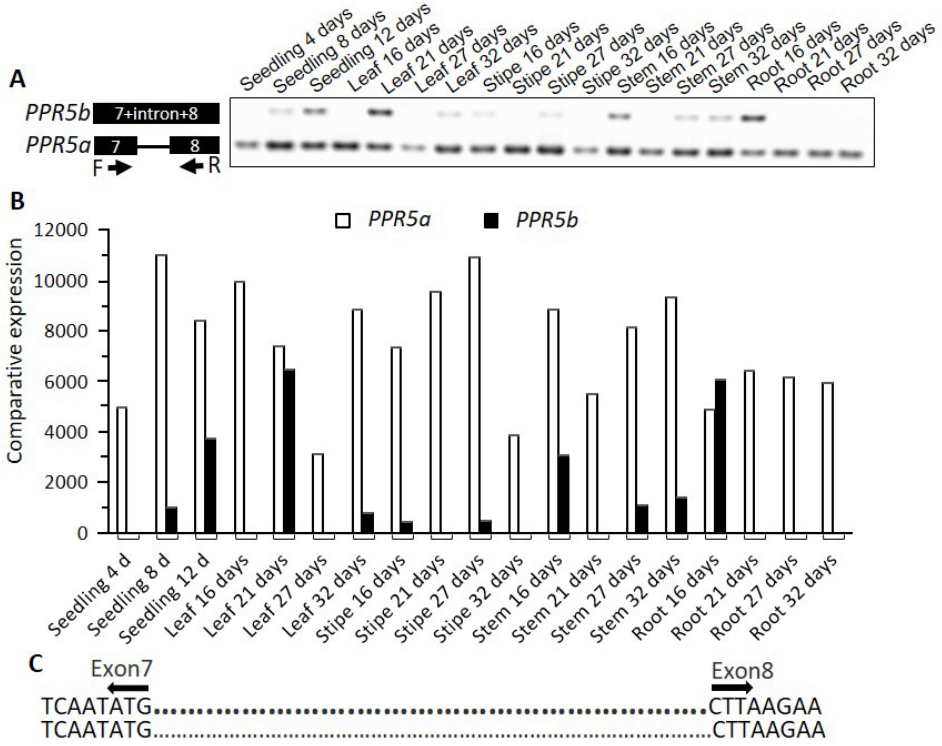

Figure 5. PCR and sequence analysis of PPR5 (accession no. AT1G30610). (A) Polyacrylamide gel electrophoresis of PCR product amplified from seedling, leaf, stipe, stem, and root tissue. Fragment size estimated from the gel in base pairs (bp). **(B)** Comparative expression analysis of the two splice isoforms in different tissues. **(C)** Genomic sequence of PPR5 from exon 7 to exon 8. Arrow indicates the exon 7 and 8 boundary, and dots indicate intron sequences. Bold dot indicate intron retained.

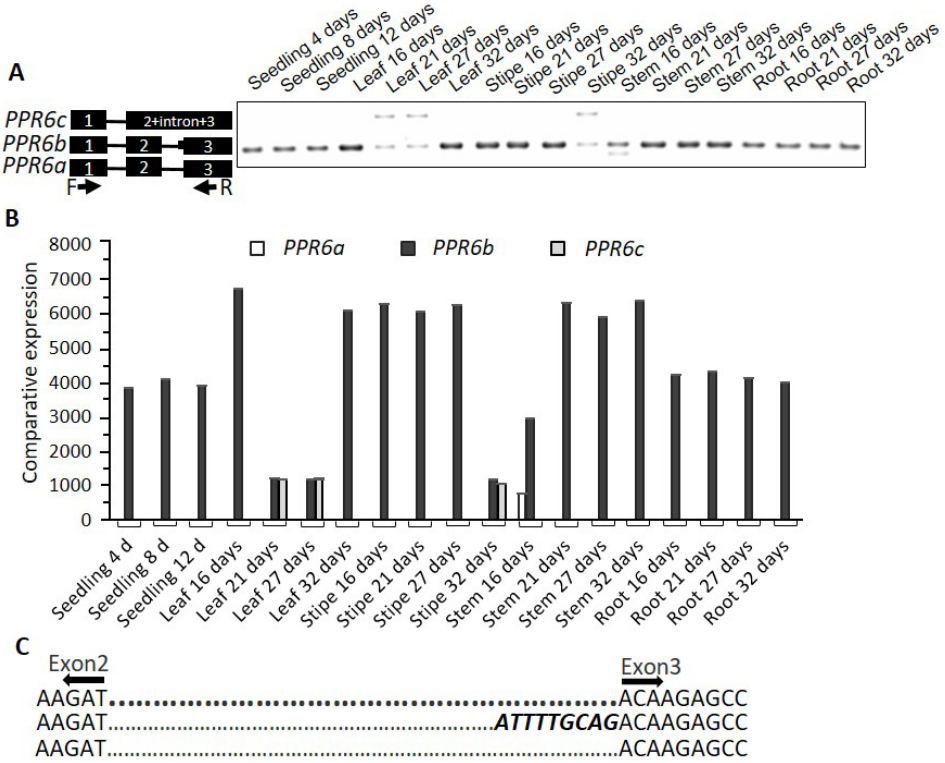

Figure 6. PCR and sequence analysis of PPR6 (accession no. AT1G05670). (A) PCR analysis of seedling, leaf, stipe stem, and root tissue. Fragment size estimated from the gel in base pairs (bp). **(B)** Comparative expression analysis of splice isoforms in different tissues. **(C)** Genomic sequence of PPR6 from exon 2 to exon 3. Arrows indicate the exon 2 and 3 boundaries, and dots indicate intron sequences. Sequences in bold and italics indicate a 3′ alternative-splicing site. Bold dot indicate intron retained.

Table 2. Summary of alternative-splicing events affecting PPR protein structure

Tentative Gene Name	Alternative-splicing event	Effect on		No. of alpha helices	No. of beta sheets	No. of random coils
		Nucleotides	Amino acids			
PPR1a	Reference isoform shorter	–	–	18	14	31
PPR1b	New 3' alternative-splicing site	15 nucleotide addition (TGACTATATTACAAG)	5 amino-acid addition (D Y I T R)	18	14	31
PPR1c	Reference isoform 3' alternative-splicing site	39 nucleotide addition (GTGTGGATTTCTTAAGTGT TATAGTGACTATATTACAAG)	13 amino-acid addition (C G F L K C Y S D Y I T R)	20	13	33
PPR2a	Reference isoform shorter	–	–	32	1	33
PPR2b	New 3' alternative-splicing site	26 nucleotide addition (TTTCGATTTTTATTCGAATC CGGAAG)	Frameshift	27	1	28
PPR5a	Reference isoform shorter	–	–	48	5	54
PPR5b	Reference isoform intron retention	84 nucleotide addition (GTAAATTTTGTAAATCCTG TAGTCCTTAAGCTTATCGA GAATTTGATTTACAAAGCT GATCTTGTTCATACCATCCA ATTTCAG)	28 amino-acid addition (V N F V N P V V L K L I E N L I Y K A D L V H T I Q F Q)	55	6	58

"–" indicate not applicable.

alternative splicing of *PPR* genes. According to the *http://www.uniprot.org* database, *PPR1* binds with iron as a cofactor, but its biological function is unknown. *PPR2*, *PPR3*, *PPR4*, *PPR5*, and *PPR6* exhibit endonuclease activity and bind to RNA, and function in RNA modification. *PPR5* likely functions in plant embryo development (*17,35*). This protein is expressed in the female gametophyte and is responsible for the initiation of gametogenesis (*36*). PPR4 is predicted to be localized to the mitochondria (*6*).

The tissue-specific expression patterns of *PPR* genes differ due to alternative splicing. In the current study, we found that retained introns were highly expressed in all tissues than 3′ and 5′ alternative-splicing sites. In different cell of Arabidopsis root tissue, intron retention is more common than other types of alternative splicing (*37*). However, it is interesting that in almost all type of tissues even in different aged condition, we found intron retention is the common phenomenon. In the current study, we detected higher tissue-specific expression of *PPR1* and *PPR2* than of the other *PPR* genes. RNA editing in *ndhB-149*, *ndhB-1255*, and *ndhD-2* does not occur in roots or in lincomycin-treated seedlings (*25*). In addition, *matK-640* is fully edited, and *accD-794*, *atpF-92*, *psbE-214*, *psbF-77*, *psbZ-50*, and *rps14-50* are completely or highly edited, in both green and non-green tissues (*25*). Based on these findings and the current results, it is likely that alternative splicing of *PPR* genes affects tissue-specific RNA editing.

We also investigated the effects of alternative splicing on protein structure and functionality. PPR1c contains a 13 amino-acid sequence, CGFLKCYSDYITR (48th-60th). Compared with the shorter isoforms, PPR1c contains a higher number of alpha helices and random coils but fewer beta sheets (Table 2). This amino-acid sequence is homologous to that of THCA synthase in *Cannabis sativa*. The major role of these residues is substrate binding rather than direct catalysis (*38*). Another homolog of this peptide is found in a juvenile hormone esterase-related protein in *Operophtera brumata*. This protein plays a major role in controlling growth and development (*39*). In PPR1b, the addition of the amino-acid sequence DYITR (48th-52th) creates a long random coil. This peptide is homologous to non-ribosomal peptide synthases (NRPSs), which help produce natural products with antimicrobial and anticancer properties (*40*). The additional 26 nt sequence in PPR2b is homologous to that in *Apis cerana* endothelin-converting enzyme 1 (ECE-1), as revealed by BLAST searches (*https://www.ncbi.nlm.nih.gov*). ECE-1 and ECE-2 can both cleave amyloid-β in mouse brain (*41*).

In this study, we found that alternative splicing in *PPR* genes adversely affects their structure and functionality. PPR proteins are highly diversified due to alternative splicing. I-TASSER analysis showed that the structures of these proteins, especially their folding ability and sometimes their ligand-binding ability, were completely altered due to alternative splicing. This process can also affect the number of alpha helices, beta sheets, and coils in a protein. Indeed, alternatively spliced exons were previously shown to affect the tertiary structures of proteins and have a great impact on protein folding ability and (ultimately) functionality (*42*). Protein-protein interaction pathways can also be altered due to tissue-specific alternative splicing (*43*).

Therefore, it is obvious that due to alterative splicing our studied PPR proteins might be greatly affected with altered even opposite function as these proteins bind to its target RNA with an algorithmic manner (*8,44*).

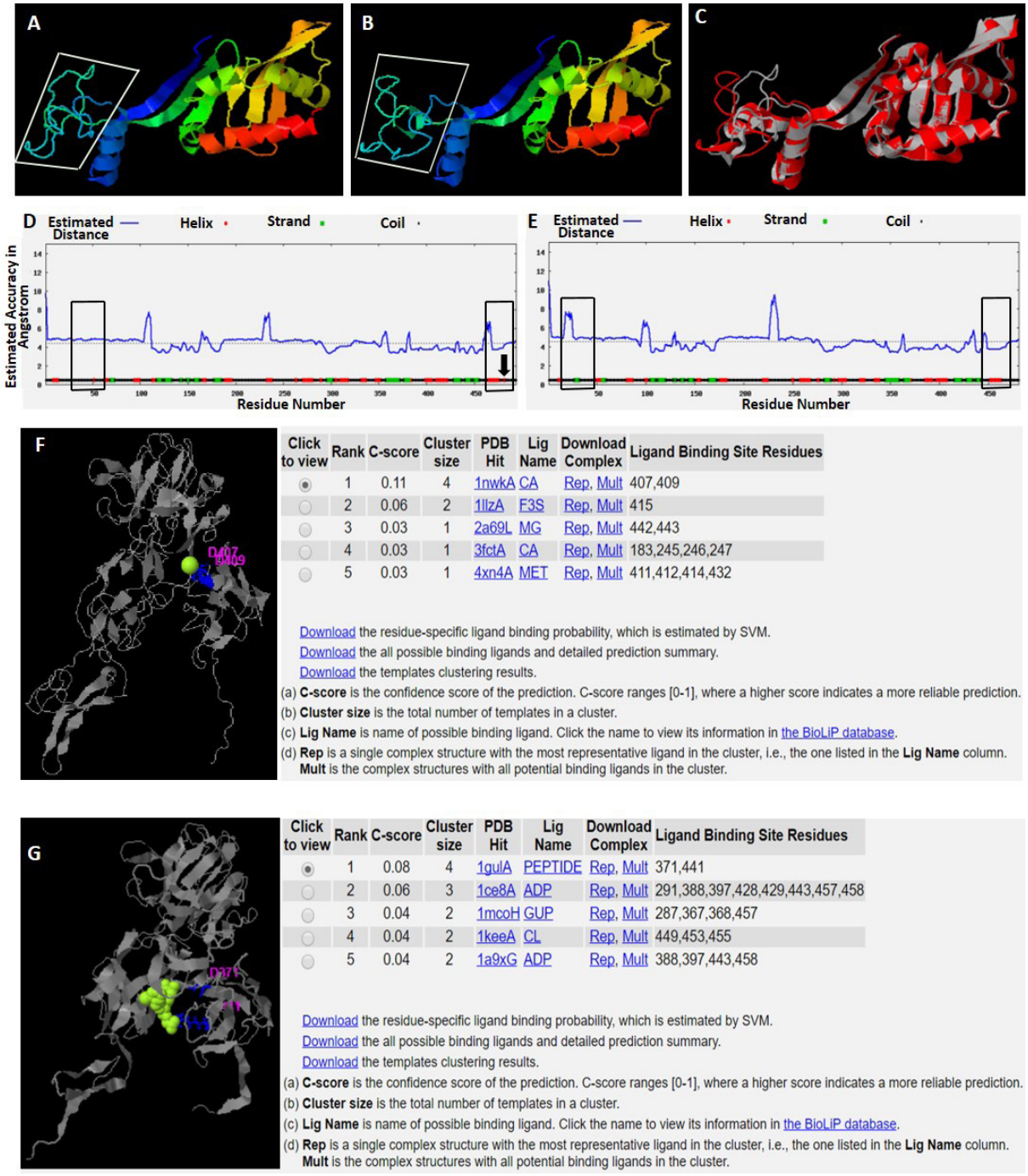

Figure 7. Effects of the addition and deletion of 13 amino acids on the structures and changes in ligand-binding site residues in PPR1, as revealed using the I-TASSER bioinformatics tool. (A) Addition of 13 amino acids (48th–60th), **(B)** Deletion of 13 amino acids, **(C)** Superposition of the two isoforms. **(D)** The beta sheet is absent in the N-terminus and an alpha helix is present in the C-terminus due to the addition of 13 amino acids, arrow indicates additional alpha helix in C-terminus. **(E)** A beta sheet is present in the N-terminus and the alpha helix is absent in the C-terminus due to a deletion of 13 amino acids. **(F-G)** Ligand-binding site is completely altered in the two isoforms.

Therefore, alternative splicing may not only alter binding location but also binding affinity. In the current study, we also determined that the secondary structures and ligand-binding activities of different isoforms from the same gene can be altered due to alternative splicing. Indeed, in the nuclear transcripts of AT1G29930.1 and AT1G52400.1 from Arabidopsis, C-to-U and U-to-C RNA editing occurs in the translation borders (*45*). These deamination and amination reactions occur in highly adjacent sites, suggesting that the deamination reaction serves as the donor of amino groups for the amination reaction (*45*), although the amination frequency is higher. Another factor might also function as an amino-group donor. The interesting thing is that the same *PPR* gene may produce the enzyme with amination and deamination activity that may be generated due to alternative splicing.

In conclusion, the findings of this study indicate that

tissue-specific alternative splicing highly diversified in plants. Alternative-splicing events in PPR transcripts have strong effects on protein diversity. More investigations of the localizations of alternatively spliced transcripts and proteins, as well as site-specific and tissue-specific RNA editing, are needed to further understand their effects on growth and development. PPRs are modular proteins that are highly reprogrammable. Therefore, it would be interesting to investigate how these types of natural editing events in transcripts affect substrate recognition and plant physiology. Additional experiments are needed to understand the precise effects of alternative-splicing and editing events on the highly programmable PPR protein family.

Acknowledgement

This work was supported by Grant-in-Aid for Scientific Research from the Japan Society for the Promotion of Science (26670167, 17H02204 and 18K19288).

References

1. Graveley BR. Alternative splicing: Increasing diversity in the proteomic world. Trends Genet. 2001; 17:100-107.
2. Lareau LF, Green RE, Bhatnagar RS, Brenner SE. The evolving roles of alternative splicing. Curr Opin Struct Biol. 2004; 14:273-282.
3. Kelemen O, Convertini P, Zhang Z, Wen Y, Shen M, Falaleeva M, Stamm S. Function of alternative splicing. Gene. 2013; 514:1-30.
4. Syed NH, Kalyna M, Marquez Y, Barta A, Brown JW. Alternative splicing in plants--coming of age. Trends Plant Sci. 2012; 17:616-623.
5. James AB, Syed NH, Bordage S, Marshall J, Nimmo GA, Jenkins GI, Herzyk P, Brown JW, Nimmo HG. Alternative splicing mediates responses of the Arabidopsis circadian clock to temperature changes. Plant Cell. 2012; 24:961-981.
6. Lurin C, Andres C, Aubourg S, *et al*. Genome-wide analysis of Arabidopsis pentatricopeptide repeat proteins reveals their essential role in organelle biogenesis. Plant Cell. 2004; 16:2089-2103.
7. Small ID, Peeters N. The PPR motif – a TPR-related motif prevalent in plant organellar proteins. Trends Biochem Sci. 2000; 25:45-47.
8. Okuda K, Nakamura T, Sugita M, Shimizu T, Shikanai T. A pentatricopeptide repeat protein is a site recognition factor in chloroplast RNA editing. J Biol Chem. 2006; 281:37661-37667.
9. Andres-Colas N, Zhu Q, Takenaka M, De Rybel B. Multiple PPR protein interactions are involved in the RNA editing system in Arabidopsis mitochondria and plastids. Proc Natl Acad Sci U S A . 2017; 114:8883-8888.
10. Bayer-Csaszar E, Haag S, Jorg A, Glass F, Hartel B, Obata T, Meyer EH, Brennicke A, Takenaka M. The conserved domain in MORF proteins has distinct affinities to the PPR and E elements in PPR RNA editing factors. Biochim Biophys Acta. 2017; 1860:813-828.
11. Choquet Y. 5' and 3' ends of chloroplast transcripts can both be stabilised by protein 'caps': A new model for polycistronic RNA maturation. EMBO J. 2009; 28:1989-1990.
12. Prikryl J, Rojas M, Schuster G, Barkan A. Mechanism of RNA stabilization and translational activation by a pentatricopeptide repeat protein. Proc Natl Acad Sci U S A. 2011; 108:415-420.
13. Delannoy E, Stanley WA, Bond CS, Small ID. Pentatricopeptide repeat (PPR) proteins as sequence-specificity factors in post-transcriptional processes in organelles. Biochem Soc Trans. 2007; 35:1643-1647.
14. Williams-Carrier R, Kroeger T, Barkan A. Sequence-specific binding of a chloroplast pentatricopeptide repeat protein to its native group II intron ligand. RNA. 2008; 14:1930-1941.
15. Gutiérrez-Marcos JF, Dal Prà M, Giulini A, Costa LM, Gavazzi G, Cordelier S, Sellam O, Tatout C, Paul W, Perez P, Dickinson HG, Consonni G. empty pericarp4 encodes a mitochondrion-targeted pentatricopeptide repeat protein necessary for seed development and plant growth in maize. Plant Cell. 2007; 19:196-210.
16. Zhou W, Lu Q, Li Q, Wang L, Ding S, Zhang A, Wen X, Zhang L, Lu C. PPR-SMR protein SOT1 has RNA endonuclease activity. Proc Natl Acad Sci U S A. 2017; 114:E1554-e1563.
17. Cushing DA, Forsthoefel NR, Gestaut DR, Vernon DM. Arabidopsis emb175 and other ppr knockout mutants reveal essential roles for pentatricopeptide repeat (PPR) proteins in plant embryogenesis. Planta. 2005; 221:424-436.
18. Okuda K, Chateigner-Boutin AL, Nakamura T, Delannoy E, Sugita M, Myouga F, Motohashi R, Shinozaki K, Small I, Shikanai T. Pentatricopeptide repeat proteins with the DYW motif have distinct molecular functions in RNA editing and RNA cleavage in Arabidopsis chloroplasts. Plant Cell. 2009; 21:146-156.
19. Chateigner-Boutin AL, Colas des Francs-Small C, Fujii S, Okuda K, Tanz SK, Small I. The E domains of pentatricopeptide repeat proteins from different organelles are not functionally equivalent for RNA editing. Plant J. 2013; 74:935-945.
20. Schallenberg-Rudinger M, Lenz H, Polsakiewicz M, Gott JM, Knoop V. A survey of PPR proteins identifies DYW domains like those of land plant RNA editing factors in diverse eukaryotes. RNA Biol. 2013; 10:1549-1556.
21. Leu KC, Hsieh MH, Wang HJ, Hsieh HL, Jauh GY. Distinct role of Arabidopsis mitochondrial P-type pentatricopeptide repeat protein-modulating editing protein, PPME, in nad1 RNA editing. RNA Biol. 2016; 13:593-604.
22. Shikanai T. RNA editing in plants: Machinery and flexibility of site recognition. Biochim Biophys Acta. 2015; 1847:779-785.
23. Barkan A, Small I. Pentatricopeptide repeat proteins in plants. Annu Rev Plant Biol. 2014; 65:415-442.
24. Doniwa Y, Ueda M, Ueta M, Wada A, Kadowaki K, Tsutsumi N. The involvement of a PPR protein of the P subfamily in partial RNA editing of an Arabidopsis mitochondrial transcript. Gene. 2010; 454:39-46.
25. Tseng C-C, Lee C-J, Chung Y-T, Sung T-Y, Hsieh M-H. Differential regulation of Arabidopsis plastid gene expression and RNA editing in non-photosynthetic tissues. Plant Mol Biol. 2013; 82:375-392.
26. Coquille S, Filipovska A, Chia T, Rajappa L, Lingford JP, Razif MFM, Thore S, Rackham O. An artificial

PPR scaffold for programmable RNA recognition. Nat Commun. 2014; 5:5729.
27. Colcombet J, Lopez-Obando M, Heurtevin L, Bernard C, Martin K, Berthome R, Lurin C. Systematic study of subcellular localization of Arabidopsis PPR proteins confirms a massive targeting to organelles. RNA Biol. 2013; 10:1557-1575.
28. Merkin J, Russell C, Chen P, Burge CB. Evolutionary dynamics of gene and isoform regulation in Mammalian tissues. Science. 2012; 338:1593-1599.
29. Stothard P. The sequence manipulation suite: JavaScript programs for analyzing and formatting protein and DNA sequences. Biotechniques. 2000; 28:1102-1104.
30. Kent WJ. BLAT – the BLAST-like alignment tool. Genome Res. 2002; 12:656-664.
31. Zhang Y. I-TASSER server for protein 3D structure prediction. BMC Bioinformatics. 2008; 9:40.
32. Roy A, Kucukural A, Zhang Y. I-TASSER: A unified platform for automated protein structure and function prediction. Nat Protoc. 2010; 5:725-738.
33. Yang J, Yan R, Roy A, Xu D, Poisson J, Zhang Y. The I-TASSER Suite: Protein structure and function prediction. Nat Methods. 2015; 12:7-8.
34. Guo L, Liu C-M. A single-nucleotide exon found in Arabidopsis. Sci Rep. 2015; 5:18087.
35. Meinke D, Sweeney C, Muralla R. Integrating the genetic and physical maps of Arabidopsis thaliana: Identification of mapped alleles of cloned essential (EMB) genes. PLoS One. 2009; 4:e7386.
36. Greco M, Chiappetta A, Bruno L, Bitonti MB. In *Posidonia oceanica* cadmium induces changes in DNA methylation and chromatin patterning. J Exp Bot. 2012; 63:695-709.
37. Li S, Yamada M, Han X, Ohler U, Benfey PN. High-resolution expression map of the Arabidopsis root reveals alternative splicing and lincRNA regulation. Dev Cell. 2016; 39:508-522.
38. Shoyama Y, Tamada T, Kurihara K, Takeuchi A, Taura F, Arai S, Blaber M, Shoyama Y, Morimoto S, Kuroki R. Structure and function of 1-tetrahydrocannabinolic acid (THCA) synthase, the enzyme controlling the psychoactivity of Cannabis sativa. J Mol Biol. 2012; 423:96-105.
39. Kontogiannatos D, Swevers L, Maenaka K, Park EY, Iatrou K, Kourti A. Functional characterization of a juvenile hormone esterase related gene in the moth Sesamia nonagrioides through RNA interference. PLoS One. 2013; 8:e73834.
40. Agrawal S, Acharya D, Adholeya A, Barrow CJ, Deshmukh SK. Nonribosomal peptides from marine microbes and their antimicrobial and anticancer potential. Front Pharmacol. 2017; 8:828.
41. Palmer JC, Tayler HM, Love S. Endothelin-converting enzyme-1 activity, endothelin-1 production, and free radical-dependent vasoconstriction in Alzheimer's disease. J Alzheimers Dis. 2013; 36:577-587.
42. Birzele F, Csaba G, Zimmer R. Alternative splicing and protein structure evolution. Nucleic Acids Res. 2008; 36:550-558.
43. Ellis JD, Barrios-Rodiles M, Colak R, Irimia M, Kim T, Calarco JA, Wang X, Pan Q, O'Hanlon D, Kim PM, Wrana JL, Blencowe BJ. Tissue-specific alternative splicing remodels protein-protein interaction networks. Mol Cell. 2012; 46:884-892.
44. Nakamura T, Yagi Y, Kobayashi K. Mechanistic insight into pentatricopeptide repeat proteins as sequence-specific RNA-binding proteins for organellar RNAs in plants. Plant Cell Physiol. 2012; 53:1171-1179.
45. Meng Y, Chen D, Jin Y, Mao C, Wu P, Chen M. RNA editing of nuclear transcripts in Arabidopsis thaliana. BMC Genomics. 2010; 11:S12-S12.

(Received August 1, 2018; Revised December 9, 2018; Accepted December 11, 2018)

Original Article

DOI: 10.5582/bst.2018.01207

The effect of His-tag and point mutation on the activity of irisin on MC3T3-E1 cells

Rujun Zeng, Yaxian Ma, Xiaoyong Qiao, Jun Zhang, Yunyao Luo, Sicong Li, Ling Liu, Liangzhi Xu*

Department of Obstetrics and Gynecology, West China Second University Hospital, Sichuan University; The Joint Laboratory for Reproductive Medicine of Sichuan University-The Chinese University of Hong Kong; Key Laboratory of Birth Defects and Related Disease of Women and Children (Sichuan University), Ministry of Education; Reproductive Endocrinology and Regulation Laboratory, West China Second University Hospital, Sichuan University, Sichuan, China.

Summary **Irisin is a myokine secreted from the cleavage of fibronectin type III domain-containing protein 5 (FNDC5) and has an effect on bone formation. There are limited studies about the structure of irisin and its functional unit. In order to clarify the candidate domain responsible for irisin action, we constructed several irisin variants and tested their influence on the proliferation and osteogenesis of MC3T3-E1 cells. On the one hand, His-tag was added to the N terminal or C terminal of irisin. On the other hand, the flexible region or salt bridge site were chosen as the candidate for point mutation. Alkaline phosphatase (ALP), Runt related transcription factor 2 (Runx2) and collagen type I alpha 1 (COL1α1) were chosen to test the differentiation efficiency. We found point mutation on flexible regions, Glu-57 and Ile-107, and adding His-tag on the C-terminal of irisin did affect its action. The osteogenic potential of irisin E57K, irisin I107F and irisin$^{C\text{-}His}$ decreased about 90.1%, 88.8% and 96.6% activity of recombinant-irisin (r-irisin) ($P < 0.05$), respectively. Point mutation on the salt bridge, Arg-75, partly decreased the effect of irisin (45 ± 11.3% of r-irisin) ($P < 0.05$). N-terminal His-tag showed almost no effect (93.5 ± 25.7% of r-irisin) ($P = 0.658$). This study suggested that the flexible region of residues 55-58 and 106-108, and C-terminal of irisin are vital for its activity. Disrupting the dimerization of irisin might result in a partly reduced effect on cell differentiation.**

Keywords: Irisin, MC3T3-E1 cell, osteogenesis, His-tag, point mutation

1. Introduction

Exercise acts as an important role on bone metabolic disorders in addition to pharmaceutical treatment. Besides mechanical interaction, it could remold bone tissue through regulating the expression of many factors such as tumor necrosis factor (*1*). Irisin is one of them and has attracted much attention since its discovery.

Irisin is composed of 112 amino acids, which can be cleaved from membrane protein human fibronectin type III domain-containing protein 5 (FNDC5) and can be detected in fat, skeletal muscle, serum and so on (*2*). Up to now, the relationship between irisin and glycolipid metabolism, muscle remodeling, non-alcohol fatty liver disease, chronic kidney disease and tumorigenesis have been reported (*3*).

Moreover, evidence suggests that irisin also contributes to bone metabolism (*4-6*). Both bone mass and bone quality of mice, with or without osteoporosis, were improved after irisin treatment (*7*). It has a direct effect on bone, including boosting bone formation and inhibiting bone absorption (*8-10*), which means it has potential in dealing with bone loss and even osteoporosis.

The concentration of irisin varies in different articles, from 0.01 to 2,000 ng/mL (*11*), which partly may be because of the detecting method. Enzyme linked immunosorbent assay (ELISA), which is the most common method, has shortages of cross reaction and inconsistent antibodies (*11,12*). Through mass

**Address correspondence to:*
Dr. Liangzhi Xu, Department of Obstetrics and Gynecology, West China Second University Hospital, Sichuan University, Chengdu, No.20, Section 3, Renmin South Road, Chengdu,Sichuan 610041, China.
E-mail: xuliangzhi@scu.edu.cn

spectrometry, Jedrychowski *et al*. reported a level of 3.6 ng/mL in human serum in the resting state, and 4.3 ng/mL after exercise (*13*). This is much lower than its dose in experiments, which suggests that irisin beyond its physiological level might have benefits.

Irisin consists of a N-terminal fibronectin III-like domain, which is attached to a flexible C-terminal structure and forms dimers (*14*). However, studies about the structure of irisin are limited and there is little known about its critical domains. His-tag is helpful in purifying or detecting protein, but it is unknown that if the activity of recombinant irisin (r-irisin) will be influenced or not by the existence and the site of the tag. Studies on irisin structure is about its synthesis, secretion and stability through mostly point mutations (*14,15*), but failed to examine its effect. In order to further understand the molecular structure of irisin, based on our previous study that r-irisin can promote the proliferation and osteogenesis of osteoblast cells (*10*), we made some changes on irisin and detected their effect on these cells.

2. Materials and Methods

2.1. *Materials*

Reagents used here included dexamethasone, ascorbic acid, beta-glycerophosphate, phenylmethanesulfonyl fluoride (PMSF) and sodium azide (NaN_3) (Sigma, USA). Recombinant irisin (r-irisin), which is without tag and synthsized from *E. coli*, was purchased from Phoenix Pharmaceuticals, Inc., Burlingame, CA, USA. BCIP/NBT alkaline phosphatase color development kit, and alkaline phosphatase assay kit was purchased from Beyotime Inst Biotech, China. Fetal bovine serum (FBS) and MEM Eagle - alpha modification (α-MEM) were purchased from Gibco, USA. The bicinchoninicacie (BCA) protein assay kit was purchased from Pierce, USA. Chromogenic substrate limulus reagent kit was purchased from Solarbio, China. The pET28a(+) vector was purchased from Novagen, USA. The MC3T3-E1 cells were provided by laboratory of transplant immunology, West China Hospital, Sichuan University.

2.2. *The plasmid construction and protein purification*

The whole FNDC5 sequences were amplified from mouse cDNA with the following primer: 5'-G AGTCGCCATGCCCCCAGG (forward) -3', 5'-GCTGCTCAGAGCAAGCACTG-3' (Reverse) and was subcloned into pTeasy vector (Transgen biotech, China) and confirmed by direct sequencing. Six histidines were added on its terminal. For the N-his tag irisin ($irisin^{N\text{-}His}$), the only irisin sequence was amplified from this plasmid with NdeI and XhoI recognizing sequence tag primers: 5'-GGAATTCCATATGGACAG CCCCTCAGCCCCT-3' (forward), 5'-GGCTCGAGT TATTACTCCTTCATGGTCACCTC-3' (Reverse), and ligated the fragment with pET28a(+) vector at NdeI and XhoI sites. For the $irisin^{C\text{-}His}$ the NcoI sites were chosen instead from NdeI with reverse primer: 5'-G GCTCGAGCTCCTTCATGGTCACCTCATCTTT-3' , and the PCR product was subcloned into pET28a(+) vector at NcoI and XhoI sites. After identification by DNA Sequencing, the plasmids were transformed into Rosetta (DE3) *E. coli*.

The plasmids containing point mutations were generated with the Fast mutagenesis System (Transgen biotech, China). Briefly, the primers containing the point mutation with 15-20 bp 5" and 10 bp 3" overlap region were designed, then PCRed the pET28a- $irisin^{N\text{-}His}$ plasmid with each pair of primers individually. The aa mutation numbers are those for FNDC5, starting with the signal peptide. The pair of oligonucleotides for PCR of $irisin^{N\text{-}His}$ E57K were (forward)5'-TGG GAT GTC CTG GAG GAT AAA GTG GTC ATT G-3', (reverse)5'-T ATC CTC CAG GAC ATC CCA GCT CAG CAC GGC-3'. The pair $irisin^{N\text{-}His}$ R75E were (forward)5'-AAG GAT GTG CGG ATG CTC GAG TTC ATT CAG G-3', (reverse)5'-TC GAG CAT CCG CAC ATC CTT CTT CTG CTG AG-3'. The pair of $irisin^{N\text{-}His}$ I107F were (forward) 5'-CAT GTG CAG GCC ATC TCC TTC CAG GGA CAG-3', (reverse) 5'-A GGA GAT GGC CTG CAC ATG GAC GAT ATA TTC-3'. All plasmids were identified by direct sequencing and transformed into Rosetta (DE3) *E. coli*.

The *E. coli* were cultured at 37ºC respectively in LB overnight, then the overnight cultures were diluted 1:100 and cultured under the same conditions continupusly. When the OD_{600} of the culture reached 0.6-0.8, 0.15mM IPTG was added and cultured at 25ºC for 3 hours to induce the expression and translation of irisin protein. The protein was purified using a Ni-sepharose 6FF column and dialyzed with PBS (pH7.4) solution. The concentration of the recombinant irisin was measured with Pierce BCA protein Assay Kit. The chromogenic substrate limulus reagent kit was used to detect the endotoxin.

2.3. *Cell culture and treatment*

The mouse osteoblastic MC3T3-E1 cells were grown in α-MEM supplemented with 10% FBS, 100 units/mL penicillin and 100 μg/mL streptomycin. All the cells were cultured in a humidified atmosphere of 95% air and 5% CO_2 at 37ºC. The culture medium was changed every 2-3 days.

The cells were divided into seven groups and treated with different r-irisin proteins at a concentration of 20nm, they were: a blank control group (con), $irisin^{N\text{-}His}$, $irisin^{C\text{-}His}$, irisin E57K, irisin R75E, irisin I107F and a commercial r-irisin.

2.4. *Cell proliferation detection*

The cells were plated into a 96-well plate at a density

of 1.5×10^4 cells/cm^2. The medium was added with the different irisin proteins after cell adherence. At 0, 24, 48 and 72 hours of culturing, cell counting kit (CCK-8) solution was added to each well and incubated for 2 hours, then the absorbance was measured at 450 nm. All experiments were performed in four replicates.

2.5. *qPCR*

Cells were seeded into 6-well plates at a density of 1.5×10^4/cm^2 and cultured in osteogenic medium composed of 10%FBS, 0.1 uM dexamethasone, 10mM β-glycerophosphate and 50 ug/mL ascorbic acid. After culturing for 3 or 14 days, cells were harvested for total RNA extraction with Trizol (Ambion, USA). According to manufacturer`s instructions, the cDNA was synthesized by Revert Aid First Strand cDNA synthesis Kit (Thermo, EU). SYBR Green Master Mix (Applied Biosystems, USA) was used to perform real-time PCR on Applied Biosystems 7500 Real-time PCR system. The 2−Δctmethod was used to calculate the relative gene expressions of alkaline phosphatase (ALP), Runt related transcription factor 2 (Runx2) and collagen type I alpha 1(COL1α1). The primers of each target gene are listed in Table 1.

2.6. *ALP detection*

Cells were plated into 6-well plates at a density of 1.5×10^4/cm^2 and grouped as described above in two replicates. All cells were cultured in osteogenic medium and the medium was changed every 3 days. After culture for 14days, the cells were fixed or harvested for ALP staining or quantification, respectively.

For ALP staining, cells were washed with PBS and fixed with 4% paraformaldehyde for 10 minutes, then rinsed with deionized water and stained to recognize ALP following the instruction of BCIP/NBT alkaline phosphatase color development kit. Images of each group were taken.

For ALP quantification, cells were washed with PBS, then lysed and collected with buffer comprised of 20 mM pH8.0 Tris-HCl, 150 mM NaCl, 1% TritonX-100, 0.02% NaN_3 and 1 mM PMSF. The collections were centrifuged and the supernatant was used to detect the ALP activity through alkaline phosphatase assay kit. After being normalized to the total protein content quantified by BCA protein assay kit, the ALP activity was standardized and compared with each other.

2.7. *Statistical analysis*

Data are presented as mean ± standard deviation (SD) and analyzed with SPSS22.0. Comparisons among two groups were evaluated by two-tailed student's *t* test. Comparisons among multiple groups were evaluated by one-way analysis of variance (ANOVA) and Turkey's test. $P < 3.35$ was considered as significant.

3. Results

3.1. *Detecting the irisin with tag or point mutation*

The recombinant plasmids were confirmed by direct DNA sequencing. The concentration of irisin$^{N\text{-}His}$, irisin$^{C\text{-}His}$, irisinE57K, irisin R75E, and irisin I107F were 0.413 ug/uL, 0.367 ug/uL, 0.179 ug/uL, 0.341 ug/uL and 0.691 ug/uL, respectively. The endotoxin of each of them was 5.71 EU/mL, 5.09 EU/mL, 5.27 EU/mL, 4.92 EU/mL, 5.39 EU/mL and 6.59 EU/mL, respectively.

3.2. *The effect of irisin with tag on the proliferation and differentiation of MC3T3-E1 cells*

Compared with the blank control group, cells cultured with irisin$^{N\text{-}His}$ or r-irisin were significantly more after 48 hours, while no difference was found between the two groups. irisin$^{C\text{-}His}$ had no effect on cell proliferation (Figure 1A).

MC-3T3 E1 cells were cultured with osteogenic medium. Three days later, irisin$^{N\text{-}His}$ and r-irisin increased the expression of ALP about 82% and 95% (1.82 ± 0.29 *vs*. 1.00 ± 0.10, 1.95 ± 0.25 *vs*. 1.00 ± 0.10, respectively). The expression of Col1α1 increased about 52% and 70% (1.52 ± 0.24 *vs*. 1.00 ± 0.12, 1.70 ± 0.20 *vs*. 1.00 ± 0.12). The expression of Runx2 increased about 64% and 77% (1.64 ± 0.13 *vs*. 1.00 ± 0.13, 1.77 ± 0.09 *vs*. 1.00 ± 0.13) (Figure 1B). After culture for 14 days, irisin$^{N\text{-}His}$ and r-irisin increased the expression of ALP about 140% and 157% (2.40 ± 0.44 *vs*. 1.00 ± 0.22, 2.57 ± 0.28 *vs*. 1.00 ± 0.22, respectively). The expression of Col1α1 increased about 253% and 273% (3.53 ± 0.40 *vs*. 1.00 ± 0.18, 3.73 ± 0.60 *vs*. 1.00 ± 0.18). The expression of Runx2 increased about 279% and 351% (3.79 ± 0.42 *vs*. 1.00 ± 0.25, 4.51 ± 0.49 *vs*. 1.00 ± 0.25). No significant differences of osteogenic-related markers were found between the irisin$^{C\text{-}His}$ group and the control (Figure 1C).

Table 1. Primer pairs used for qPCR

Target gene	Forward (5'-3')	Reverse (5'-3')
ALP	TGACCTTCTCTCCTCCATCC	CTTCCTGGGAGTCTCATCCT
Runx2	CCGTGGCCTTCAAGGTTGT	TTCATAACAGCGGAGGCATTT
COL1α1	GCTCCTCTTAGGGGCCACT	CCACGTCTCACCATTGGGG
GAPDH	TGCACCACCAACTGCTTAG	GGATGCAGGGATGATGTTC

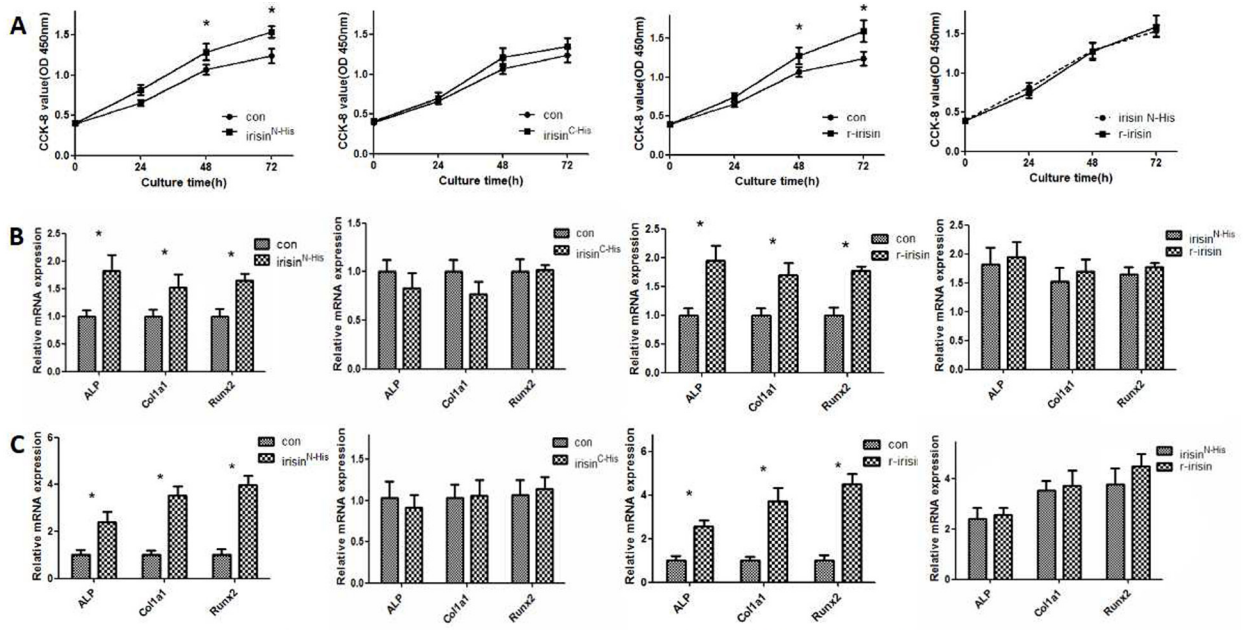

Figure 1. Effects of irisin with tag on the proliferation and differentiation of MC3T3-E1 cells. (A) At 0, 24, 48 and 72 hours of culture, cell counting kit (CCK-8) was applied to detect proliferation. **(B-C)** MC3T3-E1 cells were cultured with osteogenic medium and irisin with tags. After culture for 3 days **(B)** and 14 days **(C)**, the cells were harvested and used for real-time RT-PCR. The mRNA expression levels are shown relative to the values of the control.

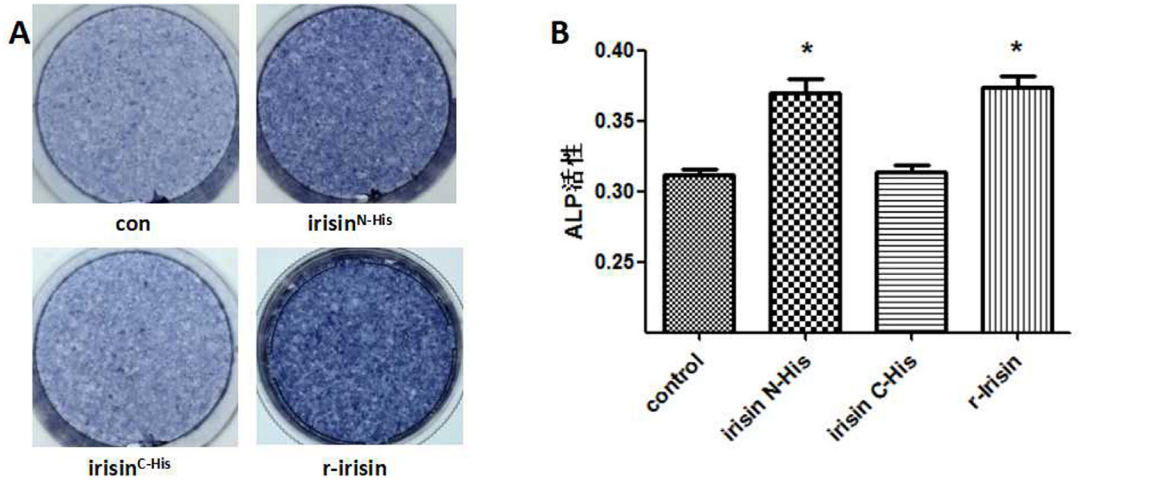

Figure 2 Effects of irisin with tag on the osteoblastic potential of MC3T3-E1 cells. After culture for 14 days, the cells were fixed and stained to recognize ALP following the instruction of BCIP/NBT alkaline phosphatase color development kit **(A)**. The cells were washed and collected to detect the ALP activity through alkaline phosphatase assay kit **(B)**.

Table 2. The ALP activity of MC3T3-E1 cells cultured with irisin with tag for 14 days. Data are shown as mean ± SD

Items	Fold r-irisin (ALP activity)	*P* value
irisin$^{N\text{-}His}$	0.935 ± 0.257	0.658
irisin$^{C\text{-}His}$	0.034 ± 0.134	< 0.01
r-irisin	1.000 ± 0.210	–

As to ALP staining and ALP quantification, the expression of ALP in irisin$^{N\text{-}His}$ or r-irisin group was higher than that in the blank control group (Figure 2). After eliminating the initial differentiation result revealed by the control group, a similar ALP activity between irisin$^{N\text{-}His}$ and r-irisin group was found. The ALP activity of irisin$^{N\text{-}His}$ group was about 93.5% of that in the r-irisin group, and the ALP activity of irisin$^{C\text{-}His}$ group was about 3.4% of that in the r-irisin group (Table 2).

3.3. *The effect of irisin with point mutation on the proliferation and differentiation of MC3T3-E1 cells*

Compared with the blank control group, cells cultured with irisin E57K was significantly more after 48 hours, and irisin R75E group showed this effect after 72 hours. No significant difference was discovered among irisin E57K, irisin R75E and r-irisin. Irisin I107F had no

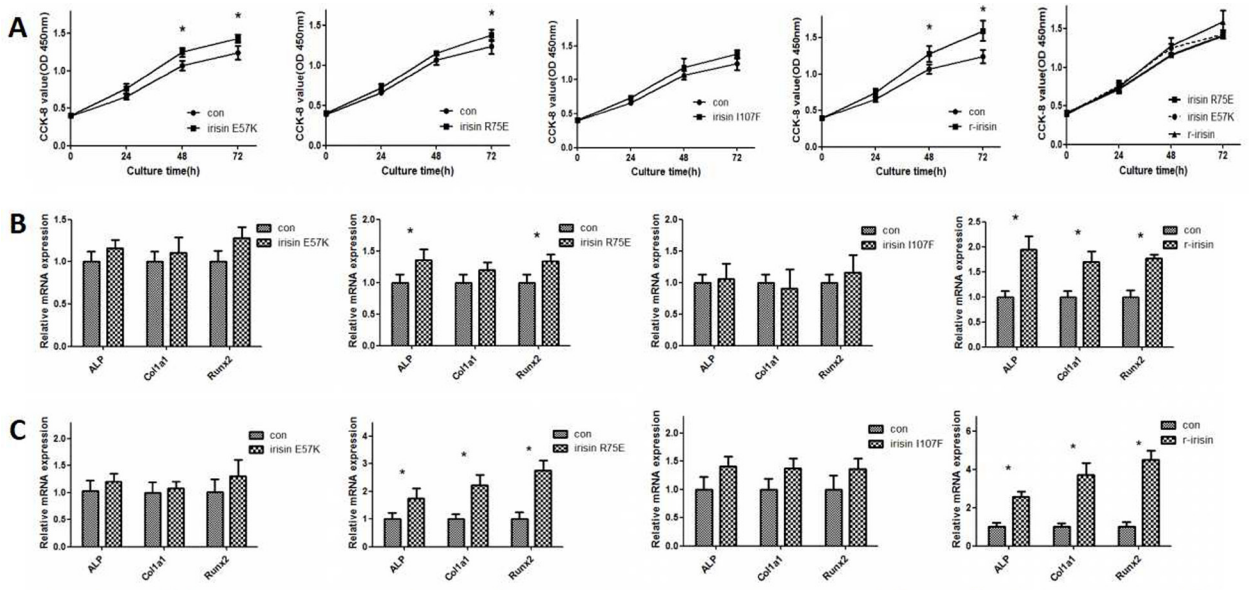

Figure 3. Effects of irisin with point mutation on the proliferation and differentiation of MC3T3-E1 cells. (A) At 0, 24, 48 and 72 hours of culture, cell counting kit (CCK-8) was applied to detect the proliferation. **(B-C)** MC3T3-E1 cells were cultured with osteogenic medium and irisin with point mutation. After culture for 3 days **(B)** and 14 days **(C)**, the cells were harvested and used for real-time RT-PCR. The mRNA expression levels are shown relative to the values of the control.

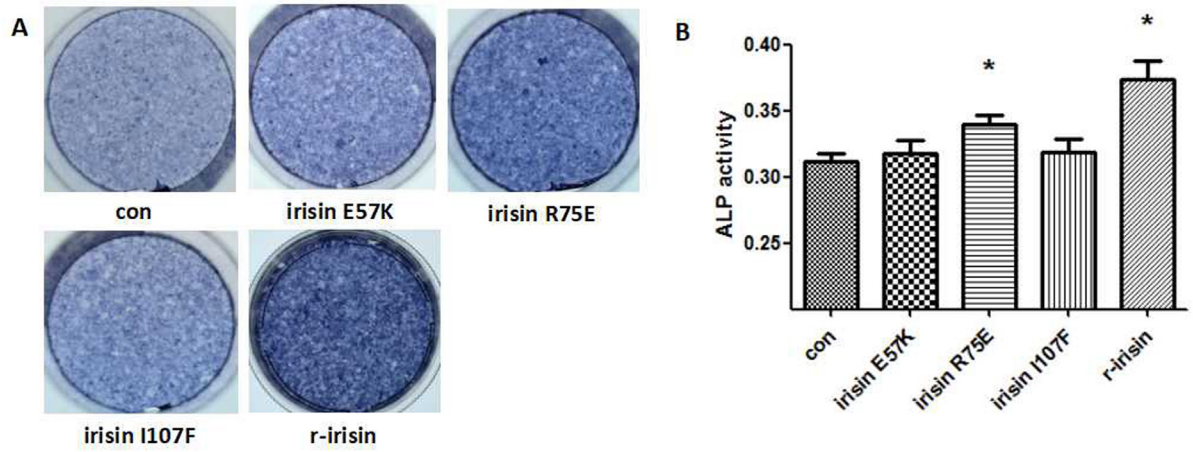

Figure 4. Effects of irisin with point mutation on the osteoblastic potential of MC3T3-E1 cells. After culture for 14 days, the cells were fixed and stained to recognize ALP following the instruction of BCIP/NBT alkaline phosphatase color development kit **(A)**. The cells were washed and collected to detect the ALP activity through alkaline phosphatase assay kit **(B)**.

effect on cell proliferation (Figure 3A).

When culturing in osteogenic medium, the mRNA expression of ALP and Runx2 were elevated by irisin R75E after 3 days (1.36 ± 0.16 *vs*. 1.00 ± 0.10, 1.34 ± 0.11 *vs*. 1.00 ± 0.13) (Figure 3B). The expression of ALP, Col1α1 and Runx2 were about 74%, 122% and 175% more than the control, respectively (1.74 ± 0.37 *vs*. 1.00 ± 0.22, 2.22 ± 0.38 *vs*. 1.00 ± 0.18, 2.75 ± 0.37 *vs*. 1.00 ± 0.25), after culturing for 14 days. No significant differences of osteogenic-related markers were found among irisin E57K, irisin I107F group and blank-control group (Figure 3C).

The ALP staining showed a higher expression of ALP in irisin R75E group, but less than the r-irisin group. While such elevation was not observed in irisin I107F or irisin E57K group (Figure 4). When the initial differentiation result, which was revealed by the blank control group, was eliminated, these three groups all revealed decreased ALP activity than the r-irisin group. The ALP activity of irisin R75E group was about 45.0% of that in the r-irisin group. The numbers were 9.9% and 11.2% for the irisin E57K group and irisin I107F group, respectively (Table 3).

Table 3. The ALP activity of MC3T3-E1 cells cultured with irisin with point mutation for 14 days. Data are shown as mean ± SD

Items	Fold r-irisin (ALP activity)	*P* value
irisin E57K	0.099 ± 0.152	< 0.01
irisin R75E	0.450 ± 0.113	< 0.05
irisin I107F	0.112 ± 0.160	< 0.01
r-irisin	1.000 ± 0.210	–

4. Discussion

In this study, we conducted 6XHis-tag or point mutation on irisin and detected their influence on the proliferation and differentiation of MC3T3-E1 cells. We found that irisin$^{N\text{-}His}$, irisin E57K and irisin R75E could boost cell proliferation. irisin$^{N\text{-}His}$ and irisin R75E had a positive effect on cell differentiation, and irisin$^{N\text{-}His}$ had the most similar effect as wild type irisin, while irisin R75E had a weaker effect than r-irisin.

Irisin has two glycosyl sites which make irisin a glycoprotein. In order to exclude the interference of glycosylation, prokaryotic cell *E. coli* was chosen to synthesize irisin in this study. Mineralized nodule could be observed in MC3T3-E1 cells after culture in induced medium for 14 days (*16*). So we detected the expression of Runx2, Col1α1 and ALP at the 3rd and 14th day of induced differentiation.

Our experiment showed that the N-terminal his-tag did not influence the effect of irisin on promoting the proliferation and differentiation of osteoblasts, but when the His-tag was on the C terminal, the protein almost completely lost its function. This suggested that the C-terminal might play a critical role. Another study found that His-tag on the C-terminal did not influence the effect of irisin on increasing oxygen consumption of cadiomyoblasts (*17*). The different cell might partly explain the difference. It needs to be mentioned that irisin$^{N\text{-}His}$ used in this study contains 18 amino acid residues before the irisin sequence, and they are MGSHHHHHHSSGLVPRGS; and irisin$^{C\text{-}His}$ has 8 residues (LEHHHHHH) following the C-terminal.

Structure analysis by crystallization suggests that irisin is composed of a β-sandwich with three β-strands on one side and four on the other, which is shown below: βA(35-43) -βB(46-52) -βC(60-69) -βC'(73-81) -βE(85-91) -βF(95-106) -βG(108-116). The flexible loops (residues 55-58 and 106-108) are considered as possible candidates to interact with other proteins (*14*). So the 57th and 107th amino acids were chosen for point mutations. We replaced the acidic glutamic, the 57th amino acid located between ligand βB and βC, with a basic lysine. The 107th amino acid, isoleucine, was replaced by a larger amino acid, phenylalanine. Our results showed that the irisin I107F did not influence the proliferation and differentiation of osteoblast cells. The irisin E57K had a significant effect on cell proliferation but failed to influence cell differentiation. This proved that residues 106-108 and 55-58 are very critical for irisin, and the pathways involved in cell proliferation and differentiation activated by irisin might be different.

Schumacher *et al*. reported that the salt bridges between Arg-75 and Glu-79 were important for maintaining irisin dimers (*14*). We used the glutamine instead of Arg-75 to interfere with formation of the salt bridge, and found that the osteogenic activity of the protein still exists but is weaker. This indicated that the salt bridge also contributes to the protein activity.

The endotoxin mixed in protein product from *E. coli* could induce inflammation and influence cell activity (*18-20*). The concentration of endotoxin in every protein sample was below the minimum concentration reported to exert an effect on osteoblasts (*21*). However, the candidate sites chosen to be changed were limited in this study and there is still a problem about identifying the receptor for irisin. Future research focusing on these might be helpful in biochemical or pharmacological exploration.

In conclusion, this research reported the influence of 6XHis-tag and point mutants of irisin on the proliferation and differentiation of osteoblasts. The flexible region of residues 55-58 and 106-108, and C-terminal of irisin are vital for its activity, and disrupting the dimerization of irisin might result in a reduced effect.

Acknowledgements

This work was supported by a grant from the National Natural Science Foundation of China [grant numbers: 81671421].

References

1. Schon HT, Weiskirchen R. Exercise-Induced Release of Pharmacologically Active Substances and Their Relevance for Therapy of Hepatic Injury. Front Pharmacol. 2016; 7:283.
2. Erickson HP. Irisin and FNDC5 in retrospect: An exercise hormone or a transmembrane receptor? Adipocyte. 2013; 2:289.
3. Chen N, Li Q, Liu J, Jia S. Irisin, an exercise-induced myokine as a metabolic regulator: An updated narrative review. Diabetes Metab Res Rev. 2016; 32:51-59.
4. Singhal V, Lawson EA, Ackerman KE, Fazeli PK, Clarke H, Lee H, Eddy K, Marengi DA, Derrico NP, Bouxsein ML, Misra M. Irisin levels are lower in young amenorrheic athletes compared with eumenorrheic athletes and non-athletes and are associated with bone density and strength estimates. PLoS One. 2014; 9:e100218.
5. Palermo A, Strollo R, Maddaloni E, Tuccinardi D, D'Onofrio L, Briganti SI, Defeudis G, De Pascalis M, Lazzaro MC, Colleluori G, Manfrini S, Pozzilli P, Napoli N. Irisin is associated with osteoporotic fractures independently of bone mineral density, body composition or daily physical activity. Clin Endocrinol (Oxf). 2015; 82:615-619.
6. Engin-Ustun Y, Caglayan EK, Gocmen AY, Polat MF. Postmenopausal Osteoporosis Is Associated with Serum Chemerin and Irisin but Not with Apolipoprotein M Levels. J Menopausal Med. 2016; 22:76-79.
7. Free patents online. IRISIN FOR CARE AND PREVENTION OF OSTEOPOROSIS. European Patent EP3081228. *http://www.freepatentsonline.com/EP3081228.html* (accessed September 19, 2018).
8. Colaianni G, Cuscito C, Mongelli T, Oranger A, Mori G,

Brunetti G, Colucci S, Cinti S, Grano M. Irisin enhances osteoblast differentiation in vitro. Int J Endocrinol. 2014; 2014:902186.
9. Graziana C, Concetta C, Teresa M, Paolo P, Cinzia B, Peng L, Ping L, Loris S, Mariasevera DC, Giorgio M. The myokine irisin increases cortical bone mass. Proc Natl Acad Sci U S A. 2015; 112:12157-12162.
10. Qiao X, Ying N, Ma Y, Yan C, Ran C, Yin W, Ying H, Xu W, Xu L. Corrigendum: Irisin promotes osteoblast proliferation and differentiation *via* activating the MAP kinase signaling pathways. Sci Rep. 2016; 6:18732.
11. Albrecht E, Norheim F, Thiede B, Holen T, Ohashi T, Schering L, Lee S, Brenmoehl J, Thomas S, Drevon C, Erickson H, Maak S. Irisin – A myth rather than an exercise-inducible myokine. Sci Rep. 2015; 5:8889.
12. Boström P, Wu J, Jedrychowski M P, *et al*. A PGC1-α-dependent myokine that drives brown-fat-like development of white fat and thermogenesis. Nature, 2013; 481:463-468.
13. Jedrychowski MP, Wrann CD, Paulo JA, Gerber KK, Szpyt J, Robinson MM, Nair KS, Gygi SP, Spiegelman BM. Detection and Quantitation of Circulating Human Irisin by Tandem Mass Spectrometry. Cell Metab. 2015; 22:734.
14. Schumacher MA, Chinnam N, Ohashi T, Shah RS, Erickson HP. The Structure of Irisin Reveals a Novel Intersubunit β-Sheet Fibronectin Type III (FNIII) Dimer: IMPLICATIONS FOR RECEPTOR ACTIVATION*. J Biol Chem. 2013; 288:33738-33744.
15. Nie YW, Liu DJ. N-glycosylation is required for FDNC5 stabilization and irisin secretion. Biochem J. 2017; 474:3167.
16. Lei Z, Gui-ying X, Lan X, Wei X, Zhi J, Shi-liang W. Establishment of an osteoblast model by inducing MC3T3-E1 subclone 14 in vitro. Chin J Hemorh. 2012; 22:16-18.
17. Xie C, Zhang Y, Tran TDN, Wang H, Li S, George EV, Zhuang H, Zhang P, Kandel A, Lai Y. Irisin Controls Growth, Intracellular Ca^{2+} Signals, and Mitochondrial Thermogenesis in Cardiomyoblasts. Plos One. 2015; 10:e0136816.
18. Bandow K, Maeda A, Kakimoto K, Kusuyama J, Shamoto M, Ohnishi T, Matsuguchi T. Molecular mechanisms of the inhibitory effect of lipopolysaccharide (LPS) on osteoblast differentiation. Biochem Biophys Res Commun. 2010; 402:755-761.
19. Nakao J, Fujii Y, Kusuyama J, Bandow K, Kakimoto K, Ohnishi T, Matsuguchi T. Low-intensity pulsed ultrasound (LIPUS) inhibits LPS-induced inflammatory responses of osteoblasts through TLR4-MyD88 dissociation. Bone. 2014; 58:17-25.
20. Wen-jv F, De-zhi Z, Xing Z, Yang G, Zhi-yang Y. Primary experimental study on the influence of LPS on osteoblast apoptosis in vitro. J Cell Mol Med. 2014; 24:8-12.
21. Guo C, Yuan L, Wang JG, Wang F, Yang XK, Zhang FH, Song JL, Ma XY, Cheng Q, Song GH. Lipopolysaccharide (LPS) induces the apoptosis and inhibits osteoblast differentiation through JNK pathway in MC3T3-E1 cells. Inflammation. 2014; 37:621.

(Received August 29, 2018; Revised December 25, 2018; Accepted December 29, 2018)

Original Article

DOI: 10.5582/bst.2018.01240

Crocin inhibits obesity *via* AMPK-dependent inhibition of adipocyte differentiation and promotion of lipolysis

Ming Gu, Li Luo, Kai Fang*

Department of Pharmacy, Union Hospital, Tongji Medical College, Huazhong University of Science and Technology, Wuhan, China.

Summary **Obesity has become a severe public health problem worldwide. Crocin, a natural product, has been reported to have a number of pharmacological activities, including anti-inflammatory, anti-cancer, neuroprotective, antihypertensive, and cardioprotective action. The aims of the current study were to identify the beneficial effects of crocin on obesity, adipocyte differentiation, and lipolysis and to evaluate the possible role of AMPK. Results indicated that crocin significantly increased AMPK phosphorylation in differentiated adipocytes *in vitro* and in adipose tissue in db/db mice. Crocin reduced lipid accumulation in differentiated adipocytes. In addition, crocin inhibited the expression of mRNA of important adipogenesis-related regulators, including CEBPα, CEBPβ, PPARγ, aP2, FAS, and CD36, in both differentiated adipocytes and adipose tissue in db/db mice. Crocin increased the expression of mRNA of key lipolysis-associated factors, including PPARα, LPL, and HSL, in both differentiated adipocytes and adipose tissue in db/db mice. In adipocytes, knockdown of AMPK significantly suppressed the crocin-induced inhibition of adipocyte differentiation and increase in lipolysis. BML-275 is an inhibitor of AMPK. In adipose tissue in db/db mice, BML-275 suppressed crocin-induced inhibition of fat formation and alleviation of a metabolic disorder. The current results suggest that crocin alleviates obesity in db/db mice and that it inhibits adipocyte differentiation in preadipocytes. Crocin inhibits adipogenesis and promotes lipolysis *via* activation of AMPK. Therefore, crocin may have promise as an option for the clinical treatment for obesity and associated metabolic diseases.**

Keywords: Obesity, crocin, AMPK, adipocyte differentiation, lipolysis

1. Introduction

Obesity and overweight have become a severe public health problem worldwide (*1*). In the United States, 17.1% of children and adolescents and 32.2% of adults were determined to be obese (*2*). In China, 21 million children were estimated to be overweight, 50% of which were considered obese (*3*). Obesity is a strong risk factor for many metabolic diseases, such as type 2 diabetes, and cardiovascular diseases (*4,5*). Obesity is a state of excessive accumulation of body fat, resulting from increased intake and storage of calories and/or decreased consumption of calories. Fat content is controlled by adipocyte differentiation and lipolysis. White adipocytes can store energy and produce numerous hormones and metabolites that modulate glucose and lipid metabolism (*6*). Increased adipocyte differentiation (*7*) and enlarged adipocytes are characteristics of obesity (*8*).

Natural products have long been used in Asia to treat various conditions such as inflammation, obesity, and diabetes (*9*). Crocin, a carotenoid compound, is a bioactive constituent of both the saffron (Crocus Sativus L.) and gardenia plants (*10*). Several studies have verified the antioxidant activities of crocin (*11-14*). Crocin has been reported to have a number of pharmacological activities, including anti-inflammatory, anti-cancer, neuroprotective, antihypertensive, and cardioprotective action (*15*). Studies have reported that crocin lowers blood glucose levels and insulin resistance, providing protection against obesity and improving the lipid profile (*16,17*). The protective effects of crocin against tissue damage in diabetes have been verified

**Address correspondence to:*
Dr. Kai Fang, Union Hospital, Tongji Medical College, Huazhong University of Science and Technology, No. 1277 Jiefang Avenue, Wuhan 430022, China.
E-mail: xinsilu930@163.com

(*14,17-19*). Crocin ameliorated the oxidative burden and inflammatory cascade and it suppressed the progression of diabetic nephropathy in diabetic rats (*11*). Crocin is effective in relieving the symptoms of obesity and diabetes, including hyperinsulinemia, hyperleptinemia, insulin resistance, and weight gain in animals that were obese or that had type 2 diabetes induced by a high fat diet and streptozotocin (*17*). In another study in which rats were fed a high-fat diet, crocin was found to alleviate functional and histopathological changes in obese rats in a dose-dependent manner (*20*). However, the mechanism by which crocin inhibits obesity is not fully understood.

AMP-activated protein kinase (AMPK) is an important sensor and central regulator of metabolism (*21*). Abnormal regulation of AMPK is associated with obesity, insulin resistance, type 2 diabetes, non-alcoholic fatty liver disease, and cardiovascular disease (*21*). AMPK has been found to regulate glucose and lipid metabolism by increasing glucose uptake, fatty acid oxidation, mitochondrial biogenesis, and autophagy while suppressing the synthesis of fatty acids, cholesterol, and protein (*22*).

Preliminary studies by the current authors indicated that crocin upregulated the phosphorylation of AMPK and that it activated AMPK signaling. The aims of the current study were to identify the beneficial effects of crocin on obesity, adipocyte differentiation, and lipolysis and to evaluate the hypothesis that crocin inhibits obesity *via* activation of AMPK-dependent inhibition of adipogenesis and promotion of lipolysis

2. Materials and Methods

2.1. *Cell culture and induction of adipocyte differentiation*

3T3-L1 preadipocytes cells were purchased from the American Type Culture Collection (ATCC; Manassas, VA, USA). 3T3-L1 cells were cultured in DMEM supplemented with heat-inactivated 10% bovine calf serum (Gibco, CA, USA), 100 mg/mL penicillin, and 100 mg/mL streptomycin in a 5% CO2 incubator at 37°C.

Induction of adipogenic differentiation was performed as previously reported (*23*). Two days after reaching confluence (designated day 0), pre-adipocytes were cultured in differentiation induction medium (DMI) with DMEM containing 10% fetal bovine serum (FBS, Gibco, CA, USA), 10 μg/mL insulin (Sigma-Aldrich, Saint Louis, MO, USA), 0.5 mM 3-isobutyl-1-methyl-xanthine (Santa Cruz, USA), and 0.25 μM dexamethasone (Sigma-Aldrich, Saint Louis, MO, USA) for 2 days. Next, cells were cultured for an additional 2 days (designated days 2-4) in maturation medium (DMEM containing 10% FBS and 10 μg/mL insulin) and then maintained in DMEM medium containing 10% FBS. The medium was replaced every two days for an additional four days (designated days 4-8) until the cells were harvested. For treatment, 20 μM crocin was added to the medium on days 0-8. The concentration of crocin used was based on previous studies (*24*).

2.2. *Lentivirus transfection*

Lentivirus (LV)-shAMPK was obtained from Santa Cruz Biotechnology (Santa Cruz, CA, USA). Preadipocytes were transfected with LV-shAMPK according to the manufacture's protocols. 3T3-L1 preadipocytes with stable knockdown of AMPK were produced.

2.3. *Lipid accumulation determination*

After the induction of adipogenic differentiation, cells were washed with phosphate-buffered saline (PBS), fixed with 10% formaldehyde for 30 min, and then washed with distilled water. The cells were then stained with BODIPY and Hoechst reagent for 20 min at room temperature. Cells were then washed with PBS and viewed under a confocal microscope (Olympus, Japan).

2.4. *Animal experiments*

All animal experiments were approved by the Institutional Animal Care and Use Committee of Union Hospital, Tongji Medical College, Huazhong University of Science and Technology and were conducted in accordance with ARRIVE and NIH guidelines for animal welfare. C57BL/KsJ-Lepdb (db/db) mice and their lean littermates (wild-type) were obtained from the Model Animal Research Center of Nanjing University. Ten-week-old male mice were housed at 22 ± 2°C and 60 ± 5% relative humidity and kept on a 12-h light/dark cycle with free access to water and a regular chow diet. db/db mice were randomly divided into three groups (db/db, Crocin, and Crocin+BML-275, n = 10 in each group). Mice in the Crocin+BML-275 group were intraperitoneally injected with BML-275 before the administration of crocin. Mice in the Crocin group were given 20 mg/kg of crocin daily. The dose of crocin was selected based on a previous study (*25*). Wild-type (WT) mice were treated with the vehicle in the same manner as the normal controls. This experiment lasted 8 weeks. Blood samples were collected, and tissue samples were flash-frozen in liquid nitrogen or collected for embedding in paraffin.

2.5. *Histological examination of adipose tissue*

A histological examination was performed to evaluate morphological changes in adipose tissue. Paraffin-embedded adipose tissue sections (5 μm) were prepared and stained with H&E. Images were captured using a light microscope (Olympus, Japan).

2.6. *Metabolic and biochemical analysis*

Before the OGTT and IPITT, mice were fasted for 12 h and 6 h, respectively. Blood glucose was measured 0, 30, 60, 90, and 120 min after the administration of glucose and insulin. Blood glucose levels were determined using tail vein blood *via* the Accu-Chek glucometer (Roche, Basel, Switzerland). At the end of the experiment, mice were fasted for 12 h and blood samples were collected from the orbital venous plexus immediately prior to sacrifice. Serum levels of triglycerides (TG), non-esterified fatty acids (NEFA), and total cholesterol (TC) were quantified using commercial kits (Nanjing Jiancheng, Nanjing, China). Serum insulin levels were determined using an enzyme-linked-immunosorbent assay (ELISA) kit (Invitrogen, Carlsbad, CA, USA).

2.7. *Real-time quantitative PCR*

Total RNA from liver tissue was isolated using TRIzol reagent (Life Technologies, Carlsbad, CA, USA). RNA samples were treated with DNase and reverse-transcribed into cDNA using Superscript II (Life Technologies, Foster City, CA). Real-time RT-PCR was performed with SYBR Green PCR Master Mix (Takara, Tokyo, Japan) in an ABI StepOnePlus Real-time PCR System. The expression of mRNA for each target gene was normalized relative to that of glyceraldehyde 3-phosphate dehydrogenase (GAPDH).

2.8. *Western blot analysis*

Liver tissues were lysed in RIPA Lysis Buffer (Beyotime, Jiangsu, China). After determination of the protein concentration using the BCA Protein Assay Kit (Beyotime, Jiangsu, China), the samples were separated with sodium dodecyl sulphate-polyacrylamide gel electrophoresis (SDS-PAGE) and transblotted onto polyvinylidene fluoride membranes (PVDF, Millipore). Membranes were then incubated with primary antibodies (diluted 1:1000; Cell Signaling Technology, USA) overnight at 4°C. Membranes were washed with TBST and then were incubated with horseradish-peroxidase (HRP)-conjugated secondary antibody (diluted 1:5,000; Thermo Fisher Scientific, USA) for 1 h at room temperature. Finally, the blots were visualized using chemiluminescence (ECL) detection reagents (Thermo Fisher Scientific, USA). Data were analyzed by calculating the integrated optical density.

2.9. *Statistical analysis*

Results are expressed as the mean ± SD. Significant differences among groups were assessed using one-way ANOVA followed by Dunnett's test. Statistical significance was defined as $p < 0.05$.

3. Results

3.1. *Crocin upregulates AMPK phosphorylation and lipid accumulation in differentiated adipocytes*

A 3T3-L1 adipogenic differentiation model was used to evaluate the effect of crocin on the course of adipocyte differentiation. Phosphorylation was inhibited with LV-shAMPK in differentiated adipocytes, but crocin significantly increased that phosphorylation, as shown in Figure 1A. Figure 1B shows that crocin markedly increased BODIPY staining in differentiated adipocytes, indicating a reduction in lipid accumulation and inhibition of adipocyte differentiation. In addition, knockdown of AMPK significantly blocked crocin's action on lipid accumulation in differentiated adipocytes (Figure 1B). Findings indicated that crocin inhibited adipocyte differentiation *via* upregulation of AMPK signaling.

3.2. *Crocin inhibits adipogenic differentiation and promotes lipolysis in differentiated adipocytes*

To investigate the mechanism of crocin-induced inhibition of lipid accumulation in differentiated adipocytes, the expression of adipogenesis-related factors and lipolysis-associated regulators was determined. As shown in Figure 2A-F, crocin reduced the expression of mRNA of important adipogenesis-related regulators, including CCAAT/enhancer binding protein α (CEBPα), CEBPβ, PPARγ, aP2, FAS, and CD36, in differentiated adipocytes. Moreover, treatment with crocin increased the expression of key lipolysis-associated regulators such as PPARα, lipoprotein lipase (LPL), and hormone-sensitive lipase (HSL) (Figure 2G-I). Results indicated that the inhibition of lipid accumulation by crocin in differentiated adipocytes may be attributed to its inhibition of adipogenic differentiation and its promotion of lipolysis. Moreover, these actions of crocin were inhibited by the knockdown of AMPK (Figures 2A-I). These findings suggest that treatment with crocin resulted in a reduction in adipocyte differentiation and an increase in lipolysis in an AMPK-dependent manner.

3.3. *Crocin inhibits adipose formation in diabetic and obese db/db mice*

To evaluate the effect of crocin on adipose formation *in vivo*, db/db mice were injected with crocin. Figure 3A and B show that AMPK phosphorylation in adipose tissue was significantly lower than that in WT mice. Treatment with crocin significantly increased AMPK phosphorylation in adipose tissue in db/db mice (Figure 3A and B). BML-275 decreased AMPK phosphorylation in adipose tissue in the presence of crocin (Figure 3A and B). Findings indicated that crocin decreased the weight of epididymal and perirenal white adipose

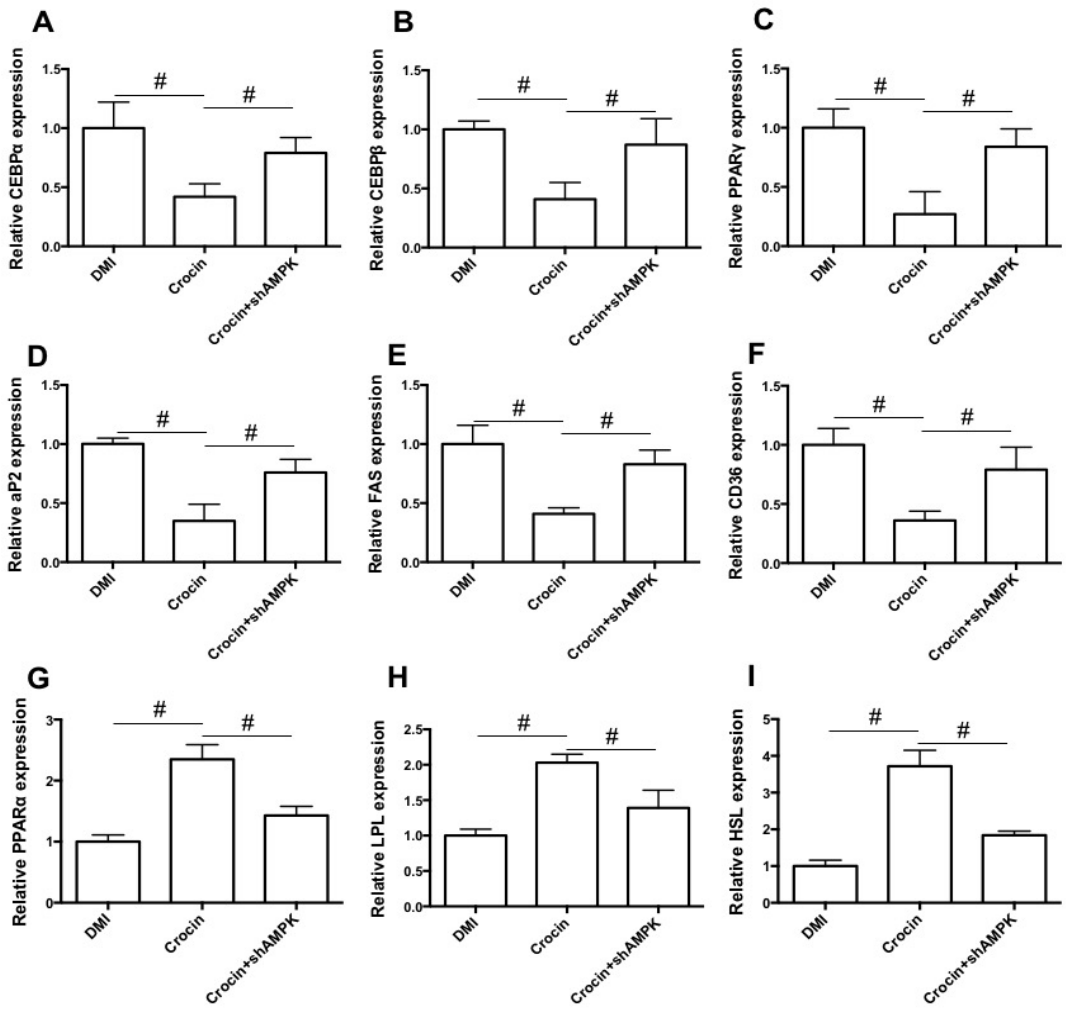

Figure 2. Effects of crocin on the expression of regulators of adipogenesis and lipolysis in differentiated adipocytes. Expression of CEBPα **(A)**, CEBPβ **(B)**, PPARγ **(C)**, aP2 **(D)**, FAS **(E)**, CD36 **(F)**, PPARα **(G)**, LPL **(H)**, and HSL **(I)** mRNA in differentiated adipocytes was determined using real-time qPCR. $^{\#}p < 0.05$ indicates a significant difference between the two groups.

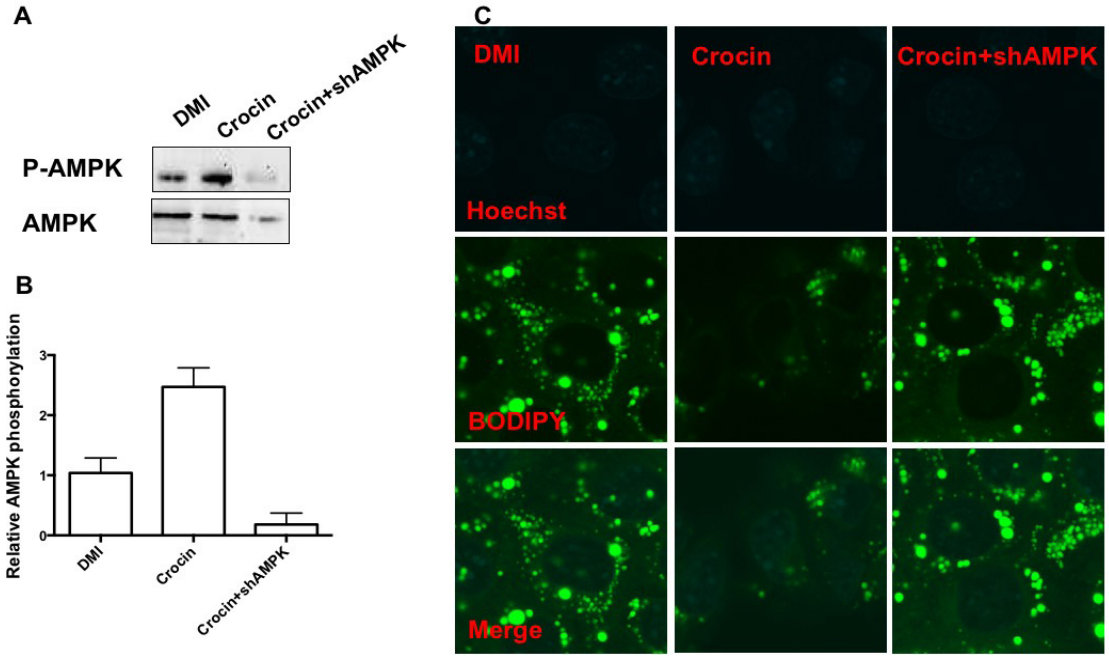

Figure 1. Effects of crocin on AMPK phosphorylation and lipid accumulation in differentiated adipocytes. (A) Western blot analysis of AMPK phosphorylation in differentiated adipocytes. **(B)** Statistical analysis of AMPK phosphorylation. **(C)** BODIPY staining of differentiated adipocytes. $^{\#}p < 0.05$ indicates a significant difference between the two groups.

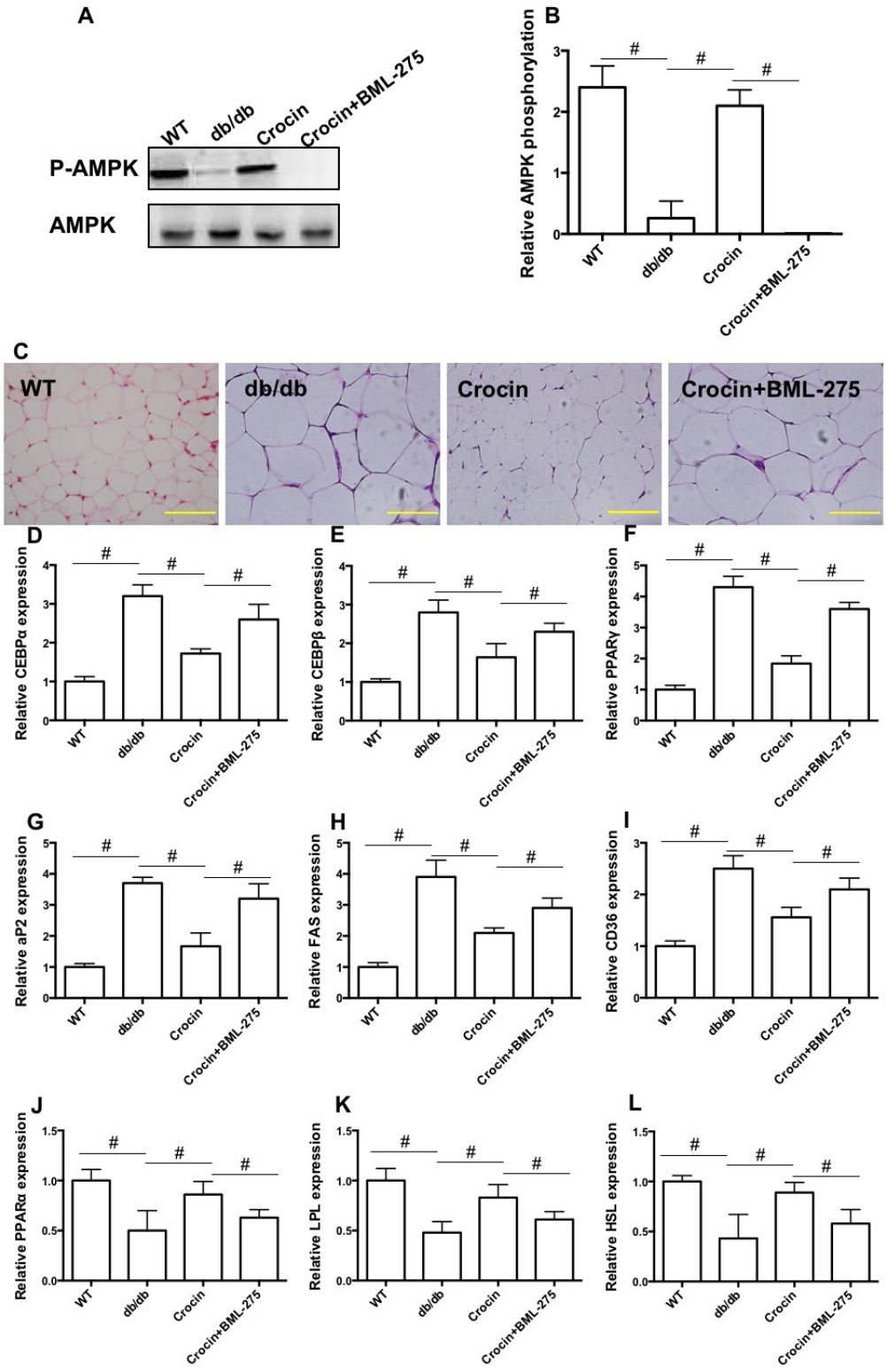

Figure 3. Effects of crocin on AMPK phosphorylation, adipocyte size, and the expression of regulators of adipogenesis and lipolysis in adipose tissue. (A) Western blot analysis of AMPK phosphorylation in differentiated adipocytes. **(B)** statistical analysis of AMPK phosphorylation. **(C)** HE staining of adipose tissue. Expression of CEBPα **(D)**, CEBPβ **(E)**, PPARγ **(F)**, aP2 **(G)**, FAS **(H)**, CD36 **(I)**, PPARα **(J)**, LPL **(K)**, and HSL **(L)** mRNA in differentiated adipocytes was determined using real-time qPCR. $^{\#}p < 0.05$ indicates a significant difference between the two groups.

tissue, though this action was inhibited by injection of BML-275, an inhibitor of AMPK (Table 1). Figure 3C shows that crocin decreased the size of adipocytes in db/db mice. However, injection of BML-275 reversed the crocin-induced shrinkage in adipocyte size in db/db mice (Figure 3C). Moreover, crocin reduced the expression of mRNA of important adipogenesis-related regulators, including CEBPα, CEBPβ, PPARγ,

Table 1. Effects of crocin on general parameters in db/db mice

Parameters	WT	db/db	Crocin	Crocin+BML-275
Body weight (g)	25.4 ± 1.7	43.7 ± 2.5$^{\#}$	34.3 ± 2.3$^{\#\#}$	39.7 ± 2.1$^{\#\#\#}$
Epididymal adipose weight (g)	0.19 ± 0.07	2.53 ± 0.23$^{\#}$	1.91 ± 0.16$^{\#\#}$	2.34 ± 0.12$^{\#\#\#}$
Perirenal adipose weight (g)	0.1 ± 0.04	1.35 ± 0.08$^{\#}$	0.98 ± 0.13$^{\#\#}$	1.22 ± 0.11$^{\#\#\#}$
Serum NEFA (mM)	0.22 ± 0.05	0.71 ± 0.12$^{\#}$	0.45 ± 0.11$^{\#\#}$	0.62 ± 0.08$^{\#\#\#}$
Serum TG (mM)	0.94 ± 0.09	1.53 ± 0.16$^{\#}$	1.14 ± 0.13$^{\#\#}$	1.38 ± 0.08$^{\#\#\#}$
Serum TC (mM)	2.02 ± 0.16	2.89 ± 0.20$^{\#}$	2.43 ± 0.11$^{\#\#}$	2.72 ± 0.12$^{\#\#\#}$
Blood glucose (mM)	5.97 ± 0.82	16.4 ± 2.81$^{\#}$	9.6 ± 1.15$^{\#\#}$	14.5 ± 2.15$^{\#\#\#}$
Serum insulin (ng/mL)	2.8 ± 0.43	18.7 ± 1.18$^{\#}$	10.9 ± 3.11$^{\#\#}$	16.3 ± 2.25$^{\#\#\#}$

WT, wild type; db/db, db/db mice; $^{\#}$, $p < 0.05$, compared with WT; $^{\#\#}$, $p < 0.05$, compared with db/db mice; $^{\#\#\#}$, $p < 0.05$, compared with Crocin treatment.

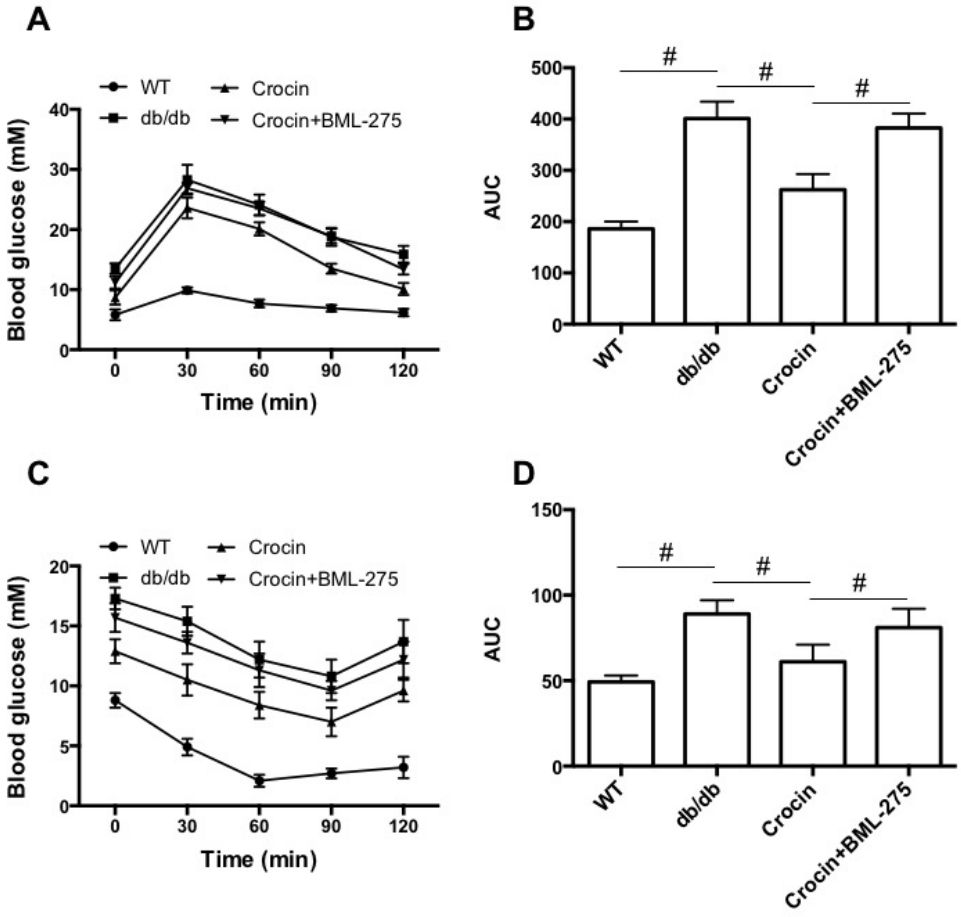

Figure 4. Effects of crocin on general glucose and lipid metabolism in db/db mice. (A) OGTT test. **(B)** area under the curve during the OGTT. **(C)** IPITT test. **(D)** area under the curve during the IPITT. $^{\#}p < 0.05$ indicates a significant difference between the two groups.

aP2, FAS, and CD36, in adipose tissue (Figure 3D-I). Treatment with crocin increased the expression of key lipolysis-associated regulators such as PPARα, LPL, and HSL in adipose tissue (Figure 3J-L). Crocin's action on adipocyte differentiation and lipolysis was inhibited by BML-275 (Figure 3D-L). Results indicated that crocin suppressed the formation of adipose by inhibiting adipogenesis and promoting lipolysis *via* AMPK-dependent regulation of key regulators.

3.4. *Crocin attenuates a metabolic disorder in diabetic and obese db/db mice*

The protective effect of crocin against systemic metabolic disorder was evaluated in db/db mice. As shown in Table 1, crocin reduced body weight, fasting blood glucose levels, and serum levels of insulin, TG, TC, and NEFA in db/db mice, but these effects of crocin were inhibited by BML-275. In addition, treatment with crocin reduced glucose levels at different times after the administration of glucose and insulin (Figure 4A-D). Improvement in glucose and insulin tolerance as a result of crocin was inhibited by BML-275. Findings suggested that crocin provided protection against a systemic metabolic disorder *via* upregulation of AMPK signaling.

4. Discussion

Obesity is a result of excessive accumulation of fat in the body (*26*), and dysregulated adipogenesis and lipolysis are involved in this process. Adipogenic differentiation and maturation of pre-adipocytes are complex processes, and a battery of regulators are involved in the regulation of the formation of adipose. In response to adipogenic stimuli, expression of CEBPβ initiates the differentiation process (*27*), which is followed by the sequential activation of various key regulators such as CEBPα and PPARγ (*28*). During differentiation, FAS and other fat synthesis-related genes are activated, leading to the synthesis of lipids droplets and storage of TG (*29*). Lipolysis, the catabolic pathway of the fatty acid cycle, is also crucial to balanced fat metabolism. Enhanced lipolysis contributes to the release of fatty acids and a decrease in fat deposition. The lipolytic process is mainly controlled by PPARα, LPL, HSL, and other key regulators. LPL is the rate-limiting enzyme for the hydrolysis of TG and very low-density lipoproteins (*30*).

The current study evaluated the effect of crocin on obesity with a focus on adipocyte differentiation and lipolysis in 3T3-L1 cells. Findings revealed that administration of crocin significantly reduced body weight and fat mass in obese mice, suggesting that crocin may be a potential option as an intervention to fight obesity and associated metabolic disorders. In addition, results indicated that crocin significantly reduced lipid accumulation in differentiated adipocytes. Moreover, crocin decreased the weight of adipose tissue in db/db mice, helping to alleviate a systemic metabolic disorder in mice. The possible mechanisms of these actions were examined, and crocin was found to inhibit the expression of adipogenesis-related factors and to promote the expression of lipolysis-associated regulators. The findings support the hypothesis that crocin inhibits the formation of adipose tissue and thus protects against systemic metabolic dysfunction.

AMPK is a serine/threonine protein that is an important regulatory sensor of cellular energy metabolism (*31*). Activated AMPK inhibits acetyl-CoA carboxylase (ACC), which is an essential enzyme for lipid biosynthesis (*32*). During adipogenesis, AMPK inhibits the expression of sterol regulatory element binding protein-1 (SREBP-1), CEBPα, PPARγ, and FAS (*33*), resulting in suppression of the differentiation of adipocytes. In addition, AMPK has been found to promote lipolysis and thus decrease the mass of adipose tissue (*34*). Preliminary studies by the current authors indicated that AMPK was activated by crocin. The current study examined whether activation of AMPK was involved in crocin's protection against obesity. Results revealed that downregulation of AMPK *via* lentivirus transfection inhibited crocin-induced suppression of lipid accumulation, downregulation of the expression of adipogenesis-related regulators, and upregulation of the expression of lipolysis-associated factors *in vitro*. BML-275 is an inhibitor of AMPK. *In vivo*, BML-275 reversed crocin's inhibition of obesity and diabetes. Results indicated that activation of AMPK was involved in crocin's protection from obesity and diabetes *via* regulation of adipocyte differentiation and lipolysis.

The current results suggest that crocin alleviated obesity in db/db mice and that it inhibited adipocyte differentiation in preadipocytes. Crocin inhibits adipogenesis and it promotes lipolysis *via* activation of AMPK. Therefore, crocin may have promise as an option for the clinical treatment for obesity and associated metabolic diseases. Further studies are needed to verify crocin's potential in other animal models and to explore the specific and non-specific biological actions of crocin.

References

1. Flier JS. Obesity wars: Molecular progress confronts an expanding epidemic. Cell. 2004; 116:337-350.
2. Ogden CL, Carroll MD, Curtin LR, McDowell MA, Tabak CJ, Flegal KM. Prevalence of overweight and obesity in the United States, 1999-2004. JAMA. 2006; 295:1549-1555.
3. Wise J. Obesity rates rise substantially worldwide. BMJ (Clinical research ed). 2014; 348:g3582.
4. Matsuda M, Shimomura I. Increased oxidative stress in obesity: Implications for metabolic syndrome, diabetes, hypertension, dyslipidemia, atherosclerosis, and cancer. Obes Res Clin Pract. 2013; 7:e330-341.
5. Haslam DW, James WP. Obesity. Lancet (London, England). 2005; 366:1197-1209.
6. Choe SS, Huh JY, Hwang IJ, Kim JI, Kim JB. Adipose tissue remodeling: Its role in energy metabolism and metabolic disorders. Front Endocrinol (Lausanne). 2016; 7:30.
7. Camp HS, Ren D, Leff T. Adipogenesis and fat-cell function in obesity and diabetes. Trends Mol Med. 2002; 8:442-447.
8. Muir LA, Neeley CK, Meyer KA, *et al*. Adipose tissue fibrosis, hypertrophy, and hyperplasia: Correlations with diabetes in human obesity. Obesity (Silver Spring, Md). 2016; 24:597-605.
9. Vasudeva N, Yadav N, Sharma SK. Natural products: A safest approach for obesity. Chin J Integr Med. 2012; 18:473-480.
10. Esposito E, Drechsler M, Mariani P, Panico AM, Cardile V, Crasci L, Carducci F, Graziano ACE, Cortesi R, Puglia C. Nanostructured lipid dispersions for topical administration of crocin, a potent antioxidant from saffron (*Crocus sativus* L.). Mater Sci Eng C Mater Biol Appl. 2017; 71:669-677.
11. Abou-Hany HO, Atef H, Said E, Elkashef HA, Salem HA. Crocin mediated amelioration of oxidative burden and inflammatory cascade suppresses diabetic nephropathy progression in diabetic rats. Chem Biol Interact. 2018; 284:90-100.
12. Li S, Liu X, Lei J, Yang J, Tian P, Gao Y. Crocin protects podocytes against oxidative stress and inflammation induced by high glucose through inhibition of NF-

kappaB. Cell Physiol Biochem. 2017; 42:1481-1492.
13. Yang X, Huo F, Liu B, Liu J, Chen T, Li J, Zhu Z, Lv B. Crocin inhibits oxidative stress and pro-inflammatory response of microglial cells associated with diabetic retinopathy through the activation of PI3K/Akt signaling pathway. J Mol Neurosci. 2017; 61:581-589.
14. Yaribeygi H, Mohammadi MT, Sahebkar A. Crocin potentiates antioxidant defense system and improves oxidative damage in liver tissue in diabetic rats. Biomed Pharmacother. 2018; 98:333-337.
15. Yosri H, Elkashef WF, Said E, Gameil NM. Crocin modulates IL-4/IL-13 signaling and ameliorates experimentally induced allergic airway asthma in a murine model. Int Immunopharmacol. 2017; 50:305-312.
16. Mashmoul M, Azlan A, Khaza'ai H, Yusof BN, Noor SM. Saffron: A natural potent antioxidant as a promising anti-obesity drug. Antioxidants (Basel, Switzerland). 2013; 2:293-308.
17. Hazman O, Aksoy L, Buyukben A. Effects of crocin on experimental obesity and type-2 diabetes. Turk J Med Sci. 2016; 46:1593-1602.
18. Altinoz E, Oner Z, Elbe H, Cigremis Y, Turkoz Y. Protective effects of saffron (its active constituent, crocin) on nephropathy in streptozotocin-induced diabetic rats. Hum Exp Toxicol. 2015; 34:127-134.
19. Sepahi S, Mohajeri SA, Hosseini SM, Khodaverdi E, Shoeibi N, Namdari M, Tabassi SAS. Effects of crocin on diabetic maculopathy: A placebo-controlled randomized clinical trial. Am J Ophthalmol. 2018; 190:89-98.
20. Mashmoul M, Azlan A, Mohtarrudin N, Mohd Yusof BN, Khaza'ai H, Khoo HE, Farzadnia M, Boroushaki MT. Protective effects of saffron extract and crocin supplementation on fatty liver tissue of high-fat diet-induced obese rats. BMC Complement Altern Med. 2016; 16:401.
21. Day EA, Ford RJ, Steinberg GR. AMPK as a therapeutic target for treating metabolic diseases. Trends Endocrinol Metab. 2017; 28:545-560.
22. Hardie DG, Ross FA, Hawley SA. AMPK: A nutrient and energy sensor that maintains energy homeostasis. Nat Rev Mol Cell Biol. 2012; 13:251-262.
23. Choi RY, Lee HI, Ham JR, Yee ST, Kang KY, Lee MK. Heshouwu (Polygonum multiflorum Thunb.) ethanol extract suppresses pre-adipocytes differentiation in 3T3-L1 cells and adiposity in obese mice. Biomed Pharmacother. 2018; 106:355-362.
24. Mousavi SH, Tayarani NZ, Parsaee H. Protective effect of saffron extract and crocin on reactive oxygen species-mediated high glucose-induced toxicity in PC12 cells. Cell Mol Neurobiol. 2010; 30:185-191.
25. Feidantsis K, Mellidis K, Galatou E, Sinakos Z, Lazou A. Treatment with crocin improves cardiac dysfunction by normalizing autophagy and inhibiting apoptosis in STZ-induced diabetic cardiomyopathy. Nutr Metab Cardiovasc Dis. 2018; 28:952-961.
26. Zhang Y, Liu J, Yao J, Ji G, Qian L, Wang J, Zhang G, Tian J, Nie Y, Zhang YE, Gold MS, Liu Y. Obesity: Pathophysiology and intervention. Nutrients. 2014; 6:5153-5183.
27. Gregoire FM, Smas CM, Sul HS. Understanding adipocyte differentiation. Physiol Rev. 1998; 78:783-809.
28. Tontonoz P, Hu E, Spiegelman BM. Stimulation of adipogenesis in fibroblasts by PPAR gamma 2, a lipid-activated transcription factor. Cell. 1994; 79:1147-1156.
29. Gregoire FM. Adipocyte differentiation: From fibroblast to endocrine cell. Exp Biol Med (Maywood). 2001; 226:997-1002.
30. Kersten S. Physiological regulation of lipoprotein lipase. Biochim Biophys Acta. 2014; 1841:919-933.
31. Kim SK, Kong CS. Anti-adipogenic effect of dioxinodehydroeckol *via* AMPK activation in 3T3-L1 adipocytes. Chem Biol Interact. 2010; 186:24-29.
32. Xi Y, Wu M, Li H, Dong S, Luo E, Gu M, Shen X, Jiang Y, Liu Y, Liu H. Baicalin attenuates high fat diet-induced obesity and liver dysfunction: Dose-response and potential role of CaMKKbeta/AMPK/ACC pathway. Cell Physiol Biochem. 2015; 35:2349-2359.
33. Rayalam S, Yang JY, Ambati S, Della-Fera MA, Baile CA. Resveratrol induces apoptosis and inhibits adipogenesis in 3T3-L1 adipocytes. Phytother Res. 2008; 22:1367-1371.
34. Cheng CY, Yang AJ, Ekambaranellore P, Huang KC, Lin WW. Anti-obesity action of INDUS810, a natural compound from Trigonella foenum-graecum: AMPK-dependent lipolysis effect in adipocytes. Obes Res Clin Pract. 2018.

(Received October 8, 2018; Revised December 29, 2018; Accepted December 31, 2018)

Original Article

DOI: 10.5582/bst.2018.01255

Danzhi Jiangtang Capsule ameliorates kidney injury *via* inhibition of the JAK-STAT signaling pathway and increased antioxidant capacity in STZ-induced diabetic nephropathy rats

Min Sun[1,*], Wenjie Bu[1], Yan Li[1], Jianliang Zhu[1], Jindong Zhao[2], Pingping Zhang[1], Lingling Gu[1], Wenna Zhang[1], Zhaohui Fang[2,*]

[1] *Anhui Provincial Key Laboratory of R&D of Chinese Material Medica, School of Life Science, Anhui University, Hefei, China;*
[2] *Department of Endocrinology, the First Affiliated Hospital of Anhui University of TCM, Hefei, China.*

Summary **Danzhi Jiangtang Capsule (DJC), a traditional Chinese medicinal formula, has been used clinically in treating diabetes and diabetic nephropathy (DN). We previously demonstrated that DJC is capable of improving renal function in patients and rats with DN, but the mechanisms underlying these therapeutic benefits of DJC are not quite clear yet. In this study, STZ-induced diabetic rats were orally administered DJC for 8 weeks. Fasting blood glucose, renal function indicators in the serum, renal index, and the expression of proteins related to JAK-STAT signaling pathway were evaluated at the end of the experiment. The kidneys were sliced for pathological histology. Antioxidant status was assessed by measuring SOD, LPO and MDA in serum. The expression levels of COX2, iNOS, SOCS and the phosphorylation status of JAK2, STAT1, and STAT3 in renal tissues were evaluated by Western blot analyses. IL-6, TNF-α, and MCP-1 expression levels in renal tissues were determined using double-antibody sandwich ELISA. Diabetic renal dysfunction and its associated pathologies were ameliorated by DJC treatment. DJC significantly reversed the high expression of COX2 and iNOS in renal tissues. Furthermore, DJC inhibited the JAK2-STAT1/STAT3-SOCS3 signaling pathway, resulting in decreased concentrations of IL-6, TNF-α, and MCP-1. Moreover, the oxidant status in the kidney was substantially ameliorated by DJC treatment. In conclusion, the ability of DJC to ameliorate diabetic renal dysfunction and the associated pathologies of this disease might be due to its antioxidant capacity and suppression of the JAK2-STAT1/STAT3 cascade.**

Keywords: Danzhi Jiangtang capsule, diabetic nephropathy, JAK-STAT signaling pathway, oxidative stress

1. Introduction

Diabetic nephropathy (DN), the most common and most serious microvascular complication of diabetic *mellitus* (DM), is a major cause of chronic renal failure or end-stage renal disease (ESRD). With the increase of the incidence of DM, the subsequent incidence of DN is increasing worldwide. Multiple mechanisms contribute to the occurrence and development of DN, such as glucose and lipid metabolic disorders, oxidative stress, accumulation of advanced glycosylation end products (AGEs) and the interaction with their receptors, and renal hemodynamic alterations. Accumulating evidence suggests that inflammation is an important pathogenic mechanism of diabetic complications (*1-4*).

Elevated levels of proinflammatory cytokines, chemokines, adhesion molecules and growth factors in renal tissues, serum and urine of diabetic patients are correlated with albuminuria (*1-4*). During inflammation,

Released online in J-STAGE as advance publication December 28, 2018.

**Address correspondence to:*
Dr. Min Sun, School of Life Science, Anhui University, Hefei 230601, Anhui, China.
E-mail: sunmin@ahu.edu.cn

Dr. Zhaohui Fang, Department of Endocrinology, the First Affiliated Hospital of Anhui University of TCM, Hefei 230031, Anhui, China.
E-mail: fangzh9097@126.com

cytokines and growth factors exert their functions mainly through activation of the Janus tyrosine kinase (JAK)-signal transducers and activators of transcription (STAT) pathway. The activated JAK-STAT signal cascade can accelerate the proliferation of glomerular mesangial cells and matrix expansion, contributing to DN (*5,6*). Thus the modulation of this pathway may prevent or alleviate the progression of DN (*5,7*). The JAK-STAT cascade is a relatively simple signaling pathway with only a few principal components. There are four members in the JAK family (JAK1, JAK2, JAK3, and TYK2) and seven members in the STAT family (STAT1, STAT2, STAT3, STAT4, STAT5A/B, and STAT6). The binding of ligands to their receptors triggers the JAK-STAT signal cascade (*5,7*) and subsequently regulates the expression of target genes encoding cytokines, chemokines, adherence molecules, and inducible enzymes such as iNOS (inducible nitric oxide synthase) and COX-2 (Cyclooxygenase 2). The JAK-STAT signaling pathway is regulated by several mechanisms, among which suppressors of cytokine signaling (SOCS) family is the most important negative regulator. SOCS family, containing at least eight members (CIS; SOCS1 to SOCS7), can be induced by many cytokines and pathogenic mediators, and thereby, serves to inhibit further signal transduction in a negative feedback loop (*7-9*).

Danzhi Jiangtang Capsule (DJC) is a traditional Chinese medicinal formula that has been shown to have good clinical efficacy in diabetes and DN. Our previous studies demonstrated that DJC inhibits oxidative stress and suppresses elevated inflammatory factors including IL (Interleukin)-8, tumor necrosis factor (TNF)-α, CXCL[The chemokine (C-X-C motif) ligand]-5, 9, and MCP-1 (monocyte chemotactic protein 1) in diabetic patients and rats (*10-13*). DJC has also been reported to inhibit NF-κB and ameliorate renal inflammation in diabetic rats (*10,14*) and to reduce the urinary albumin excretion rate (UAER) in early-stage DN patients (*10,15*).

However, the mechanisms underlying these therapeutic benefits of DJC are not quite clear yet. Therefore, the present study was carried out to evaluate the efficacy and to explore the potential underlying mechanism of DJC on DN. In this study, STZ-induced diabetic rats were treated with DJC intragastrically for 8 weeks, the antioxidant effects of DJC were evaluated and the roles of DJC in JAK-STATs signaling and SOCS proteins expression were also explored.

2. Materials and Methods

2.1. *Preparation of DJC*

DJC was provided by the Department of Pharmaceutics at the First Affiliated Hospital of Anhui University of Traditional Chinese Medicine (Hefei, Anhui, China). DJC contains 6 medicinal components at a ratio of 6:5:4:4:3:3: Radix Pseudostellariae, Radix Rehmanniae, Cortex Moutan, Rhizoma Alismatis, Semen Cuscutae Chinensis, and Leech. As mentioned in the previous study (*16*), Cortex Moutan was extracted using ethanol and the extract was dried under vacuum. The gruffs of Cortex Moutan and the other 4 medicinal components except for Leech, were mixed and extracted with water. After vacuum drying, the dried extract powder was obtained. The ground fine powder of Leech was mixed with the above-mentioned dry extract powder, and the resulting powder was prepared as capsules with each capsule containing 0.4 g of extract (equivalent to 8 g mixture of herbal medicine). The components of the DJC capsule were detected and quantitated by ultra-performance liquid chromatography (UPLC) (*17*).

2.2. *Chemicals and reagents*

Rat TNF-α and IL-6 ELISA kits were obtained from ExCell Bio Inc (Shanghai, China), and the MCP-1 kit was from Neobioscience (Shenzhen, Guangdong, China). Serum super oxide dismutase (SOD), lipid peroxidation (LPO) and malondialdehyde (MDA) kits were purchased from Jiancheng Bio-engineering Institute (Nanjing, China). The COX2, p-STAT1 (Tyr 701) and STAT1 polyclonal antibodies were obtained from SAB (Signalway Antibody Company, College Park, MD, USA). The monoclonal antibodies against p-STAT3 (Tyr 705) and STAT3 were supplied from Cell Signaling Technology (Beverly, MA, USA). p-JAK2 and JAK2 polyclonal antibodies were from Millipore (Billerica, MA, USA). The SOCS1 polyclonal antibody was from ImmunoWay Biotechnology (Plano, TX, USA). The SOCS3 and iNOS polyclonal antibodies were obtained from Santa Cruz (Santa Cruz, CA, USA). Rabbit polyclonal β-actin antibody and all of the secondary antibodies used for Western blotting were obtained from Abmart (Hangzhou, Zhejiang, China). An electrochemiluminescence (ECL) kit and BCA protein assay kit were supplied by Thermo Scientific Pierce (Rockford, IL, USA). STZ was from Sigma Chemical Co (St. Louis, MO, USA). All chemicals used in this study were analytical grade reagents and obtained commercially.

2.3. *Animals and Experimental procedures*

Male healthy Sprague-Dawley rats, weighing 80 ± 10 g (4 weeks old), were provided by the Experimental Animal Center of Anhui Medical University (Hefei, Anhui, China). After feeding with a high fat diet (containing 10% lard, 2.5% milk powder, 5% glucose, 10% egg yolk, 1% cholesterol, and 71.5% standard rat feed) for 4 weeks, the rats were intraperitoneally injected with STZ in citrate buffer (pH 4.5) at a dose of 30 mg/kg body weight weekly for 3 weeks (*18*). Non-

diabetic, normal animals fed with a normal diet were injected with vehicle and used as controls (Ctrl). The rats with fasting blood glucose (FBG) levels above 16.7 mmol/L were considered to be diabetic animals, then the diabetic rats were weighed and randomly divided into the model (DM), low-dose DJC (DJCL, 600 mg / kg.d^{-1} in tap water) and high-dose DJC (DJCH, 2,000 mg/kg.d^{-1} in tap water) groups, each consisting of 8 rats. The low dose of DJC (equivalent dose) was calculated from the human dose on the basis of estimated body surface area. Rats in the DJCH and DJCL groups were orally administered DJC for 8 consecutive weeks, while those in the control and DM groups were given an equal volume of vehicle. Rats were placed in a temperature and humidity controlled room, free access to high fat or standard rat feed and drinking water was allowed during the experiment. Furthermore, the rats were weighed on a weekly basis. FBG measurements were taken bi-weekly using a One Touch Glucometer (Life scan, Johnson & Johnson, Milpitas, California, USA). After 8 weeks of treatment, all rats were sacrificed for analysis of renal tissue. This study was approved by the Committee for the Care and Use of Laboratory Animals of Anhui University, and procedures were in accordance with the Guidelines for the Welfare and Ethics of Laboratory Animals of China.

2.4. *Determination of biochemical parameters*

After 8 weeks of DJC administration, the rats were fasted overnight, weighed and sacrificed under chloral hydrate anesthesia (300 mg/kg, IP), and their blood was collected and centrifuged at 1,400 g for 10 min to obtain serum. The serum urea nitrogen (BUN), creatinine (Cr), uric acid (UA), FBG, cholesterol (CHO), triglycerides (TG), low-density lipoprotein (LDL) and high-density lipoprotein (HDL) were determined using an automatic biochemistry analyzer (Dimension RxL Max, Siemens, US).

2.5. *Detection of oxidative stress indicators*

The activities of total SOD and the concentrations of MDA and LPO in the serum were assayed using commercial test kits from Jiancheng Bio-engineering Institute (Nanjing, China) following the manufacturer's instructions.

2.6. *Histopathological assay*

The kidney samples were dissected and fixed in 10% formalin, followed by dehydration and embedding in paraffin. Then the tissues were cut into 5-μm-thick sections and stained with H&E (hematoxylin and eosin) and PAS (periodic acid Schiff) and then were studied; photos were taken using a binocular Olympus DX45 microscope (Olympus Corporation, Tokyo, Japan).

2.7. *Renal cytokine determination*

After mashing and homogenizing, the renal tissues were centrifuged at 4,500 g for 10 min at 4°C, the supernatants were then collected, and the levels of IL-6, TNF-α and MCP-1 levels were measured using commercial enzyme-linked immunoassay (ELISA) kits according to the manufacturer's instructions. Cytokine concentrations were normalized to the amount of total protein of each sample, which was determined by BCA assay (Thermo Scientific Pierce, Rockford, IL).

2.8. *Western blotting*

Renal tissues were homogenized in ice-cold RIPA buffer (50 mM Tris pH 7.5, 150 mM NaCl, 2 mM EGTA, 2 mM $Na3VO_4$, 1 mM phenylmethane sulfonyl fluoride) containing HALT protease/phosphatase inhibitor cocktail (Sangon, Shanghai, China) and lysed for 60 min. The lysates were collected and centrifuged at 4°C for 20 min at 30,500 g. The protein concentration of the supernatant was determined using a BCA kit (Thermo Scientific Pierce, Rockford, IL). Aliquots containing 40 μg of protein were separated by electrophoresis through 10% or 12% sodium dodecyl sulfate (SDS)-polyacrylamide gel electrophoresis (PAGE) gels and then transferred to nitrocellulose membranes (Bio-Rad, Hercules, CA, USA). After blocking with 5% nonfat milk in PBST buffer (phosphate buffer saline containing 1% Tween-20) for 1 h, the membranes were probed with primary antibodies [anti-COX2 (1:500 dilution), anti-iNOS (1:300 dilution), anti-phosphor-JAK2 (1:500 dilution), anti-JAK2 (1:500 dilution), anti-phosphor-STAT1 (1:500 dilution), STAT1 (1:500 dilution), anti-phosphor-STAT3 (1:500 dilution), STAT3 (Cell 1:500 dilution), SOCS1 (1:300 dilution), SOCS3 (1:300 dilution) and actin (1:5,000 dilution)] at 4°C overnight. After washing with PBST, the membranes were probed with appropriate secondary antibodies for 2 h at room temperature and finally developed using ECL detection reagent. The antibody–antigen complexes were visualized by the FluorChem™ E System (ProteinSimple, California, US), and the relative densities of the bands were evaluated and quantified using ImageJ software (NIH, Bethesda, MD, USA).

2.9. *Statistical analysis*

Data were analyzed by GraphPad Prism 5.0 Software (GraphPad Software, San Diego, CA, USA) and are represented as means ± SEM. Statistical significance was evaluated by the One-Way Analysis of Variance (ANOVA) followed by the Student-Newman-Keuls test. $p < 0.05$ was considered to be statistically significant.

Table 1. Effect of DJC on FBG, lipid profile, and renal function parameters in diabetic rats

Parameters	Ctrl	DM	DJCL	DJCH
FBG (mmol/L)	5.32 ± 0.88	23.26 ± 4.29***	23.19 ± 3.93	19.82 ± 3.85
Body weight (g)	310.38 ± 45.43	245.14 ± 48.55*	235.50 ± 38.44	257.75 ± 31.19
Kidney weight (g)	1.58 ± 0.25	2.81 ± 0.54***	2.53 ± 0.61	2.41 ± 0.64
Renal index (KW/BW)	0.51 ± 0.07	1.13 ± 0.08***	1.08 ± 0.06	0.93 ± 0.17##
Cr (μmol/L)	38.53 ± 5.77	58.57 ± 10.24***	48.86 ± 6.367#	44.88 ± 6.38##
BUN (mmol/L)	8.61 ± 0.37	17.48 ± 4.15***	12.05 ± 3.06#	10.4 ± 5.34##
UA (μmol/L)	67.75 ± 11.04	223.71 ± 54.81***	187.15 ± 29.81***	157.63 ± 33.01***##
CHO (mmol/L)	1.24 ± 0.21	2.58 ± 0.47**	1.92 ± 0.41*#	1.72 ± 0.27##
TG (mmol/L)	0.29 ± 0.10	1.62 ± 0.36**	1.33 ± 0.28**	1.21 ± 0.33**#
HDL (mmol/L)	2.12 ± 0.25	1.28 ± 0.32**	1.52 ± 0.25**	1.71 ± 0.40*#
LDL (mmol/L)	0.32 ± 0.13	1.15 ± 0.28**	0.63 ± 0.25*##	0.46 ± 0.19#

Data are presented as the means ± SEM (n = 8 in the control and DJCH groups, n = 7 in the other groups). *p < 0.05, **p < 0.01, ***p < 0.001, *vs*. ctrl; #p < 0.05, ##p < 0.01, ###p < 0.001, *vs*. DM group.

3. Results

3.1. *Effects of DJC on the metabolic indexes and renal function in diabetic rats induced by STZ*

During the experiment, one rat in the diabetic (DM) group and one in the DJCL group died of undetermined causes. As displayed in Table 1, after 8 weeks of DJC administration, body weights of rats in the DM group were lower than those in control group (p < 0.05). Even at the high dose of 2,000 mg/kg.d^{-1}, DJC did not markedly influence the body weight of diabetic rats. As expected, FBG was obviously higher in the STZ-induced diabetic rats than those in control group (p < 0.001). DJC treatment slightly reduced FBG levels, but without significant differences. Additionally, the serum levels of CHO, TG, and LDL were markedly increased, while serum HDL was markedly reduced in diabetic rats compared with the control group (Table 1). DJCL changed serum levels of CHO and LDL, and DJCH significantly changed CHO, TG, LDL, and HDL in diabetic rats during the course of the experiment.

The renal functional alterations in the diabetic rats were evaluated by examining serum BUN, Cr, and UA. All these serum parameters in the diabetic group were significantly elevated (p < 0.001) compared with the non-diabetic group, while the parameters were obviously reduced (p < 0.01) after 8 weeks of DJC treatment. The kidney weight and renal index [kidney weight/body weight ratio (KW/BW)] in the diabetic rats substantially increased compared with the non-diabetic rats (p < 0.001). The rats in the DJC treatment groups showed a significant reduction in the renal index (p < 0.01), but no significant reduction in body weight. These results indicate that the administration of DJC is beneficial in ameliorating DN in rats.

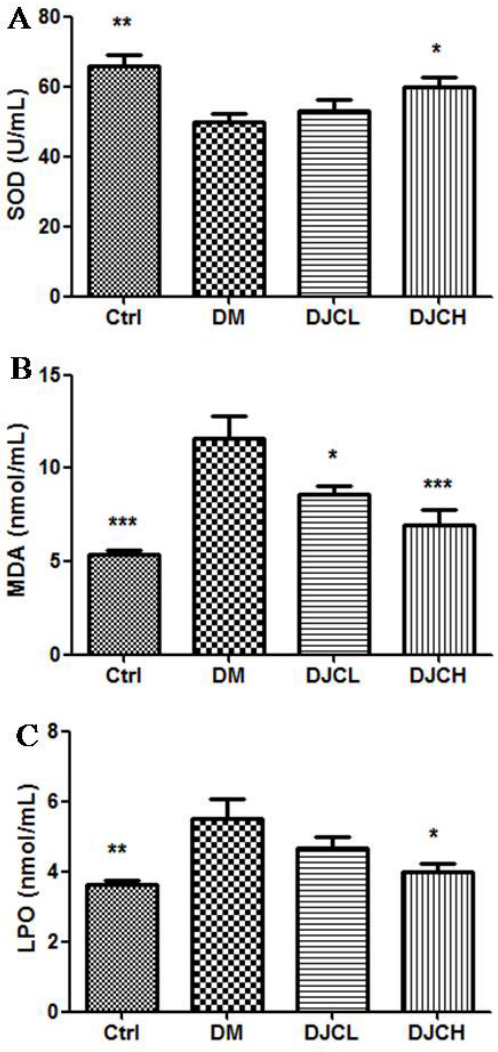

Figure 1. Effect of DJC on oxidative stress in diabetic rats. The activities of total SOD **(A)** and the concentrations of MDA **(B)** and LPO **(C)** in the serum were assayed using commercial test kits. Data are presented as the means ± SEM. *p < 0.05, **p < 0.01, ***p < 0.001, *vs*. DM group.

3.2. *Effect of DJC on antioxidant status in diabetic rats*

Compared with the non-diabetic rats, serum LPO and MDA levels were markedly increased (p < 0.01 and p < 0.001), and SOD activity was significantly decreased in the diabetic rats (p < 0.01), indicating that oxidative stress is initiated in diabetic rats (Figure 1). DJC markedly enhanced SOD activity (p < 0.05), and notably

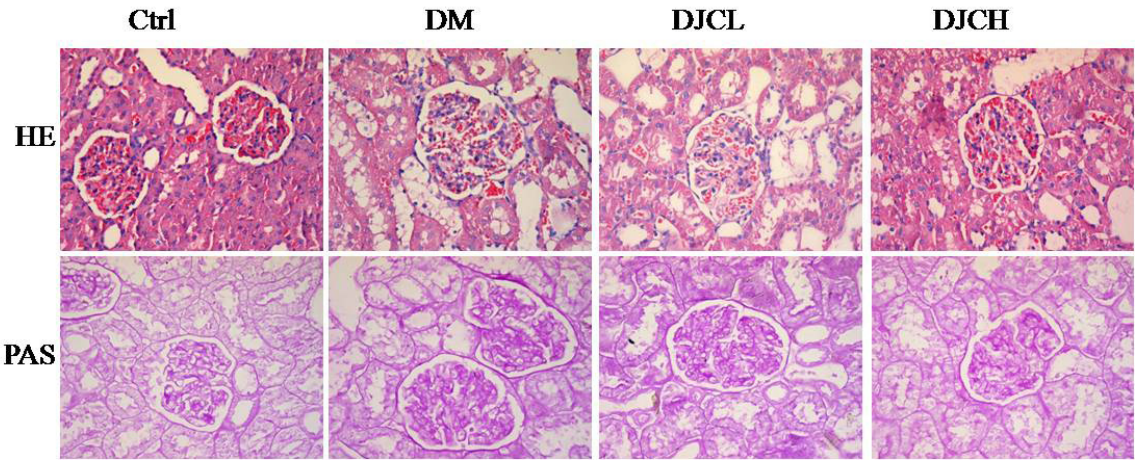

Figure 2. H&E and PAS staining of representative sections from kidney (×400).

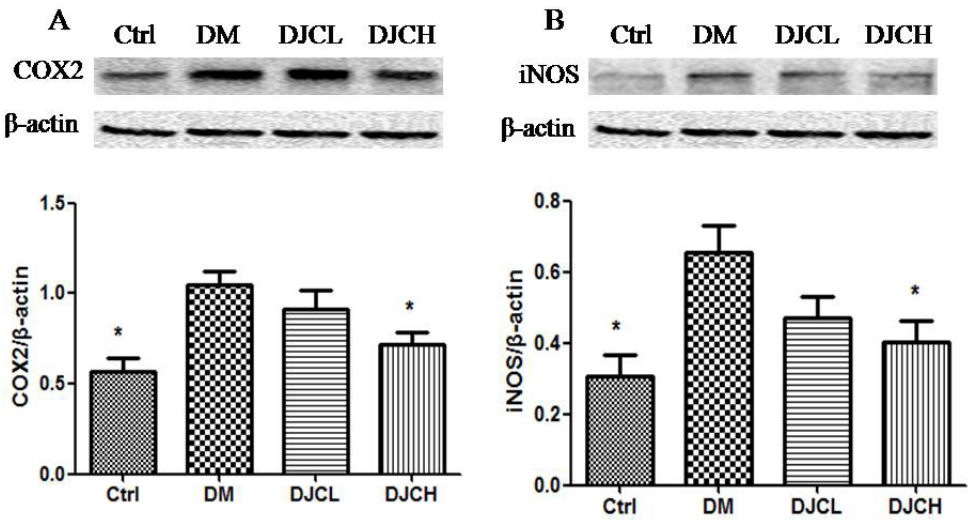

Figure 3. Effects of DJC on COX2 and iNOS expression in the diabetic rat kidneys. Total protein was extracted from the renal tissues for conducting Western blot analysis. Protein expression levels of COX2 and iNOS were normalized to the level of β-actin. **(A)** Quantitative analysis of COX2 expression; **(B)** Quantitative analysis of iNOS expression. The data are presented as the means ± SEM, $n = 3$. *$p < 0.05$, **$p < 0.01$, ***$p < 0.001$, *vs*. DM group.

decreased LPO and MDA ($p < 0.05$, $p < 0.001$). The results suggest that DJC is able to improve antioxidant capacity and attenuate oxidative damage in rats with DN.

3.3. *Effects of DJC on renal morphology in diabetic rats*

The representative histology of the kidney by H&E staining is shown in Figure 2. No obvious histopathological alternations were observed in the glomerulus, kidney tubules, or mesenchyme in the renal biopsies from the animals in the control group. However, mesangial expansion with glomerular hypertrophy, basement membrane (GBM) thickening, and tubular atrophy/dilation were clearly observed in the diabetic group. The histopathological changes were clearly attenuated after DJC treatment in rats with DN. Moreover, the DJCH group showed more improvement than the DJCL group. In PAS-stained sections of the glomeruli, the mesangial matrix fraction was notably increased in the diabetic rats compared with the non-diabetic rats. This increase in the mesangial matrix fraction of diabetic rats was suppressed by DJC treatment for 8 weeks but remained higher than the control group. Taken together, these results confirmed that DJC improved renal dysfunction in diabetic rats induced by STZ.

3. 4. *Effects of DJC on COX2 and iNOS expression levels in diabetic rat kidneys*

To explore the anti-inflammatory effects of DJC and its mechanism of action in the kidney, we evaluated its effect on the expression of iNOS and COX-2, key enzymes in the inflammatory processes of DN. As illustrated in Figure 3, the expression of COX2 and iNOS in the kidneys of diabetic rat were significantly increased

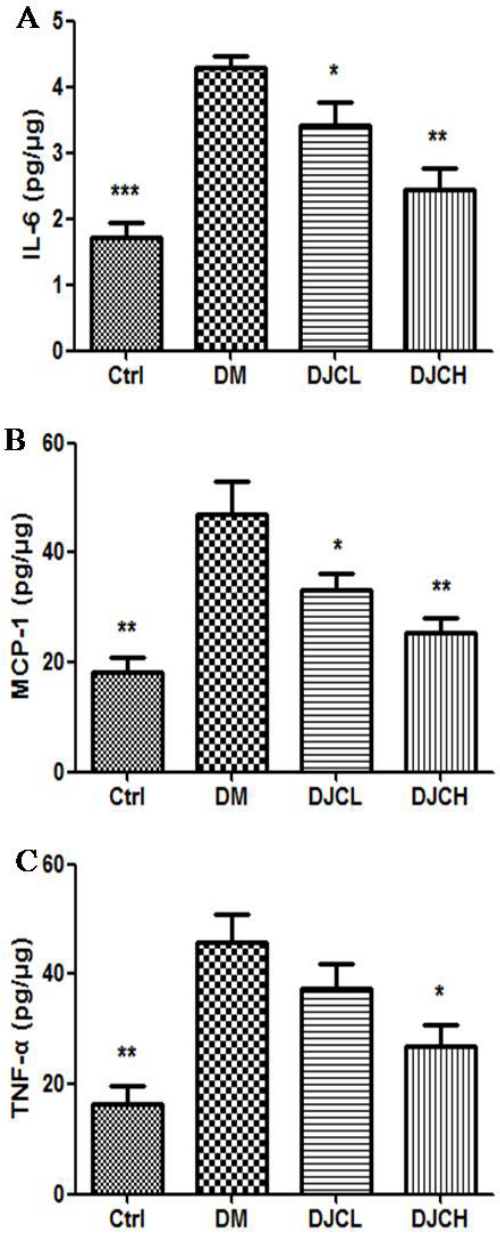

Figure 4. Effects of DJC on the inflammatory cytokine levels in diabetic rat kidneys. The renal tissues were homogenized and the supernatants were collected for cytokine detection. The levels of IL-6 **(A)**, MCP-1 **(B)** and TNF-α **(C)** levels were measured using ELISA kits. Cytokine concentrations were normalized to the amount of total protein of each sample. Data are presented as the means ± SEM ($n = 8$ in the control and DJCH groups, $n = 7$ in the other groups).**$p < 0.05$, **$p < 0.01$, ***$p < 0.001$, *vs*. DM group.

compared to the normal control group ($p < 0.05$). DJCH administration significantly attenuated the elevated expression of COX2 and iNOS ($p < 0.05$).

3. 5. *Effects of DJC on the inflammatory cytokine levels in diabetic rat kidneys*

Inflammatory cytokines are thought to play pivotal roles in the pathogenesis of DN. Cytokines including IL-6, TNF-α and MCP-1 are correlated with deterioration of renal function (*1-4*). Therefore, to validate the effect of DJC on the JAK-STAT signaling pathway, we measured the expression profiles of IL-6, MCP-1, and TNF-α, which contain STAT binding sites in their promoter regions. As shown in Figure 4, IL-6, MCP-1, and TNF-α expression levels in the diabetic group were significantly increased as compared with the non-diabetic group ($p < 0.01$), administration of DJC remarkably reduced these increased inflammatory cytokines (Figure 4, $p < 0.05$).

3. 6. *DJC ameliorates JAK-STAT signaling in diabetic rat kidneys*

JAK2, STAT1, and STAT3 are important signaling factors for the production of iNOS, COX2 and proinflammatory cytokines in the DN rat (*5-7*). Thus, to determine whether the inhibitory effect of DJC on the expression of proinflammatory cytokines and mediators is associated with inhibition of JAK-STAT signal pathway, we next examined the effect of DJC on the phosphorylation of JAK2, STAT1, and STAT3 in diabetic rat kidneys. The results demonstrated that the expression levels of tyrosine- phosphorylated JAK2, STAT1, and STAT3 were substantially increased in the diabetic group in comparison with the control group. DJC treatment significantly decreased the tyrosine-phosphorylated JAK2, STAT1, and STAT3 ($p < 0.05$, Figure 5A, 5B, 5C), implying that the anti-inflammatory activity of DJC is due to inhibition of the JAK-STAT pathway in diabetic rat kidneys.

To validate the mechanism of the JAK-STAT signaling cascade in DJC treatment, we measured the effects of DJC on SOCS1 and SOCS3 protein expression levels in DM renal tissues. As illustrated in Figure 5, the expression levels of SOCS1 and SOCS3 were significantly increased in diabetic rats compared with normal rats (Figure 5D, 5E). DJC markedly reduced the expression level of SOCS3 ($p < 0.01$), but no significant alteration was seen in SOCS1.

4. Discussion

In this study, intraperitoneal injections of STZ resulted in overt hyperglycemia. Kidney weight and renal index were significantly increased, and renal function (Cr, BUN, UA) was compromised. Consistently, mesangial cell proliferation, extracellular matrix (ECM) accumulation, mesangial expansion, glomerular hypertrophy, and thickened tubular and GBM were observed on the renal histopathological pictures of diabetic rats. These results indicate that the rat model of DN was successfully established. DJC treatment resulted in an obvious increase in renal function and improved associated pathologies, a decrease in renal index, and a slight reduction in blood glucose, while the general condition of the animals improved.

Growing evidence demonstrates that chronic

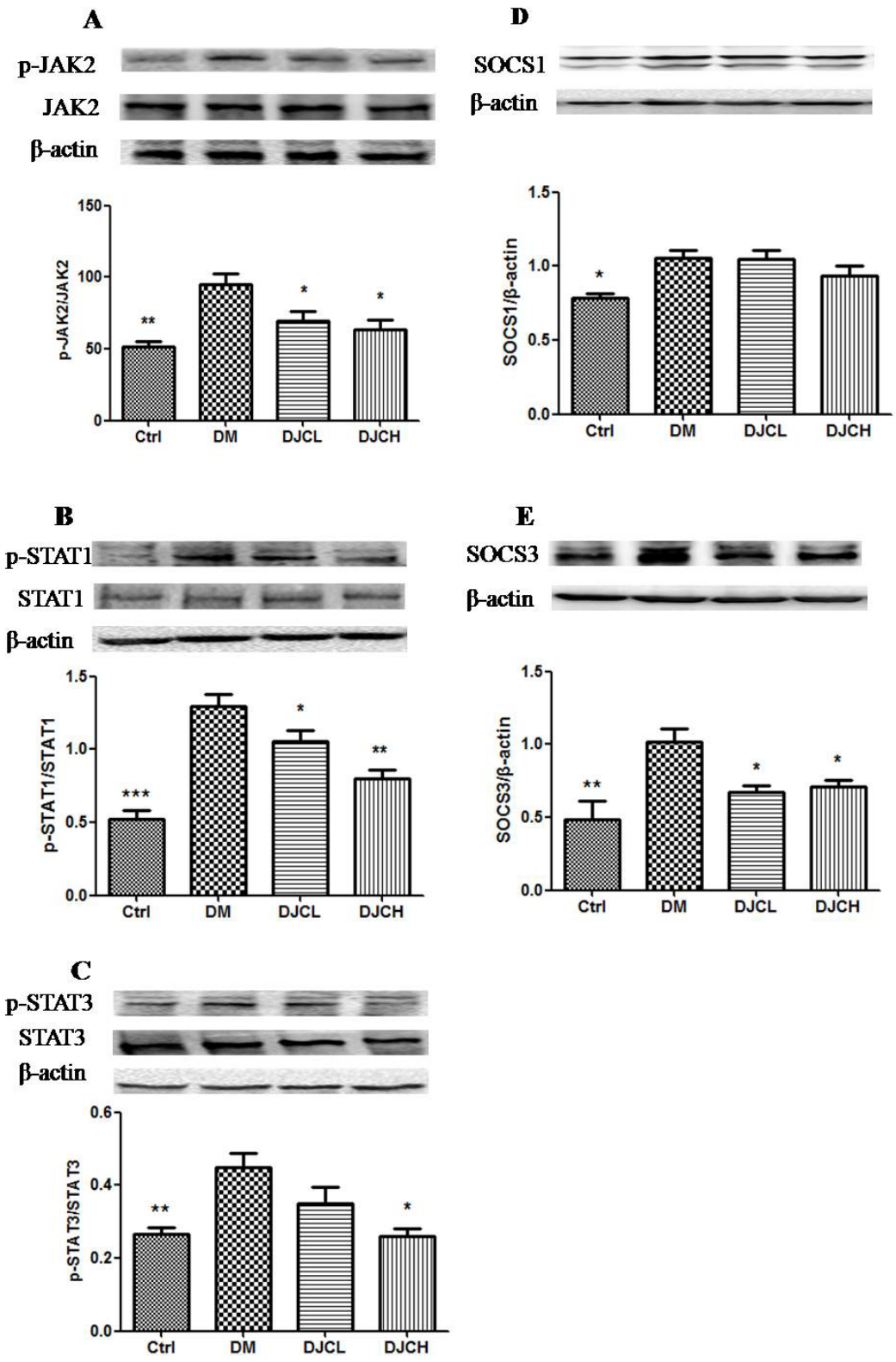

Figure 5. DJC suppressed JAK/STAT signal pathway in renal tissues of diabetic rats. Total proteins extracted from kidneys were subjected to Western blot analysis. Densitometry analysis of **(A)** p-JAK2/JAK2, **(B)** p-STAT1/STAT1, **(C)** p-STAT3/STAT3 expression, laser densitometry of the bands was shown in upper panels and this experiment was repeated three times. Densitometry analysis of **(D)** SOCS1 and **(E)** SOCS2 expression. Levels of SOCS proteins were normalized to β-actin. The columns and error bars represent the mean and SEM ($n = 3$ per group). *$p < 0.05$, **$p < 0.01$, ***$p < 0.001$, *vs*. DM.

low-grade inflammation resulting from activation of the innate immune system plays a vital role in the pathogenesis of DN (*1-4*). Cytokines, produced by various resident renal cells including monocyte-macrophages, mesangial cells, tubular epithelial cells, podocytes, and endothelial cells, promote glomerular

hypertrophy, glomerular cell proliferation, ECM accumulation and increase glomerular filtration rate (GFR) in early DN (*2,3*). The glomerular injury eventually leads to albuminuria and renal failure. Circulating levels of cytokines (*e.g*. IL-6, MCP-1, TNF-α and its receptors TNFR-1 and 2) have been found correlated with albuminuria and renal function decline in DN patients (*19*). IL-6 has been demonstrated to play an important role in stimulating mesangial cell proliferation, promoting ECM accumulation, and increasing endothelial cell permeability (*1,2,20-22*). A significant correlation between IL-6 and ECM accumulation, GBM thickening, and glomerulosclerosis was observed in type 2 diabetic patients with overt nephropathy (*22*). TNF-α promotes the recruitment of monocytes and macrophages, stimulates local generation of reactive oxygen species (ROS), reduces GFR by hemodynamic changes (*23-25*), alters endothelial permeability (*2,3,25*), and thereby increases albumin permeability. A variety of chemokines including MCP-1 can be induced by proinflammatory cytokines such as TNF-α, IL-6, and interferon-α (INF-α) (*2,26*). MCP-1 facilitates the activation of macrophages and monocytes and their migration to lesions, and induces the expression of adhesion molecules and other proinflammatory cytokines (*3,26,27*). MCP-1 has also been demonstrated to relate to the progression of glomerular lesions and deterioration of GFR. In the present study, DJC significantly suppressed the production of inflammatory cytokines including IL-6, TNF-α, and MCP-1, whose promoter regions contain a potential STAT binding site. Therefore, we subsequently detected whether the activation of the JAK-STAT signaling pathway is involved in the anti-inflammatory actions of DJC in diabetic renal tissues.

JAK2-STATs signaling is activated in many cell types exposed to high concentrations of glucose and the renal cortex in rodent models of early DN (*6,7,28*). Upon ligand binding, JAKs become activated, then phosphorylate and activate STATs. The activated STATs form dimers and translocate to the nucleus, bind to specific response elements in the promoters of target genes, and regulate the expression of target genes encoding cytokines, chemokines, adherence molecules, and inducible enzymes such as iNOS and COX-2. JAK2 and its downstream signaling components, STAT1 and STAT3 are required for the production of iNOS, COX2 and proinflammatory cytokines in diabetic rat kidneys (*6,7*). The STAT3 inhibitor, S3I-201, exhibits an inhibitory effect on renal interstitial fibroblast activation and interstitial fibrosis (*29*). In this study, we found that DJC treatment markedly reversed JAK2-STAT1/STAT3 activation. These results agree with previous observations (*30,31*) and support our hypothesis that DJC ameliorates STZ-induced renal inflammatory responses *via* suppressing the JAK-STAT signaling pathway.

SOCS is a critical negative regulator of JAK-STAT signaling. Increased expression levels of SOCS1 and SOCS3 were detected in the STZ-induced diabetic rat model, biopsies of patients with DN and renal cells cultured with high glucose (*32-34*). SOCS proteins, which are rapidly induced by cytokines, have been demonstrated to regulate JAK-STAT signaling through a classic negative feedback loop (*8,9*). Lu *et al*. (*35*) reported that Stat3SA/– animals (transgenic mice that have a reduced capacity for STAT3 activation) with STZ-induced diabetes presented with less proteinuria, decreased mesangial cell proliferation and mesangial expansion in glomeruli, reduced macrophage infiltration, matrix accumulation and inflammatory cytokine expression at the early stage of DN. In our current study, the ability of DJC to inhibit JAK-STAT signaling was verified by the observation that it reversed the elevated protein expression level of SCOS-3 in renal tissues. We also reported a similar result in mesangial cells stimulated by AGEs (*16*). Our results indicate that the elevated SOCS proteins are involved in the activated JAK-STAT signaling in diabetic renal tissues. However, we did not find the obvious inhibition of SOCS1 by DJC in this study. Collectively, the data presented here support a novel function of DJC and put forward a possible molecular mechanism for its action.

Hyperglycemia induces ROS, resulting in oxidative stress in the kidney. Oxidative stress is thought to contribute to the occurrence and development of DN (*36,37*). Increased ROS interacts with the lipid in cell membranes and causes subsequent cellular damage including lipid peroxidation, which, in turn, affect cellular function. MDA, one of the final products of LPO, is considered to be a biomarker of oxidative stress and is induced by excessive ROS. SOD, a major defender against superoxide, is part of the superoxide defense system and plays an extremely important role in protecting all aerobic life-systems from oxygen toxicity. Under diabetic conditions, the balance between the oxidant/ pro-oxidant and antioxidant defense systems is destroyed and manifested as enhanced LPO and MDA and depletion of the antioxidant defense system (*e.g*. decreased SOD), giving rise to rapid increases in intracellular ROS levels. Antioxidants have been demonstrated to attenuate renal function decline and pathological structure in diabetic rats (*37,38*). Chronic hyperglycemia generates ROS and oxidative stress, resulting in the activation of the JAK-STAT signaling pathway (*39,40*). Diverse stimuli, including Ang II, cytokines, AGEs, and hyperglycemia have been reported to contribute to the development of DN through a ROS involved JAK2/STATs signaling pathway (*4,39,40*). It is possible that inhibiting oxidative stress may suppress the JAK-STAT signaling cascade (*41,42*). Therefore, targeting oxidative stress-induced expression of inflammatory cytokines signaling *via* a JAK-STAT dependent mechanism may increase

the therapeutic effect of DN. As shown in the current study, diabetic rats exhibited significant oxidative stress, administration with DJC significantly enhanced antioxidant capacity and decreased LPO and MDA content in DN rats, indicating that DJC is capable of eliminating oxidative stress and the suppression of JAK-STAT signaling *via* the antioxidant defense system.

In conclusion, our results demonstrate that DJC amelioration of diabetic renal injury and associated pathology might be due to its antioxidant ability and suppression of the JAK2-STAT1/STAT3 cascade.

Acknowledgements

This work was supported by the research grant from the National Natural Science Foundation of China awarded (81573944), the research project for Practice Development of National TCM Clinical Research Bases (JDZX2012001), Natural Science Foundation of Anhui Provincial Education Department (KJ2013A027) and Key Technology R.D Program of Qinghai Province (2016-SF-126).

References

1. Wada J, Makino. Inflammation and the pathogenesis of diabetic nephropathy. Clin Sci (Lond). 2013; 124:139-152.
2. Navarro-González JF, Mora-Fernández C. The role of inflammatory cytokines in diabetic nephropathy. J Am Soc Nephrol. 2008; 19:433-442.
3. Wada J, Makino H. Inflammation and the pathogenesis of diabetic nephropathy. Clin Sci (Lond). 2013; 124:139-152.
4. Donate-Correa J, Martín-Núñez E, Muros-de-Fuentes M, Mora-Fernández C, Navarro-González JF. Inflammatory cytokines in diabetic nephropathy. J Diabetes Res. 2015; 2015:948417
5. Brosius FC 3rd, He JC. JAK inhibition and progressive kidney disease. Curr Opin Nephrol Hypertens. 2015; 24:88-95.
6. Marrero MB, Banes-Berceli AK, Stern DM, Eaton DC. Role of the JAK/STAT signaling pathway in diabetic nephropathy. Am J Physiol Renal Physiol. 2006; 290:F762-F768.
7. Brosius FC, Tuttle KR, Kretzler M. JAK inhibition in the treatment of diabetic kidney disease. Diabetologia. 2016; 59:1624-1627.
8. Trengove MC, Ward AC. SOCS proteins in development and disease. Am J Clin Exp Immunol. 2013; 2:1-29.
9. Linossi EM, Babon JJ, Hilton DJ, Nicholson SE. Suppression of cytokine signaling: The SOCS perspective. Cytokine Growth Factor Rev. 2013; 24:241-248.
10. Fang ZH, Cheng SH, Wu Q. Effect of Danzhi Jiangtang Capsule on NF-κB and urinary albumin excretion rate in early diabetic nephropathy patients. World Science & Technology-Modernization of TCM and Materia Medica. 2013; 15:891-895. (in Chinese)
11. Liu SS, Li ZN, Xu CQ, Xiong YY, Fang ZH. Effects of Danzhi Jiangtang Capsule on serum levels of Tumor Necrosis Factor Alpha and Chemokine (C-X-C Motif) ligand 5 in diabetic rats. Journal of Anhui University of Chinese Medicine. 2014; 33:58-61. (in Chinese)
12. Bao TT, Yang C, Chu QG. Effects of Dangzhi Jiangtang Capsules on abdominal aortic ultrastructure, MCP-1 and resistin mRNA expression in diabetic rats. Chinese Traditional Patent Medicine. 2015; 37:1888-1892. (in Chinese)
13. Li ZN, Xiong YY, Li L, Fang ZH. Effects of Danzhi Jiangtang Capsule on CXCL9 and IL-8 in diabetic model rats. Chinese Journal of Information on TCM. 2014; 21:45-47. (in Chinese)
14. Xiong YY, Li ZN, Liu SS. The influence of Danzhi Jiangtang Capsule on the expression of NF-κB in kidney tissue of diabetic rats. Global Journal of Endocrinology and Metabolism Studies. 2014; 34:6-10. (in Chinese)
15. Niu YF, Fang ah, Liu J, Shi GB. The clinical efficacy of Danhzi Jiangtang Capsule on elderly patients with early diabetic nephropathy. Modern Chinese Medicine. 2008; 10:36-38. (in Chinese)
16. Sun M, Li Y, Bu WJ, Zhao J, Zhu J, Gu L, Zhang P, Fang Z. DJC suppresses Advanced Glycation End Products-Induced JAK-STAT signaling and ROS in mesangial cells. Evid Based Complement Alternat Med. 2017; 2017:2942830.
17. Wang YZ, Jiang L, Han YQ, Zuo D, Xia LZ. UPLC fingerprint of Danzhi Jiangtang Capsule. Clinical Journal of Traditional Chinese Medicine. 2012; 24:1009-1011. (in Chinese)
18. Wang HJ, Jin YX, Shen W, Neng J, Wu T, Li YJ, Fu ZW. Low dose streptozotocin (STZ) combined with high energy intake can effectively induce type 2 diabetes through altering the related gene expression. Asia Pac J Clin Nutr. 2007; 16 Suppl 1:412-417.
19. Barutta F, Bruno G, Grimaldi S, Gruden G. Inflammation in diabetic nephropathy: Moving toward clinical biomarkers and targets for treatment. Endocrine. 2015; 48:730-742.
20. Feigerlová E, Battaglia-Hsu SF. IL-6 signaling in diabetic nephropathy: From pathophysiology to therapeutic perspectives. Cytokine Growth Factor Rev. 2017; 37:57-65.
21. Navarro-González JF, Mora-Fernández C, Muros de Fuentes M, García-Pérez J. Inflammatory molecules and pathways in the pathogenesis of diabetic nephropathy. Nat Rev Nephrol. 2011; 7:327-340.
22. Horii Y, Muraguchi A, Iwano M, Matsuda T, Hirayama T, Yamada H, Fujii Y, Dohi K, Ishikawa H, Ohmoto Y. Involvement of IL-6 in mesangial proliferative glomerulonephritis. J Immunol. 1989; 143:3949-3955.
23. Omote K, Gohda T, Murakoshi M, Sasaki Y, Kazuno S, Fujimura T, Ishizaka M, Sonoda Y, Tomino Y. Role of the TNF pathway in the progression of diabetic nephropathy in KK-A(y) mice. Am J Physiol Renal Physiol. 2014; 306:F1335-F1347.
24. Awad AS, You H, Gao T, Cooper TK, Nedospasov SA, Vacher J, Wilkinson PF, Farrell FX, Brian Reeves W. Macrophage-derived tumor necrosis factor-α mediates diabetic renal injury. Kidney Int. 2015; 88:722-733.
25. Navarro JF, Mora-Fernández C. The role of TNF-alpha in diabetic nephropathy: Pathogenic and therapeutic implications. Cytokine Growth Factor Rev. 2006; 17:441-450.
26. Moreno JA, Moreno S, Rubio-Navarro A, Gómez-

Guerrero C, Ortiz A, Egido J. Role of chemokines in proteinuric kidney disorders. Expert Rev Mol Med. 2014; 16:e3.
27. Awad AS, Kinsey GR, Khutsishvili K, Gao T, Bolton WK, Okusa MD. Monocyte/macrophage chemokine receptor CCR2 mediates diabetic renal injury. Am J Physiol Renal Physiol. 2011; 301:F1358-F1366.
28. Berthier CC, Zhang H, Schin M, *et al*. Enhanced expression of Janus kinase-signal transducer and activator of transcription pathway members in human diabetic nephropathy. Diabetes. 2009; 58:469-477.
29. Pang M, Ma L, Gong R, Tolbert E, Mao H, Ponnusamy M, Chin YE, Yan H, Dworkin LD, Zhuang S. A novel STAT3 inhibitor, S3I-201, attenuates renal interstitial fibroblast activation and interstitial fibrosis in obstructive nephropathy. Kidney Int. 2010; 78:257-268.
30. Wang X, Shaw S, Amiri F, Eaton DC, Marrero MB. Inhibition of the Jak/STAT signaling pathway prevents the high glucose-induced increase in TGF-beta and fibronectin synthesis in mesangial cells. Diabetes. 2002; 51:3505-3509.
31. Shi Y, Zhang Y, Wang C, Du C, Zhao S, Qi Z, Zhang Q, Duan H. Suppressor of cytokine signaling-1 reduces high glucose-induced TGF-beta1 and fibronectin synthesis in human mesangial cells. FEBS Lett. 2008; 582:3484-3488.
32. Liu Q, Xing L, Wang L, Yao F, Liu S, Hao J, Liu W, Duan H. Therapeutic effects of suppressors of cytokine signaling in diabetic nephropathy. J Histochem Cytochem. 2014; 62:119-128.
33. Zhou Y, Lv C, Wu C, Chen F, Shao Y, Wang Q. Suppressor of cytokine signaling (SOCS) 2 attenuates renal lesions in rats with diabetic nephropathy. Acta Histochem. 2014; 116:981-988.
34. Ortiz-Muñoz G, Lopez-Parra V, Lopez-Franco O, Fernandez-Vizarra P, Mallavia B, Flores C, Sanz A, Blanco J, Mezzano S, Ortiz A, Egido J, Gomez-Guerrero C. Suppressors of cytokine signaling abrogate diabetic nephropathy. J Am Soc Nephrol. 2010; 21:763-772.
35. Lu TC, Wang ZH, Feng X, Chuang PY, Fang W, Shen Y, Levy DE, Xiong H, Chen N, He JC. Knockdown of Stat3 activity *in vivo* prevents diabetic glomerulopathy. Kidney Int. 2009; 76:63-71.
36. Giacco F, Brownlee M. Oxidative stress and diabetic complications. Circ Res. 2010; 107:1058-1070.
37. Stanton RC. Oxidative stress and diabetic kidney disease. Curr Diab Rep. 2011; 11:330-336.
38. Nam SM, Lee MY, Koh JH, Park JH, Shin JY, Shin YG, Koh SB, Lee EY, Chung CH. Effects of NADPH oxidase inhibitor on diabetic nephropathy in OLETF rats: The role of reducing oxidative stress in its protective property. Diabetes Res Clin Pract. 2009; 83:176-182.
39. Simon AR, Rai U, Fanburg BL, Cochran BH. Activation of the JAK-STAT pathway by reactive oxygen species. Am J Physiol. 1998; 275 (6 Pt 1):C1640-C1652.
40. Duhé RJ. Redox regulation of Janus kinase: The elephant in the room. JAKSTAT. 2013; 2:e26141.
41. Schieffer B, Luchtefeld M, Braun S, Hilfiker A, Hilfiker-Kleiner D, Drexler H. Role of NAD(P)H oxidase in angiotensin II-induced JAK/STAT signaling and cytokine induction. Circ Res. 2000; 87:1195-1201.
42. Lee HB, Yu MR, Yang Y, Jiang Z, Ha H. Reactive oxygen species-regulated signaling pathways in diabetic nephropathy. J Am Soc Nephrol. 2003; 14(8 Suppl 3):S241-S245.

(Received October 21, 2018; Revised October 28, 2018; Accepted December 12, 2018)

Original Article

DOI: 10.5582/bst.2018.01263

Protective effects of metformin against osteoarthritis through upregulation of SIRT3-mediated PINK1/Parkin-dependent mitophagy in primary chondrocytes

Chenzhong Wang[§], Yi Yang[§], Yueqi Zhang, Jinyu Liu, Zhenjun Yao, Chi Zhang*

Department of Orthopedic surgery, Zhongshan Hospital, Fudan University, Shanghai, China.

Summary **Mitochondrial damage is involved in the pathogenesis of osteoarthritis. Metformin, one of the most common prescriptions for patients with type 2 diabetes, can reportedly activate Sirtuin 3 (SIRT3) expression which protects mitochondria from oxidative stress. In this study, we investigated the inhibitory property of metformin on mitochondrial damage by focusing on the interleukin-1 beta (IL-1β)-stimulated osteoarthritis model by using primary murine chondrocytes. Our results demonstrated that SIRT3 was downregulated in chondrocytes under IL-1β stimulation, where its expression was positively correlated with mitochondrial damage and reactive oxygen species (ROS) production. Metformin treatment upregulated SIRT3 expression and mitigated loss of cell viability and decreased the generation of mitochondria-induced ROS in chondrocytes stimulated with IL-1β. Metformin also attenuated IL-1β-induced expressions of catabolic genes such as matrix metalloproteinase-3 (MMP3) and MMP13 and enhanced the anabolic indicator Collagen II. These effects were mediated by phosphatase and tensin homolog (PTEN)-induced putative kinase protein 1 (PINK1)/Parkin-dependent mitophagy and the autophagic elimination of damaged mitochondria. Further, the SIRT3 inhibitor 3-TYP effectively inhibited the initiation of mitophagy, as decreased expression of PINK1 and Parkin, decreased the LC3II/LC3I, enhanced the expression of MMP3 and MMP13, and decreased the expression of Collagen II. Overall, our findings provide evidence that metformin suppresses IL-1β-induced oxidative and osteoarthritis-like inflammatory changes by enhancing the SIRT3/PINK1/Parkin signaling pathway, thereby indicating metformin's potential in prevention and treatment of osteoarthritic joint disease.**

Keywords: Osteoarthritis, mitophagy, SIRT3

1. Introduction

Osteoarthritis (OA) is a common degenerative joint disease affecting patients worldwide, which is characterized by articular cartilage degradation and elevated chondrocyte mortality, in addiction to synovial inflammation, osteophyte formation and remodeling of subchondral bone (*1*). It is well documented that mitochondrial dysfunction and damages can cause an inflammatory response, characterized by interleukin-1 beta (IL-1β) release which is a classic hallmark of OA chondrocytes (*2*).

The mitochondria is a membrane-enclosed organelle that converts nutritional molecules into adenosine triphosphate(ATP) *via* oxidative phosphorylation (OXPHOS) (*3*). Mitochondria are at the center of multiple specific pathways in cartilage homeostasis owing to their central role in catabolic and anabolic metabolism, generation of reactive oxygen species (ROS), apoptosis, and signal transduction. OA chondrocytes demonstrate impaired mitochondrial function (*4*) and decreases in mitochondrial biogenesis and OXPHOS (*5*).

Protein acetylation in mitochondria typically promotes decreased mitochondrial integrity and function (*6*).The nicotinamide adenine dinucleotide (NAD^+)-

Released online in J-STAGE as advance publication December 22, 2018.

[§]These authors contributed equally to this work.

**Address correspondence to:*
Dr. Chi Zhang, Department of Orthopedic surgery, Zhongshan Hospital, Fudan University, 180 Fenglin Road, Shanghai 200032, China.
E-mail: zhang.chi2018@aliyun.com

dependent protein deacetylase, SIRT3 (Sirtuin 3), is the major mitochondrial protein deacetylase localized to the mitochondria (*7,8*), thereby regulating mitochondrial antioxidant system and OXPHOS (*9,10*). SIRT3 protects mitochondria from oxidative stress by deacetylating superoxide dismutase (SOD2) and mitigates OA progression (*11*).Chen *et al*. recently showed that SIRT3 was regulated by AMP-activated protein kinase (AMPK) activation in human chondrocytes, which reduced mtDNA^{4977} deletion and improved mitochondrial functions (*12*). AMPK activator metformin also increased SIRT3 expression and knockdown SIRT3 by short hairpin RNA (shRNA) transfection mediated accumulation of oxidative stress (*13*). In our study, we chose metformin to induce SIRT3 expression. Meanwhile considering metformin is an autophagy-inducing drug possibly through mitophagy (*14*), we investigated the relationship between SIRT3 and mitophagy using metformin.

The role of autophagy in human chondrocytes and the pathophysiology of OA has been elucidated, which is known to modulate OA-related gene expression and apoptosis (*15*). Mitophagy is the specific autophagic elimination of damaged mitochondria, regulated by the kinase phosphatase and tensin homolog (PTEN)-induced putative kinase protein 1 (PINK1) and the E3 ubiquitin ligase Parkin in many metazoan cell types (*16*). A recent study has shown that loss of Parkin can impair the elimination of damaged/dysfunctional mitochondria in IL-1β-stimulated OA chondrocytes (*17*). Together, these data suggest that the functional role of mitophagy is critical in the pathophysiology of OA.

The relationship between SIRT3 and mitophagy has been previously reported (*18,19*) wherein depletion of SIRT3 strongly reduced mitophagy. However, to our best knowledge, the effectiveness of SIRT3-mediated mitophagy in OA has not yet been investigated. Herein, we aimed to examine the effects of SIRT3-mediated mitophagy on IL-1β-induced mitochondrial damage and inflammatory responses in primary murine chondrocytes (PMCs).

2. Materials and Methods

2.1. *Materials and chemicals*

Metformin was purchased from Sigma (St.Louis, USA). It was dissolved in dimethyl sulfoxide (DMSO) for the *in vitro* assay and was stored at a concentration of 1 M, diluted with Dulbecco's modified Eagle's medium (DMEM), and a solvent control with DMSO was performed at no more than 2‰ (v/v). 3-TYP was purchased from Selleck (Shanghai, China) and was dissolved in DMSO and stored at a concentration of 5 mM.

DMEM/F12 and fetal Bovine Serum (FBS) were from Gibco BRL (Grand Island, NY, USA). Antibodies against Parkin, LC3B and glyceraldehyde-3-phosphate dehydrogenase (GAPDH) were from Cell Signaling Technology (Boston, USA). Antibodies against PINK1, MMP3, MMP13 and Collagen IIwere from Abcam (Cambridge, UK). IL-1β was from Preprotech (Chicago,USA). Phenylmethylsulfonyl fluoride (PMSF), ethylenediamine tetraacetic acid (EDTA), 3-(4,5-dimethyl-2-thiazolyl)-2,5-diphenyl-2-tetrazolium bromide (MTT) and other chemicals were purchased from Sigma.

2.2. *PMC isolation and culture*

All experiments with mice were approved by the Ethics Committee for Animal Research (Zhongshan Hospital, Shanghai, China). Mouse articular chondrocytes were isolated from the knee of 6~8-week-old C57BL/6 male mice. Cartilage was dissected from the joint explant surfaces and then rinsed with saline. The cartilage explants were digested overnight at 37℃ in 1.5 mg/mL collagenase II solution (Gibco, CA, USA). The primary isolated chondrocytes were seeded in flasks after being filtered through a 70 μM cell strainer. Cells are cultured in DMEM/F12 (Gibco) with 10% fetal bovine serum (FBS)(Gibco). Passage 2 was used for experimentation.

2.3. *Cell viability assay*

Chondrocytes were seeded in 96-well plates. After stimulation with IL-1β for 24 h in the presence or absence of different concentrations of metformin, cell viability was evaluated using the Cell Counting Kit-8 solution (Beyotime, Shanghai, China).

2.4. *Detection of reactive oxygen species (ROS)*

Intracellular ROS generation was detected by Cellular Reactive Oxygen Species Detection Assay Kit (Beyotime). Cells were incubated with 10 μM 2′,7′-dichlorofluorescin diacetate (DCF-DA) for 30 min and then washed with phosphate buffered saline (PBS) thrice. The fluorescent signals were recorded with a fluorescent microscope (Olympus, Japan). Six random fields were selected and quantified and measured by using the Image J software (National Institutes of Health, Bethesda, Maryland, USA).

2.5. *Protein isolation and western blot analysis*

To extract whole-cell proteins, the chondrocytes were collected, washed thrice with ice-cold PBS, and then lysed using the cell lysis buffer (25 mM tris-Cl [pH 7.5], 250 mM NaCl, 5 mM ethylenediaminetetraacetic acid, 1%Nonidet-P40, 1 mM phenylmethylsulphonyl fluoride, 5 mM dithiothreitol, 2X protease and phosphatase inhibitor [Thermo Scientific, Waltham, MA, USA]) for 15 min before cell debris were removed

by centrifugation. The same amounts of protein (20 μg) were separated by sodium dodecyl sulfate-polyacrylamide gel electrophoresis (SDS-PAGE) and transferred to polyvinylidene difluoride (PVDF) membranes. The membranes were blocked with 5% non-fat dry milk for 1 h at room temperature and subsequently probed with primary antibodies overnight with gentle agitation at 4℃. After washing three times with Tris-buffered saline containing 0.1% Tween-20 (TBST) for 5 min, the membranes were incubated with the corresponding horseradishperoxidase-linked secondary antibodies (Proteintech, Wuhan, China) for 1 h at room temperature. The membranes were visualized by enhanced chemiluminescence (ECL) solution (Epizyme Bio, Shanghai, China) and the density of each band was measured on the Tanon Imager 4600 system (Tannon, China) and quantified by Image J software.

2.6. *Gene expression analyses by Real-time Quantitative Polymerase Chain Reaction (RT-qPCR)*

Total RNA was extracted using the TRIZOL reagent (Sigma, St. Louis, USA). cDNA was synthesized using 1 μg RNA isolated from mice articular chondrocytes with the First Strand cDNA synthesis kit (Takara, Dalian, China) according to the manufacturers' recommendations. Quantitative PCR analyses were performed using SYBR Green qPCR master mix system (Takara, Dalian, China) according to the manufacturers' recommendations. The target genes expressions were normalized to the mRNA levels of the housekeeping gene GAPDH. The following conditions were used for PCR amplification: incubation for 10 min at 95℃ followed by 40 amplification cycles of 15 s of denaturation at 95℃followed by 45 s of annealing-elongation at 60℃. Primers used for qPCR analysis are as follows GAPDH forward primer:5'-AGGTCGGTGTGAACGGATTTG-3', reverse primer: 5'-TGTAGACCATGTAGTTGAGGTCA-3'; SIRT3 forward primer: 5'-ATCCCGGACTTCAGATCCCC-3', reverse primer: 5'-CAACATGAAAAAGGGCTTGGG-3'.

2.7. *Mitochondrial specific fluorescence staining*

MitoTracker™ Green FM (M7514, ThermoFisher) is a mitochondrial membrane potential independent mitochondrial staining regent. The experiment was performed according to the manufacturer's protocol. Mitochondria were observed under fluorescence microscopy.

2.8. *Immunofluorescence staining*

Chondrocytes were inoculated on the culture slide (Corning, Corning, NY, USA) to facilitate microscopic observation. After 4% paraformaldehyde fixation, 0.5% Triton X-100 permeabilization and serum blocking overnight, cells were incubated with the rabbit polyclonal anti-LC3B antibodies (1:200) (CST) at 4°C overnight and then incubated with rabbit IgG (H+L) secondary antibodies (Alexa Fluor 555, 1 : 1000) (Invitrogen) at room temperature for 1 h. The fluorescent signals were recorded with a fluorescent microscope (Olympus, Japan).

2.9. *Statistical analysis*

All experiments reported in this study were replicated in six independent experiments. The results are presented as the mean ± SD. All data analyses were performed using GraphPad Prism 7 software (GraphPad Software Inc., San Diego, CA, USA). Statistical significance was assessed by unpaired *t*-test (between two groups) and one-way analysis of variance followed by least significant difference (LSD) test (among multiple groups). A P value of < 0.05 was considered statistically significant.

3. Results

3.1. *IL-1β reduces chondrocyte viability and metformin prevents it*

In the present study, IL-1β (*20*) significantly reduced chondrocytes viability in a dose dependent manner (Figure 1A). There was nearly a 40% decrease in cell

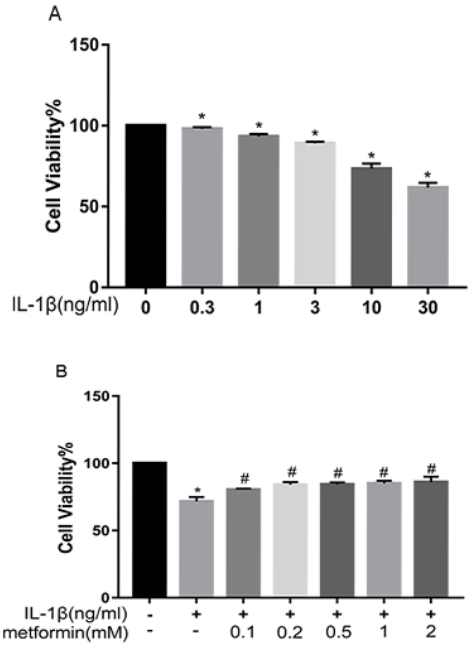

Figure 1. Effects of IL-1β and metformin on cell viability. (A) Cell Counting Kit-8 (CCK-8) results of primary murine articular chondrocytes treated with different concentrations of IL-1β (0, 0.3, 1, 3 10 and 30 ng/mL) for 24 h. **(B)** CCK-8 results of metformin-pretreated (0, 0.1, 0.2, 0.5, 1 and 2 mM) chondrocytes stimulated by 10 ng/mL IL-1β. The data in the figures represent the averages ± SD. Significant differences between groups are indicated as $^{*}P < 0.05$ compared to group NC; $^{\#}P < 0.05$ compared to the cells treated with IL-1β ($n = 6$).

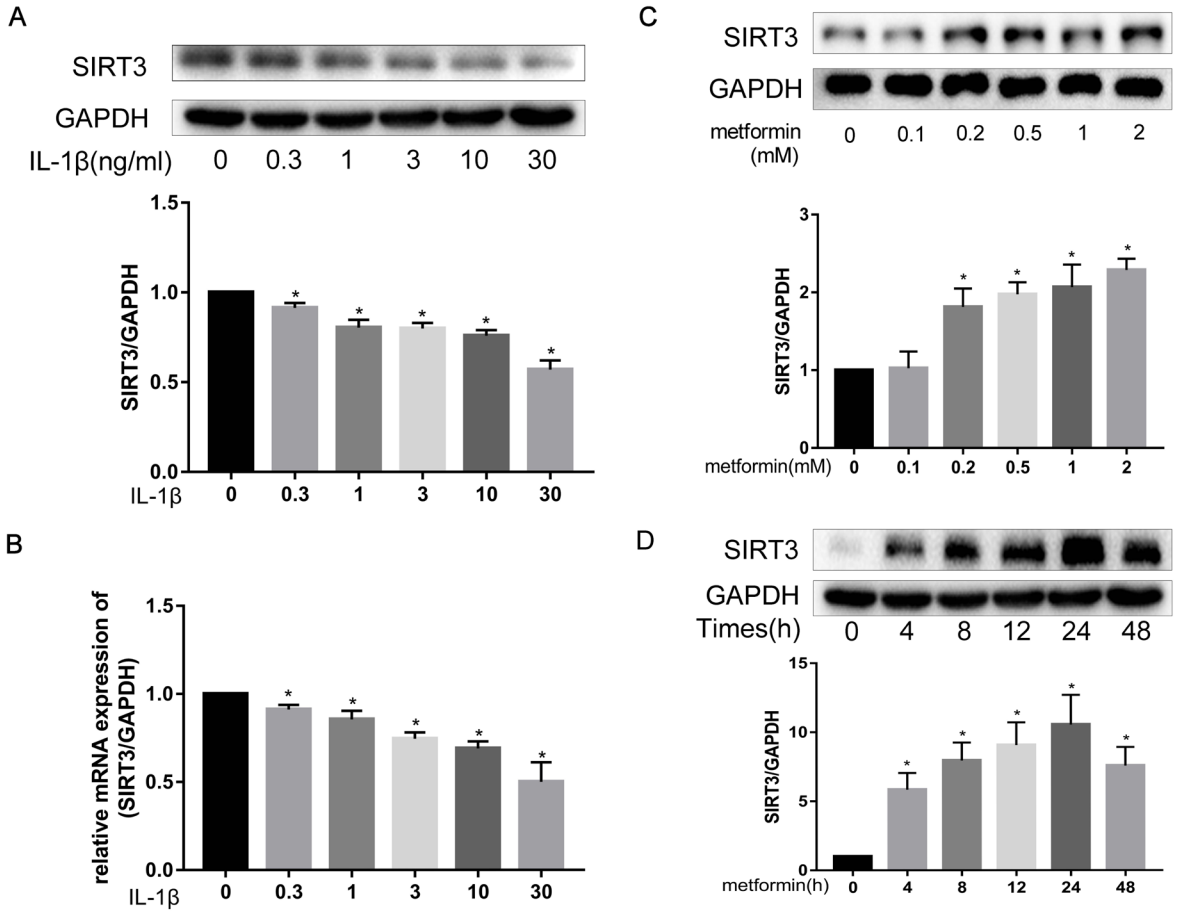

Figure 2. Effects of IL-1β and metformin on the expression of SIRT3. (A) Chondrocytes were incubated with IL-1β (0, 0.3, 1, 3, 10 and 30 ng/mL) respectively, the expression of SIRT3 proteins were detected by Western blotting. **(B)** Chondrocytes were incubated with IL-1β (0, 0.3, 1, 3, 10 and 30 ng/mL) respectively, the level of relative mRNA expression of SIRT3 were detected by qPCR. **(C)** After metformin treatment (0, 0.1, 0.2, 0.5, 1 and 2 mM) for 24 h, the expression of SIRT3 proteins were detected by Western blotting. **(D)** Chondrocytes were incubated with 1mM metformin for 0, 4, 8, 12, 24 or 48 h respectively, the expression of SIRT3 proteins were detected by Western blotting. The data in the figures represent the averages ± S.D. Significant differences between the treatment and control groups are indicated as $^{*}p < 0.05$, $n = 6$.

viability after treatment with 30 ng/mL IL-1β compared with the control group ($p < 0.01$). Metformin alone did not exhibit any toxic effects on cells (data not shown). In the presence of metformin, IL-1β-induced cell toxicity was reduced by different concentration of metformin (Figure 1B).

3.2. *SIRT3 is downregulated in chondrocytes stimulated with IL-1β, and metformin can activate SIRT3 expression*

To investigate the effect of IL-1β on the expression of SIRT3, the level of SIRT3 expression was detected by western blotting and qRT-PCR assays in chondrocytes stimulated with different concentration of IL-1β. As shown in Figure 2A-B, the expression of SIRT3 decreased in a dose dependent manner. We also detected whether SIRT3 expression was regulated by metformin in chondrocytes, the cells were treated with different concentrations or with 1 mM metformin for different time points as shown in Figure 2C-D. Metformin increased the expression of SIRT3 in a concentration- and time-dependent manner. We found that treatment with 1 mM metformin for 24 h resulted in autophagy activation reaching its highest point. According to these findings, the concentration of metformin was chosen as 1 mM and treatment course as 24 h for subsequent studies.

3.3. *Metformin ameliorates IL-1β-induced oxidative stress in chondrocytes*

As oxidative stress also plays a critical role in the progression of OA (*21*), we performed ROS staining assay and mitochondrial membrane potential detection in chondrocytes treated by IL-1β and metformin to confirm whether metformin could alleviate IL-1β-induced mitochondrial stress. As shown in Figure 3, pretreatment with metformin could significantly decrease IL-1β-induced ROS production and rescue downregulated mitochondrial membrane potential.

3.4. *Effect of metformin on mitochondrial function regulators in chondrocytes*

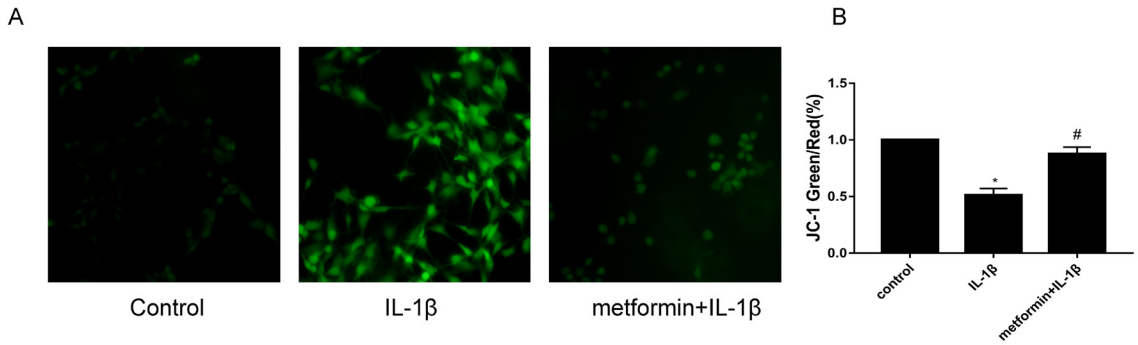

Figure 3. Metformin treatment reduces chondrocytes oxidative stress and decreases mitochondrial membrane potential. (A) ROS measurement was described as the fluorescence intensity imaged by fluorescence microscopy. **(B)** Mitochondrial membrane potential was described as relative mean fluorescence intensity of Green/Red. The data in the figures represent the averages ± S.D. Significant differences between groups are indicated as $^{*}p < 0.05$ compared to group NC; $^{\#}p < 0.05$ compared to the cells treated with IL-1β ($n = 6$).

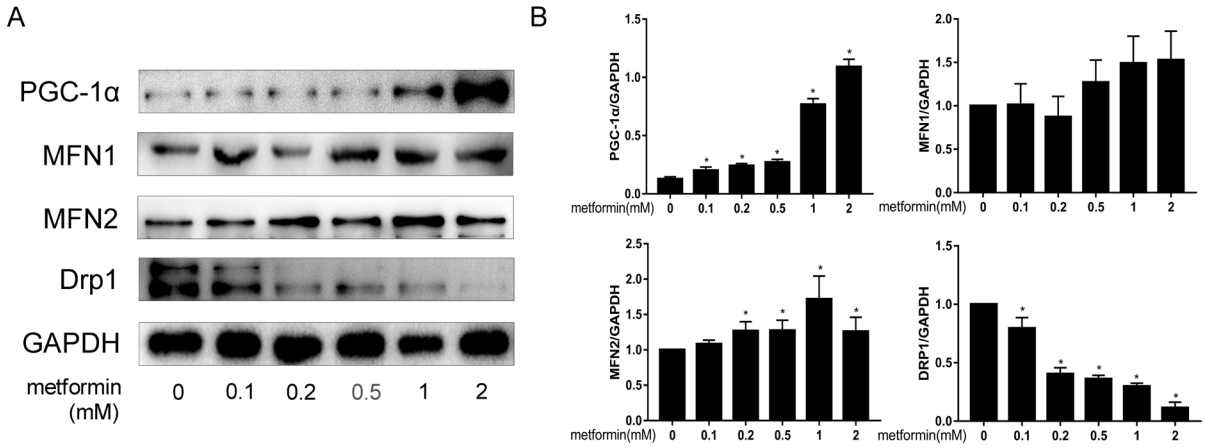

Figure 4. Effect of metformin on mitochondrial function regulators in chondrocytes. (A) The protein expression of PGC-1α, MFN1, MFN2, Drp1 in chondrocytes treated with different concentration of metformin (0, 0.1, 0.2, 0.5, 1 and 2 mM) for 24 h. **(B)** Relative level of PGC-1α, relative level of MFN1, relative level of MFN2, relative level of Drp1. The data in the figures represent the averages ± S.D. Significant differences between the treatment and control groups are indicated as $^{*}p < 0.05$, $n = 6$.

To confirm the effect of metformin on mitochondrial functional statement, we screened the change of mitochondrial fission and fusion-related protein including peroxisome proliferator-activated receptor gamma coactivator 1 Alpha (PGC-1α), mitofusin 1(MFN1), mitofusin 2(MFN2), dynamin-related protein 1(Drp1) (Figure 4). We found that the levels of PGC-1α and MFN2 protein expression increased in a concentration-dependent manner after metformin treatment while the level of Drp1 decreased. These findings indicated metformin promoted mitochondrial fusion and inhibited mitochondrial fission which elevated mitochondrial quality.

3.5. *Metformin promotes PINK1/Parkin-mediated mitophagy in chondrocytes*

To investigate the effect of metformin on autophagy, the expression of SIRT3, PINK1, Parkin and LC3B was detected by western blotting. As shown in Figure 5A, the expression of SIRT3 decreased in chondrocytes stimulated with IL-1β. Metformin upregulated the expression of SIRT3, PINK1, Parkin and the ratio of LC3II/LC3I under inflammatory cytokines stimulation.

To further confirm the effect of metformin on mitophagy, MitoTracker Green staining and LC3B immunofluorescence staining were used to detect mitophagy. Metformin significantly increased co-localization of autophagosome with mitochondria, as evidenced by the merged fluorescent signaling of LC3B and MitoTracker (Figure 6B). Taken together, these data suggest that metformin stimulates mitophagy by activating mitochondrial PINK1/Parkin signaling pathway in OA chondrocytes.

3.6. *SIRT3 inhibitor 3-TYP inhibits SIRT3-mediated PINK1/Parkin-dependent mitophagy in chondrocytes*

We further investigated the effect of SIRT3 inhibitor 3-TYP on mitophagy for the study of mechanisms involved in the SIRT3-mediated PINK1/Parkin-dependent mitophagy. Western blotting results showed pretreatment of 3-TYP inhibited the increase of PINK1, Parkin and the ratio of LC3II/LC3Ias compared to

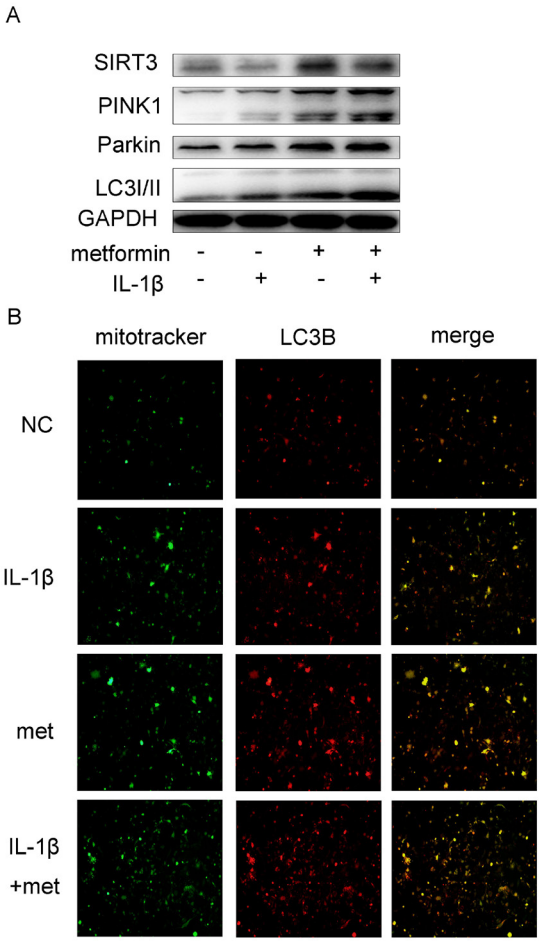

Figure 5. Metformin promotes PINK1/Parkin-mediated mitophagy in chondrocytes. (A) After 10 ng/mL IL-1β treatment with or without metformin for 24 h, the expression of SIRT3, PINK1, Parkin and LC3B were determined by Western blot analysis. **(B)** Representative colocalization images of LC3B immunofluorescent (green) and mitochondria (MitoTracker Green). Chondrocytes were pretreated without or with IL-1β for 1 h, followed by incubation with metformin for another 24 h.

chondrocytes treated with metformin alone (Figure 6).These results indicated that SIRT3 may serve as a upstream regulator of the PINK1/Parkin/LC3B pathway.

3.7. *SIRT3/PINK1/Parkin signaling pathway is involved in the pathogenesis of OA*

To confirm the protective effect of SIRT3-mediated mitophagy in chondrocytes, we screened the expression of OA markers-MMP3, MMP13 and collagen II-when chondrocytes were treated with IL-1β. As shown in Figure 7, immunoblotting revealed that inflammatory cytokine IL-1β increased matrix degrading enzymes, MMP3 and MMP13 and decreased collagen II, as compared to the levels in vehicle-treated chondrocytes. However, metformin reversed the inflammatory response caused by IL-1β, which was dented by SIRT3 inhibitor 3-TYP. These findings illustrated that the inhibition of SIRT3 enhanced the chondrocyte

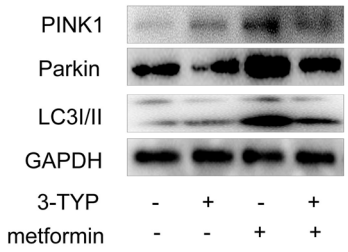

Figure 6. SIRT3 inhibitor 3-TYP inhibits SIRT3-mediated PINK1/Parkin-dependent mitophagy in chondrocytes. After 1 h of pretreatment without or with3-TYP (50 μM), chondrocytes were treated with metformin for another 24 h. The expression of PINK1, Parkin and LC3B was detected by Western blotting.

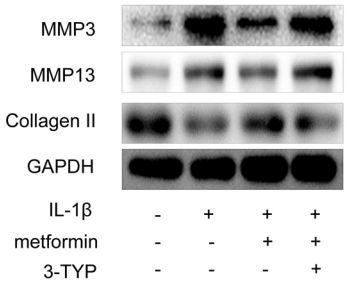

Figure 7. Effects of activation of mitophagy mediated by SIRT3 on ECM catabolism and anabolism balance. After 1 h of pretreatment without or with3-TYP (50 μM), chondrocytes stimulated with IL-1β were treated with metformin for another 24 h. The expression of MMP3, MMP13 and Collagen IIwas detected by Western blotting.

pathological phenotype *via* the PINK1/Parkin-dependent mitophagy.

4. Discussion

OA is a common disease that shows increasing incidence with age. Chondrocytes, which are the only cell type found in articular cartilages, maintain the dynamic balance between synthesis and degradation of ECM (*22*). Inflammatory cytokines, especially IL-1β, were upregulated in OA joints and have been showed to decrease the production of type II collagen and increase the levels of cartilage matrix degrading proteases in chondrocytes (*20*). Therefore, IL-1β is often used to mimic pathological conditions and establish an *in vitro* OA model. Previous studies have shown that stimulation of primary murine chondrocytes with IL-1β result in loss of mitochondrial membrane potential, significant increase in mitochondrial ROS levels, and chondrocyte death (*17*). Mitochondria dysfunction is tightly associated with oxidative stress. Therefore, we sought to establish the role of mitophagy in eliminating dysfunctional mitochondria and its impact on ROS level and chondrocyte-specific anabolic and catabolic balance under IL-1β stimulation in this study.

In this study, we investigated the role of SIRT3

on mitophagy in OA. We found that SIRT3-meidated mitophagy exerted a potent protective effect against OA progression. These beneficial effects may be the result of specific autophagic elimination of damaged mitochondria.

In our study, we found that SIRT3 was decreased in IL-1β stimulated chondrocytes, where its expression was positively correlated with mitochondrial damage and ROS production. The results that IL-1β promoted generation of ROS in chondrocytes were consistent with the phenomenon that the accumulation of ROS was elevated in degenerated articular cartilage *in vivo* (*23*). We also found that metformin treatment elevated SIRT3 expression in chondrocytes. Furthermore, metformin treatment mitigated the loss of chondrocytes viability caused by IL-1β. We also demonstrated that metformin activated SIRT3/PINK1/Parkin pathway could reverse the increased ROS level and loss of ΔΨM. Consistent with our results, studies have also shown that Parkin-mediated mitophagy may eliminate damaged mitochondria and decrease the level of ROS in human umbilical vein endothelial cells and fibroblasts (*24,25*).

We also investigate the effect of metformin on mitochondrial dynamics. The dynamic balance of mitochondrial fusion and fission is critical in the maintenance of mitochondrial membrane potential and function. We found that 24 h of metformin treatment promoted fusion level and suppressed fission level in chondrocytes. Metformin significantly enhanced the mitochondrial fusion level and restored its normal function.

Mitophagy recently emerged as an important mechanism that controls mitochondrial quality. and as a cytoprotective mechanism to maintain mitochondrial homeostasis and cell survival under conditions of stress (*26*). We found that PINK1/Parkin was elevated in IL-1β stimulated murine chondrocytes. We considered the upregulation of PINK1/Parkin as a chondrocytic response to combat pathological conditions. When metformin-mediated SIRT3 was elevated, the PINK1/Parkin pathway was more enhanced, and the immunofluorescence staining results showed enhanced mitophagy in metformin-treated and inflammation-stimulated chondrocytes as compared to the IL-1β group, indicating that the SIRT3 regulated mitophagic activity in OA chondrocytes eventually helped to eliminate damaged mitochondria.

One of the critical events during OA is the loss of chondrocyte cellularity within the articular cartilage. This phenomenon can disrupt the balance between catabolic and anabolic processes and consequently destroy the cartilage. In our studies, metformin abolished IL-1β-induced ECM catabolism by inducing mitophagy related to the activation of the SIRT3/PINK1/Parkin signaling pathway. SIRT3 inhibitor 3-TYP effectively enhanced the expression of MMP3 and MMP13 and decreased the expression of collagen II. Thus, we speculate this effect of metformin on chondrocyte ECM balance may depend on the activation of PINK1/Parkin-mediated mitophagy.

In conclusion, our data reveals that SIRT3 expression is associated with the progression of OA, it is also involved in the clearance of dysfunctional mitochondria *via* mitophagy in chondrocytes. Metformin could suppress IL-1β-induced oxidative stress *via* the activation of the SIRT3/PINK1/Parkin signaling pathway. Thus, mitophagy may become a therapeutic target for OA. Finally, owing to the association between mitophagy and OA, a wide range of drug screening targeting mitophagy may support clinical treatment of OA.

Acknowledgements

The authors thank Dr. Yi Shi, PhD, Biomedical Research Centre, Zhongshan Hospital, Fudan University, for technical assistance.

Author contributions: All listed authors have made substantial contributions to the following aspects of the manuscript: *i*) The conception and design of the study, or acquisition of data, or analysis and interpretation of data. *ii*) Drafting the article or revising it critically for important intellectual content. *iii*) Final approval of the version to be submitted.

Conflict of interest statement: None of the authors had financial or personal relationships with people or organizations that could inappropriately influence the bias of the presented work.

References

1. Glyn-Jones S, Palmer AJ, Agricola R, Price AJ, Vincent TL, Weinans H, Carr AJ. Osteoarthritis. Lancet. 2015; 386:376-387.
2. Blanco FJ, Rego I, Ruiz-Romero C. The role of mitochondria in osteoarthritis. Nat Rev Rheumatol. 2011; 7:161-169
3. Henze K, Martin W. Evolutionary biology: essence of mitochondria. Nature.2003; 426:127-128.
4. Maneiro E, Martín MA, Andres MCD, López-Armada MJ, Hoyo PD, Galdo F, Arenas J, Blanco FJ. Mitochondrial respiratory activity is altered in osteoarthritic human articular chondrocytes. Arthritis Rheum. 2003; 48:700-708.
5. Wang Y, Zhao X, Lotz M, Terkeltaub R, Liubryan R. Mitochondrial biogenesis is impaired in osteoarthritis chondrocytes but reversible *via* peroxisome proliferator-activated receptor γ coactivator 1α. Arthritis Rheumatol. 2015; 67:2141-2153.
6. Baeza J, Smallegan MJ, Denu JM. Mechanisms and dynamics of protein acetylation in mitochondria. Trends Biochem Sci. 2016; 41:231-244.
7. Onyango P, Celic I, Mccaffery JM, Boeke JD, Feinberg

AP. SIRT3, a human SIR2 homologue, is an NAD-dependent deacetylase localized to mitochondria. Proc Natl Acad Sci U S A. 2002; 99:13653-13658.
8. Lombard DB, Alt FW, Cheng HL, Bunkenborg J, Streeper RS, Mostoslavsky R, Kim J, Yancopoulos G, Valenzuela D, Murphy AJM, Biology C. Mammalian Sir2 homolog SIRT3 regulates global mitochondrial lysine acetylation. Mol Cell Biol.2007; 27:8807-8814.
9. Kincaid B, Bossywetzel E. Forever young: SIRT3 a shield against mitochondrial meltdown, aging, and neurodegeneration. Front Aging Neurosci. 2013; 5:48.
10. Ansari A, Rahman MS, Saha SK, Saikot FK, Deep A, Kim KH. Function of the SIRT3 mitochondrial deacetylase in cellular physiology, cancer, and neurodegenerative disease. Aging Cell. 2017; 16:4-16.
11. Fu Y, Kinter M, Hudson J, Humphries KM, Lane RS, White JR, Hakim M, Pan Y, Verdin E, Griffin TM. Aging promotes sirtuin 3-dependent cartilage superoxide dismutase 2 acetylation and osteoarthritis. Arthritis Rheumatol. 2016; 68:1887-1898.
12. Chen LY, Wang Y, Terkeltaub R, Liu-Bryan R. Activation of AMPK-SIRT3 signaling is chondroprotective by preserving mitochondrial DNA integrity and function. Osteoarthritis Cartilage. 2018; 26:1539-1550.
13. Karnewar S, Neeli PK, Panuganti D, Kotagiri S, Mallappa S, Jain N, Jerald MK, Kotamraju S. Metformin regulates mitochondrial biogenesis and senescence through AMPK mediated H3K79 methylation: Relevance in age-associated vascular dysfunction. Biochim Biophys Acta Mol Basis Dis. 2018; 1864:1115-1128.
14. Kim J, Yang G, Kim Y, Kim J, Ha J. AMPK activators: mechanisms of action and physiological activities. Exp Mol Med. 2016; 48:e224
15. Sasaki H, Takayama K, Matsushita T, Ishida K, Kubo S, Matsumoto T, Fujita N, Oka S, Kurosaka M, Kuroda R. Autophagy modulates osteoarthritis-related gene expression in human chondrocytes. Arthritis Rheum. 2012; 64:1920-1928.
16. Youle RJ, Narendra DP. Mechanisms of mitophagy. Nat Rev Mol Cell Biol. 2011; 12:9-14.
17. Ansari MY, Khan NM, Ahmad I, Haqqi TM. Parkin clearance of dysfunctional mitochondria regulates ROS levels and increases survival of human chondrocytes. Osteoarthritis Cartilage. 2017; 26:1087-1097.
18. Yu W, Gao B, Na L, Wang J, Qiu C, Zhang G, Min L, Zhang R, Li C, Gang J. Sirt3 deficiency exacerbates diabetic cardiac dysfunction: Role of Foxo3A-Parkin-mediated mitophagy. Biochim Biophys Acta Mol Basis Dis. 2016; 1863:1973-1983.
19. Feng J, Lu C, Dai Q, Sheng J, Xu M. Pharmacology. SIRT3 facilitates amniotic fluid stem cells to repair diabetic nephropathy through protecting mitochondrial homeostasis by modulation of mitophagy. Cell Physiol Biochem. 2018; 46:1508-1524.
20. Goldring MB, Birkhead JR, Suen LF, Yamin R, Mizuno S, Glowacki J, Arbiser JL, Apperley JF. Interleukin-1 beta-modulated gene expression in immortalized human chondrocytes. J Clin Invest. 1994; 94:2307-2316.
21. Lepetsos P, Papavassiliou AG. ROS/oxidative stress signaling in osteoarthritis. Biochim Biophys Acta. 2016; 1862: 576-591.
22. Zhang Y, Vasheghani F, Li YH, Blati M, Simeone K, Fahmi H, Lussier B, Roughley P, Lagares D, Pelletier JP, Martel-Pelletier J, Kapoor M. Cartilage-specific deletion of mTOR upregulates autophagy and protects mice from osteoarthritis. Ann Rheum Dis. 2015; 74:1432-1440.
23. Jallali N, Ridha H, Thrasivoulou C, Underwood C, Butler PE, Cowen T. Vulnerability to ROS-induced cell death in ageing articular cartilage: the role of antioxidant enzyme activity. Osteoarthritis Cartilage. 2005; 13:614-622.
24. Rojansky R, Cha MY, Chan DC. Elimination of paternal mitochondria in mouse embryos occurs through autophagic degradation dependent on PARKIN and MUL1. eLife. 2016; 5:pii:e17896.
25. Zhu W, Yuan Y, Liao G, Li L, Liu J, Chen Y, Zhang J, Cheng J, Lu Y, Mesenchymal stem cells ameliorate hyperglycemia-induced endothelial injury through modulation of mitophagy. Cell Death Dis. 2018; 9:837.
26. Eiyama A, Okamoto K. PINK1/Parkin-mediated mitophagy in mammalian cells. Curr Opin Cell Biol. 2015; 33:95-101.

(Received October 31, 2018; Revised December 14, 2018; Accepted December 16, 2018)

Original Article

DOI: 10.5582/bst.2018.01232

Integrating multiple of the median values of serological markers with the risk cut-off value in Down syndrome screening

Yuan Zhou[1,§], Yan Du[1,2,§], Bin Zhang[1,*], Ling Wang[1,2,3,4,*]

[1] *Obstetrics and Gynecology Hospital of Fudan University, Shanghai, China;*
[2] *The Academy of Integrative Medicine of Fudan University, Shanghai, China;*
[3] *Shanghai Key Laboratory of Female Reproductive Endocrine-related Diseases, Shanghai, China;*
[4] *Laboratory for Reproductive Immunology, Hospital & Institute of Obstetrics and Gynecology, IBS, Fudan University Shanghai Medical College, Shanghai, China.*

Summary **To assess the predictive value of integrating multiple of the median (MOM) with the risk cut-off value for serological screening of Down syndrome. In this retrospective study, women with singleton pregnancies who underwent triple serological screening for Down syndrome were followed, and their screening results and pregnancy outcomes were recorded. The range of MoM value of each indicator was calculated, different protocols integrating various MoM values with the risk cut-off value were compared. A total of 120,269 women with singleton pregnancy were screened and included in the analysis, of those 52 fetuses were confirmed as trisomy-21 by amniocentesis chromosomal karyotyping. Using a risk cut-off value of 1:380, 8,809 samples tested positive and the screen positive rate was 7.32% (8,809/120,269). The normal reference ranges (5-95%) of the MoM value of AFP, β-hCG, and uE3 were 0.60-1.72, 0.43-2.21 and 0.60-1.58, respectively. The detection rate of each screening protocol integrating different MoM percentile values was between 75% and 79%, the positive rate was between 7% and 18%, and the false positive rate was between 7% and 18%. Protocol-6 which combined the screening risk cut-off value and β-hCG MoM ≥ 97.5% percentile is an optimal protocol with a relatively high detection rate (78.8%) and low false positive rate (8.2%). Integrating MoM values of serological indicators can appropriately increase detection rate when interpreting the results of Down syndrome screening.**

Keywords: Down syndrome, serological screening, multiple of the median, prediction

1. Introduction

Down syndrome, also known as trisomy-21 syndrome, is the most common aneuploid type with a reported incidence between 1/1000 and 1/650 (*1,2*). Serological screening is widely used in prenatal screening for Down syndrome for fetal risk assessment (*3*). For cases with high-risk serological screening results, further prenatal diagnosis is recommended for confirmation. The serological screening mainly includes quadruple test [AFP (alpha fetoprotein), β-hCG (human chorionic gonadotropin), uE3 and Inh-A (Inhibin-A)] and triple test (AFP, β-hCG and uE3) in the second trimester, and the latter is widely used in China (*4*).

Multiple of the median (MoM) value is referred to as the ratio of the actual measured value of the three markers over the normal median value of the corresponding gestational weeks (days). When interpreting the results of Down syndrome screening, there are different notions on whether or not to include MoM values of each serological indicator and no consensus has been reached yet. Some researchers suggest that AFP MoM ≤ 0.5 and β-hCG MoM≥2.5 can be used as suitable cut-off values for screening Down syndrome pregnancy (*5*). And others only use median of MoM (mMoM) as a quality control measure but do not include in the screening criteria (*6-8*). From our clinical experiences, we have found that MoM value has certain clinical significance. In this retrospective

[§]These authors contributed equally to this work.
**Address correspondence to:*
Dr. Bin Zhang and Dr. Ling Wang, Hospital and Institute of Obstetrics and Gynecology, IBS, Fudan University, 419 Fangxie Road, Shanghai 200011, China.
E-mail: shentuzhangbin@163.com (BZ), Dr.wangling@fudan.edu.cn (LW)

study, we mainly aimed to evaluate the clinical value of integrating different MoM percentile values with the risk cut-off value for serological screening of Down syndrome.

2. Materials and Methods

2.1. *Study population*

This retrospective study was conducted at the Obstetrics and Gynecology Hospital of Fudan University. A total of 122,671 pregnant women who underwent second trimester (14 weeks^{+0} to 21 weeks^{+6}) triple serological test (AFP, β-hCG, and uE3) for Down syndrome screening during the period of June 2007 to July 2016 were included. Of those women, 120,269 women were with singleton pregnancy. Gestational week was confirmed with the last menstruation period and fetal crown-rump length (CRL). The pregnancy outcome of all those women was followed up.

The study protocol conformed to the ethical guidelines of the 2000 Declaration of Helsinki and was approved by the institutional review board at Obstetrics and Gynecology Hospital of Fudan University. Oral informed consent was obtained from all participants.

2.2. *Serological screening*

For each pregnant woman, 2 ml of maternal peripheral blood was extracted, and conserved at 4℃ after separation of serum. Serological markers (AFP, β-hCG and uE3) were detected within 3 days using chemiluminescent immunoassay (*9*). Instruments and reagents were provided by BECKMAN COULTER (USA). Chemiluminescence detection was performed using Beckman Coulter Access2 Automatic Immunoassay System (BECKMAN COULTER, USA) according to the manufacturer's instructions.

After chemiluminescent immunoassay, TCsoft prenatal screening software was used to calculate the screening risk. Values included in the software were serological markers (AFP, β-hCG and uE3), birthday of the mother, gestational weeks, height, weight, history of pregnancy, and fetal numbers (*10*). It automatically calculated the risk of Down syndrome, Open spina bifida (OSB) and Trisomy 18 syndrome (Final risk = age related risk* AFP likelihood ratio* β-hCG likelihood ratio* uE3 likelihood ratio). Using the software, the cut-off value for Down syndrome risk was set at 1:380 (*11*).

2.3. *MoM calculation and correction for each serological marker*

MoM value is the ratio of the actual measured value of the indicator to the normal median of the gestational weeks (days). In order to eliminate the influence of gestational weeks on markers when calculating the screening risk of Down syndrome, the MoM values of various serological indicators were calculated (*12*). In addition, a quality control system based on the mMoM was utilized to control the quality of the prenatal screening for Down syndrome. The ideal mMoM value should be within the range of 1.0 ± 0.05 (*7,8*). The mMoM values of the three markers (AFP, β-hCG, uE3) in our hospital in the last decade were 0.83, 1.00, and 1.00 respectively. The mMoM value of the AFP marker was significantly off 1.00 (median = 0.83, range: 0.73-0.94). In order to control for systematic error, all MoM AFP values were divided by 0.83 to correct for this deviation (*6,13*).

2.4. *Statistical analyses*

Mean and standard deviation (SD) were calculated for continuous variables, and were compared using Student's *t* test. Number and frequency were calculated for categorical variables, and were compared using Chi-square tests. Wilcoxon rank sum test was used to compare MoM values of each serological marker. Positive rate (screening positive cases/total cases), detection rate (true positive cases detected/true positive cases total), false positive rate (false positive cases/true negative cases total), positive predictive value (true positive cases detected/total positive cases detected) were calculated for each screening protocol.

All above analyses were two sided and were performed by SPSS 16.0 for Windows (SPSS Inc., Chicago, IL, USA). A P value of < 0.05 was considered statistically significant.

3. Results

3.1. *Population characteristics*

A total of 120,269 women with singleton pregnancies were included in the final analysis. Of those screened, 52 fetuses were confirmed as trisomy-21 by chromosomal karyotyping during amniocentesis or blood test after birth. The prevalence rate of Down syndrome in our population was 0.04% (52/120,269). Table 1 shows the population characteristics of the two groups. Compared to women without Down syndrome pregnancies, the average age of pregnant women in the Down syndrome pregnancy group was significantly older (31.15 ± 4.17 *vs*. 29.23 ± 3.44, $P < 0.05$). There was no statistically significant difference in weight, gestational age, smoking and gestational diabetes status between the two groups ($P > 0.05$ for all).

3.2. *Results of screening and follow-up outcome*

As shown in Table 2, using a risk cut-off value of greater than 1:380 (*11,13*), 8,809 samples tested

Table 1. Characters of the Down syndrome pregnancy group and the group without Down syndrome pregnancy

Items	Down syndrome pregnancy group (N = 52)	Control group (N = 120,217)	P
Age (years), Mean ± SD	31.15 ± 4.21	29.23 ± 3.44	< 0.001
AMA			
Yes	8	6,324	0.001
No	44	113,875	
Weight (kg)	57.32 ± 7.77	57.91 ± 8.88	
Gestational age (weeks)	16.65 ± 0.99	16.89 ± 1.27	0.63
Smoking			0.18
Yes	1	1,692	0.75
No	51	118,525	
GDM			
Yes	0	533	0.63
No	52	119,684	

AMA, advanced maternal age, defined as ≥ 35 years of age; GDM, gestational diabetes mellitus; SD, standard deviation.

Table 2. Second trimester serological screening results of Down syndrome

Screening	Down syndrome pregnancy group	Control group	Total
Positive (≥ 1:380)	39	8,770	8,809
Negative (< 1:380)	13	111,447	111,460
Total	52	120,217	120,269

Table 3. Percentile distribution of the MoM values of each indicator in 120,269 samples

Percentile (%)	AFP MoM	β-hCG MoM	uE3 MoM
2.5	0.550	0.357	0.540
5	0.604	0.426	0.603
50	0.995	0.994	0.999
95	1.719	2.213	1.576
97.5	1.930	2.603	1.718

AFP, alpha fetoprotein; β-hCG, human chorionic gonadotropin; MoM, multiple of median.

positive among 120,269 samples and the screen positive rate was 7.32% (8,809/120,269). Of the 8,809 samples, 39 (39/8,809, 0.4%) cases of Down syndrome were confirmed. Among the screening negative women, 13 were false negative cases classified using serological screening risk cut-off value of Down syndrome.

3.3. *Distribution of MoM values for each indicator*

Table 3 lists the different percentile distributions of the MoM values for each indicator. Compared to the control group, the Down syndrome pregnancy group had a higher β-hCG value, but lower AFP and uE3 values ($P < 0.05$ for all).

3.4. *Down syndrome cases*

Among the 52 women with Down syndrome pregnancies, one was a smoker, while none of them had gestational diabetes. Ten cases (10/52, 19.23%) were delivered, while 42 cases (42/52, 80.77%) were confirmed by amniocentesis chromosomal karyotyping and underwent induced labor. Eight of the 10 (8/10, 80%) live birth Down syndrome cases were screened as low risk using the risk cut-off value of less than 1:380, another 2 (2/10, 20%) cases were classified as high screening risk but refused amniocentesis. The detailed information of 10 cases of live birth Down syndrome cases is presented in Table 4.

Thirty-seven of the 42 (37/42, 88.10%) cases that underwent induced labor were screened as high risk (risk cut-off value of ≥ 1:380) and received amniocentesis chromosomal karyotyping; another 5 cases (5/42, 11.90%) were screened as low risk using the risk cut-off value of less than 1:380 but ultrasonographic screening indicated fetal abnormality, and were then confirmed by amniocentesis chromosomal karyotyping (Table 5). In total, twenty-six of the 52 (26/52, 50%) confirmed cases were detected with soft ultrasound markers for Down syndrome, including 6 cases of absent or hypoplastic nasal bone, 6 cases of nuchal fold thickness ≥ 6 mm, 5 cases of ventricular septal defect, 3 cases of ventriculomegaly, 2 cases of dilation of the renal pelvis, and 4 cases with multiple risk markers.

3.5. *False negative cases*

Among the confirmed 52 Down syndrome cases, 13 (13/52, 25%) were classified as false negative cases using serological screening of Down syndrome. The information of these 13 cases is shown in Table 6. The average age of the false negative cases was less than 35 (mean = 29.97, SD = 2.96). The risk of Down syndrome was between 1:1423 and 1:475. The MoM value of AFP was less than 0.7 for 4 cases, the MoM value of β-hCG was more than 2.0 for 2 cases, and the MoM value of uE3 was less than 0.7 for 2 cases. Five of the 13 (5/13, 38.46%) false negative cases underwent amniocentesis chromosomal karyotyping after ultrasound indication of fetal anomalies and then underwent induced labor, while the other 8 cases were delivered.

Table 4. Information of the 10 live birth Down syndrome cases

Case Number	AFP MoM	β-hCG MoM	uE3 MoM	Gestational age (week)	Weight (kg)	Down syndrome risk	Maternal age (year)	Clinical information						
								Ultrasound	Gestational age at delivery (week)	Delivery mode	Sex of newborn	Weight of newborn (g)	Chromosome examination	Outcome
1	0.62	1.1	0.93	15.4	66	345	35.55	Nasal bone hypoplasia	37.1	CS	Male	3065	Trisomy-21	Live
2	1.03	1.47	0.65	15.4	57	508	30.35	Ventricular septal defect	38.2	VD	Male	3450	Trisomy-21	Live
3	1.18	1.37	0.72	15.4	66	730	31.85	-	39.5	VD	Male	3660	Trisomy-21	Live
4	1.01	0.91	0.94	15.6	55	3601	26.58	Placental previa	36.3	CS	Male	2380	Trisomy-21	Dead
5	0.59	2.5	0.84	16.3	63	169	26.66	-	32.2	VD	Male	1795	Trisomy-21	Dead
6	0.63	1.69	0.83	16.1	54	435	23.89	-	37.4	VD	Female	2530	Trisomy-21	Live
7	0.75	1.05	0.99	16.1	49	754	34.49	-	38.3	CS	Female	3120	Trisomy-21	Live
8	0.87	1.26	0.79	17.6	50	391	34.48	Breech fetus	37.6	CS	Female	3010	Trisomy-21	Live
9	0.88	1.99	1.06	17.6	72	787	29.53	-	40.0	VD	Female	4050	Trisomy-21	Live
10	1.11	1.06	0.65	17.6	53	1380	29.23	Breech fetus	37.6	CS	Male	2830	Trisomy-21	Live

AFP, alpha fetoprotein; β-hCG, human chorionic gonadotropin; CS, cesarean section; MoM, multiple of median; VD, vaginal delivery.

Table 5. Down syndrome screening results and pregnancy outcomes

Items	Induced labor	Delivery	Total
High risk (< 1:380)	37	2	39
Low risk (≥ 1:380)	5	8	13
Total	42	10	52

3.6. *Comparison of different screening protocols*

We integrated the risk cut-off value with different combinations of the serological marker MoM percentile values to form different screening protocols, and summarized positive rate, detection rate, false positive rate, and positive predictive value of each protocol (Table 7). In general, integrating the risk cut-off value with different MoM percentile values of each indicator improved the detection rate of Down syndrome up to 79%.

Generally, the positive rate and false positive rate for most of the screening protocols were below 20%. It is observed that two protocols (3 and 6), which combined the screening risk and serological β-hCG MoM value, increased the detection rate to almost 80% while did not significantly increase the positive rate and false positive rate (both below 10%).

4. Discussion

The diagnosis of Down syndrome is mainly dependent on invasive prenatal examination and postpartum chromosome examination. The reported pregnancy loss rate for invasive prenatal diagnosis is between 0.3% and 1%, and varies depending on the skill and experience of the operators and specialist centers (*14*). Therefore, it is necessary to improve the detection rate of prenatal screening and reduce the false positive rate, thus reducing the invasive prenatal diagnostic procedure. Current prenatal screening is divided into early pregnancy screening and mid-pregnancy screening, based on the conditions and initial diagnostic time window of the medical institutions where the pregnant woman receives prenatal care. During the early pregnancy (11 weeks to 13^{+6} weeks), evaluation of Down syndrome risk is often based on the comprehensive analysis of maternal age, fetal neck translucency (NT) thickness, serum β-hCG and pregnancy-associated plasma protein A (PAPP-A). The detection rate of early pregnancy screening is between 80% and 82%, with a false positive rate of 3% (*14*). During the second trimester, serological triple (AFP, β-hCG, uE3) or quadruple (AFP, β-hCG, uE3 and Inh A) test integrating computation of maternal age risk is commonly used. Studies from other countries have reported that the quadruple test performed better than the triple test, with a detection rate close to 80%, and a false positive rate of 3% (*15,16*). However, in most parts

Table 6. Information of the 13 false negative cases

Case number	Gestational age (week)	Age (year)	Age risk	Risk of Down syndrome	AFP MoM	β-hCG MoM	uE3 MoM	Pregnancy outcome	Ultrasound
1	15.4	30.35	1:930	1:508	0.85	1.47	0.65	Delivered	Ventricular septal defect
2	15.4	31.85	1:760	1:730	0.98	1.37	0.72	Delivered	-
3	15.6	26.58	1:1,282	1:3,601	0.84	0.91	0.94	Delivered	-
4	16.1	23.89	1:1,423	1:435	0.52	1.69	0.83	Delivered	-
5	16.5	29.29	1:1,043	1:609	0.76	3.68	1.25	Induced labor	Nuchal fold thickness ≥ 6mm
6	16.1	34.49	1:477	1:754	0.63	1.05	0.99	Delivered	-
7	16.3	32.68	1:666	1:1,197	0.71	1.51	1.16	Induced labor	Nuchal fold thickness ≥ 6mm
8	16.5	29.00	1:1,071	1:3,980	0.93	1.29	1.19	Induced labor	Nuchal fold thickness ≥ 6mm
9	17.6	34.48	1:475	1:391	0.72	1.26	0.79	Delivered	Breech fetus
10	17.1	28.42	1:1,128	1:538	0.66	1.39	0.71	Induced labor	Nasal bone hypoplasia
11	17.6	29.53	1:1,014	1:787	0.73	1.99	1.06	Delivered	-
12	17.6	29.23	1:1,047	1:1,380	0.92	1.06	0.65	Delivered	Breech fetus
13	18.1	29.84	1:981	1:657	0.46	2.73	1.27	Induced labor	Head edema, tetralogy of fallot

AFP, alpha fetoprotein; β-hCG, human chorionic gonadotropin; MoM, multiple of median.

Table 7. Comparisons of different screening protocols

Number	Screening protocol	Positive rate (number of cases)	Detection rate	False positive rate	Positive predictive value
1	Risk cut-off value (1:380)	7.2% (8,614)	75.0% (39/52)	7.1%	1/221
2	Risk cut-off value + AFP MoM ≤ 5% (0.604)	11.3% (13,534)	76.9% (40/52)	11.2%	1/338
3	Risk cut-off value + β-hCG MoM ≥ 95% (2.213)	9.8% (11,733)	78.8% (41/52)	9.7%	1/286
4	Risk cut-off value + uE3 MoM ≤ 5% (0.603)	9.8% (11,733)	75.0% (39/52)	10.5%	1/324
5	Risk cut-off value + AFP MoM ≤ 2.5% (0.550)	9.2% (11,015)	75.0% (39/52)	9.1%	1/282
6	Risk cut-off value + β-hCG MoM ≥ 97.5% (2.603)	8.2% (9,910)	78.8% (41/52)	8.2%	1/242
7	Risk cut-off value + uE3 MoM ≤ 2.5% (0.540)	8.8% (10,536)	75.0% (39/52)	8.7%	1/270
8	Risk cut-off value + AFP MoM ≤ 0.7	17.8% (21,406)	78.8% (41/52)	17.8%	1/522
9	Risk cut-off value + β-hCG MoM ≥ 2.0	11.5% (13,807)	78.8% (41/52)	11.4%	1/337
10	Risk cut-off value + uE3 MoM ≤ 0.7	15.7% (18,860)	78.8% (41/52)	15.7%	1/460

AFP, alpha fetoprotein; β-hCG, human chorionic gonadotropin; MoM, multiple of median.

of China, early pregnancy screening rate is low because of missing time or technical limitations (*17*). The main method of screening fetal chromosomal abnormality in China is serological triple test, and further diagnostic procedures are recommended for high-risk pregnant women. Down syndrome screening in second trimester is a simple procedure with relatively low cost, which can be widely applied in China especially in less developed and resource limited regions.

It was reported that in the early time of second trimester, the AFP value of normal pregnant women had increased by 15-20% per week, serum uE3 value had increased by 20-25% per week, while serum β-hCG had decreased from the peak at 15 weeks and decreased slowly after 20 weeks (*18*). An early study reported that the AFP MoM of Down syndrome pregnancy was under 1.0 (*19*). A subsequent study found that the serum β-hCG of Down syndrome pregnancy was more than twice that of normal pregnancy, and the uE3 value was lower than normal pregnancy (*20*). Similarly, our data showed that the values of both AFP MoM and uE3 MoM decreased, while the value of β-hCG MoM increased. It is important to consider the serological screening test results, since clear deviations from the normal range also indicate an increased risk of chromosome abnormality. In our study, the screening risk of all 13 false negative cases were below the cut-off value (1:380); however, MoM values of some cases deviated significantly from the normal range. For example, the AFP MoM value of case number 4 was 0.52 (< 97.5%), the β-hCG MoM value of case number 5 was 3.68 (> 97.5%); and for case number 13, the AFP MoM value was 0.46 (< 97.5%) and the β-hCG MoM value was 3.68 (> 97.5%). Therefore, the MoM value of the serological markers should be taken into consideration when interpreting Down syndrome screening report, which could reduce the occurrence of false negative cases.

MoM values provide a simple way to compare the deviation of an individual from the overall population. When using software to calculate Down syndrome risk, the level of serological markers in pregnant women was correlated with their race, age, gestational age, weight, diabetes and smoking, and the correction of gestational age and weight is most significant (*21*). Several regression equations have been developed for risk estimate correction (*6,13,22*). In our hospital, gestational age was corrected by ultrasonographic measurements, and weight was corrected by the reciprocal correction equation (*22*).

Both the positive rate and false positive rate increase with the increase of detection rate, which may lead to unnecessary invasive prenatal diagnostic procedures. Generally, the positive rate and false positive of an optimal screening protocol should be below 10%. It is observed that protocol-3 and protocol-6 combining screening risk and different serological β-hCG MoM values (protocol-3: screening risk > 1:380 and β-hCG MoM value more than 2.213; protocol-6: screening risk > 1:380 and β-hCG MoM value > 2.603) increased the detection rate up to almost 80% while did not significantly increase the positive rate and false positive rate. It is of significant importance to incorporate ultrasound screening findings when interpreting serological examination results, so as to improve the detection rate of Down syndrome. As shown among the 13 false negative cases (Table 6), 6 cases showed abnormal soft indexes of ultrasound, including NF thickened, nasal bone hypoplasia, cardiac abnormalities, and head edema.

With the advancement of non-invasive prenatal testing technology, more and more pregnant women have chosen non-invasive prenatal testing (NIPT) to screen for fetal chromosome abnormalities (*23*). NIPT has the advantage of high accuracy and noninvasiveness (*23*). An increasing amount of data has shown that NIPT can be used in medium risk groups as stated by the International Society for Prenatal Diagnosis (*24*). In economically developed regions, for pregnant women with critical Down syndrome screening risk or abnormal serological indicator MoM values, using NIPT is advantageous. But in less developed regions, traditional Down syndrome screening remains the main method for chromosome abnormality screening. Therefore, choosing an appropriate screening protocol is particularly important. The detection rate of our protocol-3 and protocol-6 was close to 80%, in combination with prenatal ultrasound screening, and can detect most Down syndrome pregnancies.

As a routine method of prenatal examination in China, the Down syndrome triple serological screening test has the advantages of efficiency, economy and convenience. The main purpose of this study was to incorporate different MoM values of serological markers into the existing Down syndrome screening test, so as to increase the efficiency of Down syndrome screening. Our study with a relatively large sample size utilizing data from the last decade in our hospital showed a similar positive rate, detection rate and false positive rate to reports from other countries and regions (*25,26*). Protocols (protocol-3 and protocol-6) which combined serum β-hCG MoM value > 95% (2.213) or > 97.5% (2.603) with the traditional screening risk showed high detection rate, low positive rate and false positive rate, and could increase the efficiency. However, the results need to be further evaluated in a validation study. In addition, the overall incidence rate of Down syndrome was lower in our dataset, which may be related to a pre-selection of pregnant women in our hospital.

In conclusion, the efficiency of combining screening risk with serological marker MoM values to screen for Down syndrome needs to be prospectively evaluated in different centers with large sample sizes. Selection of an optimal screening protocol should be based on the population characteristics of each center.

Acknowledgements

This work was supported by the National Natural Science Foundation of China No. 31571196 (to Ling Wang), the Science and Technology Commission of Shanghai Municipality 2015 YIXUEYINGDAO project No.15401932200 (to Ling Wang), the FY2008 JSPS Postdoctoral Fellowship for Foreign Researchers P08471 (to Ling Wang), the National Natural Science Foundation of China No. 30801502 (to Ling Wang), the Shanghai Pujiang Program No. 11PJ1401900 (to Ling Wang), Development Project of Shanghai Peak Disciplines-Integrative Medicine No.20150407.

References

1. Stoll C, Dott B, Alembik Y, Roth MP. Associated congenital anomalies among cases with Down syndrome. Eur J Med Genet. 2015; 58:674-80.
2. V Plaiasu. Down Syndrome – Genetics and Cardiogenetics. Maedica (Buchar). 2017; 12:208-213.
3. Spencer, K. Screening for Down syndrome. Scand J Clin Lab Invest Suppl. 2014; 244:41-7.
4. Palomaki GE, Eklund EE, Neveux LM, Lambert Messerlian GM. Evaluating first trimester maternal serum screening combinations for Down syndrome suitable for use with reflexive secondary screening via sequencing of cell free DNA: High detection with low rates of invasive procedures. Prenat Diagn. 2015; 35:789-96.
5. Jiang T, Sun YJ, Xu QJ, Sun Y, Zhang XJ, Cao L, Z W, Zhang J, Huang ML, Chen CH, Lin YS, Xu ZF. Results of second-trimester prenatal screening using two serum markers for Down's syndrome in 60 931 pregnant women. Chin J Perinat Med. 2011; 14:74-77. (Article in Chinese)
6. Malone, FD, Canick JA, Ball RH, *et al*. First-trimester or second-trimester screening, or both, for Down's syndrome. N Engl J Med. 2005; 353:2001-2011.
7. Alldred SK, Deeks JJ, Guo B, Neilson JP, Alfirevic Z. Second trimester serum tests for Down's Syndrome screening. Cochrane Database Syst Rev. 2012; 6:CD009925.
8. Alldred SK, Takwoingi Y, Guo B, Pennant M, Deeks JJ, Neilson JP, Alfirevic Z. First and second trimester serum tests with and without first trimester ultrasound tests for Down's syndrome screening. Cochrane Database Syst Rev. 2017; 3:CD012599.
9. Ananth CV, Wapner RJ, Ananth S, D'Alton ME, Vintzileos AM. First-Trimester and Second-Trimester Maternal Serum Biomarkers as Predictors of Placental Abruption. Obstet Gynecol. 2017; 129:465-472.
10. Reynolds TM, Vranken G, Van Nueten J. Weight correction of MoM values: Which method? J Clin Pathol. 2006; 59:753-758.
11. Zhang Y, Hu J, Qiu C. Clinical application of TCSoft Down's syndrome screening software for prenatal screening in middle period pregnant women. Lab Med Clin. 2013; 10 (Suppl I):55-58. (Article in Chinese)
12. Wald NJ. Prenatal screening for open neural tube defects and Down syndrome: Three decades of progress. Prenat Diagn. 2010; 30:619-621.
13. Jiang Y, Liu J, Liu S, Hao N, Zhou J, Qi QZ, Zhou XY, Bian XM. The Application Instance of Monitoring and Audit of Median values of Mom in Prenatal Screening of Down's Syndrome. Journal of Practical Obstetrics and Gynecology. 2014; 30:103-107. (Article in Chinese)
14. Akolekar R, Beta J, Picciarelli G, Ogilvie C, D'Antonio F. Procedure-related risk of miscarriage following amniocentesis and chorionic villus sampling: A systematic review and meta-analysis. Ultrasound Obstet Gynecol. 2015;45:16-26.
15. Benn P, Borell A, Chiu R, *et al*. Position statement from the Aneuploidy Screening Committee on behalf of the Board of the International Society for Prenatal Diagnosis. Prenat Diagn. 2013; 33:622-9.
16. Agarwal Gupta N, Kabra M. Diagnosis and management of Down syndrome. Indian J Pediatr. 2014; 81:560-7.
17. Dong Y, Yan X. Significance and feasibility of combined serological and ultrasound screening for early diagnosis of fetal Down's syndrome. Chinese Journal of Practical Gynecology and Obstetrics. 2010; 12:895-898. (Article in Chinese)
18. Gomes MS, Carlos-Alves M, Trocado V, Arteiro D, Pinheiro P. Prediction of adverse pregnancy outcomes by extreme values of first trimester screening markers. Obstet Med. 2017; 10:132-137.
19. Merkatz IR, Nitowsky HM, Macri JN, Johnson WE. An association between low maternal serum alpha-fetoprotein and fetal chromosomal abnormalities. Am J Obstet Gynecol. 1984; 148:886-94.
20. Wald NJ, Kennard A, Densem JW, Cuckle HS, Chard T, Butler L. Antenatal maternal serum screening for Down's syndrome: Results of a demonstration project. BMJ. 1992; 305:391-394.
21. Huang T, Meschino WS, Okun N, Dennis A, Hoffman B, Lepage N, Rashid S, Aul R, Farrell SA. The impact of maternal weight discrepancies on prenatal screening results for Down syndrome. Prenat Diagn. 2013; 33:471-476.
22. Zhang B, Liu X. Influence of maternal weight on MoM and screening performance in second trimester prenatal triple marker screening. Laboratory Medicine. 2014; 29:1101-1106. (Article in Chinese)
23. Du Y, Lin J, Lan L, Dong Y, Zhu J, Jiang W, Pan X, Lu Y, Li D, Wang L. Detection of chromosome abnormalities using current noninvasive prenatal testing: A multi-center comparative study. Biosci Trends. 2018; 12:317-324.
24. Benn P, Borrell A, Chiu RW, *et al.* Position statement from the Chromosome Abnormality Screening Committee on behalf of the Board of the International Society for Prenatal Diagnosis. Prenat Diagn. 2015; 35:725-734.
25. Kazerouni NN, Currier B, Malm L, Riggle S, Hodgkinson C, Smith S, Tempelis C, Lorey F, Davis A, Jelliffe-Pawlowski L, Walton-Haynes L, Roberson M. Triple-marker prenatal screening program for chromosomal defects. Obstet Gynecol. 2009; 114:50-58.
26. Abou-Youssef HS, Kamal MM, Mehaney DA. Triple test screening for Down syndrome: An Egyptian-tailored study. PLoS One. 2014; 9:e110370.

(Received September 27, 2018; Revised December 17, 2018; Accepted December 29, 2018)

Original Article

DOI: 10.5582/bst.2018.01285

En bloc resection for intra-abdominal/retroperitoneal desmoid-type fibromatosis with adjacent organ involvement: A case series and literature review

Zhen Wang, Jianhui Wu, Ang Lv, Xiuyun Tian, Chunyi Hao*

Key Laboratory of Carcinogenesis and Translational Research (Ministry of Education, Beijing), Department of Hepato-Pancreato-Biliary Surgery, Peking University Cancer Hospital and Institute, Beijing, China.

Summary **Surgical treatment for intra-abdominal/retroperitoneal desmoid-type fibromatosis (IA/RPDF) is still controversial. Studies regarding en bloc resection in IA/RPDF with adjacent organ involvement are scanty. This study aims to evaluate the safety and effectiveness of en bloc resection in IA/RPDF with adjacent organ involvement. This retrospective clinical study included 21 patients who were diagnosed with IA/RPDF and underwent tumor resection at a single center between March 2013 and June 2018. All patients included in the study underwent surgery with curative intent, and IA/RPDF with adhesive organs was removed en bloc. The safety of surgical treatment was verified by the analysis of intraoperative bleeding, postoperative morbidity and perioperative mortality. The efficacy of surgical treatment was evaluated based on the status of tumor infiltration of adjacent organs and patient follow-up results. Complete macroscopic (R0 or R1) resection was achieved in all cases. A median of 2 (range, 1-7) organs were resected. The median operating time was 300 (90-650) minutes. The median intraoperative bleeding was 300 (20-4,500) milliliters. For postoperative pathological diagnosis at our center, tumor infiltrated at least one organ in each patient. Infiltration was noted in 45 resected organs (45/57, 78.9%). Grade III-V postoperative morbidity developed in one patient (4.8%). During the follow-up, one patient developed local recurrence. No DF-related death was noted during the follow-up. The 3-year disease-free survival rate was 94.1% (95% confidence interval: 83.6-100%). Therefore, en bloc resection of the tumor and involved adjacent organs is a safe and effective treatment modality for IA/RPDF.**

Keywords: Desmoid-type fibromatosis, retroperitoneum, surgery

1. Introduction

Desmoid-type fibromatosis (DF) is a rare monoclonal, fibroblastic proliferation characterized by locally infiltrative but rarely metastatic lesions (*1,2*). The local recurrence rate is high and varies between 15% and 77% (*3,4*). DF can occur in many locations, the most common being the extremities and abdominal wall. It can also occur in the abdominal cavity and retroperitoneum. Desmoid tumors have been reported to occur in 7.5% to 16% of patients with familial adenomatous polyposis (FAP) and the relative risk of developing desmoid tumors is much higher in patients with FAP than in the general population (*5,6*). FAP-related tumors more commonly arise in the intra-abdominal region (*7*).

The consensus for treatment of DF has changed over the past decade, with most centers moving away from primary radical surgery toward a front-line "watchful waiting" policy (*1,2,8-11*). However, most of the results of previous studies were based on the analysis of extra-abdominal DF (*1,2,8-11*). There are limited studies on intra-abdominal/retroperitoneal DF (IA/RPDF), and most previous studies were case reports. The effectiveness of surgical treatment for IA/RPDF remains controversial. Given the lower risk of complications and recurrence rates than extremity DF

**Address correspondence to:*
Dr. Chunyi Hao, Key Laboratory of Carcinogenesis and Translational Research (Ministry of Education, Beijing), Department of Hepato-Pancreato-Biliary Surgery, Peking University Cancer Hospital and Institute, #52 Fucheng Road, Haidian District, Beijing 100142, China.
E-mail: haochunyi@bjmu.edu.cn

following surgical resection, some investigators have suggested that there should be a low threshold for surgery in the treatment of intra-abdominal DF (*2,12*). However, other investigators have recommended that surgical treatment should be chosen with caution according to the changing consensus regarding extra-abdominal DF therapy (*1,13*).

Several studies show that margin status does not affect recurrence and has no prognostic significance in desmoid tumors (*14-16*). However, some large retrospective studies have reported higher recurrence rates for patients with positive margins when compared to negative margins (*15,17,18*). Considering that DF is characteristically locally infiltrative, *en bloc* resection in IA/RPDF with adjacent organ involvement may help reduce relapse and improve prognosis. Studies regarding *en bloc* resection in IA/RPDF with adjacent organ involvement are scanty.

Hence, to assess the safety and efficacy of *en bloc* resection in IA/RPDF with adjacent organ involvement, we conducted a retrospective case series analysis and literature review.

2. Materials and Methods

2.1. *Data source and patient selection*

A retrospective clinical study was conducted, with data retrieved on 21 consecutive patients with IA/RPDF who were treated at the Peking University Cancer Hospital Sarcoma Center between March 2013 and June 2018. All patients included in the study underwent surgery with curative intent, and IA/RPDF with adhesive organs were removed *en bloc*. The median follow-up period was 24 (range, 4-68) months. The ethics committee of Peking University Cancer Hospital and Institute approved the study.

2.2. *Pathological diagnosis*

All resected tumors were delivered to the Department of Pathology after the operation. Overall tumor size was defined as the sum of the perpendicular maximum diameters. All margins were perpendicularly sampled, with two or more sections taken from all margins. Additional sections were taken from the closest margin. Serial sampling of all resected organs and surrounding fat was performed. Two sarcoma pathologists independently diagnosed the tumor pathology.

2.3. *Definitions*

Different from the DF located in extremities and abdominal wall, it is difficult to achieve a reliable assessment of the margin status of IA/RPDF (*19*). Thus, surgical resection was described as macroscopically complete (R0 or R1) or incomplete (R2) (*19*). Postoperative complications were graded according to the Clavien-Dindo classification (*20*). Postoperative pancreatic fistulae (POPF) were defined according to the International Study Group on Pancreatic Fistula definition (*21*).

2.4. *Follow-up*

At our center, patients were prospectively followed up via clinical examination, chest radiography, and abdominopelvic computed tomography or magnetic resonance imaging every 3 months for the first year, every 6 months for the subsequent 4 years, and yearly thereafter.

2.5. *Statistical analysis*

Data extracted from the database, computerized hospital notes, and pathology records were analyzed. Data are presented as median and range or number and percentage, as appropriate. We analyzed the local disease-free survival (DFS) from the date of operation to the date of last follow-up. Statistical analyses were performed using SPSS version 24.0 (IBM Corp., Armonk, NY, USA) and R version 3.4.0 (*http://www.r-project.org*).

3. Results

3.1. *Patient characteristics*

Data from 21 patients, comprising 11 male (52.4%) and 10 female (47.6%), were retrospectively analyzed in our study. The median age was 35 (range, 21-73) years. DF was located in the abdominal cavities of 6 (28.6%) patients, and in the retroperitoneum of 15 (71.4%) patients. Seventeen (81.0%) patients received primary surgical treatment, while 4 patients underwent surgery after tumor recurrence. Meanwhile, DF in 3 patients (14.3%) was considered to be related to FAP due to a history of colon polyposis. All the patients achieved macroscopically complete resection (R0 and R1). The clinicopathologic characteristics of all the patients are displayed in Table 1.

3.2. *Details of surgery*

All patients included in the study underwent surgery with curative intent, and the surgical policy was to remove tumors with adhesive organs *en bloc* (Figure 1). Complete macroscopic (R0 or R1) resection was achieved in all cases. The median number of resected organs was 2 (range, 1-7). The median operating time was 300 (90-650) minutes. The median intraoperative bleeding was 300 (20-4,500) milliliters. The tumor of the patient with the largest amount of intraoperative bleeding was located in the pelvic cavity, and the

amount of bleeding in the presacral venous plexus was large. Except in this patient, the maximum volume of intraoperative blood lost was 1,000 milliliters. The details of operating time and intraoperative bleeding are displayed in Table 2.

The small intestine, including the duodenum, was the organ most commonly resected (14/21, 66.7%), followed by the colon (12/21, 57.1%). Of the 4 patients (4/21, 19.0%) who underwent nephrectomy, 1 had a tumor that invaded the kidney and 3 had a tumor that encapsulated the proximal ureter for a long length, making it difficult to reconstruct the ureters. Two patients (2/21, 9.5%) underwent distal pancreatectomy, and 1 patient (1/21, 4.8%) underwent partial resection of the uncinate process. Three patients (3/21, 14.3%) underwent resection of the iliac vessels and artificial vessels replacement because the vessels adhered to the resected tumor; among them, 1 patient underwent resection of the iliac artery and vein, while the remaining 2 patients underwent resection of the iliac vein alone. The details of resected organs are displayed in Table 2 and Table 3.

Table 1. Patient characteristics

Characteristics	*n* (%)
Age, (years; median [range])	35 (21–73)
Sex	
Male	11 (52.4)
Female	10 (47.6)
Presentation	
Primary	17 (81.0)
Recurrent	4 (19.0)
Tumor site	
Abdomen	6 (28.6)
Retroperitoneum	15 (71.4)
Number of tumors	
Single	17 (81.0)
Multiple	4 (19.0)
Tumor size	
≤ 10 cm	11 (52.4)
> 10 cm	10 (47.6)
FAP-related desmoid-type fibromatosis	
Yes	3 (14.3)
No	18 (85.7)
Number of organs resected [median (range)]	2 (1–7)
Resection margins	
Macroscopically complete	21(100.0)
Macroscopically incomplete	0 (0)

FAP, familial adenomatous polyposis.

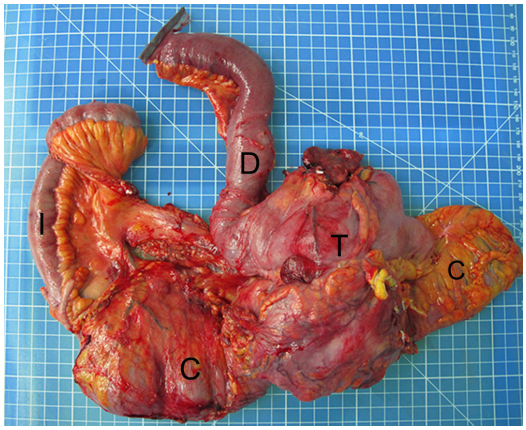

Figure 1. The resected specimen of *en bloc* resection of intra-abdominal/retroperitoneal desmoid-type fibromatosis and involved adjacent organs. The tumor and adjacent organs were resected *en bloc*. The tumor invaded the duodenum and colon. **T**, tumor; **C**, colon; **D**, duodenum; **I**, ileum.

Table 2. Details of resected organs, intraoperative bleeding, duration of operating time, infiltrated organs and postoperative morbidities of patients

Items	Resected organs	Intraoperative bleeding (mL)	Duration of operating time (minutes)	Infiltrated organs	Post-operative morbidities
Case 1	Colon, ovary, kidney, AG, ureter, IA, IV	1,000	650	IA, IV, ureter, colon	Gastroparesis
Case 2	SI	300	135	SI	
Case 3	Colon, ureter, SI	200	300	Colon, ureter, SI	Grade A POPF
Case 4	Colon, pancreas, spleen	500	300	Colon, pancreas	
Case 5	Pancreas, stomach, spleen	50	210	Pancreas, stomach, spleen	
Case 6	Colon, SI, ureter	100	190	SI, ureter	
Case 7	SI	800	180	SI	
Case 8	Colon, SI	1,000	210	Colon, SI	
Case 9	SI	100	90	SI	
Case 10	SI	50	480	SI	
Case 11	Colon, stomach	50	300	Stomach	Hemorrhage
Case 12	Pancreas, SI	50	480	Pancreas, SI	
Case 13	SI	900	180	SI	Gastroparesis
Case 14	Colon, SI	200	210	Colon, SI	Incomplete intestinal obstruction
Case 15	Colon, SI	50	150	Colon, SI	
Case 16	SI, ureter, kidney	800	210	SI, ureter	
Case 17	Kidney, AG, ureter, ovary, AW, colon, IV	20	600	Kidney, ovary, AW, colon	
Case 18	Colon, kidney, ureter	300	330	Colon, ureter	
Case 19	Colon, SI, AW	800	460	Colon, SI, AW	
Case 20	Rectus, uterus, ovary, ureter, IV	4,500	630	rectum, ureter, IV	
Case 21	Colon, SI	1,000	380	Colon, SI	

AG, adrenal gland; AW, abdominal wall; IA, iliac artery; IV, iliac vein; POPF, postoperative pancreatic fistula; SI, small intestine.

3.3. *Infiltration details*

All tumors were diagnosed as DF, and tumor infiltrated at least one organ in each patient. The median number of infiltrated organs was 2 (range, 1-5) in each patient. Infiltration was noted in 45 resected organs (45/57, 78.9%). The tumors commonly infiltrated the small intestine, and all the resected small intestines were infiltrated by DF while some of the DF lesions even infiltrated the submucosae of the small intestines (Figure 2A). DF infiltrated all the resected abdominal walls, stomachs, rectums, pancreata (Figure 2B), and iliac vessels (Figure 2C). Among 4 patients who underwent nephrectomy, only 1 (1/4, 25%) kidney infiltration by DF, and the remaining 3 had tumor infiltration of the ureters. The details of infiltration are displayed in Table 2 and Table 3.

3.4. *Postoperative morbidity and follow-up*

Grade II postoperative morbidity developed in 4 patients (19.0%); 2 of them experienced gastroparesis, 1 experienced incomplete intestinal obstruction, and 1 experienced grade A POPF. Grade III postoperative morbidity developed in 1 patient (4.8%). This patient experienced postoperative hemorrhage and required reoperation. No patient died of surgery.

During the follow-up, 1 patient developed local recurrence in the 15th month after surgery, and the tumor progressed despite non-steroidal anti-inflammatory drug treatment. Thus, the patient underwent secondary surgery, and no recurrence was noted during follow-up (20 months). The 3-year DFS rate was 94.1% (95% confidence interval: 83.6-100%). No DF-related death was noted during the follow-up. The patients' functional ability was scored according to the Barthel Index (*22*), with all patients scoring 100.

Table 3. Resection and infiltration details of intra-abdominal/retroperitoneal desmoid-type fibromatosis at our center

Items	Resected number	Infiltrated number (%)
Small intestine	14	14 (100)
Colon	12	10 (83.3)
Ureter	7	6 (85.7)
Vessel	4	4 (100)
Kidney	4	1 (25)
Pancreas	3	3 (100)
Ovary	3	1 (33.3)
Stomach	2	2 (100)
Abdominal wall	2	2 (100)
Spleen	2	1 (50)
Adrenal gland	2	0 (0)
Rectum	1	1 (100)
Uterus	1	0 (0)
Total	57	45 (78.9)

FAP, familial adenomatous polyposis.

4. Discussion

The consensus for treatment of DF has changed over the past decade, with most centers moving away from primary radical surgery toward a front-line "watchful waiting" policy (*1,2,8-11*). However, most of the results of previous studies were based on the analysis of extra-abdominal DF (*1,2,8-11*). There are limited studies on IA/RPDF, and most previous studies were case reports (Table 4) (*23-42*). A case series of IA/RPDF treated with *en bloc* resection of the tumor with adhesive organs is reported for the first time in this study. Complete macroscopic resection was achieved in all cases.

Although the "watchful waiting" policy was recommended as the first-line management for extra-abdominal DF, it is a controversial one for IA/RPDF (*2,12,43*). Several previous studies have reported tumor location as a risk factor for recurrence after surgery, and a lower rate of recurrence for intra-abdominal DF than for tumors located in the extremities (*1,18*). Lev *et al.* reported that the most common sites of local recurrence were the extremities (16/57 [28%]), superficial trunk (7/71 [10%]), and viscera (4/47 [9%]) (*18*). The response rate to medical therapy varies from 15-60% (*44-47*), and grade 3-4 toxicities occurred in approximately 13-43% of patients (*46,48-50*). Considering the uncertain effect of medical therapy and the occurrence of adverse effects, there is insufficient evidence that drug therapy is better than surgery in the treatment of IA/RPDF. Furthermore, for patients with symptoms, awaiting spontaneous regression or drug onset is intolerable. Therefore, there should be a low threshold for surgery in the treatment

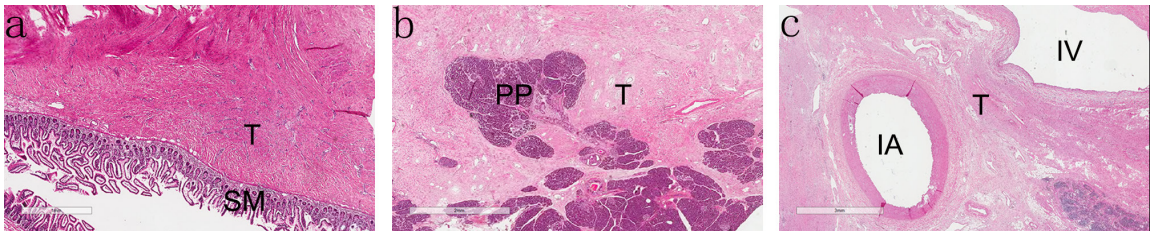

Figure 2. Intra-abdominal/retroperitoneal desmoid-type fibromatosis infiltrating the adjacent organs. (A) Desmoid-type fibromatosis infiltration of the submucosa of the small intestine. **(B)** Desmoid-type fibromatosis infiltration of the pancreatic parenchyma. **(C)** Desmoid-type fibromatosis infiltration of the iliac vessels. **T**, tumor; **SM**, submucosa of the small intestine; **PP**, pancreatic parenchyma; **IA**, iliac artery; **IV**, iliac vein.

Table 4. Summary of 23 cases of intra-abdominal/retroperitoneal desmoid-type fibromatosis published in the PubMed database between 2006 and 2017

Authors	Age	Sex	Site	Size (cm)	Resected organs	Complication	Recurrence	Follow up time (months)
Yong W. 2013 (24)	31	Male	Abdomen	10.0	None	No	No	/
Deepak V. 2010 (25)	46	Female	Abdomen	6.2	colon	No	No	3
Koichi T. 2006 (34)	73	Female	Abdomen	6.3	Small intestine	No	No	48
B. Kreuzberg 2007 (26)	48	Female	Abdomen	/	Small intestine, colon, uterus	No	No	/
B. Kreuzberg 2007 (26)	60	Female	Retroperitoneum	/	None	No	Yes	24
B. Kreuzberg 2007 (26)	43	Male	Retroperitoneum	/	None	No	No	/
Mohammad K. 2010 (33)	37	Male	Abdomen	6.0	None	No	No	8
Jae Young C. 2010 (36)	46	Female	Retroperitoneum	5.5	Colon, ureter	No	No	/
Christos N. 2010 (42)	65	Male	Abdomen	12.0	Small intestine	Bowel ischemia	No	/
Coskun P. 2010 (27)	57	Male	Abdomen	10.0	Small intestine, colon	No	No	/
Bouhabl S. 2011 (41)	71	Male	Abdomen	19.0	Small intestine	No	No	12
Sung Hoon J. 2009 (40)	49	Female	Abdomen	7.5	Colon, ovary, oviduct	No	No	/
Liang-Yu S. 2012 (39)	56	Male	Retroperitoneum	3.6	None	No	No	6
Mohammed K. 2012 (28)	47	Male	Abdominal	28.0	Small intestine	No	No	6
Marek W. 2010 (38)	44	Female	Abdominal	10.1	Small intestine	No	No	/
Cemli C. 2011 (37)	35	Female	Abdominal	6.0	Colon	No	No	/
Kinyanjui J. 2012 (32)	41	Male	Abdomen	/	Small intestine	No	No	/
LH Tan 2010 (35)	58	Female	Abdomen	4.5	Small intestine	No	No	6
Menegazzo M. 2013 (23)	35	Female	Abdomen	34.0	Small intestine	No	No	25
Norihito O. 2013 (30)	45	Male	Abdomen	9.0	Pancreas, spleen	No	No	27
Norihito O. 2013 (30)	74	Female	Abdomen	6.0	Small intestine	Bowel obstruction	No	7
Mari M. 2017 (31)	45	Female	Abdomen	5.5	Pancreas, spleen, stomach	No	No	/
Hirotoshi K. 2014 (29)	55	Male	Abdomen	1.2	Small intestine	No	No	/

of intra-abdominal DF, particularly for patients with symptoms that are difficult to endure (*8*).

For postoperative pathological diagnosis, DF infiltrated at least one organ in each patient. Infiltration was noted in 78.9% resected organs. Some of the IA/RPDF lesions even infiltrated the submucosa of the small intestine. All these results indicate that IA/RPDF has a high infiltration tendency, such that it frequently infiltrates organs. Although margin status remains a controversial topic in the management of desmoid tumors, it is often agreed that R0 resections are ideal (*13*). Considering the high infiltration tendency of IA/RPDF, to reduce the local recurrence, achieving negative surgical margins by *en bloc* resection of the tumor and adjacent organs is recommended.

In our present study, grade III-V postoperative morbidity occurred in 1 of the patients, and only 1 patient developed local recurrence during the follow-up. The 3-year DFS rate was 94.1%. No DF-related death was noted during the follow-up. Among the 23 patients previously reviewed, grade III-V postoperative morbidity occurred in only 1 of the patients, and no patient developed local recurrence and died during the follow-up (Table 4) (*23-42*). Based on the above results, *en bloc* resection in IA/RPDF with adjacent organ involvement is a safe and effective treatment modality. However, the varied anatomical locations of the DF within abdominal cavity and retroperitoneum result in local invasion to different adjacent organs, and there is no standard surgical approach or procedure for IA/RPDF treating. We have reported details of anterior approach to *en bloc* resection in left sided retroperitoneal sarcoma with adjacent organ involvement, which also can be applied in left sided retroperitoneal DF (*51*).

Most DF are sporadic, but the incidence of DF associated with FAP has been reported to be 7.5 to 16% (*5,6*). FAP-related tumors more commonly arise in the intra-abdominal region (*7*). FAP-related DF has a high recurrence rate after surgical resection (*12,52*). However, in our study, no recurrence occurred in the patient with FAP-related DF during follow-up, suggesting that *en bloc* resection in IA/RPDF with adjacent organ can effectively control the tumor. This was confirmed by a 10-year review of the management of FAP-associated DF (*53*). However, larger-scale, prospective observational studies with longer follow-up periods are needed to validate the most appropriate treatments for IA/RPDF and FAP-associated DF.

This study has certain limitations. Although it was a case series of IA/RPDF in patients who underwent *en bloc* resection of the tumor and adjacent organs, because of its low incidence, the sample size was relatively small, which might influence the accuracy of our results. Further multicenter and larger sample studies are needed to provide more reliable results.

In conclusion, according to the case series study and literature review, *en bloc* resection of the tumor and adjacent organ involvement is a safe and effective treatment modality for IA/RPDF.

Acknowledgements

We would like to thank all faculty members who assisted us in this study. This work was supported by

the Beijing Municipal Administration of Hospitals' Ascent Plan (approval No.: DFL20181104), Beijing Municipal Administration of Hospitals Clinical Medicine Development of Special Funding Support (approval No.: XMLX201708), the Capital Health Research and Development of Special Funds (approval No.: 2016-2-2151), and National Natural Science Funding (approval No.: 31770836).

References

1. Kasper B, Baumgarten C, Garcia J, Bonvalot S, Haas R, Haller F, Hohenberger P, Penel N, Messiou C, van der Graaf WT, Gronchi A, Desmoid Working G. An update on the management of sporadic desmoid-type fibromatosis: A European Consensus Initiative between Sarcoma PAtients EuroNet (SPAEN) and European Organization for Research and Treatment of Cancer (EORTC)/Soft Tissue and Bone Sarcoma Group (STBSG). Ann Oncol. 2017; 28:2399-2408.
2. Otero S, Moskovic EC, Strauss DC, Benson C, Miah AB, Thway K, Messiou C. Desmoid-type fibromatosis. Clinical radiology. 2015; 70:1038-1045.
3. Ballo MT, Zagars GK, Pollack A, Pisters PW, Pollack RA. Desmoid tumor: Prognostic factors and outcome after surgery, radiation therapy, or combined surgery and radiation therapy. J Clin Oncol. 1999; 17:158-167.
4. Sorensen A, Keller J, Nielsen OS, Jensen OM. Treatment of aggressive fibromatosis: A retrospective study of 72 patients followed for 1-27 years. Acta Orthop Scand. 2002; 73:213-219.
5. Fallen T, Wilson M, Morlan B, Lindor NM. Desmoid tumors – a characterization of patients seen at Mayo Clinic 1976-1999. Familial cancer. 2006; 5:191-194.
6. Nieuwenhuis MH, Casparie M, Mathus-Vliegen LM, Dekkers OM, Hogendoorn PC, Vasen HF. A nation-wide study comparing sporadic and familial adenomatous polyposis-related desmoid-type fibromatoses. Int J Cancer. 2011; 129:256-261.
7. Koskenvuo L, Ristimaki A, Lepisto A. Comparison of sporadic and FAP-associated desmoid-type fibromatoses. J Surg Oncol. 2017; 116:716-721.
8. Kasper B, Baumgarten C, Bonvalot S, Haas R, Haller F, Hohenberger P, Moreau G, van der Graaf WT, Gronchi A. Management of sporadic desmoid-type fibromatosis: A European consensus approach based on patients' and professionals' expertise - a sarcoma patients EuroNet and European Organisation for Research and Treatment of Cancer/Soft Tissue and Bone Sarcoma Group initiative. European journal of cancer (Oxford, England:1990). 2015; 51:127-136.
9. Bonvalot S, Eldweny H, Haddad V, Rimareix F, Missenard G, Oberlin O, Vanel D, Terrier P, Blay JY, Le Cesne A, Le Pechoux C. Extra-abdominal primary fibromatosis: Aggressive management could be avoided in a subgroup of patients. Eur J Surg Oncol. 2008; 34:462-468.
10. Fiore M, Rimareix F, Mariani L, Domont J, Collini P, Le Pechoux C, Casali PG, Le Cesne A, Gronchi A, Bonvalot S. Desmoid-type fibromatosis: A front-line conservative approach to select patients for surgical treatment. Ann Surg Oncol. 2009; 16:2587-2593.
11. Briand S, Barbier O, Biau D, Bertrand-Vasseur A, Larousserie F, Anract P, Gouin F. Wait-and-see policy as a first-line management for extra-abdominal desmoid tumors. The Journal of bone and joint surgery American volume. 2014; 96:631-638.
12. Wilkinson MJ, Fitzgerald JE, Thomas JM, Hayes AJ, Strauss DC. Surgical resection for non-familial adenomatous polyposis-related intra-abdominal fibromatosis. Br J Surg. 2012; 99:706-713.
13. Howard JH, Pollock RE. Intra-Abdominal and Abdominal Wall Desmoid Fibromatosis. Oncology and therapy. 2016; 4:57-72.
14. Crago AM, Denton B, Salas S, Dufresne A, Mezhir JJ, Hameed M, Gonen M, Singer S, Brennan MF. A prognostic nomogram for prediction of recurrence in desmoid fibromatosis. Ann Surg. 2013; 258:347-353.
15. Huang K, Wang CM, Chen JG, Du CY, Zhou Y, Shi YQ, Fu H. Prognostic factors influencing event-free survival and treatments in desmoid-type fibromatosis: Analysis from a large institution. Am J Surg. 2014; 207:847-854.
16. Mullen JT, Delaney TF, Kobayashi WK, Szymonifka J, Yeap BY, Chen YL, Rosenberg AE, Harmon DC, Choy E, Yoon SS, Raskin KA, Petur Nielsen G, Hornicek FJ. Desmoid tumor: Analysis of prognostic factors and outcomes in a surgical series. Ann Surg Oncol. 2012; 19:4028-4035.
17. Peng PD, Hyder O, Mavros MN, Turley R, Groeschl R, Firoozmand A, Lidsky M, Herman JM, Choti M, Ahuja N, Anders R, Blazer DG, 3rd, Gamblin TC, Pawlik TM. Management and recurrence patterns of desmoids tumors: A multi-institutional analysis of 211 patients. Ann Surg Oncol. 2012; 19:4036-4042.
18. Lev D, Kotilingam D, Wei C, Ballo MT, Zagars GK, Pisters PW, Lazar AA, Patel SR, Benjamin RS, Pollock RE. Optimizing treatment of desmoid tumors. J Clin Oncol. 2007; 25:1785-1791.
19. Anaya DA, Lev DC, Pollock RE. The role of surgical margin status in retroperitoneal sarcoma. J Surg Oncol. 2008; 98:607-610.
20. Dindo D, Demartines N, Clavien PA. Classification of surgical complications: A new proposal with evaluation in a cohort of 6336 patients and results of a survey. Ann Surg. 2004; 240:205-213.
21. Bassi C, Marchegiani G, Dervenis C, *et al*. The 2016 update of the International Study Group (ISGPS) definition and grading of postoperative pancreatic fistula: 11 years after. Surgery. 2017; 161:584-591.
22. Mahoney FI, Barthel DW. Functional Evaluation: The Barthel Index. Md State Med J. 1965; 14:61-65.
23. Menegazzo M, Tonello M, Bardini R. A 13 kg intra-abdominal mass: A case of mesenteric fibromatosis. Updates Surg. 2013; 65:237-240.
24. Wang Y, Cui NY, Li L, Zhang R, Hao YZ, Xue LY, Zhou CW, Jiang YX. An abdominal desmoid-type fibromatosis. Quantitative imaging in medicine and surgery. 2013; 3:228-230.
25. Venkat D, Levine E, Wise WE. Abdominal pain and colonic obstruction from an intra-abdominal desmoid tumor. Gastroenterology & hepatology. 2010; 6:662-665.
26. Kreuzberg B, Koudelova J, Ferda J, Treska V, Spidlen V, Mukensnabl P. Diagnostic problems of abdominal desmoid tumors in various locations. European journal of radiology. 2007; 62:180-185.
27. Polat C, Aktepe F, Turel S, Yazicioglu B, Ozkececi T, Arikan Y. A giant mesenteric fibromatosis case presenting with mechanical intestinal obstruction and

successfully resected with partial duodeno-jejunectomy and right hemicolectomy. Clinics (Sao Paulo). 2010; 65:110-113.
28. Gari MK, Guraya SY, Hussein AM, Hego MM. Giant mesenteric fibromatosis: Report of a case and review of the literature. World J Gastrointest Surg. 2012; 4:79-82.
29. Kobayashi H, Sugihara K. Intra-abdominal desmoid tumor after resection for gastrointestinal stromal tumor of the small intestine: Case report. Japanese journal of clinical oncology. 2014; 44:982-985.
30. Ogawa N, Iseki H, Tsunozaki H, Hayashi M, Baba H, Matsuyama T, Uetake H, Sugihara K. Intra-abdominal desmoid tumor difficult to distinguish from a gastrointestinal stromal tumor: Report of two cases. Surgery today. 2014; 44:2174-2179.
31. Mizuno M, Kawaguchi Y, Kawanishi A, Kawashima Y, Maruno A, Ogawa M, Tomioku M, Furukawa D, Nabeshima K, Nakamura K, Hirabayashi K, Mine T. An Intra-Abdominal Desmoid Tumor, Embedded in the Pancreas, Preoperatively Diagnosed as an Extragastric Growing Gastrointestinal Stromal Tumor. Case reports in oncology. 2017; 10:301-307.
32. Kinyanjui J, Butler N, Lambrianides A. Large Intra-abdominal desmoid tumour: Complete resection with preservation of function. J Surg Case Rep. 2012; 2012:8.
33. Khan M, Bozas G, Cooke J, Wedgwood K, Maraveyas A. Mesenteric desmoid tumor developing on the site of an excised gastrointestinal stromal tumor. Rare Tumors. 2010; 2:e33.
34. Tamura K, Tani M, Kinoshita H, Yamaue H. Mesenteric desmoid tumor of the interposed jejunal pouch after total gastrectomy. World J Surg Oncol. 2006; 4:27.
35. Tan CH, Pua U, Liau KH, Lee HY. Mesenteric desmoid tumour masquerading as a fat-containing cystic mass. Br J Radiol. 2010; 83:e200-203.
36. Choi JY, Kang KM, Kim BS, Kim TH. Mesenteric fibromatosis causing ureteral stenosis. Korean J Urol. 2010; 51:501-504.
37. Caliskan C, Korkut MA. Mesenteric fibromatosis of the ileocolic area: A case report. Indian J Surg. 2011; 73:149-151.
38. Wronski M, Ziarkiewicz-Wroblewska B, Slodkowski M, Cebulski W, Gornicka B, Krasnodebski IW. Mesenteric fibromatosis with intestinal involvement mimicking a gastrointestinal stromal tumour. Radiol Oncol. 2011; 45:59-63.
39. Shih LY, Wei CK, Lin CW, Tseng CE. Postoperative retroperitoneal desmoid tumor mimics recurrent gastrointestinal stromal tumor: A case report. World journal of gastroenterology. 2012; 18:6172-6176.
40. Jung SH, Paik CN, Jung JH, Lee KM, Chung WC, Yang JM. Simultaneous Colonic Obstruction and Hydroureteronephrosis due to Mesenteric Fibromatosis. Gut Liver. 2009; 3:215-217.
41. Bouhabel S, Leblanc G, Ferreira J, Leclerc YE, Dube P, Sideris L. Solitary fibrous tumor arising in the mesentery: A case report. World J Surg Oncol. 2011; 9:140.
42. Stoidis CN, Spyropoulos BG, Misiakos EP, Fountzilas CK, Paraskeva PP, Fotiadis CI. Surgical treatment of giant mesenteric fibromatosis presenting as a gastrointestinal stromal tumor: A case report. J Med Case Rep. 2010; 4:314.
43. Burtenshaw SM, Cannell AJ, McAlister ED, Siddique S, Kandel R, Blackstein ME, Swallow CJ, Gladdy RA. Toward Observation as First-line Management in Abdominal Desmoid Tumors. Ann Surg Oncol. 2016; 23:2212-2219.
44. Desurmont T, Lefevre JH, Shields C, Colas C, Tiret E, Parc Y. Desmoid tumour in familial adenomatous polyposis patients: Responses to treatments. Familial cancer. 2015; 14:31-39.
45. Hansmann A, Adolph C, Vogel T, Unger A, Moeslein G. High-dose tamoxifen and sulindac as first-line treatment for desmoid tumors. Cancer. 2004; 100:612-620.
46. de Camargo VP, Keohan ML, D'Adamo DR, Antonescu CR, Brennan MF, Singer S, Ahn LS, Maki RG. Clinical outcomes of systemic therapy for patients with deep fibromatosis (desmoid tumor). Cancer. 2010; 116:2258-2265.
47. Garbay D, Le Cesne A, Penel N, Chevreau C, Marec-Berard P, Blay JY, Debled M, Isambert N, Thyss A, Bompas E, Collard O, Salas S, Coindre JM, Bui B, Italiano A. Chemotherapy in patients with desmoid tumors: A study from the French Sarcoma Group (FSG). Ann Oncol. 2012; 23:182-186.
48. Gega M, Yanagi H, Yoshikawa R, Noda M, Ikeuchi H, Tsukamoto K, Oshima T, Fujiwara Y, Gondo N, Tamura K, Utsunomiya J, Hashimoto-Tamaoki T, Yamamura T. Successful chemotherapeutic modality of doxorubicin plus dacarbazine for the treatment of desmoid tumors in association with familial adenomatous polyposis. J Clin Oncol. 2006; 24:102-105.
49. Weiss AJ, Horowitz S, Lackman RD. Therapy of desmoid tumors and fibromatosis using vinorelbine. Am J Clin Oncol. 1999; 22:193-195.
50. Azzarelli A, Gronchi A, Bertulli R, Tesoro JD, Baratti D, Pennacchioli E, Dileo P, Rasponi A, Ferrari A, Pilotti S, Casali PG. Low-dose chemotherapy with methotrexate and vinblastine for patients with advanced aggressive fibromatosis. Cancer. 2001; 92:1259-1264.
51. Wang Z, Wu JH, Lv A, Li CP, Tian XY, Hao CY. Anterior Approach to En Bloc Resection in Left-Sided Retroperitoneal Sarcoma with Adjacent Organ Involvement: A Study of 25 Patients in a Single Center. Med Sci Monit. 2018; 24:961-969.
52. Clark SK, Neale KF, Landgrebe JC, Phillips RK. Desmoid tumours complicating familial adenomatous polyposis. Br J Surg. 1999; 86:1185-1189.
53. Latchford AR, Sturt NJ, Neale K, Rogers PA, Phillips RK. A 10-year review of surgery for desmoid disease associated with familial adenomatous polyposis. Br J Surg. 2006; 93:1258-1264.

(Received November 27, 2018; Revised December 27, 2018; Accepted December 29, 2018)

Brief Report

DOI: 10.5582/bst.2018.01267

A freeze-and-thaw method to reuse agarose gels for DNA electrophoresis

Noboru Sasagawa

Department of Applied Biochemistry, School of Engineering, Tokai University, Hiratsuka, Kanagawa, Japan.

Summary **A novel protocol to reuse agarose following agarose gel electrophoresis was established in this study. By repeated freeze-and-thaw of the agarose gel, ethidium bromide and other buffer components in the gel were safely removed from the gel without generation of any toxic fume. The agarose recovered using this method can be used for further electrophoretic experiments without any issues.**

Keywords: Agarose, agarose gel electrophoresis, ethidium bromide

1. Introduction

It is widely known that agarose gels for electrophoresis are reusable. Used gels can be boiled and melted again, and poured into a template gel tray, as is done for new agarose gels. However, agarose gels are commonly stained with ethidium bromide (EtBr; 3,8-diamino-5-ethyl-6-phenylphenanthridinium bromide, $C_{21}H_{20}BrN_3$). EtBr is a toxic substance that forms fumes and vapor during the boiling and melting steps; this can lead to inhalation of EtBr molecules. Therefore, boiling and melting EtBr-stained agarose gels is not recommended.

Dialysis of used agarose gel can help remove EtBr, but it is not suitable on a day to day basis since 100 L of distilled water is needed for diluting the EtBr in 100 mL of agarose to a final dilution of 10^{-3}. A method consisting of repeated gel washing/dialyzing for reusing agarose gels has been reported (*1,2*). This method reduces the amount of water, but its execution is difficult owing to the fragility of agarose gels, which causes them to break easily. Here, I report a safe, easy, and suitable method for effectively removing EtBr from used agarose gels.

2. Materials and Methods

Standard agarose was purchased from different providers (*e.g.*, STAR Agarose RSV-AGRP from Rikaken, Aichi, Japan). Agarose gels contained agarose 1% (w/v) dissolved in Tris-acetate-ethylenediaminetetraacetic acid buffer (TAE buffer; 40 mM Tris, 40 mM acetic acid, and 1 mM EDTA). Agarose gel electrophoresis was performed at 100 V for 45 min by standard protocol (*3*) using TAITEC PICO-1 (Saitama, Japan). After electrophoresis, the agarose gels were stained with EtBr by incubating them in TAE buffer containing EtBr (0.1 ng/mL final concentration) for 30-60 min. Finally, the gels were photographed.

3. Results and Discussion

The protocol for reusing agarose gels proposed in this paper is summarized in Figure 1. Stained gels were collected in clean paper cartons or plastic bags. When a carton or bag was filled with gels, it was left in a –20°C freezer overnight. Using paper cartons or plastic bags is essential because the glass or plastic bottles crack during freezing. The next day, the containers were settled upside-down on a kitchen mesh or colander on top of a bucket and incubated at room temperature until completely thawed. The resulting solution seeped through the gels, which contains EtBr, can be collected and decontaminated following standard protocols (*4,5*).

Generally, buffers and solutions freeze disproportionally because of freezing-point depression. In a buffer, pure water freezes faster and the concentrated buffer freezes later. In the thaw step, the concentrated buffer elutes first and the pure water elutes later. The "Freeze-out" or "Freeze-concentrate" technique based on this principle has been widely used to concentrate molecules from diluted buffers and solutions (*6*). The

**Address correspondence to:*
Dr. Noboru Sasagawa, Department of Applied Biochemistry, School of Engineering, Tokai University, Hiratsuka, Kanagawa 259-1292, Japan.
E-mail: noboru.sasagawa@tokai.ac.jp

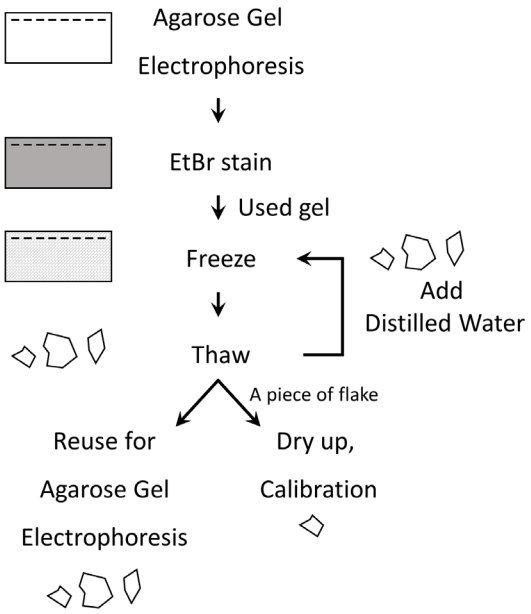

Figure 1. Scheme of the freeze-and-thaw method proposed in this manuscript.

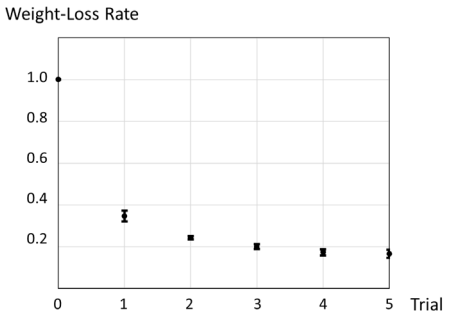

Figure 2. Weight loss of the agarose by freeze-and-thaw. Repeated freeze-and-thaw of agarose gel reduces gel weight but does not completely remove contaminant solutions (n = 3). The thawed agarose gels were placed back in the –20°C freezer without any additional water.

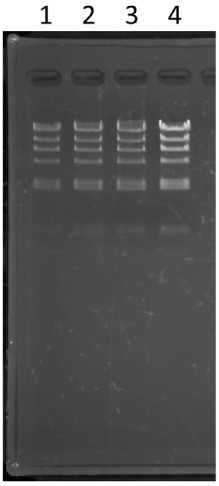

Figure 3. Agarose gel electrophoresis using recycled agarose (1%). Lambda DNA/*Hin* dIII digest was applied for the electrophoresis. DNA at volumes 125, 250, 375, and 500 μg was applied to lanes 1, 2, 3, and 4, respectively.

TAE buffer in the agarose gel freezes in the same way as in the freeze-concentrate technique. This property contributes to the effective removal of EtBr and agarose purification. Another attractive feature is that agarose gel changes its structure to flakes. The freezing step causes ice crystals to form in the agarose gel, destroying its mesh structure resulting in wet flakes of agarose. This "cake-to-flake" conversion causes the agarose gel to reduce its volume. The smaller the volume, the less water is needed for dilution of unnecessary content.

It is well known that DNA is separated from agarose gel by the freeze-squeeze method (*7*). Therefore, the freeze-and-thaw step and "cake-to-flake" conversion are also useful for removing nucleic acids from the agarose gel.

Figure 2 shows the effectivity of the freeze-and-thaw steps to remove solutions from the agarose gels. In this experiment, the thawed agarose gels were subjected to five freeze-and-thaw cycles without adding additional water. In the initial freeze-and-thaw step, a large amount of solution (including water, EtBr, and other molecules) was eluted.

However, repeated freeze-and-thaw steps did not seem to result in complete removal of water. Therefore, adding distilled water to the thawed gel before re-freezing it is the more effective way of removing the buffer and other contaminants. The ratio of the wet weight of the agarose gel before- and after- the initial freeze-and-thaw is 0.35 (s.d. = 0.03), indicating that the freeze-and-thaw step is more effective for removing electrophoresis buffer than simple dialysis. It also means that 5 cycles of freeze-and-thaw result in and EtBr dilution of 10^{-3} when 100 mL of distilled water is added to 100 mL of agarose gel before each re-freezing step. In conclusion, a total of 500 mL of distilled water is needed to reuse 100 mL of agarose gel (200 times more water is necessary to achieve the same level of purification by dialysis). Moreover, no fume or vapor is generated in this method.

Gel flakes are kept in the refrigerator as dumplings. A piece of flake from the dumpling is weighed (wet weight). Then, it is completely dried by simply leaving in the air and weighed again (dry gel weight). This dry-up calibration reveals the agarose concentration in the wet gel flake which enables to calculate the adequate agarose gel concentration for electrophoresis. In my experience, the wet gel flakes contain 3-7% agarose. Based on this calibration step, the residual gel dumpling is boiled, melted, and poured into a bottle in the appropriate concentrations and buffers and then cooled until hard. This melting step is also a good chance for filtrating dust from the agarose. The reused agarose gels can be used for gel electrophoresis, as previously described (*3*), without any difficulties (Figure 3).

In conclusion, I propose a novel protocol for reusing

agarose after agarose gel electrophoresis. This method is simple, free from EtBr toxicity, and very easy to execute. Furthermore, no special equipment is needed to use this method. Although five days are needed to complete the protocol, only a simple freeze-and-thaw process is needed at each step; thus, only 5-10 min are needed for completing each step.

Acknowledgements

I would like to thank Editage (www.editage.jp) for English language editing.

References

1. Palacios G, Giménez C, García ED. Recycling agarose. Plant Mol Biol Rep. 2000; 18:47-49.
2. Seng TY, Singh R, Faridah QZ, Tan SG, Alwee SS. Recycling of superfine resolution agarose gel. Genet Mol Res. 2013; 12:2360-2367.
3. Sambrook J, Fritsch EF, Maniatis T. Molecular Cloning: A Laboratory Manual, 2nd ed.; Cold Spring Harbor Laboratory Press, NY, US, 1989.
4. Lunn G, Sansone EB. Ethidium bromide: Destruction and decontamination of solutions. Anal Biochem. 1987; 162:453-458.
5. Quillardet P, Hofnung M. Ethidium bromide and safety – Readers suggest alternative solutions. Trends Genet. 1988; 4:89-90.
6. Wilson TE, Evans DJ, Theriot ML. Freezing-out technique applied to the concentration of biologically active materials. Appl Microbiol. 1964; 12:96-99.
7. Tautz D, Renz M. An optimized freeze-squeeze method for the recovery of DNA fragments from agarose gels. Anal Biochem. 1983; 132:14-19.

(Received November 3, 2018; Revised December 27, 2018; Accepted December 29, 2018)

Brief Report

DOI: 10.5582/bst.2018.01218

Purification, crystallization and preliminary X-ray crystallographic studies on the C-terminal domain of the flagellar protein FliL from *Helicobacter pylori*

Kar Lok Chan[1], Mayra A. Machuca[1], Mohammad Mizanur Rahman[1], Mohammad Firoz Khan[1], Daniel Andrews[1], Anna Roujeinikova[1,2,*]

[1] *Infection and Immunity Program, Monash Biomedicine Discovery Institute, Department of Microbiology, Monash University, Clayton, Victoria, Australia;*
[2] *Department of Biochemistry and Molecular Biology, Monash University, Clayton, Victoria, Australia.*

Summary **FliL is an inner membrane protein, occupying a position between the rotor and the stator of the bacterial flagellar motor. Its proximity to, and interactions with, the MS (membrane and supramembranous) ring, the switch complex and the stator proteins MotA/B suggests a role in recruitment and/or stabilization of the stator around the rotor, although the precise role of FliL in the flagellum remains to be established. In this study, recombinant C-terminal domain of *Helicobacter pylori* FliL (amino-acid residues 81-183) has been expressed in *Escherichia coli* and purified to > 98% homogeneity. Purified recombinant protein behaved as a monomer in solution. Crystals were obtained by the hanging-drop vapour-diffusion method using ammonium phosphate monobasic as a precipitant. These crystals belong to space group *P*1, with unit-cell parameters *a* = 62.5, *b* = 82.6, *c* = 97.8 Å, *α* = 67.7, *β* = 83.4, *γ* = 72.8°. A complete data set has been collected to 2.8 Å resolution using synchrotron radiation. This is an important step towards elucidation of the function of FliL in the bacterial flagellar motor.**

Keywords: Flagellar motor, Helicobacter pylori, protein crystallization, X-ray crystallography

1. Introduction

Helicobacter pylori infection of the human stomach is associated with chronic gastritis and gastric ulcers and has a strong correlation with gastric cancer (*1-4*). Motility by means of a tuft of sheathed, unipolar flagella is an essential colonization factor (*5,6*). The flagellum has two major components, the cell wall-embedded basal body, that spans both inner and outer membrane, and the extracellular filament composed of flagellins (*7*). The basal body consists of the cytoplasmic C-ring, the MS (membrane and supramembranous) ring, the rod, the export apparatus and the stator. The basal body serves as a rotary motor that spins the filament, with the energy for rotation derived from the proton-motive force (*8*). Rotation is driven by the interaction of the C-ring with several circumferentially positioned stator complexes, composed of the cytoplasmic protein MotA and peptidoglycan-anchored MotB (*7,9,10*).

Whilst it is well understood that MotA/MotB complex functions as a proton channel that does bind efficiently to the cell wall and is 'plugged' until it incorporates into the motor (*11-14*), little is known about the mechanism by which the stator assembles around the rotor and switches into a proton-conducting state. Previous studies of the flagellar motor in *Salmonella* and *E. coli* suggested that conserved protein FliL, which contains a single transmembrane helix and an approximately 150 a.a. long periplasmic domain, plays an important role in the stator assembly, as it has been shown to interact with the stator proteins MotA and MotB, as well as the rotor components FliF (MS ring) and FliG (C ring) (*15*). Deletion of *Salmonella fliL* caused only a small reduction in swimming, but eliminated swarming (*16*). It is thought that FliL is required for *Salmonella* swarming, when the motor

**Address correspondence to:*
Dr. Anna Roujeinikova, Infection and Immunity Program, Monash Biomedicine Discovery Institute Department of Microbiology, Department of Biochemistry and Molecular Biology, Monash University, Clayton, Victoria, Australia.
E-mail: anna.roujeinikova@monash.edu

must produce sufficient torque to move through viscous mediums (high load), because it enhances the interaction between MotA and MotB, increases the time that the stator is engaged with the rotor and/or improves the efficiency of proton flow through the motor (*15*). In addition, it has been suggested that FliL may assist the release of the MotB plug helices from the membrane and thus activate the stator complexes upon their assembly into the motor, as point mutations within the plug suppressed the motility defect of the *Salmonella* Δ*fliL* mutant (*15*).

The deletion of the *fliL* gene in *Rhodobacter sphaeroides* impaired its motility (*17*). It has been proposed that in *R. sphaeroides*, FliL, together with MotF, promotes the opening of the proton channel through FlgT, which interacts with MotB and triggers the release of the plug (*18-20*). Similarly, a *fliL* mutant of *Caulobacter crescentus* had non-functional flagella, indicating the essential role of FliL in flagellar rotation (*21*). FliL defect in *Proteus mirabilis* resulted in the impairment of motility and the synthesis of flagellin proteins, and it has been suggested that *P. mirabilis* FliL may also serve as a surface sensor that regulates the gene expression (*22-24*).

In *Borrelia burgdorferi*, the deletion of FliL altered the periplasmic flagellar orientation and caused motility impairment (*25*). Crucially, cryo-electron tomography of the *B. burgdorferi* flagellar motor revealed that FliL is located between the rotor and the stator (*25*), a position consistent with the hypothetical role of FliL in the assembly and/or stabilization of the stator around the rotor. Similarly, in the recent cryo-electron tomography study of the *H. pylori* flagellar motor, the putative FliL ring is clearly seen between the MS ring and the stator, although the role of FliL in the motor function in *H. pylori* remains to be established (*26*).

FliL shares no significant sequence similarity to any protein of a known structure. However, it is anticipated that determination of the crystal structure of its soluble periplasmic domain will provide a critical insight into its function through identification of functional homologues with a similar fold, as protein structure is more conserved than sequence. The production of the crystals of the periplasmic domain of FliL from *Vibrio alginolyticus* was reported (*27*), but no structure is available yet. Here, we report the cloning, purification, crystallization and the preliminary X-ray crystallographic analysis of the C-terminal periplasmic domain of *H. pylori* FliL.

2. Materials and Methods

2.1. *Gene cloning and overexpression*

The membrane topology and disordered regions of FliL from *H. pylori* strain SS1 (Genbank ID AQM65563.1) were predicted by using the TOPCONS (*http://topcons.net/*) (*28*) and DISOPRED3 (*http://bioinf.cs.ucl.ac.uk/disopred*) (*29*) servers, respectively (Figure 1). The coding sequence for the C-terminal domain of FliL (FliL-C, comprising amino-acid residues 81-183) was codon optimized for expression in *Escherichia coli*, synthesized and ligated into the pET151/D-TOPO vector (Invitrogen, Waltham, MA, USA) by GenScript (Piscataway, NJ, USA) to produce an expression vector that harbors an N-terminal His_6 tag followed by a tobacco etch virus (TEV) protease cleavage site. The 109-residue recombinant protein used for crystallization comprised residues 81-183 of FliL plus six additional residues from the TEV cleavage site (GIDPFT).

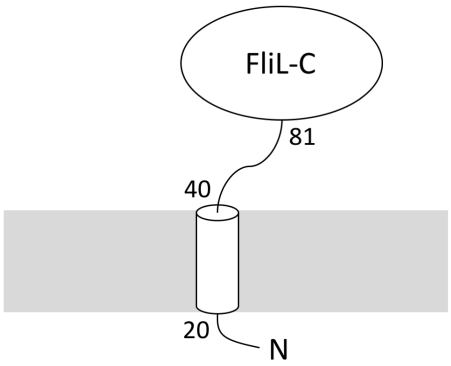

Figure 1. The predicted membrane topology of *H. pylori* FliL and the boundaries of the periplasmic domain CtaB FliL-C characterized in this study.

Escherichia coli strain BL21(DE3)-RIPL cells (Stratagene, La Jolla, CA, USA) were transformed with the expression vector and cultured at 37°C in LB medium containing 50 mg/L ampicillin. Overexpression of FliL-C was induced with 1 mM isopropyl-D-1-thiogalactopyranoside at an OD_{600} of 0.6. The cells were grown for a further 4 h at 37°C and then harvested by centrifugation at 4,800 g for 15 min at 4°C.

2.2. *Purification and determination of the oligomeric state*

Protein was purified by following the procedure based on that described in (*30*). Briefly, the cell pellet was resuspended in buffer A (20 mM Tris-HCl pH 8.0, 150 mM NaCl, 1 mM phenylmethanesulfonyl fluoride) and lyzed using an Avestin EmulsiFlex-C5 high-pressure homogenizer (Avestin, Ottawa, Canada). Cell debris was removed by centrifugation at 10,000 g for 20 min (4°C). NaCl and imidazole were then added to the supernatant to final concentrations of 500 and 10 mM, respectively, after which the supernatant was loaded onto a 5 mL Ni-NTA affinity column (GE Healthcare, Chicago, IL, USA) pre-equilibrated in buffer B (20 mM Tris-HCl pH 8.0, 500 mM NaCl, 20 mM imidazole), washed with 10 column volumes of the same buffer and eluted with buffer C (20 mM Tris-HCl pH 8.0, 500 mM NaCl, 500 mM imidazole). The hexahistidine tag was cleaved off using TEV protease (Invitrogen, Waltham, MA, USA) while dialyzing the sample against buffer

D [20 mM Tris-HCl pH 8.0, 150 mM NaCl, 2 mM dithiothreitol, 1% (v/v) glycerol] at 10°C overnight. NaCl and imidazole were then added to the sample to final concentrations of 500 and 20 mM, respectively, and the TEV protease and the uncleaved protein were removed by passing the sample through the Ni-NTA column. The flowthrough was concentrated to 2 mL in a VivaSpin 10,000 Da cutoff concentrator and passed through a Superdex 200 HiLoad 26/60 gel-filtration column (GE Healthcare) equilibrated with buffer E (10 mM Tris-HCl pH 8.0, 150 mM NaCl). Protein concentration was determined using the Bradford assay (*31*), and protein purity was evaluated using SDS-PAGE. The oligomeric state of FliL-C in solution was determined by calculating the molecular weight (MW) using a calibration plot of log MW versus the retention volume [$V_{retention}$ (mL) = 549.3 – 73.9 × log MW] (*32*).

2.3. *Protein buffer optimization*

Thermal shift analysis of protein stability in different buffers was performed using a Rotor-Gene Q Real-time PCR instrument (QIAGEN, Hilden, Germany). FliL-C was concentrated to 1.0 mM in buffer E and then diluted 100 fold with a series of test buffers containing 10×SYPRO Orange reagent (purchased from Sigma-Aldrich, St. Louis, MO, USA as 5000× stock, catalogue number S5692) in a final volume of 25 µL. The samples were thermally denatured by heating them from 35°C to 90°C at a ramp rate of 0.5°C/min. Protein denaturation was monitored by following SYPRO Orange fluorescence emission (λ_{ex} 530 nm/λ_{em} 555 nm). The denaturation data were fit to a derivation of the Boltzmann equation for the two-state unfolding model to obtain the midpoint of denaturation (the melting temperature T_m) (*33*). All experiments were performed in triplicates.

2.4. *Crystallization*

FliL-C was concentrated to 8 mg/ml and centrifuged for 20 min at 13,000 g to clarify the solution. The crystallization screening was carried out by the hanging-drop vapour-diffusion method using an automated Phoenix crystallization robot (Art Robbins Instruments, Sunnyvale, CA, USA) and commercial screens JBS Classic HTS1, JBS Classic HTS2, JBS JCSG++ (Jena Bioscience, Jena, Germany), Crystal Screen HT, and PEG/Ion HT (Hampton Research, Laguna Niguel, CA). The crystallization droplets comprised 100 nL protein solution mixed with 100 nL reservoir solution, and were equilibrated against 50 µL reservoir solution in a 96-well Art Robbins CrystalMation Intelli-Plate (Hampton Research). Clusters of needle-like crystals appeared after one day in condition G5 of the JBS Classic HTS2 screen, which contained 0.5 M ammonium di-hydrogen phosphate and 0.2 M trisodium citrate, and in condition A11, which contained 1.0 M ammonium phosphate monobasic and 0.1 M trisodium citrate dehydrate pH 5.6. Optimization of the condition to improve the crystal quality yielded thin plate-like crystals using 0.4 M ammonium phosphate monobasic and 0.1 M trisodium citrate dehydrate pH 5.6 and a protein concentration of 12 mg/mL. These crystals had maximum dimensions of 0.1 × 0.03 × 0.02 mm.

2.5. *Data collection and processing*

Prior to data collection, the FliL-C crystals were briefly soaked in a cryoprotectant solution (0.48 M ammonium phosphate monobasic, 0.12 M trisodium citrate dehydrate pH 5.6, 20% (v/v) glycerol), and then flash-frozen by plunging in liquid nitrogen. A complete X-ray diffraction data set was collected to 2.8 Å from a single cryo-cooled crystal on the MX1 beamline of the Australian Synchrotron. A total of 360 images were collected using a 0.5° oscillation. The data were processed and scaled using XDS (*34*) and *AIMLESS* from the Collaborative Computational Project, Number 4 (*CCP4*) suite (*35*). Data collection and processing statistics are summarized in Table 1. Calculation of the self- rotation function was performed using the *POLARRFN* program (*35*).

3. Results and Discussion

H. pylori FliL (183 a.a.) was predicted to contain one N-terminal transmembrane (TM) helix (amino-acid residues 20-40), with the protein's amino-terminus in the cytoplasm, followed by a disordered linker region (residues 41-85) connecting the TM helix to the periplasmic domain (Figure 1). For the purpose of protein production for crystallization, the domain boundaries of the recombinant periplasmic domain FliL-C have

Table 1. Data collection and processing. Values in parentheses correspond to the highest resolution shell

Diffraction source	MX1 beamline, Australian Synchrotron
Wavelength (Å)	0.95
Temperature (K)	100
Detector	ADSC Quantum 210r CCD
Rotation per image (º)	0.5
Total rotation range (º)	180
Space group	*P*1
a, b, c (Å)	62.5, 82.6, 97.8
α, β, γ (º)	67.7, 83.4, 72.8
Mosaicity (º)	0.6
Resolution range (Å)	54.16-2.80 (2.91-2.80)
Total No. of reflections	81,483 (9,191)
No. of unique reflections	41,760 (4,676)
Completeness (%)	98.1 (97.6)
Multiplicity	2.0
$\langle I/\sigma(I)\rangle$	5.2 (1.6)
$CC_{1/2}$ (%)	98.5 (71.3)
R_{merge}	0.103 (0.323)
Overall *B* factor from Wilson plot (Å^2)	30.7

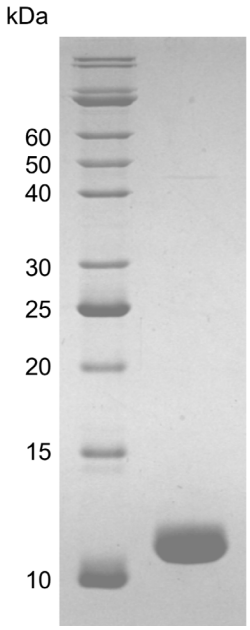

Figure 2. Coomassie Blue-stained 16.5% SDS–PAGE gel of recombinant FliL-C.

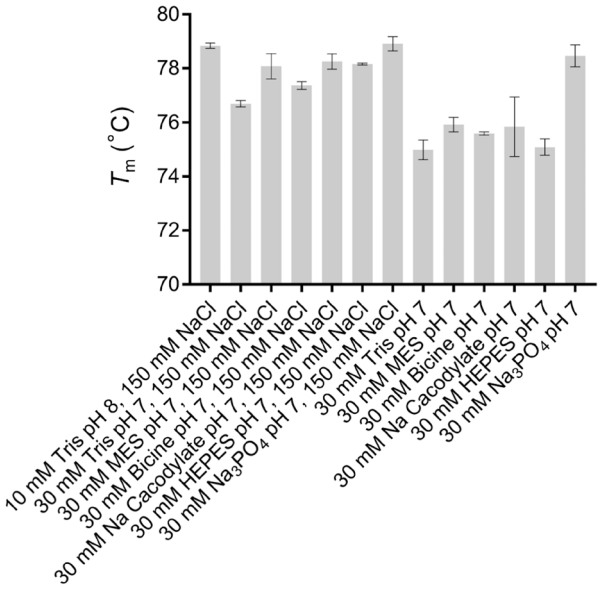

Figure 3. Comparison of the melting temperature T_m of the 10 μM solution of FliL-C in different buffers. Results are means ± S.D. for three independent replicates.

been set at residues 81-183. FliL-C was over-expressed in BL21(DE3)-RIPL cells from the pET151/D-TOPO plasmid, upon induction of T7 polymerase, and purified to > 98% electrophoretic homogeneity based on Coomassie Blue staining of the SDS-PAGE gel (Figure 2). It migrated on SDS-PAGE with an apparent molecular weight of ~12 kDa, which is close to the value calculated from the amino-acid sequence (12.18 kDa).

When subjected to gel filtration, the protein eluted as a single symmetrical peak (data not shown). The particle weight value estimated from the mobility of the gel-filtration column calibrated using globular proteins of a known mass gave the value of approximately 11.2 kDa, which suggested that *H. pylori* FliL-C is monomeric in solution under the tested conditions. This result is in agreement with the previous report on the periplasmic domain of *Vibrio alginolyticus* FliL, which is also primarily monomeric in solution in the concentration range used in this study (*27*).

In preparation for crystallization experiments, we have assessed the protein stability in different buffers using a thermal shift assay (Figure 3), and ascertained that gel-filtration buffer E (10 mM Tris-HCl pH 8.0, 150 mM NaCl) was optimal, as the melting temperature in this buffer was one of the highest among all tested conditions. Thus, no buffer exchange step was needed between gel filtration and crystallization. Crystals of FliL-C were obtained using a sparse-matrix crystallization approach. A complete X-ray diffraction data set was collected for a cryo-cooled crystal of FliL-C (Figure 4) to 2.8 Å using the Australian Synchrotron facility. Autoindexing of the diffraction data using *XDS* was consistent with space group *P*1, with unit-cell parameters $a = 62.5$, $b = 82.6$, $c = 97.8$ Å, $\alpha = 67.7$, $\beta = 83.4$, $\gamma = 72.8°$. The average $I/\sigma(I)$ value

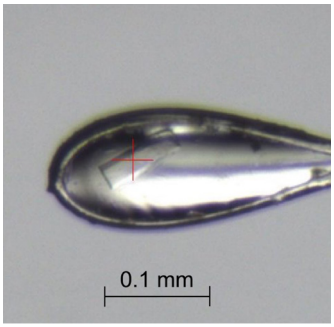

Figure 4. The FliL-C crystal mounted in the cryo-loop prior to data collection at the MX1 station of the Australian Synchrotron.

was 5.2 for all reflections (resolution range 54.2-2.8 Å) and 1.6 in the highest resolution shell (2.91-2.80 Å). Data processing gave an R_{merge} of 0.103 for intensities (0.323 in the highest resolution shell), and these data were 98% complete (98% completeness in the outer shell).

Estimation of the Matthews coefficient V_M (*36*) gave plausible values for 8 ($V_M = 4.6$ Å^3/Da) to 18 ($V_M = 2.1$ Å^3/Da) protein molecules in the asymmetric unit. The $\chi = 90$, $\chi = 120$ and $\chi = 180°$ sections of the self-rotation function were unremarkable. Thus, we are currently not able to establish the protein content of the asymmetric unit. A search for heavy-atom derivatives with the aim to solve the structure using multiple isomorphous replacement and/or multi-wavelength anomalous dispersion methods is underway. Production of the recombinant periplasmic domain of *H. pylori* FliL in its pure form will enable proteomics-based identification of its interacting partners in the flagellar motor. Furthermore, generation of well-ordered, reproducible crystals will allow determination of its 3-D

structure which would be an important step towards our understanding of its function in the bacterial flagellum.

Acknowledgements

Part of this research was undertaken on the MX1 beamline of the Australian Synchrotron, Victoria, Australia. We thank the AS staff for their assistance with data collection. We are also grateful to Dr. Danuta Maksel and Dr. Geoffrey Kong at the Monash Macromolecular Crystallisation Facility for assistance with the robotic crystallization trials. Mayra A. Machuca was a recipient of a PhD scholarship from the Departamento Admistrativo de Ciencia, Tecnología e Innovación COLCIENCIAS.

References

1. Warren JR, Marshall BJ. Unidentified curved bacilli on gastric epithelium in active chronic gastritis. Lancet. 1983; 1:1273-1275.
2. Watanabe T, Tada M, Nagi H, Sasaki S, Nakao M. *Helicobacter pylori* infection induces gastric cancer in Mongolian gerbils. Gastroenterology. 1998; 115:642-648.
3. Honda S, Fujioka T, Tokieda M, Satoh R, Nishizono A, Nasu M. Development of *Helicobacter pylori*-induced gastric carcinoma in mongolian gerbils. Cancer Res. 1998; 58:4255-4259.
4. Forman D, Coleman M, Debacker G, *et al*. An international association between *Helicobacter pylori* infection and gastric cancer. Lancet. 1993; 341:1359-1362.
5. Eaton KA, Morgan DR, Krakowka S. Motility as a factor in the colonisation of gnotobiotic piglets by *Helicobacter pylori*. J Med Microbiol. 1992; 37:123-127.
6. Geis G, Suerbaum S, Forsthoff B, Leying H, Opferkuch W. Ultrastructure and biochemical studies of the flagellar sheath of *Helicobacter pylori*. J Med Microbiol. 1993; 38:371-377.
7. Terashima H, Kojima S, Homma, M. Chapter 2: Flagellar Motility in Bacteria. Structure and Function of Flagellar Motor. In: International Review of Cell and Molecular Biology, Vol. 270, 2008; pp. 39-85.
8. Manson MD, Tedesco P, Berg HC, Harold FM, Van der Drift C. A protonmotive force drives bacterial flagella. Proc Natl Acad Sci U S A. 1977; 74:3060-3064.
9. Roujeinikova A. Crystal structure of the cell wall anchor domain of MotB, a stator component of the bacterial flagellar motor: Implications for peptidoglycan recognition. Proc Natl Acad Sci U S A. 2008; 105:10348-10353.
10. Reboul CF, Andrews DA, Nahar MF, Buckle AM, Roujeinikova, A. Crystallographic and molecular dynamics analysis of loop motions unmasking the peptidoglycan-binding site in stator protein MotB of flagellar motor. PLoS one. 2011; 6:e18981.
11. O'Neill J, Xie M, Hijnen M, Roujeinikova A. Role of the MotB linker in the assembly and activation of the bacterial flagellar motor. Acta Crystallogr D Biol Crystallogr. 2011; 67:1009-1016.
12. Andrews DA, Nesmelov YE, Wilce MC, Roujeinikova A. Structural analysis of variant of *Helicobacter pylori* MotB in its activated form, engineered as chimera of MotB and leucine zipper. Sci Rep. 2017; 7:13435.
13. Wilson ML, Macnab RM. Co-overproduction and localization of the *Escherichia coli* motility proteins motA and motB. J Bacteriol. 1990; 172:3932-3939.
14. Hosking ER, Vogt C, Bakker EP, Manson MD. The *Escherichia coli* MotAB proton channel unplugged. J Mol Biol. 2006; 364:921-937.
15. Partridge JD, Nieto V, Harshey RM. A new player at the flagellar motor: FliL controls both motor output and bias. MBio. 2015; 6:e02367.
16. Attmannspacher U, Scharf BE, Harshey RM. FliL is essential for swarming: motor rotation in absence of FliL fractures the flagellar rod in swarmer cells of *Salmonella enterica*. Mol Microbiol. 2008; 68:328-341.
17. Suaste-Olmos F, Domenzain C, Mireles-Rodríguez JC, Poggio S, Osorio A, Dreyfus G, Camarena L. The flagellar protein FliL is essential for swimming in *Rhodobacter sphaeroides*. J Bacteriol. 2010; 192:6230-6239.
18. Fabela S, Domenzain C, De la Mora J, Osorio A, Ramirez-Cabrera V, Poggio S, Dreyfus G, Camarena L. A distant homologue of the FlgT protein interacts with MotB and FliL and is essential for flagellar rotation in *Rhodobacter sphaeroides*. J Bacteriol. 2013; 195:5285-5296.
19. Suaste-Olmos F, Domenzain C, Mireles-Rodríguez JC, Poggio S, Osorio A, Dreyfus G, Camarena L. The flagellar protein FliL is essential for swimming in *Rhodobacter sphaeroides*. J Bacteriol. 2010; 192:6230-6239.
20. Ramírez-Cabrera V1, Poggio S, Domenzain C, Osorio A, Dreyfus G, Camarena L. A novel component of the *Rhodobacter sphaeroides* Fla1 flagellum is essential for motor rotation. J Bacteriol. 2012; 194:6174-6183.
21. Jenal U, White J, Shapiro L. *Caulobacter* flagellar function, but not assembly, requires FliL, a non-polarly localized membrane protein present in all cell types. J Mol Biol. 1994; 243:227-244.
22. Cusick K, Lee YY, Youchak B, Belas R. Perturbation of FliL interferes with *Proteus mirabilis* swarmer cell gene expression and differentiation. J Bacteriol. 2012; 194:437-447.
23. Lee YY, Patellis J, Belas R. Activity of *Proteus mirabilis* FliL is viscosity dependent and requires extragenic DNA. J Bacteriol. 2013; 195:823-832.
24. Lee YY, Belas R. Loss of FliL alters *Proteus mirabilis* surface sensing and temperature-dependent swarming. J Bacteriol. 2015; 197:159-173.
25. Motaleb MA, Pitzer JE, Sultan SZ, Liu J. A novel gene inactivation system reveals altered periplasmic flagellar orientation in a *Borrelia burgdorferi fliL* mutant. J Bacteriol. 2011; 193:3324-3331.
26. Qin Z, Lin W, Zhu S, Franco AT, Liu J. Imaging the motility and chemotaxis machineries in *Helicobacter pylori* by cryo-electron tomography. J Bacteriol. 2017; 199:e00695-16.
27. Kumar A, Isumi M, Sakuma M, Zhu S, Nishino Y, Onoue Y, Kojima S, Miyanoiri Y, Imada K, Homma M. Biochemical characterization of the flagellar stator-associated inner membrane protein FliL from *Vibrioalginolyticus*. J Biochem. 2017; 161:331-337.
28. Tsirigos KD, Peters C, Shu N, Kall L, Elofsson A. The TOPCONS web server for consensus prediction of

membrane protein topology and signal peptides. Nucleic Acids Res. 2015; 43:W401-407.
29. Jones DT, Cozzetto D. DISOPRED3: precise disordered region predictions with annotated protein-binding activity. Bioinformatics. 2015; 31:857-863.
30. Woon AP, Tohidpour A, Alonso H, Saijo-Hamano Y, Kwok T, Roujeinikova A. Conformational analysis of isolated domains of *Helicobacter pylori* CagA. PLoS one. 2013; 8:e79367.
31. Bradford MM. A rapid and sensitive for the quantitation of microgram quantitites of protein utilizing the principle of protein-dye binding. Anal Biochem. 1976; 72:248-254.
32. Modak JK, Revitt-Mills SA, Roujeinikova A. Cloning, purification and preliminary crystallographic analysis of the complex of *Helicobacter pylori* α-carbonic anhydrase with acetazolamide. Acta Crystallogr Sect F Struct Biol Cryst Commun. 2013; 69:1252-1255.
33. Orwig SD, Lieberman RL. Biophysical characterization of the olfactomedin domain of myocilin, an extracellular matrix protein implicated in inherited forms of glaucoma. PLoS one. 2011; 6:e16347.
34. Kabsch W. XDS. Acta Crystallogr D Biol Crystallogr. 2010; 66:125-132.
35. Winn MD, Ballard CC, Cowtan KD, Dodson EJ, Emsley P, Evans PR, Keegan RM, Krissinel EB, Leslie AG, McCoy A. Overview of the CCP4 suite and current developments. Acta Crystallogr D Biol Crystallogr. 2011; 67:235-242.
36. Matthews BW. Solvent content of protein crystals. J Mol Biol. 1968; 33:491-497.

(Received September 11, 2018; Revised December 10, 2018; Accepted December 21, 2018)

Brief Report

DOI: 10.5582/bst.2018.01279

Comparative study of preciseness in the regional variation of influenza in Japan among the National Official Sentinel Surveillance of Infectious Diseases and the National Database of Electronic Medical Claims

Yasushi Ohkusa[1], Tamie Sugawara[1], Kenzo Takahashi[2,*], Miwako Kamei[3]

[1] *National Institute of Infectious Diseases, Tokyo, Japan;*
[2] *Teikyo University Graduate School of Public Health, Tokyo, Japan;*
[3] *School of Pharmacy, Nihon University, Chiba, Japan.*

Summary **In Japan, national official surveillance for influenza has been performed at about 5,000 sentinel hospitals/clinics by the National Official Sentinel Surveillance of Infectious Diseases (NOSSID). Meanwhile, all electronic medical claims nationwide in the National Database of Electronic Medical Claims (NDBEMC) were recently disclosed by the Ministry of Health, Labour and Welfare of Japan. We compared the regional variation of influenza incidence among prefectures between the NOSSID and NDBEMC. The data were extracted from NOSSID and the NDBEMC for the 2010/2011 through 2013/2014 seasons. We compared the data of both datasets season by season by using Spearman's rank correlation in each season. Spearman's rank correlation values for the four seasons were 0.7823, 0.3907, 0.4961 and 0.4543, and their *p*-values were less than 0.00005, 0.0066, 0.0004 and 0.0013, respectively. Statistically, regional variation of influenza incidence in NOSSID is not imprecise, but its correlation with the NDBEMC dataset is not so high. It is important to note this fact when interpreting regional variation in NOSSID.**

Keywords: Influenza, National Database for Electronic Medical Claims, National Official Sentinel Surveillance, regional variation

1. Introduction

Official surveillance, especially for influenza, is sentinel surveillance in many countries such as the United States (*https://www.cdc.gov/flu/weekly/overview.htm*), Europe (*http://flunewseurope.org/System*) and Japan. Because sentinel surveillance is not comprehensive, its interpretation or preciseness should be evaluated more comprehensively and precisely, as so called "big data," and not as timely information. "Big data" has not been available in the past, and thus sentinel surveillance has been considered to be the gold standard without evaluation its preciseness. However, recently, we have had access to "big data" with which to evaluate sentinel surveillance.

*Address correspondence to:
Dr. Kenzo Takahashi, Teikyo University Graduate School of Public Health, 2-11-1 Kaga, Itabashi-ku, Tokyo 173-8605, Japan.
E-mail: kenzo.takahashi.chgh@med.teikyo-u.ac.jp

Based on the Law Related to the Prevention of Infectious Diseases and Medical Care for Patients of Infections (The Infectious Diseases Control Law) in Japan, national official surveillance for influenza has been performed at about 5,000 sentinel hospitals/clinics, which represent about one tenth of the pediatric or internal medicine facilities nationwide. We call this system the National Official Sentinel Surveillance of Infectious Diseases (NOSSID) (*1,2*). As there has been no comparable surveillance so far, the preciseness of NOSSID cannot be evaluated. Recently, however, data of almost all electronic medical claims nationwide have been disclosed in the "National Database of Health Insurance Claims and Specific Health Checkups of Japan" (*3*) by the Ministry of Health, Labour and Welfare (MHLW) of Japan (*4-7*). We call this the National Database of Electronic Medical Claims (NDBEMC). This data covered 98.4% of all medical claims made in 2015 (*8*). All doctors must record a diagnosis for medical claims; therefore, this data must necessarily constitute

the most reliable data source to date. Exceptionally, only small clinics operated by only one doctor older than 65 years of age were exempted from providing non-electronic medical claim information as an interim measure.

In Japan, almost all influenza patients receive a rapid diagnostic test. Therefore, influenza patients in Japan are not patients with influenza-like-illness; rather, they are patients actually diagnosed as having influenza by a rapid diagnostic test. Information in both NOSSID and the NDBEMC is reported by the diagnosing doctor. For NOSSID, doctors have to report their diagnostic information to the public health center weekly. NDBEMC contains the information they send monthly to the health insurer when submitting electronic medical claims, which includes the diagnosis.

Our previous study evaluated the number of influenza patients from NOSSID nationwide (*9*). In the present study, we focus on the regional variation of influenza incidence among prefectures in NOSSID in comparison with that in the NDBEMC. So far, as there is no more comprehensive information available than that from sentinel surveillance, we have to believe that the sentinel surveillance data is accurate. For example, the MHLW or mass media have sometimes reported the highest influenza incidence in a prefecture based on sentinel surveillance. However, we questioned whether the information was true or credible. This study attempted to answer this question by using NDBEMC, which has the most comprehensive data, to evaluate the preciseness of NOSSID by comparing the data of NOSSID with that of NDBEMC.

2. Materials and Methods

2.1. *Data and study period*

NOSSID for influenza has about 5,000 sentinels, which represent almost one tenth of all pediatric or internal medicine clinics/hospitals nationwide. Among these 5,000 sentinels, 3,000 are pediatric clinics/hospitals and 2,000 are clinics/hospitals for adult patients. They report the number of influenza patients per sentinel weekly by prefecture. Age, sex, and other characteristic of the patients were not available. We used the published data of the number of reported patients by prefecture weekly.

The NDBEMC can be used to count patients diagnosed as having influenza. We used the reported number of patients who had been diagnosed as having influenza, excluding suspected cases but including complex cases, by prefecture and by month in the NDBEMC. Age, sex, and other characteristic of the patients were also not available in this application. In May 2015, approximately 98.4% of all electronic medical claims were covered (*8*). Data from the NDBEMC were available from April 2009 through March 2015. We obtained permission to use this data for research purposes.

The influenza season was defined as the period spanning September to August of the following year or, equivalently, from the 36th epidemiological week to the 35th epidemiological week of the following year. The study period was from the 2010/2011 season through the 2013/2014 season.

2.2. *Statistical analysis*

Data from NOSSID were aggregated in the season by prefecture and divided by the number of sentinels in each prefecture. Data from the NDBEMC were aggregated in the season by prefecture and divided by the population in each prefecture. The mid-year population during each season was adopted as the population for each prefecture. Since the data distribution was not linear, thus we decided to apply non-parametric method. We compared the rank of influenza incidence by prefecture in both datasets season by season for the study period so as to solve objective in the present study. We used Spearman's rank order correlation among prefecture in the incidence of influenza in each season. We adopted 5% as a significant level.

2.3. *Ethical considerations*

This study used only anonymous data that had been de-linked from individual patient information. Therefore, ethical issues related to medical institutions and pharmacies do not pertain in this study. The NOSSID data were open to all. Author MK was approved to use the NDBEMC data by the MHLW on July 27, 2016 (Research project: Estimation of the number of patients of infectious diseases).

3. Results and Discussion

Figure 1 shows the regional variations in the incidence rate in the NDBEMC over the four seasons, and Figure 2 shows the regional variations in the total number of patients per sentinel in NOSSID. These figures show that the influenza incidence in the 2013/2014 season, which is shown as a black line in the graphs, was higher than that for other three seasons in almost all prefectures in the NDBEMC, whereas in NOSSID, there was no clearly dominating season in almost all prefectures.

Table 1 shows the prefecture rankings for the number of influenza cases in both datasets. We can see some discrepancies among the NDBEMC and NOSSID. For example, Okinawa was on top for three seasons in NOSSID and in second place in the 2012/2013 season. It was also second in the NDBEMC for three seasons, but it was 43rd, which was 5th from the bottom, in the 2012/2013 season. Conversely, the top prefectures in the NDBEMC did not appear in the top ten of NOSSID in the same season except for Hiroshima in the 2012/2013

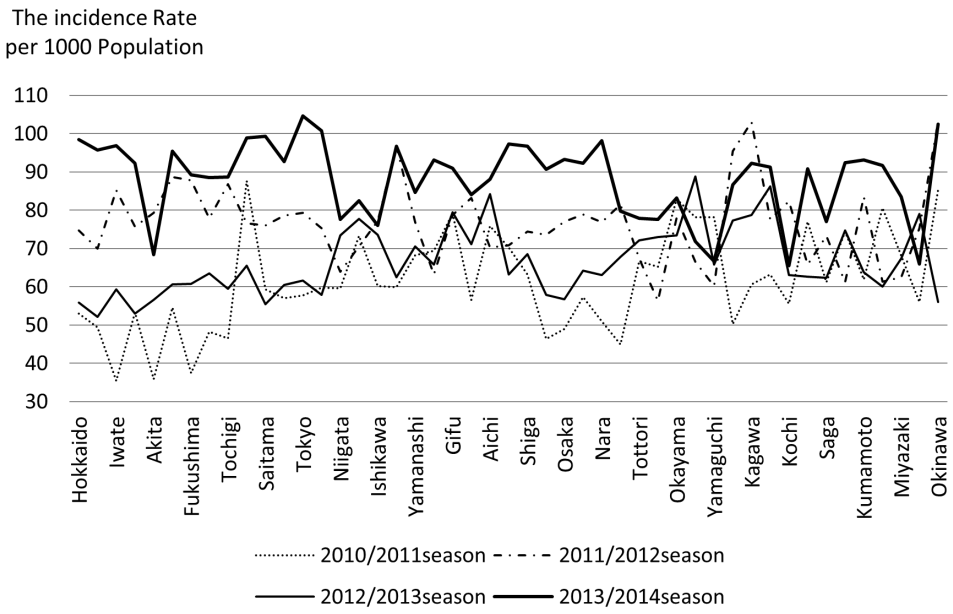

Figure 1. Incidence rate per 1000 population in the NDBEMC by prefecture for the four seasons. *Note*: The NDBEMC is the National Database of Electronic Medical Claims. This figure shows the cumulative incidence, which is the number of newly diagnosed influenza patients from the 2010/2011 season through the 2013/2014 season in the NDBEMC divided by the population by prefecture. The influenza season is defined as September to August of the following year. The bold black line shows the situation in the 2013/2014 season, the thin black line shows the 2012/2013 season, the gray line shows the 2011/2012 season, and the dashed line shows the 2010/2011 season.

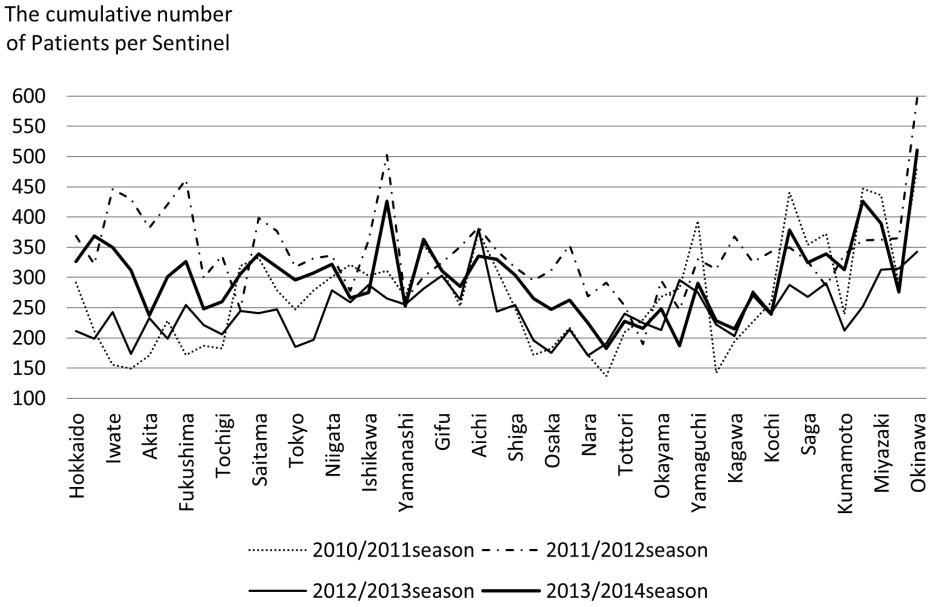

Figure 2. Cumulative number of patients per sentinel in NOSSID by prefecture for the four seasons. *Note*: NOSSID is the National Official Sentinel Surveillance for Infectious Diseases. This figure shows the cumulative number of influenza patients in one season per sentinel by prefecture. The influenza season for NOSSID extends from the 36th epidemiological week to the 35th epidemiological week of the following year. The epidemiological week in Japan is defined as Monday through Sunday. The first epidemiological week is the week including the first of January if that day was Monday-Wednesday. If that day was Thursday-Saturday, then the first epidemiological week starts from the first Monday of the year. The bold black line shows the situation in the 2013/2014 season, the thin black line shows the 2012/2013 season, the gray line shows the 2011/2012 season, and the dashed line shows the 2010/2011 season.

season. Spearman's rank correlation coefficients for the four seasons were 0.7823, 0.3907, 0.4961 and 0.4543, and their *p*-values were less than 0.00005, 0.0066, 0.0004 and 0.0013, respectively.

It shows some discrepancies between the rankings of the NDBEMC and NOSSID. For example, Okinawa prefecture was the top prefecture in three of the four seasons in the NOSSID ranking, but it was never ranked on top in the NDBEMC. In the exceptional season of 2012/2013, Okinawa prefecture was ranked second in

Table 1. Ranking by prefecture of the incidence rate per 1,000 population in the NDBEMC and the cumulative number of patients per sentinel in NOSSID for the four seasons

Ranking	Season							
	2010/2011		2011/2012		2012/2013		2013/2014	
	NDBEMC	NOSSID	NDBEMC	NOSSID	NDBEMC	NOSSID	NDBEMC	NOSSID
1	Gunma	Okinawa	Kagawa	Okinawa	Hiroshima	Aichi	Tokyo	Okinawa
2	Okinawa	Oita	Okinawa	Fukui	Ehime	Okinawa	Okinawa	Oita
3	Okayama	Fukuoka	Fukui	Fukushima	Aichi	Kagoshima	Kanagawa	Fukui
4	Oita	Miyazaki	Tokushima	Iwate	Gifu	Miyazaki	Saitama	Miyazaki
5	Gifu	Yamaguchi	Yamagata	Miyagi	Kagoshima	Gifu	Gunma	Fukuoka
6	Hiroshima	Aichi	Fukushima	Yamagata	Kagawa	Hiroshima	Hokkaido	Aomori
7	Yamaguchi	Nagasaki	Tochigi	Saitama	Toyama	Nagasaki	Nara	Nagano
8	Fukuoka	Nagano	Iwate	Aichi	Tokushima	Fukuoka	Mie	Iwate
9	Aichi	Saga	Kumamoto	Akita	Nagasaki	Ishikawa	Iwate	Saitama
10	Nagasaki	Saitama	Shizuoka	Chiba	Ishikawa	Nagano	Shiga	Nagasaki
11	Toyama	Toyama	Kochi	Hokkaido	Okayama	Niigata	Fukui	Aichi
12	Mie	Gunma	Wakayama	Kagawa	Niigata	Ehime	Aomori	Mie
13	Nagano	Gifu	Tokyo	Kagoshima	Shimane	Yamaguchi	Yamagata	Hokkaido
14	Yamanashi	Mie	Akita	Miyazaki	Tottori	Saga	Osaka	Fukushima
15	Miyazaki	Fukui	Hyogo	Oita	Shizuoka	Fukui	Nagano	Saga
16	Tottori	Ishikawa	Gifu	Ishikawa	Yamanashi	Shizuoka	Kumamoto	Niigata
17	Shimane	Niigata	Chiba	Hyogo	Shiga	Toyama	Chiba	Chiba
18	Ehime	Hokkaido	Okayama	Shizuoka	Wakayama	Yamanashi	Nagasaki	Kumamoto
19	Shiga	Kagoshima	Ibaraki	Fukuoka	Miyazaki	Fukushima	Hyogo	Miyagi
20	Kumamoto	Hiroshima	Ehime	Mie	Yamaguchi	Shiga	Kagawa	Gifu
21	Saga	Chiba	Ishikawa	Kochi	Nagano	Oita	Miyagi	Kanagawa
22	Kagawa	Kanagawa	Osaka	Kumamoto	Gunma	Chiba	Oita	Gunma
23	Ishikawa	Okayama	Yamanashi	Niigata	Hyogo	Gunma	Ehime	Shiga
24	Fukui	Yamanashi	Nara	Tochigi	Kumamoto	Mie	Gifu	Yamagata
25	Kanagawa	Kochi	Gunma	Kanagawa	Ibaraki	Iwate	Fukuoka	Tokyo
26	Niigata	Shizuoka	Saitama	Yamaguchi	Mie	Kochi	Kyoto	Yamaguchi
27	Saitama	Shiga	Miyagi	Saga	Nara	Saitama	Fukushima	Shizuoka
28	Tokyo	Tokyo	Kagoshima	Ehime	Kochi	Tottori	Tochigi	Kagoshima
29	Hyogo	Kumamoto	Kanagawa	Gifu	Fukuoka	Akita	Ibaraki	Ishikawa
30	Chiba	Shimane	Hokkaido	Aomori	Fukui	Shimane	Aichi	Ehime
31	Shizuoka	Yamagata	Shiga	Tokyo	Saga	Tokushima	Tokushima	Toyama
32	Kagoshima	Ehime	Kyoto	Shiga	Tokyo	Ibaraki	Yamanashi	Kyoto
33	Kochi	Hyogo	Saga	Tokushima	Fukushima	Hyogo	Shizuoka	Hyogo
34	Yamagata	Aomori	Mie	Osaka	Yamagata	Okayama	Miyazaki	Tochigi
35	Miyagi	Tottori	Toyama	Nagano	Chiba	Kumamoto	Okayama	Yamanashi
36	Hokkaido	Kagawa	Aichi	Ibaraki	Oita	Hokkaido	Toyama	Okayama
37	Nara	Ibaraki	Aomori	Kyoto	Tochigi	Tochigi	Wakayama	Ibaraki
38	Tokushima	Tochigi	Tottori	Okayama	Iwate	Kagawa	Tottori	Osaka
39	Aomori	Osaka	Hiroshima	Wakayama	Kyoto	Yamagata	Shimane	Kochi
40	Osaka	Nara	Fukuoka	Nagasaki	Kanagawa	Aomori	Niigata	Akita
41	Ibaraki	Fukushima	Niigata	Toyama	Osaka	Kanagawa	Saga	Tokushima
42	Tochigi	Kyoto	Nagano	Nara	Akita	Kyoto	Ishikawa	Tottori
43	Kyoto	Akita	Miyazaki	Yamanashi	Okinawa	Wakayama	Hiroshima	Nara
44	Wakayama	Iwate	Oita	Tottori	Hokkaido	Tokyo	Akita	Shimane
45	Fukushima	Miyagi	Nagasaki	Gunma	Saitama	Osaka	Yamaguchi	Kagawa
46	Akita	Tokushima	Yamaguchi	Hiroshima	Miyagi	Miyagi	Kagoshima	Hiroshima
47	Iwate	Wakayama	Shimane	Shimane	Aomori	Nara	Kochi	Wakayama

Note: NDBEMC is the National Database of Electronic Medical Claims. The influenza season in the NDBEMC is defined as September to August of the following year. NOSSID is the National Official Sentinel Surveillance for Infectious Diseases. The influenza season in NOSSID extends from the 36th epidemiological week to the 35th epidemiological week of the following year.

NOSSID but fifth from the bottom in the NDBEMC. Similarly, Wakayama prefecture was ranked as the least flu-prevalent prefecture in the two seasons of 2010/2011 and 2013/2014 in NOSSID, but it was never ranked as the lowest in the NDBEMC. The exceptional case was Shimane prefecture in the 2011/2012 season. It ranked as the least prevalent prefecture in both datasets. These discrepancies between the two datasets may have caused the low rank correlation of around 0.5, even though the four p values were quite small, and the null hypothesis that the two datasets were independent was rejected in all seasons.

We can surmise three reasons for the low rank correlation. First, in principle, the sentinels in NOSSID were chosen randomly. However, they were determined as the outcome of bargaining between the local government and the regional medical associations, and thus, in fact, the sentinels were not selected randomly. For example, if a local government would like to know about the early stage of an outbreak, they might ask

larger hospitals and clinics to be sentinels. This process may bias the NOSSID data. The second reason relates to bias in the proportion of sentinels. Among the 5,000 sentinels in NOSSID, about 3,000 are pediatric clinics/hospitals and 2,000 are clinics/hospitals for adult patients. Thus, the coverage in children is much higher than that in adults, even though its ratio is not well known because the age distribution of the pediatric and adult patients was not published by prefecture. Therefore, NOSSID may reflect epidemics in children much more accurately than in adults. In contrast, the NDBEMC has no such bias in age because almost all electronic claims are included. This difference in the two datasets may have caused the low rank correlation. The third reason might be incompleteness of the NDBEMC. As explained above, the coverage of the NDBEMC was quite high but not 100%. The information defect may occur at small clinics operated by only one older doctor. In such cases, the doctor can report records by handwriting, rather than electronically, and this interim measure can cause this defect. If there were systematic variations in the proportion or size of these small clinics to which the interim measure was applied, among regions, the lack of these clinics' data might cause bias in the NDBEMC and thus a subsequent lower rank correlation with NOSSID. However, since such a defect might affect a very small proportion of the data at least in the national average, and there is no specific reason for systematic variations in the proportion or size of these small clinics among regions, the possibility of this effect might be small.

There were some limitations in this study. First, we examined regional variation in influenza, but we do not know whether similar phenomena might be observed in other infectious diseases including respiratory syncytial virus infection; gastrointestinal infections; varicella; hand, foot and mouth disease; erythema infectiosum; or pertussis. Therefore, we cannot extend the obtained result to NOSSID itself.

Second, though we do not know the age distribution of the patients with influenza in NOSSID, we will be able to obtain it from the NDBEMC with a future application. Such information on age distribution may be insightful in interpreting regional variation. As mentioned before, the sentinels in NOSSID were designed to bias to pediatric patients rather than adult. Conversely, NEDEMC does not have those bias in age distribution. This difference might cause some discrepancies in two data set.

Third, as we have examined no research in countries other than Japan, we cannot apply the obtained results to sentinel surveillance itself, especially as related to other countries. As medical claims or records in other countries are available, we need to verify the preciseness of the sentinel surveillance.

In conclusion, we found that regional variation in the influenza data in NOSSID was not imprecise statistically, but its correlation with the NDBEMC dataset was not so high. It is important to note this fact when interpreting regional variation in the NOSSID data. The examination of infectious diseases other than influenza remains as a future challenge.

Acknowledgements

We acknowledge the MHLW for their permission to use the NDBEMC.

References

1. Hashimoto S, Murakami Y, Taniguchi K, Shindo N, Osaka K, Fuchigami H, Nagai M. Annual incidence rate of infectious diseases estimated from sentinel surveillance data in Japan. J Epidemiol 2003; 13:136-141.
2. Kawado M, Hashimoto S, Murakami Y, Izumida M, Ohta A, Tada Y, Shigematsu M, Yasui Y, Taniguchi K, Nagai M. Annual and weekly incidence rates of influenza and pediatric diseases estimated from infectious disease surveillance data in Japan, 2002-2005. J Epidemiol 2007; 17:S32-S41.
3. Ministry of Health, Labour and Welfare, Japan. National Database of Health Insurance Claims and Specific Health Checkups of Japan. *https://www.mhlw.go.jp/file/06-Seisakujouhou-12400000-Hokenkyoku/0000193322.pdf* (accessed October 5, 2018). (in Japanese)
4. Health Insurance Bureau, Ministry of Health, Labour and Welfare, Japan. Expert Meeting of Providing the Information of Medical Claims and Others. The report of providing the information of medical claims and health check-up for metabolic syndrome to the third party. 2013. (in Japanese).
5. Health Insurance Bureau, Ministry of Health, Labour and Welfare. Expert Meeting of Providing the Information of Medical Claims and Others. The guideline for providing the information of medical claims and health check-up for metabolic syndrome. (updated 2013 Aug) 2011. (in Japanese).
6. Nakamura Y, Sugawara T, Ohkusa Y, Taniguchi K, Miyazaki C, Momoi M, Okabe N. Severe abnormal behavior incidence after administration of neuraminidase inhibitors using the national database of medical claims. J Infect Chemother 2018; 24:177-181.
7. Miura K, Miyagawa N, Murakami Y, Okayama A. Outlines of the national database on medical expenditure and health check-up. Hoken Iryo Kagaku 2013; 62:31-35. (in Japanese)
8. Health Insurance Claims Review & Reimbursement services (2015): Status of medical claims by claim form (Diagnosed in April, 2015). *http://www.ssk.or.jp/tokeijoho/tokeijoho_rezept/tokeijoho_04_h27.files/seikyu_2704.pdf.* (accessed July 3, 2018). (in Japanese)
9. Nakamura Y, Sugawara T, Kawanohara H, Ohkusa Y, Kamei M, Oishi K. Evaluation of the estimated number of influenza patients from National Sentinel Surveillance using National Database of Electronic Medical Claims. Jpn J Infect Dis 2015; 68:27-29.

(Received November 15, 2018; Revised December 24, 2018; Accepted December 29, 2018)

Brief Report

DOI: 10.5582/bst.2018.01296

Stent placement for benign portal vein stenosis following pancreaticoduodenectomy in a hybrid operating room

Yutaka Sawai[1], Takashi Kokudo[1], Yoshihiro Sakamoto[1], Hidemasa Takao[2], Yusuke Kazami[1], Yujiro Nishioka[1], Nobuhisa Akamatsu[1], Junichi Arita[1], Junichi Kaneko[1], Kiyoshi Hasegawa[1,*]

[1] *Hepato-Biliary-Pancreatic Surgery Division, Artificial Organ and Transplantation Division, Department of Surgery, Graduate School of Medicine, The University of Tokyo, Tokyo, Japan;*
[2] *Department of Radiology, Graduate School of Medicine, The University of Tokyo, Tokyo, Japan.*

Summary **Benign portal vein stenosis is a rare complication following pancreaticoduodenectomy. Because a direct surgical approach to the portal vein is difficult due to severe adhesions following pancreaticoduodenectomy, portal vein stent placement is considered a good treatment option. Herein, we report 3 cases of severe portal vein stenosis following pancreaticoduodenectomy that were treated with portal venous stent placement in a hybrid operating room, combining a conventional operating room with an angiography suite. High-resolution images on digital subtraction angiography provide better contrast and support accurate stent placement compared to using a mobile C-arm.**

Keywords: Digital subtraction angiography, portal hypertension, hepato-biliary-pancreatic surgery

1. Introduction

Benign portal vein (PV) stenosis is a rare complication following hepato-biliary-pancreatic surgery, such as hepatectomy and pancreaticoduodenectomy (PD) (*1,2*). The most frequent cause of stenosis is postoperative inflammation, which leads to portal hypertension and subsequent gastrointestinal hemorrhage from varices (*3*). Because a direct surgical approach to the PV is difficult due to adhesions following hepato-biliary-pancreatic surgery, PV stent placement is considered a good treatment option for benign PV stenosis (*4*).

Here, we report 3 cases of severe PV stenosis following PD treated with portal venous stent placement in a hybrid operating room (OR), which combines a conventional OR with a digital subtraction angiography (DSA) unit (*5*).

Released online in J-STAGE as advance publication December 28, 2018.

**Address correspondence to:*
Dr. Kiyoshi Hasegawa, Hepato-Biliary-Pancreatic Surgery Division, Artificial Organ and Transplantation Division, Department of Surgery, Graduate School of Medicine, The University of Tokyo, 7-3-1 Hongo, Bunkyo-ku, Tokyo 113-8655, Japan.
E-mail: kihase-tky@umin.ac.jp

We place this study into appropriate perspective with the most recent clinical practice guidelines.

2. Patients and Methods

2.1. *Patients*

From August 2016 to July 2017, 62 patients underwent PD, including five hepatopancreatic duodenectomies (HPDs), at the University of Tokyo Hospital. Two patients developed acute PV stenosis with symptoms (patients 1 and 3). Patient 2 was referred from another hospital for surgical resection of remnant pancreatic cancer following PD. In total, 3 patients underwent PV stent placement for severe PV stenosis following PD in a hybrid OR in our hospital from April 2017 to October 2017. Portal vein stent placement was considered when a patient developed symptoms due to portal vein stenosis. However, in patient 2, portal vein stent placement was indicated to avoid complication, such as ascites, related to portal vein stenosis after distal pancreatectomy. Table 1 shows the patient characteristics prior to stent placement. After the surgery, all three patients developed benign PV stenosis at 2, 52, and 3 months. Patient 1 developed melena 6 months after PD, and PV stenosis was identified on computed tomography (CT) scan (Figure 1). In patient 2,

Table 1. Preoperative Patient Characteristics

Patient Characteristics	Patient 1	Patient 2	Patient 3
Age, years	68	68	75
Sex (Male/Female)	Male	Female	Female
Primary lesion	CC	PC	CC
Pathological TNM staging*	T3aN1M0	T3N0M0	T3bN1M0
ASA score	2	2	2
BMI, kg/m^2	30.0	19.2	19.4
Albumin, g/dL	3.5	3.4	2.7
Total bilirubin, mg/dL	0.7	0.9	0.6
AST, U/L	19	50	60
ALT, U/L	14	16	30
PT-INR	1.04	0.92	1.11
Comorbidities			
Hypertension	yes	yes	no
Diabetes mellitus	yes	yes	no
Tobacco use (ever)	no	yes	no
Alcohol use (ever)	no	yes	no
PD			
Operative time, min	597	494	689
Estimated blood loss, mL	840	884	1680
Portal vein resection	no	no	yes
Additional right hemihepatectomy	no	no	yes
RBC transfusion required	no	yes	yes
Characteristics after PD			
Major abdominal complications**			
POPF	yes**	no	no
Cholangitis	no	yes	no

*According to the American Joint Committee on Cancer Classification (*8*). **International Study Group of Postoperative Pancreatic Fistula Grade B (*9*). TNM, tumor, lymph node, metastasis; ASA, American Society of Anesthesiologists; AST, aspartate transaminase; ALT, alanine transaminase; PT-INR, prothrombin time-international normalized ratio; CC, cholangiocarcinoma; PC, pancreatic cancer; POPF, postoperative pancreatic fistula; RBC, red blood cells.

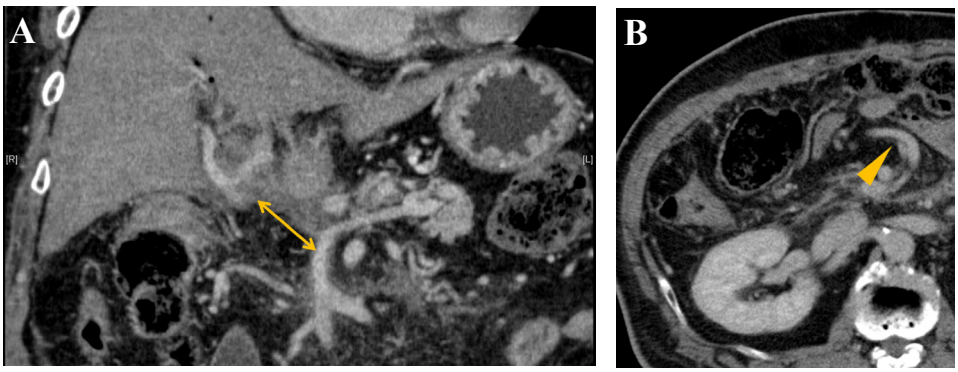

Figure 1. Preoperative findings. (A) Coronal image on contrast-enhanced CT showing extrahepatic portal vein stenosis (arrow). **(B)** Axial image on contrast-enhanced CT showing the dilated collateral vessel from the first jejunal vein (arrow head).

preoperative CT scan revealed severe PV stenosis with surrounding soft tissue density area. No malignant cells were found in the soft tissue on repeated endoscopic ultrasound-guided fine needle aspiration (EUS-FNA); thus the PV stenosis might be because of postoperative cholangitis associated with severe stenosis resulting from choledocojejunostomy. Stent placement was performed to relieve stenosis 17 months after PD. Patient 3 developed a liver abscess 2 months after HPD with CT scan revealing PV stenosis. The study was approved by the institutional ethics committee (approval number: CL2017037).

2.2. *Surgical technique*

For our three patients, we used an open trans-ileocecal approach to the portal venous system in a hybrid OR because safe puncture using a percutaneous approach was difficult. In patients 1 and 2, the portal vein diameter of the umbilical portion was small (5 mm) and portal vein flow was difficult to detect. In patient 3, although the portal vein diameter was relatively thick (9 mm), liver abscess existed at the puncture tract.

During transileocolic PV stent placement, a midline incision was made on the lower abdomen. A vascular

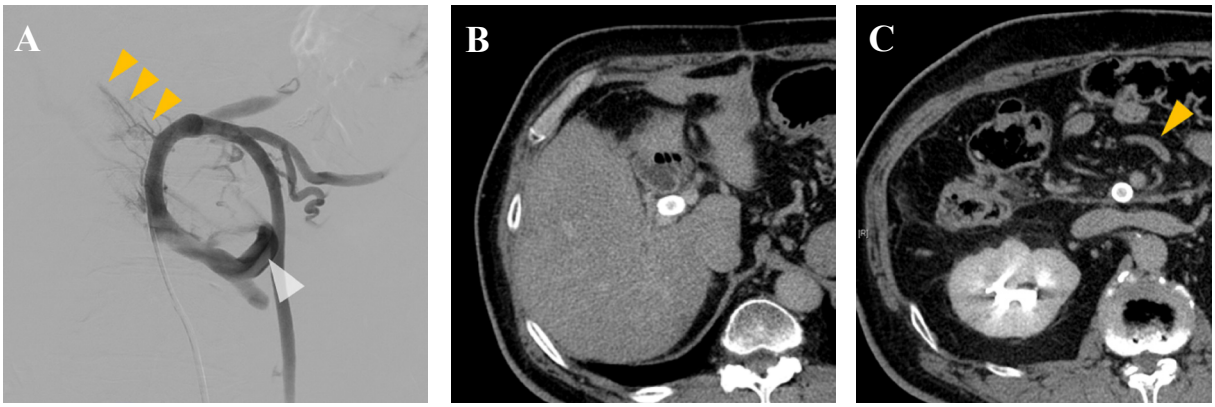

Figure 2. Intraoperative and postoperative findings. (A) Portography showing portal vein stenosis (yellow arrow head) and collateral vessels from the first jejunal vein (white arrow head). **(B, C)** Contrast-enhanced CT images 3 months after stent placement showing stent patency **(B)** and collateral vessel shrinkage **(C**, yellow arrow head**)**.

Table 2. Intraoperative and Postoperative Outcomes of Stent Placement

Variables	Patient 1	Patient 2	Patient 3
Intraoperative outcome			
Operative time, min	164	140	154
Estimated blood loss, mL	115	50	0
Decrease in pressure gradient between the PV and SMV, cm H_2O	7.5	18.4	8.5
Postoperative morbidity			
Clavien-Dindo classification	0	0	0
Postoperative hospital stay, d	11	7	9

*According to Dindo et al's classification (*10*). PV, portal vein; SMV, superior mesenteric vein.

sheath was introduced into the peripheral ileal vein following ileal mesentery dissection. The severity and length of the PV stenosis were examined by high-resolution portography using DSA (Figure 2A). A metallic stent was placed following balloon dilatation of the stenotic site, and additional balloon dilatation of the PV from inside of the stent was performed. Portal pressure gradient was measured before and after stent placement.

Anticoagulant therapy with heparin was administered for 1 week following stent placement and then switched to warfarin (*5*) for 6 months. Intraoperative and postoperative outcomes are shown in Table 2.

3. Results and Discussion

The portal system was clearly visualized in all three patients using DSA in a hybrid OR. The pressure gradient at the stenotic site was 10.5, 21.2, and 9.5 cmH_2O, respectively. It improved to 3.0, 2.8 and 1.0 cmH_2O after stent placement. Postoperative courses were uneventful in all patients. The postoperative hospital stay was 11, 7, and 9 days, respectively.

Contrast-enhanced CT scan was performed 1 week after the surgery confirmed PV stent patency. In patient 1, stent patency and collateral vessel shrinkage were detected on contrast-enhanced CT 3 months after stent placement (Figure 2B, C).

Patients 1 and 3 were symptom free following stent placement for 9 and 3 months, respectively, and patient 2 underwent resection of remnant pancreatic cancer 1 month after stent placement and was complication free for 7 months. The latest stent patency for each patient was confirmed on contrast-enhanced CT at 9, 1, and 5 months following stent placement, respectively.

We herein report 3 cases of stent placement for severe benign PV stenosis in a hybrid OR with high-resolution DSA. To our knowledge, this is the first study to report successful PV stent placement owing to the use of hybrid OR.

A hybrid OR combines a conventional OR with an angiography suite, providing radiologists with the same environment as an angiography room outside of the surgical unit. Compared to using a mobile C-arm, better contrast resolution on DSA facilitates optimal balloon inflation and supports accurate stent placement. In the present cases, stent placement using high-resolution DSA images in a hybrid OR contributed to successful stent placements.

In an angiography room, the percutaneous transhepatic approach is ultrasound guided and less invasive but is performed under local anesthesia, and the patient must undergo interventional treatment for 2-3 hours. Additionally, using the retrograde approach to the main PV, the guidewire is sometimes difficult

to advance beyond the stenotic site (*3*). On the other hand, the transileocecal approach requires laparotomy under general anesthesia, but it is possible to advance a guidewire through the thin portal branches, which are difficult to approach using percutaneous transhepatic access. Furthermore, it is easier to place a stent at the stenotic site using an antegrade approach than using a retrograde approach. A hybrid OR is superior to the angiography suite or a regular OR as the approach can be switched immediately whenever necessary. Therefore, referral to a specialized institution with a high-resolution hybrid OR may be beneficial in patients with severe PV stenosis.

Benign PV stenosis is a rare complication following hepatobiliary-pancreatic surgery (*1,2*), and is possibly caused by postoperative inflammation, such as pancreatic fistula. In the present cases, the origin of benign PV stenosis was probably due to inflammation after the surgery. Malignancy was ruled out using contrast-enhanced CT, positron emission tomography CT (PET-CT), and biopsy. Patients often develop symptoms of portal hypertension, such as gastrointestinal hemorrhage, ascites, and thrombocytopenia, when PV stenosis is > 80% (*6*). In our study, stenosis was > 90% in each case, and two of three patients suffered from complications.

Kato *et al*. (*3*) performed stent placement in 29 patients using a percutaneous transhepatic approach in 22 patients and using laparotomy via the transileocolic vein in seven patients. In total, 7 patients had stent occlusion: three had acute thrombosis, one had thrombosis at 80 days after stenting, and three had tumor growth. The patency rate was 76%, and the mean stent patency period was 17.3 ± 21.4 months. They also found that presence of a collateral vein is a significant variable related to the development of stent occlusion. Scant evidence supports using anticoagulant therapy following stent placement (*7*). In the present cases, warfarin was administered for 6 months after the surgery.

As a major limitation of this study, we did not compare this new approach to previous technique. Future study is necessary to clearly demonstrate the usefulness of a hybrid operating room for this relatively rare situation.

In conclusion, benign PV stenosis is a good indication for PV stent placement. A hybrid OR with high-resolution DSA contributed to the success of PV stent placement.

References

1. Monge JJ, Judd ES, Gage RP. Radical pancreatoduodectemy: A 22-year experience with the complications, mortality rate, and survival rate. Ann Surg. 1964; 160:711-722.
2. Watanobe I, Ito Y, Akimoto E, Sekine Y, Haruyama Y, Amemiya K, Miyano S, Kosaka T, Machida M, Kitabatake T, Kojima K. Postoperative portal vein thrombosis and gastric hemorrhage associated with late-onset hemorrhage from the common hepatic artery after pancreaticoduodenectomy. Korean J Hepatobiliary Pancreat Surg. 2016; 20:44-47.
3. Kato A, Shimizu H, Ohtsuka M, Yoshitomi H, Furukawa K, Miyazaki M. Portal vein stent placement for the treatment of postoperative portal vein stenosis: Long-term success and factor associated with stent failure. BMC Surg. 2017; 17:1-6.
4. Jeon UB, Kim CW, Kim TU, Choo KS, Jang JY, Nam KJ, Chu CW, Ryu JH. Therapeutic efficacy and stent patency of transhepatic portal vein stenting after surgery. World J Gastroenterol. 2016; 22:9822-9828.
5. Yamakado K, Nakatsuka A, Tanaka N, Fujii A, Isaji S, Kawarada Y, Takeda K. Portal venous stent placement in patients with pancreatic and biliary neoplasms invading portal veins and causing portal hypertension: Initial experience. Radiology. 2001; 220:150-156.
6. Shan H, Xiao XS, Huang MS, Ouyang Q, Jiang ZB. Portal venous stent placement for treatment of portal hypertension caused by benign main portal vein stenosis. World J Gastroenterol. 2005; 11:3315-3318.
7. Funaki B, Rosenblum JD, Leef J a, Zaleski GX, Farrell T, Lorenz J, Brady L. Percutaneous treatment of portal venous stenosis in children and adolescents with segmental hepatic transplants: Long-term results. Radiology. 2000; 215:147-151.
8. American Joint Comittee on Cancer. AJCC Cancer Staging Manual, 8th Edition. 2016.
9. Bassi C, Marchegiani G, Dervenis C, *et al*. The 2016 update of the International Study Group (ISGPS) definition and grading of postoperative pancreatic fistula: 11 years after. Surg. 2017; 161:584-591.
10. Dindo D, Demartines N, Clavien P-A. Classification of Surgical Complications. Ann Surg. 2004; 240:205-213.

(Received December 12, 2018; Revised December 18, 2018; Accepted December 24, 2018)

BST
BioScience Trends

Guide for Authors

1. Scope of Articles

BioScience Trends is an international peer-reviewed journal. BioScience Trends devotes to publishing the latest and most exciting advances in scientific research. Articles cover fields of life science such as biochemistry, molecular biology, clinical research, public health, medical care system, and social science in order to encourage cooperation and exchange among scientists and clinical researchers.

2. Submission Types

Original Articles should be well-documented, novel, and significant to the field as a whole. An Original Article should be arranged into the following sections: Title page, Abstract, Introduction, Materials and Methods, Results, Discussion, Acknowledgments, and References. Original articles should not exceed 5,000 words in length (excluding references) and should be limited to a maximum of 50 references. Articles may contain a maximum of 10 figures and/or tables.

Brief Reports definitively documenting either experimental results or informative clinical observations will be considered for publication in this category. Brief Reports are not intended for publication of incomplete or preliminary findings. Brief Reports should not exceed 3,000 words in length (excluding references) and should be limited to a maximum of 4 figures and/or tables and 30 references. A Brief Report contains the same sections as an Original Article, but the Results and Discussion sections should be combined.

Reviews should present a full and up-to-date account of recent developments within an area of research. Normally, reviews should not exceed 8,000 words in length (excluding references) and should be limited to a maximum of 100 references. Mini reviews are also accepted.

Policy Forum articles discuss research and policy issues in areas related to life science such as public health, the medical care system, and social science and may address governmental issues at district, national, and international levels of discourse. Policy Forum articles should not exceed 2,000 words in length (excluding references).

Case Reports should be detailed reports of the symptoms, signs, diagnosis, treatment, and follow-up of an individual patient. Case reports may contain a demographic profile of the patient but usually describe an unusual or novel occurrence. Unreported or unusual side effects or adverse interactions involving medications will also be considered. Case Reports should not exceed 3,000 words in length (excluding references).

News articles should report the latest events in health sciences and medical research from around the world. News should not exceed 500 words in length.

Letters should present considered opinions in response to articles published in BioScience Trends in the last 6 months or issues of general interest. Letters should not exceed 800 words in length and may contain a maximum of 10 references.

3. Editorial Policies

Ethics: BioScience Trends requires that authors of reports of investigations in humans or animals indicate that those studies were formally approved by a relevant ethics committee or review board.

Conflict of Interest: All authors are required to disclose any actual or potential conflict of interest including financial interests or relationships with other people or organizations that might raise questions of bias in the work reported. If no conflict of interest exists for each author, please state "There is no conflict of interest to disclose".

Submission Declaration: When a manuscript is considered for submission to BioScience Trends, the authors should confirm that 1) no part of this manuscript is currently under consideration for publication elsewhere; 2) this manuscript does not contain the same information in whole or in part as manuscripts that have been published, accepted, or are under review elsewhere, except in the form of an abstract, a letter to the editor, or part of a published lecture or academic thesis; 3) authorization for publication has been obtained from the authors' employer or institution; and 4) all contributing authors have agreed to submit this manuscript.

Cover Letter: The manuscript must be accompanied by a cover letter signed by the corresponding author on behalf of all authors. The letter should indicate the basic findings of the work and their significance. The letter should also include a statement affirming that all authors concur with the submission and that the material submitted for publication has not been published previously or is not under consideration for publication elsewhere. The cover letter should be submitted in PDF format. For example of Cover Letter, please visit http://www.biosciencetrends.com/downcentre.php (Download Centre).

Copyright: A signed JOURNAL PUBLISHING AGREEMENT (JPA) form must be provided by post, fax, or as a scanned file before acceptance of the article. Only forms with a hand-written signature are accepted. This copyright will ensure the widest possible dissemination of information. A form facilitating transfer of copyright can be downloaded by clicking the appropriate link and can be returned to the e-mail address or fax number noted on the form (Please visit Download Centre). Please note that your manuscript will not proceed to the next step in publication until the JPA Form is received. In addition, if excerpts from other copyrighted works are included, the author(s) must obtain written permission from the copyright owners and credit the source(s) in the article.

Suggested Reviewers: A list of up to 3 reviewers who are qualified to assess the scientific merit of the study is welcomed. Reviewer information including names, affiliations, addresses, and e-mail should be provided at the same time the manuscript is submitted online. Please do not suggest reviewers with known conflicts of interest, including participants or anyone with a stake in the proposed research; anyone from the same institution; former students, advisors, or research collaborators (within the last three years); or close personal contacts. Please note that the Editor-in-Chief may accept one or more of the proposed reviewers or may request a review by other qualified persons.

Language Editing: Manuscripts prepared by authors whose native language is not English should have their work proofread by a native English speaker before submission. If not, this might delay the publication of your manuscript in BioScience Trends.

The Editing Support Organization can provide English proofreading, Japanese-English translation, and Chinese-English translation services to authors who want to publish in BioScience Trends and need assistance before submitting a manuscript. Authors can visit this organization directly at http://www.iacmhr.com/iac-eso/support.php?lang=en. IAC-ESO was established to facilitate manuscript preparation by researchers whose native language is not English and to help edit works intended for international academic journals.

4. Manuscript Preparation

Manuscripts should be written in clear, grammatically correct English and submitted as a Microsoft Word file in a single-column format. Manuscripts must be paginated and typed in 12-point Times New Roman font with 24-point line spacing. Please do not embed figures in the text. Abbreviations should be used as little as possible and should be explained at first mention unless the term is a well-known abbreviation (*e.g.* DNA). Single words should not be abbreviated.

Title Page: The title page must include 1) the title of the paper (Please note the title should be short, informative, and contain the major key words); 2) full name(s) and affiliation(s) of the author(s), 3) abbreviated names of the author(s), 4) full name, mailing address, telephone/fax numbers, and e-mail address of the corresponding author; and 5) conflicts of interest (if you have an actual or potential conflict of interest to disclose, it must be included as a footnote on the title page of the manuscript; if no conflict of

interest exists for each author, please state "There is no conflict of interest to disclose"). Please visit Download Centre and refer to the title page of the manuscript sample.

Abstract: The abstract should briefly state the purpose of the study, methods, main findings, and conclusions. For article types including Original Article, Brief Report, Review, Policy Forum, and Case Report, a one-paragraph abstract consisting of no more than 250 words must be included in the manuscript. For News and Letters, a brief summary of main content in 150 words or fewer should be included in the manuscript. Abbreviations must be kept to a minimum and non-standard abbreviations explained in brackets at first mention. References should be avoided in the abstract. Key words or phrases that do not occur in the title should be included in the Abstract page.

Introduction: The introduction should be a concise statement of the basis for the study and its scientific context.

Materials and Methods: The description should be brief but with sufficient detail to enable others to reproduce the experiments. Procedures that have been published previously should not be described in detail but appropriate references should simply be cited. Only new and significant modifications of previously published procedures require complete description. Names of products and manufacturers with their locations (city and state/country) should be given and sources of animals and cell lines should always be indicated. All clinical investigations must have been conducted in accordance with Declaration of Helsinki principles. All human and animal studies must have been approved by the appropriate institutional review board(s) and a specific declaration of approval must be made within this section.

Results: The description of the experimental results should be succinct but in sufficient detail to allow the experiments to be analyzed and interpreted by an independent reader. If necessary, subheadings may be used for an orderly presentation. All figures and tables must be referred to in the text.

Discussion: The data should be interpreted concisely without repeating material already presented in the Results section. Speculation is permissible, but it must be well-founded, and discussion of the wider implications of the findings is encouraged. Conclusions derived from the study should be included in this section.

Acknowledgments: All funding sources should be credited in the Acknowledgments section. In addition, people who contributed to the work but who do not meet the criteria for authors should be listed along with their contributions.

References: References should be numbered in the order in which they appear in the text. Citing of unpublished results, personal communications, conference abstracts, and theses in the reference list is not recommended but these sources may be mentioned in the text. In the reference list, cite the names of all authors when there are fifteen or fewer authors; if there are sixteen or more authors, list the first three followed by *et al.* Names of journals should be abbreviated in the style used in PubMed. Authors are responsible for the accuracy of the references. Examples are given below:

Example 1 (Sample journal reference):
Inagaki Y, Tang W, Zhang L, Du GH, Xu WF, Kokudo N. Novel aminopeptidase N (APN/CD13) inhibitor 24F can suppress invasion of hepatocellular carcinoma cells as well as angiogenesis. Biosci Trends. 2010; 4:56-60.

Example 2 (Sample journal reference with more than 15 authors):
Darby S, Hill D, Auvinen A, *et al.* Radon in homes and risk of lung cancer: Collaborative analysis of individual data from 13 European case-control studies. BMJ. 2005; 330:223.

Example 3 (Sample book reference):
Shalev AY. Post-traumatic stress disorder: diagnosis, history and life course. In: Post-traumatic Stress Disorder, Diagnosis, Management and Treatment (Nutt DJ, Davidson JR, Zohar J, eds.). Martin Dunitz, London, UK, 2000; pp. 1-15.

Example 4 (Sample web page reference):
Ministry of Health, Labour and Welfare of Japan. Dietary reference intakes for Japanese. *http://www.mhlw.go.jp/houdou/2004/11/h1122-2a.html* (accessed June 14, 2010).

Tables: All tables should be prepared in Microsoft Word or Excel and should be arranged at the end of the manuscript after the References section. Please note that tables should not in image format. All tables should have a concise title and should be numbered consecutively with Arabic numerals. If necessary, additional information should be given below the table.

Figure Legend: The figure legend should be typed on a separate page of the main manuscript and should include a short title and explanation. The legend should be concise but comprehensive and should be understood without referring to the text. Symbols used in figures must be explained.

Figure Preparation: All figures should be clear and cited in numerical order in the text. Figures must fit a one- or two-column format on the journal page: 8.3 cm (3.3 in.) wide for a single column, 17.3 cm (6.8 in.) wide for a double column; maximum height: 24.0 cm (9.5 in.). Please make sure that the symbols and numbers appeared in the figures should be clear. Please make sure that artwork files are in an acceptable format (TIFF or JPEG) at minimum resolution (600 dpi for illustrations, graphs, and annotated artwork, and 300 dpi for micrographs and photographs). Please provide all figures as separate files. Please note that low-resolution images are one of the leading causes of article resubmission and schedule delays. All color figures will be reproduced in full color in the online edition of the journal at no cost to authors.

Units and Symbols: Units and symbols conforming to the International System of Units (SI) should be used for physicochemical quantities. Solidus notation (*e.g.* mg/kg, mg/mL, mol/mm^2/min) should be used. Please refer to the SI Guide www.bipm.org/en/si/ for standard units.

Supplemental data: Supplemental data might be useful for supporting and enhancing your scientific research and BioScience Trends accepts the submission of these materials which will be only published online alongside the electronic version of your article. Supplemental files (figures, tables, and other text materials) should be prepared according to the above guidelines, numbered in Arabic numerals (*e.g.*, Figure S1, Figure S2, and Table S1, Table S2) and referred to in the text. All figures and tables should have titles and legends. All figure legends, tables and supplemental text materials should be placed at the end of the paper. Please note all of these supplemental data should be provided at the time of initial submission and note that the editors reserve the right to limit the size and length of Supplemental Data.

5. Submission Checklist

The Submission Checklist will be useful during the final checking of a manuscript prior to sending it to BioScience Trends for review. Please visit Download Centre and download the Submission Checklist file.

6. Online Submission

Manuscripts should be submitted to BioScience Trends online at http://www.biosciencetrends.com. The manuscript file should be smaller than 5 MB in size. If for any reason you are unable to submit a file online, please contact the Editorial Office by e-mail at office@biosciencetrends.com.

7. Accepted Manuscripts

Proofs: Galley proofs in PDF format will be sent to the corresponding author via e-mail. Corrections must be returned to the editor (proof-editing@biosciencetrends.com) within 3 working days.

Offprints: Authors will be provided with electronic offprints of their article. Paper offprints can be ordered at prices quoted on the order form that accompanies the proofs.

Page Charge: Page charges will be levied on all manuscripts accepted for publication in BioScience Trends ($140 per page for black white pages; $340 per page for color pages). Under exceptional circumstances, the author(s) may apply to the editorial office for a waiver of the publication charges at the time of submission.

(*Revised February 2013*)

Editorial and Head Office:
Pearl City Koishikawa 603
2-4-5 Kasuga, Bunkyo-ku
Tokyo 112-0003 Japan
Tel: +81-3-5840-8764
Fax: +81-3-5840-8765
E-mail: office@biosciencetrends.com

BST
BioScience Trends

JOURNAL PUBLISHING AGREEMENT (JPA)

Manuscript No.:

Title:

Corresponding Author:

The International Advancement Center for Medicine & Health Research Co., Ltd. (IACMHR Co., Ltd.) is pleased to accept the above article for publication in BioScience Trends. The International Research and Cooperation Association for Bio & Socio-Sciences Advancement (IRCA-BSSA) reserves all rights to the published article. Your written acceptance of this JOURNAL PUBLISHING AGREEMENT is required before the article can be published. Please read this form carefully and sign it if you agree to its terms. The signed JOURNAL PUBLISHING AGREEMENT should be sent to the BioScience Trends office (Pearl City Koishikawa 603, 2-4-5 Kasuga, Bunkyo-ku, Tokyo 112-0003, Japan; E-mail: **office@biosciencetrends.com**; Tel: **+81-3-5840-8764**; Fax: **+81-3-5840-8765**).

1. Authorship Criteria

As the corresponding author, I certify on behalf of all of the authors that:
1) The article is an original work and does not involve fraud, fabrication, or plagiarism.
2) The article has not been published previously and is not currently under consideration for publication elsewhere. If accepted by BioScience Trends, the article will not be submitted for publication to any other journal.
3) The article contains no libelous or other unlawful statements and does not contain any materials that infringes upon individual privacy or proprietary rights or any statutory copyright.
4) I have obtained written permission from copyright owners for any excerpts from copyrighted works that are included and have credited the sources in my article.
5) All authors have made significant contributions to the study including the conception and design of this work, the analysis of the data, and the writing of the manuscript.
6) All authors have reviewed this manuscript and take responsibility for its content and approve its publication.
7) I have informed all of the authors of the terms of this publishing agreement and I am signing on their behalf as their agent.

2. Copyright Transfer Agreement

I hereby assign and transfer to IACMHR Co., Ltd. all exclusive rights of copyright ownership to the above work in the journal BioScience Trends, including but not limited to the right 1) to publish, republish, derivate, distribute, transmit, sell, and otherwise use the work and other related material worldwide, in whole or in part, in all languages, in electronic, printed, or any other forms of media now known or hereafter developed and the right 2) to authorize or license third parties to do any of the above.

I understand that these exclusive rights will become the property of IACMHR Co., Ltd., from the date the article is accepted for publication in the journal BioScience Trends. I also understand that IACMHR Co., Ltd. as a copyright owner has sole authority to license and permit reproductions of the article.

I understand that except for copyright, other proprietary rights related to the Work (*e.g.* patent or other rights to any process or procedure) shall be retained by the authors. To reproduce any text, figures, tables, or illustrations from this Work in future works of their own, the authors must obtain written permission from IACMHR Co., Ltd.; such permission cannot be unreasonably withheld by IACMHR Co., Ltd.

3. Conflict of Interest Disclosure

I confirm that all funding sources supporting the work and all institutions or people who contributed to the work but who do not meet the criteria for authors are acknowledged. I also confirm that all commercial affiliations, stock ownership, equity interests, or patent-licensing arrangements that could be considered to pose a financial conflict of interest in connection with the article have been disclosed.

Corresponding Author's Name (Signature):

Date: